Effect of Age & Unilateral Dopamine Depletion on Striatal NMDA Receptor Function

Submitted by

Thabelo Khoboko

Submitted in fulfilment of the requirements for the degree of Master of Science in Medicine (M.Sc.Med) in the Faculty of Health Sciences at the University of Cape Town

Supervised by

Professor Vivienne A. Russell

Dr Lauriston Kellaway

DECLARATION

I, *Thabelo Khoboko*, hereby declare that the work on which this thesis is based is my original work (except where acknowledgments indicate otherwise), and that neither the whole work nor any part of it has been, is being, or is to be submitted for another degree in this or any other university.

I empower the University Of Cape Town to reproduce for the purpose of research either the whole or any portion of the contents in any manner whatsoever.

Signature

December 2005

Date

PRESENTATIONS

Parts of this dissertation have been presented at:

INTERNATIONAL BRAIN RESEARCH ORGANIZATION (IBRO) / SOCIETY FOR NEUROSCIENTISTS OF AFRICA (SONA) CONFERENCE

Cape Town – Republic of South Africa
April 2005
Results of this study were presented at the international meeting held in Cape Town

SUMMER PROGRAM IN NEUROSCIENCE, ETHICS AND SURVIVAL (SPINES)

Marine Biological Laboratory, Woods Hole – United States of America
July 2004
Preliminary data was presented to the MBL community as part of student presentations

ACKNOWLEDGMENTS

At the University of Cape Town I would like to thank my supervisors and all my colleagues who contributed to the development of this study. Most especially I would like to thank Professor Vivienne Russell for her constant interrogations that helped to air all the cobwebs from the corners of my mind!! Thank you for the guidance and for helping me grow as a scientist.

I am grateful to the International Brain Research Organization (IBRO) for making such a tremendous effort to develop neuroscience globally but I am most grateful for their efforts in Africa. The African Neuroscience Schools continually provide incredible opportunities for students to vastly broaden their knowledge with international researchers at the fore of their field. The schools are truly unique in creating a professional yet intimate environment for students to develop relationships with their peers on the continent and to foster relationships with mentors. Thank you to my IBRO mentors, for your hard work and dedication.

My deepest gratitude to Professor Rita Levi Montalcini and her foundation for investing in the growth of African female neuroscientists. As a recipient of such generosity words fail to express my indebtedness.

To Ntate Njabulo and 'M'e Mpho Ndebele, thank you for physical, mental and spiritual nourishment. Cape Town could not have been my home for so long without you and because of you it will always be my home. I have always valued and will always cherish your encouragement, faith and guidance. You have given me strength when I had none.

To my family, I am nothing without your love. You are the source and the foundation of all that I am. Through all the pain we are still strong and we are still moving on. To my sister, Keromang, you died before the completion of this project and with you the meaning of it died. One day we'll meet again in the

land of our ancestors and I'll tell you how I made it through without you even when I lost all faith...I remain blessed with your love. Robala ka khotso.

TABLE OF CONTENTS

List of Abbreviations

AC	Adenylyl cyclase
AChE	Acetylcholinesterase
aka	Also known as
AKAP	A kinase anchoring protein
AMPA	α-amino-3-hydroxy-5-methyl-4-isoxazole
ANOVA	Analysis of variance
AP	Anterior-posterior
ATP	Adenosine trisphosphate
Ca^{2+}	Calcium
$^{45}Ca^{2+}$	Radioactive calcium-45
CaM	Calmodulin
Ca^{2+}-CaM	Calcium-calmodulin complex
CaMKII	Ca^{2+}-CaM dependent kinase II
cAMP	Cyclic adenosine monophosphate
Cd^{2+}	Cadmium
CKII	Casein kinase II
CNS	Central nervous system
CREB	cAMP/ Ca^{2+} response element binding protein
DAG	Diacylglycerol
DARPP-32	Dopamine and cAMP-regulated phosphoprotein Mr 32kDa
DV	Dorso-ventral
ER	Endoplasmic reticulum
ERK	Extracellular signal regulated protein
F-actin	Filamentous actin
GABA	γ-aminobutyric acid
GPe	External globus pallidus
GPi	Internal globus pallidus
GPv/VP	Ventral globus pallidus
GTP	Guanosine trisphosphate
G-protein	GTP binding regulatory protein
IP_3	Inositol trisphosphate
K^+	Potassium
L-dopa	3, 4 dihydroxyphenylalanine
MAGUK	Membrane associated guanylate kinase
MAP2	Microtubule associated protein 2
MFB	Medial forebrain bundle
Mg^{2+}	Magnesium
mg	Milli gram
mGluR	Metabotropic glutamate receptor
ms	Milli second
ML	Medio-lateral
µm	Micro metre
µl	Micro litre
Na^+	Sodium
NMDA	N-methyl-D-aspartate
nmol	Nano mole
OMPFC	Orbito-medial prefrontal cortex
6-OHDA	6-hydroxydopamine
PDZ	PSD-95 Drosophila discs large (Dlg) zona occludens –1(zo-1) protein
PKA	cAMP dependent protein kinase
PKC	Ca^{2+}/phospholipids dependent protein kinase
PLC	Phospholipase C
Po	Open probability
PP-1	Protein phosphatase 1
PSD	Postsynaptic density
PP-2B	Protein phosphatase 2B (calcineurin)
SAP	Synapse associated protein
s.c.	Subcutaneously
Ser	Serine
SMA	Supplementary motor area
SNAP	Synaptosome associated protein 25
SNARE	Synaptosome associated protein receptor
SN	Substantia nigra
SNc	Substantia nigra pars compacta
SNr	Substantia nigra pars reticulata
STEP	Striatal enriched tyrosine phosphatase
STN	Subthalamic nucleus
TH	Tyrosine hydroxylase
Thr	Threonine
VTA	Ventral tegmental area
YELK	Internalization motif

List of Figures

List of Tables

Chapter 5

ABSTRACT

Parkinson's disease is characterized by the loss of dopamine neurons of the substantia nigra pars compacta (SNc) resulting in the loss of dopamine innervation into the striatum. Dopamine is involved in modulating N-methyl-D-aspartate (NMDA) receptor activity in the striatum and consequently NMDA receptor function is influenced by the pathophysiology of Parkinson's disease. Parkinson's disease is more frequently observed in older rather than younger patients. During development and aging, synaptic NMDA receptor function is altered through decreases in receptor expression and alterations of receptor subunit composition in the synaptic membrane. These changes in turn alter NMDA mediated calcium (Ca^{2+}) currents. Ca^{2+} ionic fluxes enable the receptors to play a critical role in the regulation of synaptic function. Following loss of striatal dopamine, NMDA receptor function has been reported to be upregulated by increased protein phosphorylation and through changes in subunit composition. Two hypotheses were tested in the current study. The first study tested the hypothesis that NMDA receptor mediated influx of radioactive calcium-45 ($^{45}Ca^{2+}$) into striatal sections will be significantly reduced with increasing age in male Long Evans rats (16 weeks old) compared to younger male adolescent rats (7 week old rats). In the second study, we tested the hypothesis that NMDA receptor upregulation following dopamine depletion in the striatum will result in increases of NMDA stimulated influx of $^{45}Ca^{2+}$ into striatal sections.

Using the method developed for measuring $^{45}Ca^{2+}$ uptake into rat cortical sections by Lehohla *et al* (2000), preliminary assays were conducted on n=14 rats to determine whether incubation of striatal sections (350 µm) in buffer containing NMDA (100 µM) for 2 mins was effective in stimulating measurable increases in $^{45}Ca^{2+}$ accumulation into the striatal sections and to determine the reproducibility of the assay. Striatal sections incubated in buffer without NMDA served as controls. Results from the preliminary experiments showed that the effect of NMDA (100 µM) on $^{45}Ca^{2+}$ uptake was calculated by subtracting the basal uptake of the control sections from total uptake of the stimulated sections. $^{45}Ca^{2+}$ accumulation was expressed as nanomoles $^{45}Ca^{2+}$ per milligram protein (nmol $^{45}Ca^{2+}$ / mg protein). There was a significant increase in total $^{45}Ca^{2+}$ accumulation into striata incubated with NMDA relative to the basal $^{45}Ca^{2+}$ uptake of non-stimulated sections.

To test our first hypothesis, NMDA stimulated $^{45}Ca^{2+}$ uptake into dorsal and ventral striatal sections from 7 week old adolescent male Long Evans rats (n=7) and 16 week old adult Long Evans rats (n=6) was measured. NMDA stimulated $^{45}Ca^{2+}$ uptake into anterior (6.73 ± 0.81 nmol $^{45}Ca^{2+}$ / mg protein) and posterior (4.35 ± 0.61 nmol $^{45}Ca^{2+}$ / mg protein) dorsal striata of the left hemisphere of 7 week old rats was significantly greater than NMDA stimulated $^{45}Ca^{2+}$ uptake into anterior (2.07 ± 0.86 nmol $^{45}Ca^{2+}$ / mg protein) and posterior (1.49 ± 0.62 nmol $^{45}Ca^{2+}$ / mg protein) dorsal striata of the same hemisphere in 16 week old rats (ANOVA, $p<0.05$). Similarly in the right hemisphere, NMDA stimulated $^{45}Ca^{2+}$ uptake into anterior (5.30 ± 0.86 nmol $^{45}Ca^{2+}$ / mg protein) and posterior (5.73 ± 0.72 nmol $^{45}Ca^{2+}$ / mg protein) dorsal striata of 7 week old rats was also significantly greater than NMDA stimulated $^{45}Ca^{2+}$ uptake into anterior (2.86 ± 0.57 nmol $^{45}Ca^{2+}$ / mg protein) and posterior (2.14 ± 0.46 nmol $^{45}Ca^{2+}$ / mg protein) dorsal striata of 16 week old rats. NMDA stimulated $^{45}Ca^{2+}$ uptake into dorsal striata of 7 week old rats were 2 - 3 fold greater than that of 16 week old rats. In the ventral striata, NMDA stimulated $^{45}Ca^{2+}$ uptake was significantly greater in the posterior striata (7.34 ± 1.43 nmol $^{45}Ca^{2+}$ / mg protein) of the left hemisphere of 7 week old rats than (2.55 ± 0.66 nmol $^{45}Ca^{2+}$ / mg protein) 16 week old rats (ANOVA, $p<0.05$). However, there were no significant differences in the right posterior ventral striata or the anterior ventral striata of either hemisphere.

To test whether dopamine loss altered NMDA stimulated $^{45}Ca^{2+}$ accumulation into rat striatal sections, an established unilateral 6-hydroxydopamine (6-OHDA) rat model of Parkinson's disease was used to induce degeneration of the nigrostriatal pathway. 6-OHDA (13.5 µg/ 4.5 µl containing 0.02% ascorbic acid in sterile saline) was infused into the medial forebrain bundle (MFB) of the nigrostriatal pathway (co-ordinates: lateral relative to the midline, 1.6 mm; anterior posterior relative to the interaural line, 4.70 mm and dorso-ventral from dura, 8.4mm –Paxinos and Watson, 1986) of the left hemisphere of Long Evans rats. Sham operated rats were infused with only saline and were used as a control. In developing the surgical technique, cresyl violet histological representation of the infusion needle targeting the MFB target site were obtained. Behavioural testing using apomorphine (0.5 mg/kg, s.c.) induced rotations were conducted to assess the extent of lesion two weeks post surgery. Greater than 100 contralateral rotations in response to apomorphine were taken as an indication of a successful lesion. Rats were selected for NMDA stimulated $^{45}Ca^{2+}$ uptake assay on the basis of this criterion. Immunocytochemistry for tyrosine hydroxylase (TH) in coronal sections of the rat brain and brain stem was conducted 5 weeks post surgery and 3 weeks

post behavioural testing on n=4 rats to obtain visual confirmation of the extent of degeneration of dopamine producing neurons within the midbrain and the extent of dopamine loss in the striatum. Near complete loss of TH within the left lesioned hemisphere was observed in rats conducting >100 contralateral rotations and confirmed a loss of dopamine neurons in the midbrain and axon terminals in the striatum in response to 6-OHDA infusion into the MFB.

$^{45}Ca^{2+}$ uptake assays were conducted on striatal sections of parkinsonian rats 5 weeks post surgery and 3 weeks following behavioural testing. NMDA stimulated $^{45}Ca^{2+}$ uptake into the anterior dorsal striatal sections (3.49 ± 0.57 nmol $^{45}Ca^{2+}$ / mg protein) of the right unlesioned hemisphere of sham operated rats (n=9) was not significantly different from NMDA stimulated $^{45}Ca^{2+}$ uptake into the same anterior dorsal striatum (3.90 ± 0.80 nmol $^{45}Ca^{2+}$ / mg protein) of 6-OHDA lesioned rats (n=10). NMDA stimulated uptake into posterior dorsal striata of the same unlesioned right hemisphere was 4.20 ± 0.93 nmol $^{45}Ca^{2+}$ / mg protein and 4.51 ± 0.89 nmol $^{45}Ca^{2+}$ / mg protein in the sham operated and 6-OHDA lesioned rats respectively. In the lesioned left hemisphere, NMDA stimulated $^{45}Ca^{2+}$ uptake into the anterior dorsal striatum of the sham operated rats (3.54 ± 0.66 nmol $^{45}Ca^{2+}$ / mg protein) showed no significant difference from $^{45}Ca^{2+}$ uptake into anterior dorsal striata of 6-OHDA lesioned rats (3.83 ± 0.64 nmol $^{45}Ca^{2+}$ / mg protein). NMDA stimulated $^{45}Ca^{2+}$ uptake into striata obtained from parkinsonian rats was not significantly different from NMDA stimulated $^{45}Ca^{2+}$ uptake into striata obtained from sham operated rats.

In the current study, we were able to demonstrate that 100 µM NMDA stimulated significant uptake of radioactive Ca^{2+} ions into striatal tissue to provide a measure of striatal NMDA receptor function. To our knowledge this is the first study to measure NMDA mediated Ca^{2+} influx into the striatum in vitro. Furthermore, using 7 week and 16 week old male rats, we were able to demonstrate that NMDA receptor mediated $^{45}Ca^{2+}$ influx in the dorsal striatum decreases two to three fold over nine weeks of young adult development. The results of NMDA stimulated $^{45}Ca^{2+}$ uptake following dopamine depletion did not confirm our hypothesis that NMDA upregulation in parkinsonian rats would result in increased NMDA receptor meditated Ca2+ influx into striatal sections. The data obtained from parkinsonian rats may indicate that upregulation of NMDA receptors as a function of increased phosphorylation following dopamine depletion may serve a different function that does not involve increased channel gating.

CHAPTER 1

NMDA RECEPTORS

1.1 The significance of NMDA receptors

Parkinson's disease is an age related disease in which symptoms of tremor, akinesia and bradykinesia are attributed to disruption of processing within basal ganglia circuitry following the selective degeneration of dopamine producing neurons of the substantia nigra pars compacta (SNc) which causes a loss of dopamine striatal innervation (Marsden and Obeso, 1994; Olanow and Tatton, 1999; Saper, 1999). The role of N-methyl-D-aspartate (NMDA) receptors has gained prominence in Parkinson's disease research as the structure and function of these receptors is altered following dopamine depletion in parkinsonian animal models. Dopamine plays a critical role in modulating cortical glutamatergic excitation of the striatal medium spiny neurons through the interaction of dopamine activated intracellular signaling cascades with NMDA mediated intracellular signaling cascades (Reynolds and Wickens, 2002). The effects of dopamine depletion on medium spiny neurons are multiple; increased neuronal firing, altered dendritic spine morphology and altered synaptic NMDA receptor expression (Kish *et al*, 1999; Arbuthnott *et al*, 2000; Tseng *et al*, 2001; Reynolds and Wickens, 2002; Yasumoto *et al*, 2002; Dunah *et al*, 2003).

Calcium (Ca^{2+}) activated intracellular signals mediated by NMDA receptors play a vital role in regulating dendritic spine morphology and synaptic receptor expression hence Ca^{2+} is prominently involved in synaptic function and developmental and activity dependent modifications attributed to synaptic plasticity (Arbuthnott *et al*, 2000; Allen, 2004; Cavazzini *et al*, 2005). The efficiency of the NMDA receptors is regulated through phosphorylation (Conti and Weinberg, 1999). Not surprisingly then that in addition to the synaptic changes that occur, the phosphorylation state of NMDA receptor subunits has been found to be greatly altered following dopamine depletion (Oh *et al*, 1998; Dunah *et al*, 2000) and it has been suggested that NMDA receptor function is upregulated (Chase *et al*, 1998). In the clinical treatment of Parkinson's disease, attenuation of NMDA receptor activity is a strategy developed using NMDA antagonists as adjuncts to dopamine replacement therapy, L-DOPA (Montastruc *et al*, 1997). In animal models of Parkinson's disease, NMDA antagonists are reported to have similar anti-parkinsonian effects as dopamine receptor agonists (Nash and Brotchie, 2002).

The prominent involvement of NMDA receptors in synaptic function and their involvement in Parkinson's disease has resulted in extensive study of these receptor channels and has motivated the development of the current study to investigate the effects of age and dopamine depletion (two influential factors involved in Parkinson's disease) on NMDA receptor function.

In this chapter, the structure and regulation of NMDA receptors and their regulation of synaptic function through Ca^{2+} mediated mechanisms is discussed. An extensive discussion on the mechanisms involved in the interaction between NMDA mediated and dopamine mediated intracellular signaling cascades during striatal neural processing follows in Chapter 2. In Chapter 3 striatal processing and significance in the basal ganglia circuitry is examined.

1.2 NMDA receptors and glutamate neurotransmission

NMDA receptors are a subtype of ionotropic glutamate receptors expressed in the vertebrate central nervous system (CNS) (Nakanishi, 1992). Glutamate is the major excitatory neurotransmitter in the CNS and the highest density of glutamate receptors in the basal ganglia is found in the medium spiny projection neurons of the striatum (Schmidt and Kretschmer, 1997). The striatum receives extensive glutamatergic projections originating from the associative, limbic and motor cortices and the thalamic nuclei (Parent, 1990; Smith and Bolam, 1990; Haber *et al*, 2000; Yelnik, 2002). These excitatory afferents form synaptic contacts with dendritic spines of striatal projection neurons upon which NMDA receptors are localized (Blackstone and Sheng, 1999; van Rossum and Hanisch, 1999). Other ionotropic glutamate receptors expressed on dendritic spines are the α-amino-3-hydroxy-5-methyl-4-isoxazole propionic acid (AMPA) receptors and kainate receptors (Nakanishi, 1992). The ligand gated ionotropic glutamate receptors gate influxes of cations - potassium (K^+), sodium (Na^+) or Ca^{2+} ions into the striatal spiny neurons through an integral cation specific receptor channel to generate current flow (Girault *et al*, 1986; Johnson and Ascher, 1987; Nakanishi, 1992; Hille, 2001).

In addition to stimulating ionotropic receptors, glutamate activates metabotropic glutamate receptors (mGluRs) and these also increase intracellular ionic levels by activating the release of Ca^{2+} from intracellular stores (Nakanishi, 1994; Blackstone and Sheng, 1999; Awad *et al*, 2000). mGluRs potentiate NMDA mediated signaling by elevating intracellular Ca^{2+} levels (Blackstone and Sheng, 1999; Awad *et al*, 2000). Relative to the other ionotropic receptors, NMDA receptors have the

greatest affinity to glutamate, generate prolonged excitatory transmission upon activation (Figure 1.1) and have a very high Ca^{2+} ion permeability (higher than K^+ and Na^+) (MacDermott *et al*, 1986; Johnson and Ascher, 1987; Forsythe and Westbrook, 1988; Nakanishi, 1992; Burnashev *et al*, 1996; Götz *et al*, 1997; Conti and Weinberg, 1999). While activation of a single AMPA receptor channel opening permits an influx of ≈ 10 – 100 Ca^{2+} ions, a single opening of NMDA receptor channel conducts ≈ 1000 Ca^{2+} ions (Conti and Weinberg, 1999).

The high permeability to Ca^{2+} ions enable NMDA receptors to play a critical role in synaptic function (Nakanishi, 1992; Mori and Mishina, 1995; Blackstone and Sheng, 1999). Ca^{2+} is the currency of NMDA mediated signal transduction pathways involved in the regulation and modification of synaptic efficiency. Through regulated spatiotemporal patterns, Ca^{2+} activated signaling cascades influence synapse formation, dendritic spine morphology, gene transcription, glutamate receptor expression on synaptic membranes, ion channel regulation, neuronal excitability and consequently the firing response of striatal spiny neurons to glutamate stimulation (Bourne and Nicoll, 1993; Mori and Mishina, 1995; Wickens and Wilson, 1998; Carroll and Zukin, 2002; Cohen-Cory, 2002; Reynolds and Wickens, 2002; Saimi and Kung, 2002; Sheng and Kim, 2002). In this way NMDA receptors regulate synaptic strengthening and weakening.

1.3 Structure of NMDA receptors and receptor activation

NMDA receptor channels at postsynaptic sites are generally expressed as diheteromeric complexes comprised of two NR1 receptor subunits co-assembled with two NR2 subunits to form an NR1/NR2 complex (Mori and Mishina, 1995; Cull-Candy *et al*, 2001). NR3 subunits are also expressed in specific brain regions and these co-assemble with existing NR1/NR2 NMDA receptor complexes to influence NMDA receptor channel conductance and Ca^{2+} permeability (Cull-Candy *et al*, 2001; Matsuda *et al*, 2003). There are eight splice variants of NR1 subunits, and these confer specific functional characteristics to seemingly similar heteromeric channels e.g. NR1-*1b*/NR2B NMDA receptors have higher deactivation time constants than NR1-*1a*/NR2B NMDA receptors (Mori and Mishina, 1995; Cull-Candy *et al*, 2001; Pauly *et al*, 2005). Of the NR2 subunits, there are four identified subtypes; NR2A, NR2B NR2C and NR2D (Mori and Mishina, 1995). NR1 subunits generally bind with a specific NR2 subunit e.g. NR1/NR2A or NR1/NR2B, however the receptor channels can also be expressed as triheteromers comprised of two different NR2 subunits e.g.

NR1/NR2A-NR2B (Kennedy, 1997; Luo *et al*, 1997; van Zundert *et al*, 2004). The NR2 subunits confer the high glutamate affinity of the receptors but differ in ligand sensitivities, kinetic properties and in their interactions with intracellular proteins thereby confer differential synaptic responses to glutamate activation (Mori and Mishina, 1995; Cull-Candy *et al*, 2001; Qian and Johnson, 2002).

Each NR2 subtype confers different ligand binding affinities for both glutamate and glycine to the NMDA receptors (measured as the efficient concentration for half maximal response, EC_{50}) but it is the NR1 subunits that influence glycine modulation of receptor function (Nakanishi, 1992; Mori and Mishina, 1995). Glycine is amongst one of numerous modulators that have binding sites on the NMDA receptors as illustrated in Figure 1.2 (Mori and Mishina, 1995; Conti and Weinberg, 1999; Shulman and Hyman, 1999; Cull-Candy *et al*, 2001). NR1/NR2A NMDA receptors have the lowest affinity for ligand binding with EC_{50} measurements of 1.7 μM for glutamate and 2.1 μM for glycine. NR1/NR2B NMDA receptors have a relatively greater affinity of 0.8 μM for glutamate and 0.3 μM for glycine while the NR1/NR2C NMDA receptors have a similar affinity (0.7 μM for glutamate and 0.2 μM for glycine). NR1/NR2D NMDA receptors have the greatest ligand binding affinity with 0.4 μM and 0.9 μM for glutamate and glycine respectively (Mori and Mishina, 1995). Maximal activation of NMDA receptor channels depends on glutamate binding to the receptors and simultaneous co-activation by endogenous glycine (Johnson and Ascher, 1987; Mori and Mishina, 1995; Qian and Johnson, 2002). Glycine functions as an allosteric modulator of signal transduction by NMDA receptors (Wroblewski *et al*, 1989) and potentiates NMDA receptor mediated Ca^{2+} currents (Wang *et al*, 1996; Berger *et al*, 1998). However, D-serine has been established to be a more potent endogenous ligand, occupying the glycine site (Berger *et al*, 1998; Mothet *et al*, 2000). Binding of ligands to the receptors induces a conformational change that alters the shape of the extracellular channel opening (Qian and Johnson, 2002).

Each NMDA subunit is composed of four hydrophobic transmembrane segments, TM1 to TMIV that span the lipid bilayer with the exception of TMII that does not transgress the entire bilayer (Nakanishi, 1992; Mori and Mishina, 1995; Conti and Weinberg, 1999). The subunits have an extracellular N-terminal domain and an intracellular C-terminal domain extending from TM1 and TMIV respectively; NR2 subunits have longer C-termini than NR1 subunits (Conti and Weinberg, 1999). The selectivity of the channel pore to cations is conferred by an anionic ring formed by asparagine amino acid

residues of the TMII segments through their inward orientation forming a channel pore (Burnashev *et al*, 1992; Nakanishi, 1992; Loftis and Janowsky, 2003). Configuration of the asparagine residues is the main structural determinant of Ca^{2+} permeability and magnesium (Mg^{2+}) sensitivity through the receptor channel (Burnashev *et al*, 1992).

Amongst the glutamate receptors, NMDA receptors are unique in that they are both ligand and voltage gated (Mori and Mishina, 1995). The unique voltage gating of NMDA receptors is conferred by the Mg^{2+} block of channels that persists at hyperpolarised potentials (Nowak *et al*, 1984). When agonist binds to the receptors *during* membrane depolarization which relieves the Mg^{2+} block, Ca^{2+} ions are admitted through the receptor channels, as a result NMDA receptors respond to simultaneous glutamate postsynaptic stimulation and membrane depolarization (Hille, 2001). In the absence of ligand binding and due to the Mg^{2+} block, NMDA receptor channels have low open probability (Po) at rest (Nowak *et al*, 1984; Rosenmund *et al*, 1995). Channel open probability is an indicator of NMDA mediated Ca^{2+} currents (Erreger *et al*, 2005). The NMDA NR1 subunits have the greatest influence on Ca^{2+} permeability and Mg^{2+} blockade (Nakanishi, 1992). Despite asparagine residues being located on the TMII segments of both NR1 and NR2 subunits, mutations of NR2 asparagine residues do not affect Ca^{2+} permeability instead they reduce Mg^{2+} sensitivity. On the other hand, NR1 asparagine mutations decrease Ca^{2+} permeability and only slightly affect Mg^{2+} sensitivity (Burnashev *et al*, 1992).

1.4 Developmental influences on subunit expression

Development has a major effect on the differential expression of the subunits. In the embryonic and neo-natal rat brain, NR2D and NR2B NMDA receptor subtypes are highly expressed but within post-natal week two, NR2D expression is drastically reduced and NR2B expression becomes restricted in the forebrain while NR2A expression increases throughout the brain (Mori and Mishina, 1995). Altering NMDA receptor subtype composition changes the kinetics of the NMDA receptor channels hence the ionic Ca^{2+} conductances. NR1/NR2D channels are open for a relatively long period; these channels have decay time constants of ≈ 5000 ms (Mori and Mishina, 1995). The time constant for both NR1/NR2B and NR1/NR2C NMDA channels is ≈ 400 ms while NR1/NR2A NMDA channels have the fastest gating constant of ≈ 120 ms (Mori and Mishina, 1995). The kinetics of the different NMDA receptor channels function to regulate different signaling mechanisms mediated by Ca^{2+} i.e.

rapid increases activate mechanisms that are not activated by slower ionic increases hence subunit composition may confer temporal activation of signaling mechanisms (Cull-Candy *et al*, 2001; Erreger *et al*, 2005). The high glutamate affinity and slow gating kinetics of NR2D containing receptors may account for their high levels of expression during pre-natal development when neurons are developing to increase the efficiency of glutamate usage during early development.

Within the developed CNS, NR1 subunits are expressed indiscriminately throughout the brain, but the expression of the NR2 subtypes exhibits more regional specialization (Nakanishi, 1992; Mori and Mishina, 1995; Erreger *et al*, 2005). In the striatum, spiny projection neurons predominantly express NR1/NR2A and NR1/NR2B NMDA receptor complexes (Chen and Reiner, 1996; Götz *et al*, 1997; Loftis *et al*, 2003). These NMDA receptor complexes are both expressed in the cerebral cortex and hippocampus, but have differential expression in the cerebellar granule cells where NR2A subtypes are most highly expressed and in the thalamus and olfactory bulb where NR2B subtypes are highly expressed (Monyer *et al*, 1992; Götz *et al*, 1997). NR2C subtype expression is restricted to the cerebellum while NR2D generally have a low expression in the developed adult brain (Monyer *et al*, 1992; Nakanishi, 1992; Mori and Mishina, 1995). Expression of NR2D mRNA in adult rat brain tissue has been observed on striatal somatostatin interneurons along with NR2A and NR2B subtypes (Chen and Reiner, 1996).

1.5 Dendritic localization of NMDA receptors and development of spines

NMDA mediated intracellular Ca^{2+} signalling mechanisms are localized at dendritic spines where the receptors are themselves organised (Blackstone and Sheng, 1999). On the dendritic spines, NMDA receptors are localized within a prominent protein lattice known as the postsynaptic density (PSD) and are associated with scaffolding proteins, kinases, phosphatases and signalling molecules (Kennedy, 1997; Scannevin and Huganir, 2000; Cull-Candy *et al*, 2001; Lin *et al*, 2004). PSD is directly opposite to the presynaptic terminal (Eccles, 1964; Blackstone and Sheng, 1999). The close proximity of signalling molecules, kinases and phosphatases to NMDA receptors within dendritic spines ensures precise signalling as the correct enzymes are organised with specific proteins; protein kinases and phosphatases either bind directly to the receptor channels or are anchored to the cytoskeleton by scaffolding proteins (Pawson and Scott, 1997). There are multiple kinases and phosphatases involved in regulating NMDA receptor function and NMDA receptors contain

multiple consensus sites for phosphorylation by several different kinases (Blank *et al*, 1997). Phosphorylation is a structural modification to ion channels mediated by protein kinases involving addition of charged phosphate ion molecule from adenosine trisphosphate (ATP) (Smart, 1997) and at PSD, NMDA receptor function is regulated through its phosphorylation state by the activity of kinases and phosphatases co-localized with NMDA receptors (Lin *et al*, 2004). Phosphorylation is a reversible process regulated by protein phosphatases.

In early development, neurons are initially without spines and these develop as dendritic protusions in response to innervation by incoming fibres to create synaptic contacts. Activation of NMDA receptors on dendrites induces transient and moderate increases in Ca^{2+} ions resulting in rapid elongation of dendritic filopodia and the formation of novel spines (Jontes and Smith, 2000; Segal *et al*, 2000). Dendritic filopodia dynamically extend outwards from dendritic shaft to interact with the approaching axon growth cone in response to depolarizing synaptic activation (Jontes and Smith, 2000; Segal *et al*, 2000; Cohen-Cory, 2002). Blocking NMDA receptors inhibits dendritic growth (Cohen-Cory, 2002). An excess of synaptic contacts is initially made to provide a diverse pool of synapses for pruning selection of potential patterns of connectivity to establish pathways and for stabilization of dendritic spines (Jontes and Smith, 2000). Synaptic pruning is important for this process but can be blocked by NMDA antagonists (Segal *et al*, 2000).

1.6 NMDA receptors and regulation of dendritic spine morphology and architecture

In addition to aiding the formation of dendritic spines NMDA receptors are necessary in the regulation of spine morphology and architecture. The framework of dendritic spines is comprised of cytoskeletal proteins, filamentous actin (F-actin) microfilaments and microtubules to which NMDA receptors are indirectly linked through binding to microfilament crosslinking structural proteins, namely α-actinin, spectrin (fodrin), and microtubule associated protein 2 (MAP2) as illustrated in Figure 1.3 (Kennedy, 1997; Blackstone and Sheng, 1999; van Rossum and Hanisch, 1999; Kasai *et al*, 2003). In Parkinson's disease and during aging morphological alterations occur and dendritic spine density is significantly reduced resulting in reduction of excitatory synapses (Ingham *et al*, 1998; Meshul *et al*, 1999; Arbuthnott *et al*, 2000). Binding of the crosslinking structural proteins to NMDA receptors stabilizes the actin cytoskeleton (van Rossum and Hanisch, 1999; Jontes and Smith, 2000; Kasai *et al*, 2003). Non-NMDA receptors do not influence dendritic morphology as they

are not directly associated with microfilament cross-linking proteins (van Rossum and Hanisch, 1999).

The morphology of dendritic spines is dynamic and is influenced by intracellular Ca^{2+} (Blackstone and Sheng, 1999; Kasai *et al*, 2003; Carlisle and Kennedy, 2005). Large increases of NMDA receptor mediated Ca^{2+} ions can cause shrinkage of spines (Segal *et al*, 2000). Indeed, Korkotian and Segal (2001) demonstrated that dendritic spines may undergo rapid actin dependent contraction described as a 'twitch', lasting up to 2s before the spine regains its original shape. 'Twitches' occur in response to Ca^{2+} transients (Korkotian and Segal, 2001). Spines are remodeled through disassembly of existing stable actin filament networks followed by re-assembly and stabilization, specifically the shape of the dendritic head can be altered within seconds in response to synaptic activity (Carlisle and Kennedy, 2005). The geometry of dendritic spines strongly influences the distribution of receptor binding sites and the impact of excitatory neurotransmission (Clements, 1996). Small heads on spines present a small synaptic area and weak glutamate sensitivity as they accommodate a small number of glutamate receptor binding sites; transformation into large spines facilitates an increased number of synaptic receptors (Kasai *et al*, 2003).

NMDA receptor binding to structural proteins is modulated by Ca^{2+} ions. α-actinin binds with NMDA receptors at the C terminal of NR2B subunits at the CO region of the NR1 C terminal when intracellular Ca^{2+} levels are low (Ehlers *et al*, 1996; Blackstone and Sheng, 1999; van Rossum and Hanisch; Samai and Kung, 2004). Ca^{2+} binding to α-actinin causes a reduction in the binding affinity of the CO region for α-actinin resulting in its dissociation from NR1 (Krupp *et al*, 1999). Dissociation of structural proteins from NR1 causes depolymerization of dendritic cytoskeletal microfilaments and alters the architecture and geometry of dendritic spines (van Rossum and Hanisch, 1999). The dissociation of α-actinin from NR1 is also induced by binding of calmodulin (CaM) to CO. NMDA mediated Ca^{2+} influx activates calcium sensing and calcium binding proteins; in particular CaM (Saimi and Kung, 2002). CaM exists in a soluble form in the cytoplasm and nucleus but has binding sites at synaptic membrane structures (Saimi and Kung, 2002). When bound with Ca^{2+}, a Ca^{2+}-CaM complex forms and CaM is able to bind to its target proteins at the PSD such as NR1 subunits (Saimi and Kung, 2002). α-actinin and Ca^{2+}-CaM bind competitively on NR1 (Ehlers *et al*, 1996; Blackstone and Sheng, 1999; Krupp *et al*, 1999; Samai and Kung, 2004). Ca^{2+}-CaM displaces α-

actinin binding on NR1 thereby induces depolymerization (van Rossum and Hanisch, 1999). Ca^{2+}-CaM binding to NR1 CO region also influences the NMDA receptor open probability; this is discussed in Chapter 2 (Krupp *et al*, 1999).

NMDA mediated Ca^{2+} influx influences both the depolymerization of cytoskeletal proteins and also increases the stability of dendritic cytoskeleton. Partial dissolution of the cytoskeletal framework through α-actinin dissociation from NMDA subunits is followed by increased tubulin concentration and polymerization of tubulin molecules mediated by MAP2 dephosphorylation (van Rossum and Hanisch, 1999). MAP2 stabilizes dendritic microtubules (Blackstone and Sheng, 1999). Following NMDA mediated Ca^{2+} influx, Ca^{2+} activation of calcineurin phosphatase dephosphorylates MAP2 to enable it to bind microtubules. Phosphorylation of MAP2 reduces its affinity for structural microtubules thereby reducing the stability of the dendritic cytoskeleton; calcineurin dephosphorylation increases binding of microtubules and increases dendritic stability (van Rossum and Hanisch, 1999). In addition to binding of microtubules, there is an increase in synaptic glutamate receptor expression that occurs following initial spectrin induced depolymerization (van Rossum and Hanisch, 1999).

1.7 Membrane associated guanylate kinases (MAGUKs)

At the PSD, NMDA receptors are bound to membrane associated guanylate kinases (MAGUKs). MAGUKs stabilize the receptors at the synapse, regulate synaptic distribution of the receptors and influence the gating properties of the receptors hence intracellular Ca^{2+} concentrations that occur in response to glutamate neurotransmission (Carroll and Zukin, 2002; Dunah *et al*, 2004; Lin *et al*, 2003; van Zundert *et al*, 2004; Ying Lin, 2004). The MAGUKs most prominently associated with NMDA receptors are synapse associated protein 102 (SAP-102) (which binds to a 102 amino acid residue long recognition motif) and postsynaptic density 95 (PSD-95) (also named SAP-90) (Kennedy, 1997). SAP-102 expression increases gradually from birth and is reduced in adulthood, whereas PSD-95 shows significant increased expression from postnatal weeks 2 and 3 to adulthood (van Zundert *et al*, 2004). The binding of NMDA receptors to either PSD-95 or SAP-102 is subject to developmental shift and preferential binding to specific NR2 subunits (Tovar and Westbrook, 2002; Loftis *et al*, 2003; van Zundert *et al*, 2004). In immature neonatal hippocampal neurons, SAP-102 is most highly expressed and preferentially binds NR2B containing NMDA receptors at the

postsynaptic membrane; PSD-95 subsequently increases binding of NR2A containing NMDA subunits (Loftis *et al*, 2003; van Zundert *et al*, 2004). This follows the developmental pattern of NR2 subunit expression with NR2B subunits expressed early in development and NR2A expression subsequently increasing (Mori and Mishina, 1995). PSD-95 binds to C-terminal domain of NMDA receptors at the PSD-95 Drosophila discs large (Dlg) zona occludens-1 (ZO-1) protein (PDZ) recognition motif (named after the first three proteins found to contain the recognition site) on NR1 and NR2 subunits to stabilize NMDA receptors at the postsynaptic membrane and reduce the rate of NR2 mediated NMDA receptor internalization (Krupp *et al*, 1998; Scannevin and Huganir, 2000; Carroll and Zukin, 2002; Lin *et al*, 2003; Lin *et al*, 2004). Deletion of PDZ motif disrupts PSD-95 binding and NMDA receptor localization at the synaptic site (Scannevin and Huganir, 2000; Lin *et al*, 2003; Lin *et al*, 2004).

1.8 NMDA receptor translocation and trafficking

Receptor translocation from the synaptic site is a key feature of developing synapses. Increasing expression of PSD-95 causes translocation of SAP-102 binding NR2B NMDA receptors to the extrasynaptic site (van Zundert *et al*, 2004). At developing cerebellar granule neurons and developing hippocampal synapses, NMDA receptors are not fixed but undergo exchange between synaptic and extrasynaptic pools (Rumbaugh and Vicini, 1999; Tovar and Westbrook, 2002). The high glutamate affinity for NR1/NR2B receptors suggests greater efficiency when activated at the extrasynaptic region during glutamate spillover thereby, allowing more efficient usage of glutamate neurotransmission. NR2B binds glutamate 30 times longer than NR2A hence have longer open times permitting greater Ca^{2+} influx (Erreger *et al*, 2005).

Translateral displacement of receptors to the extrasynaptic site also serves to target them for internalization, particularly at immature synapses (Carroll and Zukin, 2002). Phosphorylation of serine and tyrosine residues of the NR1 and NR2 subunits regulates internalization. Phosphorylation of NR1 serine residues by PKC disrupts their binding to PSD-95 resulting in translocation (Carroll and Zukin, 2002). At the extrasynpatic site, tyrosine phosphorylation of NR2 regulates the ability of the endocytic adaptor protein (APZ) to recognize the internalisation motif (YELK) expressed by the NR2 subunits (Carroll and Zukin, 2002). Internalisation of receptors

reduces synaptic NMDA mediated Ca^{2+} influx thereby reduces activation of Ca^{2+} mediated signaling influencing synaptic efficacy (Carroll and Zukin, 2002).

1.9 Kinases and phosphatases and NMDA receptor regulation

Apart from preferential localization of NR2A containing receptors at the synapse, organization of PSD-95 at the central synaptic site mediates the interaction of NMDA receptor with kinases and phosphatases that regulate the phosphorylation state of NMDA receptors (Blackstone and Sheng, 1999). Dopamine mediated intracellular signals play a significant role in activating some protein kinases that regulate NMDA receptor activity and Ca^{2+} currents. That role is compromised in Parkinson's disease.

cAMP dependent protein kinase (PKA) and Ca^{2+}/phospholipid dependent protein kinase (PKC)

Dopamine activated protein kinases are directly associated with NMDA receptors and these modulate NMDA receptor function. There are two subtypes of dopamine receptors, D1 subtype and D2 subtype; each activates differing protein kinases and signal cascades. D1 receptor subtype stimulates production of cyclic adenosine monophosphate (cAMP), which activates cAMP dependent protein kinase (PKA). D2 receptor subtype activates production of diacylglycerol (DAG) which co-stimulates the Ca^{2+}/phospholipid dependent protein kinases (PKC) with Ca^{2+}; PKC contains a DAG binding site and a Ca^{2+} binding site (Sim and Scott, 1999). A more extensive discussion of dopamine receptors and modulation of NMDA receptors follows in Chapter 2.

PKA is anchored to the scaffolding proteins, A-kinase anchoring proteins (AKAPs) at the PSD; specifically PKA is bound to AKAP79/150 or Yotiao anchoring proteins (Coghlan *et al*, 1995; Klauck *et al*, 1996; Pawson and Scott, 1997; Sim and Scott, 1999; Colledge *et al*, 2000). AKAP79/150 is recruited to PSD by binding to PSD-95 to bring it in close proximity to NMDA receptors (Colledge *et al*, 2000). When anchored to AKAP79/150, PKA is inactive and is localized with PKC and calcineurin phosphatase (PP-2B); the kinases anchor to AKAP79/150 independently of eachother (Coghlan *et al*, 1995; Klauck *et al*, 1996; Pawson and Scott, 1997; Sim and Scott, 1999; Colledge *et al*, 2000). Yotiao binds directly to NMDA receptor on the C1 region of NR1 C terminal (Sim and Scott, 1999). At Yotiao, PKA co-localizes with the tonically active protein phosphatase 1 (PP-1) (Sim and Scott, 1999; Loftis and Janowsky, 2003). Yotiao anchoring of PKA and PP-1 limits NMDA ionic

flow by maintaining the dephosphorylation state of the channel (Sim and Scott, 1999). Apart from Yotiao anchoring, PP-1 is localised to dendritic spines by neuronal actin binding protein (neurabin) or spinophilin both of which are F-actin associated scaffolding proteins (Allen, 2004).

There is dynamic interplay between the co-localized enzymes and their close localisation presumably serves to improve the efficiency of this dynamic interaction. For instance, PKA phosphorylation enhances NMDA mediated currents (Colwell and Levine, 1995; Blank *et al*, 1997). This potentiation is regulated by PP-1 to which PKA is co-localized at Yotiao (Blank *et al*, 1997). PP-1 inhibits PKA phosphorylation (Svennigsson *et al*, 2004; Håkansson *et al*, 2004; Nishi *et al* 2005). PKA activation also induces receptor exocytosis from the endoplasmic reticulum (ER) and trafficking of the receptors to the synaptic membrane surface. This function requires PKC co-activation (Carroll and Zukin, 2002). NMDA receptor subunits are assembled in the endoplasmic reticulum (ER) to form functional channels and are targeted selectively to the postsynaptic membrane where they are expressed together with AMPA receptors and dopamine receptors (Carroll and Zukin, 2002; Salter, 2003). PKA and PKC phosphorylate NR1 serine residues, Ser^{897} and Ser^{896} respectively and these serine residues flank ER retention motif on NR1 subunit (Tingley *et al*, 1997; Scott *et al*, 2003; Carroll and Zukin, 2002). Co-ordinated phosphorylation triggers ER release of assembled NMDA receptors resulting in receptor trafficking to the membrane surface subsequently increasing Ca^{2+} intracellular levels (Carroll and Zukin, 2002; Scott *et al*, 2003). Other proteins are also involved in the exocytosis and trafficking of 'new' NMDA receptors include synaptosome associated protein receptor (SNARE) and synaptosome associated protein 25 (SNAP) (Carroll and Zukin, 2002).

PKC has a highly prominent role in NMDA receptor function. In addition, to phosphorylating NR1 Ser^{896} to stimulate delivery of NMDA receptors to the cell surface, PKC phosphorylates NR1 Ca^{2+}-CaM binding region to reduce the subunit affinity to CaM affecting both NMDA receptor kinetics and dendritic cytoskeletal stability (Hisatsune *et al*, 1997; Tingley *et al*, 1997; Smart *et al*, 1998; Snyder *et al*, 1998; Oh *et al*, 1998; Krupp *et al*, 1999). PKC phosphorylation of the CaM binding site at immature synapses disrupts NMDA receptor-PSD-95 binding resulting in translateral displacement receptors to the extrasynaptic site where they are targeted for internalisation (Carroll and Zukin, 2002). PKC activation can enhance NMDA currents by reducing the Mg^{2+} block through phosphorylation of NR2B C terminus serine residues Ser^{1303} and Ser^{1323} and NR1 C terminus Ser^{889}

and Ser^{890} (Chen *et al*, 1992; Blank *et al*, 1997; Snyder *et al*, 1998; Loftis and Janowsky, 2003). Serine phosphorylation of NR2 subunits does not only function to directly modulate receptor channel function but is also a mechanism for preventing other enzymes binding to the NMDA subunits. PKC phosphorylation of NR2A Ser^{1416} inhibits Ca^{2+}-CaM dependent kinase (CaMKII) binding to the subunit (Gardoni *et al*, 2001). PKC phosphorylation is regulated by PP-1 (Snyder *et al*, 1998).

Ca^{2+}-CaM dependent kinase (CaMKII)

In response to high levels of intracellular Ca^{2+}, cytoplasmic Ca^{2+}-CaM dependent kinase (CaMKII) dissociates from F-actin and Ca^{2+}-CaM binding to CaMKII induces autophosphorylation of its threonine residue, Thr^{286}. Autophosphorylation enables the kinase to remain active until Thr^{286} dephosphorylation (Tao-Cheng *et al*, 2001; Lisman *et al*, 2002). PP-1 regulates most CaMKII phosphorylation activity (Allen, 2004) and most importantly PP-1 dephosphorylates CaMKII autophosphorylation of threonine residue, Thr^{286}. Protein phosphatase 2A can also dephosphorylate Thr^{286} (Strack *et al*, 2000; Allen, 2004; Tao-Cheng *et al*, 2005). Dissociation from F-actin results in translocation of CaMKII to the synaptic membrane to bring the kinase within close proximity with AMPA receptors which it phosphorylates at serine residue Ser^{831} to potentiate the receptor activity; CaMKII potentiation of AMPA receptor activity prolongs neuronal response to excitation and is a key factor in long term potentiation (Leonard *et al*, 1999; Scannevin and Huganir, 2000; Lisman *et al*, 2002).

At the synaptic membrane, CaMKII binds to NR1, NR2A and NR2B (Leonard *et al*, 1999; Tao-Cheng *et al*, 2001). Binding of CaMKII to NR2A is considerably weaker than NR2B binding (Strack *et al*, 2000). CaMKII phosphorylates NR2B at the region of serine residues $Ser^{260\text{-}1309}$ (Strack *et al*, 2000; Loftis *et al*, 2003). CaMKII itself can regulate its association with NMDA receptors. Phosphorylation of NR2B Ser^{1303} promotes dissociation of the kinase from NR2B (Strack *et al*, 2000; Loftis *et al*, 2003). As mentioned earlier, PKC phosphorylation of NR2A also prevents CaMKII forming complexes with NR2 subunits.

In addition to its role in synaptic potentiation, CaMKII plays a significant role in regulating the stability of NMDA receptors to MAGUK through its regulation of casein kinase II (CKII) activity. CKII phosphorylates NR2B Ser^{1480} residue at the PDZ recognition motif resulting in disruption of the

NMDA receptor from the MAGUKs, PSD-95 and SAP-102 (Chung *et al*, 2004). The result is receptor internalisation or lateral translocation to extrasynaptic site. CKII is tonically active and functions to control basal activity of NMDA receptors (Lieberman and Mody, 1999). The phosphorylation of Ser^{1480} is increased after NMDA receptor inactivation, and though the effect of PSD-95/NMDA binding has been found to result in increased channel gating, CKII phosphorylation inducing dissociation results in increased duration of channel openings (Lieberman and Mody, 1999). The role of tonically active CaMKII in regulating CKII phosphorylation is to regulate the frequency of channel opening (Lieberman *et al*, 1999; Chung *et al*, 2004).

NMDA receptor activation can induce dephosphorylation of Ser^{1480} (Lieberman and Mody, 1999) as NMDA receptor mediated Ca^{2+} influx activates calcineurin (a.k.a. protein phosphatase 2B, PP-2B). Calcineurin dephosphorylates CKII mediated phosphorylation (Lieberman and Mody, 1999). In addition, calcineurin regulates NMDA synaptic responses potentiated by PKA (Lieberman and Mody, 1999; Krupp *et al*, 2002; Rycroft and Gibb, 2004). As a result, the phosphatase diminishes the amplitude of NMDA excitatory postsynaptic currents and shortens the duration of receptor channel openings (Raman *et al*, 1996; Lieberman and Mody, 1994). Calcineurin is inhibited when it is bound to AKAP79/150, where it co-localizes with PKA and PKC (Pawson and Scott, 1997). The phosphate is only bound when AKAP79/150 is not binding to PSD-95 i.e. when the complex is not targeted to PSD (Coghlan *et al*, 1995; Klauck *et al*, 1996; Pawson and Scott, 1997; Colledge *et al*, 2000).

1.10 NMDA receptors and gene expression

An important function of NMDA receptors in neurons is the regulation of gene expression, which plays an important role in synaptic plasticity. Ca^{2+} is involved in the activation and regulation of transcription (Kornhauser et al, 2002). Immediate early gene expression i.e. c-fos gene expression in striatal medium spiny neurons is activated by phosphorylation of cAMP/Ca^{2+} response element binding protein (CREB) following phosphorylation of extracellular signal regulated protein kinases (ERK 1 / 2) mediated by co-activation of NMDA receptors and D1 dopamine receptors (Valjent *et al*, 2005; Yang *et al*, 2004). ERK phosphorylation requires NMDA mediated Ca^{2+} to induce immediate early gene expression (Konradi *et al*, 1996). mGluR coactivation with NMDA receptors also increases ERK phosphorylation (Yang *et al*, 2004) as mGluRs mediate increases of intracellular Ca^{2+} levels. CREB phosphorylation leads to the activation of target genes (Kornhauser *et al*, 2002).

CREB phosphorylation occurs at Ser^{133} residue and requires D1 activation to activate transcription (Hardingham *et al*, 1998). The role of D1 activation is necessary as D1 activated phosphorylation of DARPP-32 indirectly prevents ERK dephosphorylation by striatal enriched tyrosine phosphatase (STEP) (Valjent *et al*, 2005; Dunah and Standaert, 2001). STEP was first isolated in rat striatum and was found to be located at the PSD (Salter and Kalia, 2004). DARPP-32 inhibits protein phosphatase 1 (PP-1) which dephosphorylates PKA phosphorylated STEP; phosphorylation of STEP prevents ERK dephsphorylation (Valjent *et al*, 2005). In synaptic plasticity gene expression is a mechanism for inducing long term adaptive modifications (Hardingham *et al*, 1998).

1.11 Summary

The greatest density of NMDA receptors in the basal ganglia is found in the striatum. Ca^{2+} influx is regulated by the variable subunit composition of NMDA receptors as different subunits have different glutamate binding affinities and kinetics. Subunit composition is influenced by development and activity during which NMDA receptor expression at the synapse is subject to translocation and internalization to influence synaptic efficacy. The stability of NMDA receptors at dendritic spines and their function is regulated by a number of kinases (PKA, PKC and CaMKII) and phosphatases (calcineurin, PP-1) through a series of phosphorylation and dephosphorylation reactions of serine and tyrosine residues on the NR1 and NR2 subunits. NMDA mediated Ca^{2+} strongly influences development of dendritic spines and regulation of dendritic spine morphology. The dynamic structure of dendritic spines is a useful mechanism for facilitating activity dependent synaptic modifications. A long term strategy for inducing synaptic modifications is through gene expression which is also influenced by NMDA mediated Ca^{2+} currents.

IMAGES

Figure 1.1 NMDA receptors conduct longer currents than other ionotropic glutamate receptors

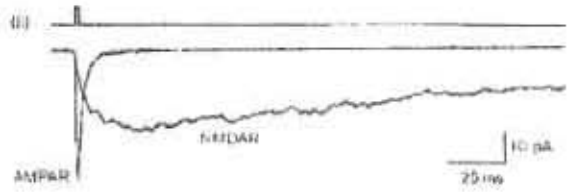

Stimulation of Ca^{2+} influx through neuronal AMPA receptor and NMDA receptor channels activated by brief application of glutamate. Recording was made at -80mV in Mg^{2+} free extracellular solution. AMPA receptors conducted short duration currents whereas NMDA mediated currents lasted longer. Image from Burnashev (1996).

Figure 1.2 Structure of NMDA receptors

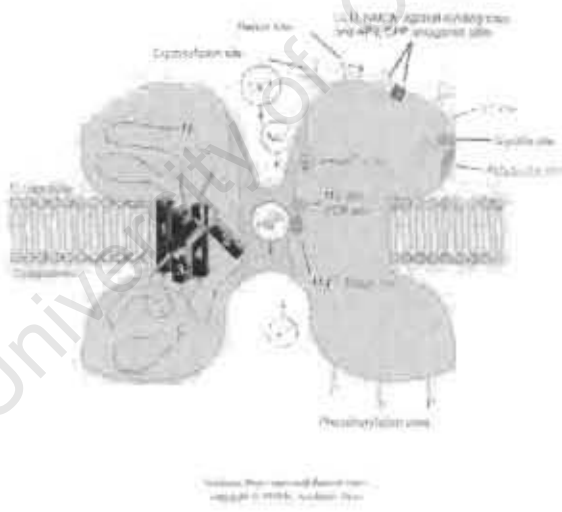

The image of an NMDA receptor shows the transmembrane segments on the right and the binding sites for the receptor agonists and modulators. NMDA receptors have many modulators. Spermine may decrease affinity for glutamate and cause voltage dependent inhibition, ethanol reduces NMDA response, while nitric oxide and photons suppress NMDA receptor activation. Other modulators include sulfhdryl, extracellular zinc (Zn^{2+}), opioid peptides and polyamines (Mori and Mishina, 1995; Conti and Weinberg, 1999; Cull-Candy *et al*, 2001). Image from Zigmond *et al* (1999).

Figure 1.3 NMDA receptor and dendritic spine architecture

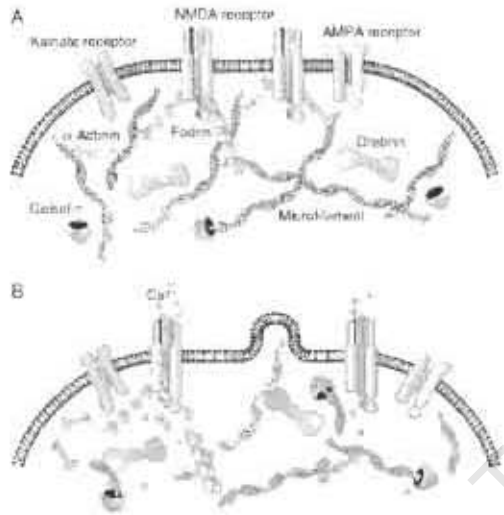

Actin dynamics in dendritic spines. Dendritic spines contain a dense protein network that is composed essentially of actin and actin-regulating proteins intermingled with postsynaptic density. The direct interaction between crosslinking proteins, α-actinin and fodrin (spectrin) and the NMDA receptor is shown. Image from van Rossum and Hanish (1999).

Figure 1.4 NMDA colocalisation with kinases and phosphatases at the PSD

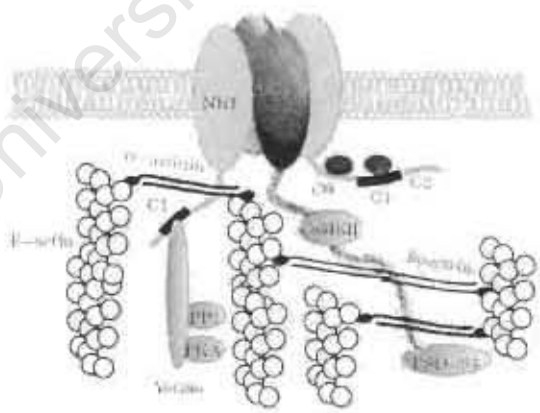

Anchoring to the actin cytoskeleton and PSD-95 independent interactions of NMDA receptors. Asscociation of NMDA receptor subunits with protein kinases and phosphatases is illustrated. Image from Blackstone and Sheng (1999)

CHAPTER 2

STRIATAL MEDIUM SPINY NEURONS

Mechanisms regulating the responsivity of medium spiny neurons to cortical stimulation, are integral to the function of NMDA receptors. The interaction between dopamine and glutamate activates an array of signaling cascades that cause phosphorylation (catalyzed by kinases) and dephosphorylation (catalyzed by phosphatases) reactions to occur to influence the efficiency of NMDA receptors (Conti and Weinberg, 1999). Dopamine modulation of neuronal excitability involves alteration of intrinsic voltage gated conductances to influence the firing threshold to enhance or attenuate the neuronal firing response of neurons to glutamate mediated by NMDA receptors (Wickens and Wilson, 1998; Lin *et al*, 2003). Consequently, the functional state of the medium spiny neurons is 'profoundly affected' by the activity of their dopamine receptors (Chase and Oh, 2000). Dopamine modulates cortico-striatal-thalamo-cortical circuits and influences neural processing in these circuits through ascending spirals of neuronal connectivity that involve the midbrain dopamine neurons (Albin *et al*, 1989; Haber *et al*, 2000). Precursors of dopamine synthesis i.e. 3,4 dihydroxyphenylalanine (L-dopa) and agonists of dopamine receptors have been shown to alleviate akinesia and rigidity in the treatment of Parkinson's disease (Montastruc *et al*, 1997).

2.1 Dopamine receptors

There are two families of dopamine receptors – D1 and D2 dopamine receptors. D1 type receptors include D1a and D1b subtypes. The D2 type receptors include D2, D3 and D4 subtypes (Surmeier *et al*, 1996). The subsets of dopamine receptors are based on their affinity to dopamine agonist coupling to intracellular signals (Surmeier *et al*, 1996). The dopamine receptors are coupled to guanosine trisphosphate (GTP) binding regulatory proteins (G-proteins) that bind to the cytoplasmic side of the plasma membrane (Hille, 2001). D1 type dopamine receptor subtypes are coupled to stimulatory (G_s) and G_q G-proteins. D2 type dopamine receptors are coupled to inhibitory (G_i) proteins. This differential coupling is significant as it confers the excitatory and inhibitory effects of dopamine on glutamate transmission. The opposing roles are clearly demonstrated by the effect of dopamine receptor function on firing activity of medium spiny neurons during cortical stimulation. When D1 receptors are blocked, the excitability of the spiny neurons in response to the cortical

stimulation is decreased suggesting a facilitatory role for the D1 receptors (West and Grace, 2002). Whereas blocking D2 receptors increases the excitable responsiveness of the neurons, suggestive of an inhibitory role in modulating spiny neuron response (West and Grace, 2002).

2.2 *D1 mediated signaling*

Upon dopamine stimulating the receptors, G-proteins are activated and they dissociate into their constituent subunits, G_{α}-GTP complex and $G_{\beta\gamma}$ dimer that act to signal to effector molecules e.g. enzymes and ion channels (Shulman and Hyman, 1999; Hille, 2001). Stimulation of D1 dopamine receptors results in $G_{\alpha s}$-GTP complex activating adenylyl cyclase 1 (AC-1), AC-II or AC-III all of which can catalyze cyclic adenosine 3', 5' monophosphate (cAMP) production from ATP leading to the activation of cAMP dependent protein kinase (PKA) (Bourne and Nicoll, 1993; Storm and Wong, 1996; Shulman and Hyman, 1999; Svennigsson *et al*, 2004). PKA phosphorylates NMDA NR1 subunits on the serine residue, Ser^{897} (Snyder *et al*, 1998; Flores-Hernandez *et al*, 2002; Svennigsson *et al*, 2004). Kinases phosphorylate proteins by catalyzing the transfer of a phosphate molecule from ATP to target proteins. This binding is a reversible reaction with phosphate groups being removed by protein phosphatases through the process of dephosphorylation (Hille, 2001).

The activity of PKA is inhibited by protein phosphatase 1 (PP-1) (Svennigsson *et al*, 2004; Håkansson *et al*, 2004; Nishi *et al*, 2005). Consequently, efficiency of PKA phosphorylation is largely reliant upon the phosphorylation of the PP-1 inhibitor, dopamine and cAMP – regulated phosphoprotein, Mr 32 kDA (DARPP-32) molecule at its threonine residue, Thr^{34} (Allen, 2004; Håkansson *et al*, 2004; Svennigsson *et al*, 2004). When phospho Thr^{34} DARPP-32 binds to PP-1 it prevents PP-1 antagonism of PKA mediated reactions thereby prevents dephosphorylation of protein residues phosphorylated by PKA (Flores-Hernandez, 2002; Svennigsson *et al*, 2004; Nishi *et al*, 2005). D1 signals potentiate NMDA currents and these are enhanced by inhibition of PP-1 and are significantly reduced in DARPP-32 knock-out mice (Blank *et al*, 1997; Flores-Hernandez *et al*, 2002). DARPP-32 protein is prevalent and selectively enriched in all striatal medium spiny neurons (Aizman *et al*, 2000; Allen, 2004; Svennigsson *et al*, 2004; Nishi *et al*, 2005). Immunofluorescence studies demonstrate that striatal neurons expressing NMDA receptors also express DARPP-32 (Wang *et al*, 2004).

2.3 D2 mediated signaling

Through D2 mediated signaling, phosphorylation of Thr^{34} may be reversed. D2 activated $G_{\beta\gamma i}$ dimer co-activates phospholipase C (PLC) to cleave phosphotidylinositol 4,5, bisphosphate (PIP_2) to its constituents, DAG and inositol trisphospshate (IP_3) (Hille, 2001). IP_3 is involved in stimulating the release of Ca^{2+} from the smooth endoplasmic reticulum intracellular stores (Svennigsson *et al*, 2004). Increased concentrations of intracellular Ca^{2+} as a consequence of both NMDA stimulation and endoplasmic release results in the activation of Ca^{2+} dependent protein phosphatases, PP-2A and PP-2B (calcineurin) (Svennigsson *et al*, 2004; Nishi *et al*, 2005). Calcineurin dephosphorylates phospho Thr^{34} DARPP-32 (Svennigsson *et al*, 2004). The rate of calcineurin dephosphorylation of phospho Thr^{34} DARPP-32 can be decreased by phosphorylation of DARPP-32 serine residues by casein kinases (Svennigsson *et al*, 2004).

D2 mediated signaling further opposes D1 signals through the inhibition of cAMP production; D2 receptor stimulation activates $G_{\alpha i}$-GTP complex which inhibits AC-1 activity (Svennigsson *et al*, 2004). D2 recruitment of calcineurin and inhibition of AC-1, regulate D1 mediated phosphorylation of L-type Ca^{2+} channels and NMDA receptor channels resulting in a significant reduction in channel activity (Snyder *et al*, 1998; Hernandez-Lopez *et al*, 2000; Flores-Hernandez *et al*, 2002; Svennigsson *et al*, 2004). Paradoxically, D2 receptors potentiate NMDA receptor function through DAG activation. D2 signaling cascades activate the Ca^{2+}/phospholipid dependent kinase (PKC) through DAG. D2 activation of PKC by DAG requires co-activation by Ca^{2+} ions following NMDA activation (Bliss and Collingridge, 1993; Svennigsson *et al*, 2004). PKC phosphorylates NMDA NR1 subunits on the serine residues, Ser^{889} and Ser^{890} (Snyder *et al*, 1998) and increases the open probability of the receptor channel. PP-1 dephosphorylation reactions are not restricted to PKA, PKC phosphorylated sites are also dephosphorylation by PP-1 (Snyder *et al*, 1998). Consequently, PKC also phosphorylates the threonine Thr^{34} residue on the DARPP-32 (Svennigsson *et al*, 2004).

D1 and D2 signals converge

There is co-operative convergence of D1 and D2 mediated signals. $G_{\alpha s}$-GTP (D1 activated) co-activates AC-II with $G_{\beta\gamma i}$ (D2 activated) to stimulate cAMP production (Bourne and Nicoll, 1993). Secondly, the $G_{\alpha q}$-GTP subunit required for activation of PLC, is the result of D1 dopamine receptor activation (Hille, 2001; Svennigsson *et al*, 2004). Thirdly, PP-2A, mobilized through D2 stimulation,

is involved in the dephosphorylation of phospho Thr^{75} DARPP-32 (Svennigsson *et al*, 2004). DARPP-32 Thr^{75} residues are phosphorylated by cyclin dependent kinase (cdk5) to convert DARPP-32 into an inhibitor of PKA (Svennigsson *et al*, 2004; (Nishi *et al*, 2005). Dephosphorylation of phospho Thr^{75} DARPP-32 prevents PKA inhibition. Through these intricate signaling mechanisms, dopamine modulates neuronal excitability.

2.4 Dopamine and NMDA signaling

The activities of PKA and PKC are regulated by the phosphorylation state of DARPP-32 which can protect PKA and PKC phosphorylated proteins from dephosphorylation by PP-1. However, DARPP-32 inhibition of PP-1 is dependent on phosphorylation of its Thr^{34} site and this is regulated to a certain extent by NMDA Ca^{2+}-CaM signals. Phosphorylation of Thr^{34} DARPP-32 requires optimal intracellular concentrations of Ca^{2+} of ≈0.3 μM and extracellular dopamine concentrations of 5 μM (Kotter, 1994). However, basal concentrations of Ca^{2+} are <0.1 μM and dopamine levels are ≈ 5 – 50 nM (Kotter, 1994), suggesting DARPP-32 Thr^{34} phosphorylation can only occur when both NMDA receptors and dopamine receptors are activated.

Ca^{2+}-CaM co-activates AC-1 with D1 stimulated $G_{\alpha s}$-GTP and this leads to cAMP production followed by PKA activation (Bourne and Nicoll, 1993; Storm and Wong, 1996; Shulman and Hyman, 1999). As a result NMDA receptor activation enhances D1 receptor mediated cAMP accumulation (Pei *et al*, 2004). Tseng and O'Donnell (2004) determined that D1 potentiation of NMDA mediated neuronal response was dependent on PKA activation and intracellular Ca^{2+}, but was not dependent on membrane depolarization. This determination is contrary to the fact that membrane bound adenylyl cyclase molecules are voltage sensitive and undergo conformational change leading to cAMP stimulation during membrane depolarization (Storm and Wong, 1996). This implies that PKA can only be activated following membrane depolarization and indeed, D1 potentiation of neuronal firing only occurs at depolarized potentials (Hernandez-Lopez *et al*, 1997).

Dopamine activated PKC is co-activated following NMDA mediated Ca^{2+} influx to circumvent Ca^{2+} induced inhibition of NMDA receptors (Krupp *et al*, 1999). When NMDA receptors are activated during the depolarized 'up' state, Ca^{2+} influx through the receptor channels increases the intracellular levels. Influx of Ca^{2+} ions through NMDA receptor channels substantially increases the intracellular

ionic concentration from <0.1 μM to ≈ 1 μM leading to binding to calcium binding proteins such as CaM to form Ca^{2+}CaM complex (Kotter, 1994). Increases of the intracellular concentration of Ca^{2+} ions, results in negative feedback mechanism involving Ca^{2+} induced inhibition to down regulate NMDA receptor gating (Xin *et al*, 2005) and limit the rise of intracellular levels (Raman *et al*, 1996). Ca^{2+} induced inhibition of the NMDA receptor involves Ca^{2+}-CaM binding to the NMDA NR1 subunit inducing a fourfold decrease in the open probability of the NMDA receptor channel causing the channels to inactivate (Ehlers *et al*, 1996; Krupp *et al*, 1999). PKC phosphorylates Ser^{890} and Ser^{889} on the NR1 Ca^{2+}-CaM binding site to prevent NMDA receptor channel inactivation (Smart, 1997; Oh *et al*, 1998; Snyder *et al*, 1998; Krupp *et al*, 1999).

Prior to NMDA receptor activation, α-actinin binds to the NR1 subunit at the CaM binding site, this prevents receptor inactivation (Krupp *et al*, 1999). However, when the NMDA channel has been activated, Ca^{2+} ions bind to the α-actinin causing it to dissociate from NR1 thereby allowing the possibility of Ca^{2+} induced inactivation of the receptor channel (Krupp *et al*, 1999). While NMDA mediated Ca^{2+}-CaM signals potentiate dopamine mediated signals, they can also attenuate them through the dephosphorylation of Thr^{34} DARPP-32 by Ca^{2+} dependent phosphatases, calcineurin and to some extent PP-2A (Svennigsson *et al*, 2004). Activation of glutamate receptors promotes dephosphorylation of DARPP-32 at both threonine residues, Thr^{34} and Thr^{75} through calcineurin and PP-2A respectively (Nishi *et al*, 2005). However, Ca^{2+}-CaM activation does not occur immediately upon the entry of Ca^{2+} ions through NMDA, it is activated 1-5 min following glutamate stimulation of the NMDA receptors to regulate Ca^{2+} influx through the receptor channel (Nishi *et al*, 2005) suggesting dopamine/glutamate interaction is under temporal regulation. In addition, Ca^{2+} dependent inactivation by CaM is observed in NR2A or NR2D NMDA receptors but not in NR2B and NR2C NMDA receptors (Blackstone and Sheng, 1999). Finally, stimulation of the IP_3 receptors and ryanodine receptors on the smooth endoplasmic reticulum to induce intracellular Ca^{2+} release is reliant on co-binding of Ca^{2+}-CaM (Samai and Kung, 2004).

2.5 Electroresponsive properties and neuronal excitability

Having considered the intracellular mechanisms involved in integration of dopamine and NMDA mediated glutamate signals, the question still remains as to how voltage gated ionic conductances regulate medium spiny neuronal firing. Electroresponsive properties of medium spiny neurons are

influenced by aging and dopamine depletion. During aging medium spiny neurons exhibit lower spontaneous firing rates and have higher firing thresholds (Cepeda *et al*, 1989). In Parkinson's disease there are increases in neuronal firing (Kish *et al*, 1999; Tseng *et al*, 2001; Wichmann and DeLong, 2003). The striatal neuronal firing response is the result of integration of the convergence of cortical and nigral neurotransmission with voltage gated ionic conductances that confer the intrinsic electroresponsive properties (Stern *et al*, 1998). The differential inhibitory and excitatory dopamine influences, are dependent on membrane potentials (Reynolds and Wickens, 2002). Dopamine reduces cell excitability during neuronal hyperpolarized resting state (Lin *et al*, 2003) but potentiates firing at depolarized potentials (Hernandez-Lopez *et al*, 1997).

The normal firing activity of medium spiny neurons is characterized by shifts between depolarized 'up' and hyperpolarized 'down' states that are driven by the presence or absence of coordinated cortical and thalamic inputs respectively (Nisenbaum and Wilson, 1995; Wickens and Wilson, 1998; Chapier *et al*, 1999; Mahon *et al*, 2003b). There is coherence between these voltage dependent states and cortical activity. Striatal membrane potentials are correlated with cortical activity which shifts the resting membrane potentials towards less negative potentials during the 'up' state (Chapier *et al*, 1999; Tseng *et al*, 2001; Mahon *et al*, 2003a). Decortication blocks the membrane oscillation to the 'up' state (Kerr and Plenz, 2002). NMDA receptors are activated during this state (Reynolds and Wickens, 2002) and consequently mediate glutamate excitatory impact to induce neuronal firing.

The functional state of the majority of the spiny neurons (73%) (Sandtrom and Rebec, 2003) is described as *silent* owing to their high resistance to excitability due to hyperpolarized membrane potentials (Calabresi *et al*, 1990; Wickens and Wilson, 1998; Venance and Glowinski, 2003). However, spiny neurons that exhibit spontaneous activity have been described (Wickens and Wilson, 1998; Venance and Glowinski, 2003). There are no morphological differences between these two types of neurons but the membrane potential during the 'up' state is higher in the spontaneously active neurons, suggesting a possible difference in K^+ conductances (Wickens and Wilson, 1998; Venance and Glowinski, 2003).

The 'up' states are periods of large numbers of correlated, synchronous cortical neurotransmission resulting in subthreshold depolarization (-40 to -55 mV) of the membrane potential that facilitates

neuronal firing of action potentials (Nisenbaum, 1995; Nisenbaum and Wilson; 1995; Mahon *et al*, 2003). During the 'down' state, intrinsic potassium (K^+) ion conductances confer the hyperpolarized resting membrane potential (-80 to -95 mV) (Nisenbaum and Wilson, 1995; Chapier *et al*, 1999; Mahon *et al*, 2003b; Wickens and Wilson, 1998; Kerr and Plenz, 2002). Glutamate neurotransmission during the down state stimulates AMPA, kainate and mGlu and not the NMDA receptors due to the persisting voltage dependent Mg^{2+} block on NMDA receptors (Reynolds and Wickens, 2002). Hyperpolarisation is significant as it is an effective deterrent from uncoordinated asynchronous cortical afferents; these are too weak to overcome the high activation threshold of hyperpolarisation (Llinás, 1988; Nisenbaum and Wilson, 1995; Chapier *et al*, 1999; Mahon *et al*, 2003b; Wickens and Wilson, 1998; Kerr and Plenz, 2002).

2.6 *Excitability and dopamine modulation*

The electroresponsive properties of striatal neurons are mediated by different types of potassium (K^+) currents (Nisenbaum and Wilson, 1995; Llinás, 1988; Calabresi *et al*, 1990; Nisenbaum and Wilson, 1995). Inwardly rectifying K^+ currents (I_{Kir}) are responsible for high activation resistance of the spiny neurons conferred by the hyperpolarized resting membrane potentials (Nisenbaum and Wilson, 1995; Chapier *et al*, 1999; Venance and Glowinski, 2003). Dopamine activation of D1 receptors fortifies the resistance to uncoordinated excitability by increasing the activity of I_{Kir} (Lin *et al*, 2003; Venance and Glowinski, 2003) and reduces neuronal firing output at hyperpolarized potentials (-82 mV) (Hernandez-Lopez *et al*, 1997). Partially due to I_{Kir}, D1 receptor mediated potentiation of NMDA currents is minimal at hyperpolarized potentials (Cepeda *et al*, 1998). NMDA receptors are also under Mg^{2+} regulating block during membrane hyperpolarisation and this contributes strongly to minimal NMDA mediated currents during the 'down state'.

The inward K^+ currents are deactivated when coordinated excitatory neurotransmission shifts the membrane potential towards more positive potentials (Mahon *et al*, 2003). Blocking I_{Kir} has a similar effect as it causes a membrane potential shift from hyperpolarized -85 mV values to depolarized -67.7 mV potentials (Nisenbaum and Wilson, 1995). Consequently, D1 mediated potentiation of NMDA currents and neuronal firing is significantly greater at subthreshold depolarized potentials when K^+ conductances are blocked (Hernandez-Lopez *et al*, 1997; Cepeda *et al*, 1998).

As potentials become less negative, the fast activating, slow inactivating K^+ currents (I_{As}) are recruited. The slow inactivation properties of I_{As} maintain the membrane at subthreshold potentials thereby reducing the rate of depolarization to limit the initial response of the neuron to transient uncorrelated cortical inputs (Gable and Nisenbaum, 1998; Mahon *et al*, 2003). The effect is a transitional latency period (ramp potential) before action potential generation during the 'up' state (Gable and Nisenbaum, 1998; Mahon *et al*, 2003). By reducing the rate of depolarization, I_{As} hinders action potential generation mediated by sodium currents (I_{Na}). In most excitable cells, I_{Na} currents are recruited to further depolarize the membrane towards firing threshold (Llinás, 1988; Kerr and Plenz, 2002). Na^+ channels have rapid inactivation kinetics; consequently, their open probability is significantly reduced by slow depolarization (Wickens and Wilson, 1998). Only when depolarizing glutamate inputs are sufficient to inactivate I_{As} channels allowing ramp potential to reach threshold, will I_{Na} facilitate neuronal discharge to occur; the membrane depolaristaion during the 'up' state does not always result in action potential generation (Nisenbaum and Wilson, 1995; Wickens and Wilson, 1998; Mahon *et al*, 2003).

However, medium spiny neuron spikes are largely dependent on voltage activated Ca^{2+} conductances rather than Na^+ ions (Llinás, 1988). As a result, blocking Na^+ channels is not effective in inhibiting neuronal excitability, whereas activation of striatal neurons is blocked by cadmium (Cd^{2+}) (a calcium channel blocker) and Mg^{2+} (an NMDA receptor channels blocker) (Llinás, 1988). Furthermore, stimulation of cortical afferents elicits striatal excitation which is attenuated when voltage gated Ca^{2+} currents are blocked with Cd^{2+} (Calabresi *et al*, 1990). Ca^{2+} ionic conductance through L-type channels play a significant role in dopamine modulation of NMDA response to glutamate neurotransmission.

Influx of Ca^{2+} ions during the 'up' state of the medium spiny neurons is also modulated by PKA phosphorylation of L-type Ca^{2+} voltage gated channels which are only active during depolarization (Carter and Sabatini, 2004; Svennigsson *et al*, 2004). $I_{L(Ca2+)}$ currents increase the period of depolarization and allow NMDA receptors to remain open for longer (Cepeda *et al*, 1998). Dopamine D1 activation mediates PKA potentiation of $I_{L(Ca2+)}$ currents and D1 enhancement of NMDA currents is dependent upon this potentiation (Hernandez-Lopez *et al*, 1997; Cepeda *et al*, 1998; Shulman and Hyman, 1999; Hille, 2001; Håkansson *et al*, 2004; Svennigsson *et al*, 2004,

Nishi *et al*, 2005). Blocking the $I_{L(Ca2+)}$ currents reduces D1 mediated enhancement of NMDA currents (Cepeda *et al*, 1998). PKA activation follows cAMP production after D1 receptor activation (Svennigsson *et al*, 2004).

2.7 Summary

Complexity of dopamine modulatory roles in striatal regulation of corticostriatal innervation is attributed to a multiplicity of receptor subtypes stimulated by dopamine and glutamate, in addition to the voltage dependent conductances mediated by K^+, Na^+ and Ca^{2+} ions. Neural processing with the medium spiny neurons is regulated by an array of intracellular signaling cascades mediated by NMDA receptor stimulation and dopamine receptor stimulation. The G-protein coupled dopamine receptors stimulate intracellular signaling cascades that interact with excitatory glutamate NMDA mediated signals. The phosphorylation state of DARPP-32 plays a critical role in the convergence of intracellular cascades and in regulating the phosphorylation state of NMDA receptors to modulate their function. NMDA signaling is largely mediated through influx of Ca^{2+} ions through the receptors. Neuronal firing is dependent not on only the interaction of afferents, but on the voltage gated ionic conductances that confer the electroresponsive properties of the neurons. Efficient processing of all the abovementioned inputs is critical to regulate the responsivity of the medium spiny neurons to cortical stimulation.

CHAPTER 3

THE STRIATUM & THE BASAL GANGLIA CIRCUITRY

Loss of dopamine neurotransmission in the striatum due to degeneration of midbrain nuclei characterizes the pathophysiology of Parkinson's disease (Albin *et al*, 1989). Dopamine depletion has profound effects not just on NMDA receptors in the striatum but also leads to global dysfunction of basal ganglia circuitry as demonstrated by increased activity of the subthalamic nucleus (STN) and basal ganglia output nuclei leading to motor disorders such as tremor, akinesia and bradykinesia in Parkinson's disease (Bergman and Deuschl, 2002; Wichman and DeLong, 2003). Stimulation of striatal NMDA receptors can also result in increased basal ganglia inhibitory output (Morari *et al*, 1996). Disruption of the basal ganglia circuitry necessitate discussion into the connectivity of the striatum with other basal ganglia nuclei.

3.1 Anatomy of the Basal Ganglia

The striatum is one of several subcortical nuclei that form the basal ganglia. The interconnected nuclei of the basal ganglia span the telencephalic, diencephalic and mesencephalic regions of the brain. The neostriatum (caudate nucleus, putamen and nucleus accumbens) is a telencephalic structure, the pallidum (medial/internal globus pallidus, lateral/external globus pallidus, ventral globus pallidus) and subthalamic nucleus are predominantly diencephalic structures and the mesencephalic nuclei are the SN (pars compacta, SNc, and pars reticulata, SNr) and the ventral tegmental area (VTA) (Yelnik, 2002).

The basal ganglia nuclei function together to integrate sensorimotor, limbic, memory-related and conditional cues from the prefrontal cortices (orbital, medial and dorsolateral), the motor cortices (primary motor cortex, pre-motor cortex, supplementary motor cortex), the somatosensory cortex, the hippocampus, the cingulate cortex, the thalamus, the amygdala, the dorsal raphe nucleus and the pedunculopontine nucleus to influence and modulate motivational, cognitive and motor behaviours (Albin *et al*, 1989; Graybiel, 1990; Parent, 1990; Smith and Bolam, 1990; Smith *et al*, 1998; Devan and White, 1999; Haber *et al*, 2000; Gonzalo *et al*, 2002; Yelnik, 2002). The striatum is the major recipient of these afferents particularly the cortical inputs via the corticostriatal pathway.

There are segregated basal ganglia-thalamocortical circuits which process motor, cognitive and limbic information and are each comprised of the two parallel direct and indirect pathways which cause phasic increase or decreases in the activity of the basal ganglia output nuclei.

3.2 The Striatum

The striatum is a vast structure commonly divided into the dorsal striatum comprised of the caudate nucleus and the putamen, and the ventral striatum comprised mainly of the nucleus accumbens (Kiyatkin and Rebec, 1996; Voorn *et al*, 2004). This division is based on differential cortical and nigral afferents to these areas. Sensorimotor and cognitive inputs are arranged in the dorsolateral and central dorsal striatum respectively, while the limbic input is located mainly within the ventromedial striatum (Haber *et al*, 2000). The dorsal striatum has been commonly attributed to processing of sensorimotor associative inputs while ventral striatum is associated with processing emotional and motivational inputs from limbic cortices, amygdala and hippocampus (Albin *et al*, 1989; Alexander and Crutcher, 1990; Parent, 1990; Voorn *et al*, 2004). However, there are no definitive boundaries between the dorsal and ventral striata, neither are there any differences in their cytoarchitecture or chemoarchitecture (Voorn *et al*, 2004). Furthermore, both striata contain medium spiny neurons with the same electroresponsive properties and the same intracellular processing mechanisms (Voorn *et al*, 2004). However, despite the similar cytoarchitecture, the differences of cortical afferents may contribute to firing activity. Spontaneously active ventral striatal spiny neurons exhibit faster basal firing rates than their dorsal counterparts (Voorn *et al*, 2004). The spiny neurons of the ventral striatum also exhibit greater reward related responses than dorsal spiny neurons (Schultz, 2002).

A characteristic feature of the neostriatum is its chemoarchitecture based on acetylcholinesterase (AChE) expression that creates a mosaic pattern of striosomal patches amidst the extrastriosomal matrix which covers ≈80% of the striatum (Graybiel, 1990). The matrix zones have a high concentration of AChE while the striosomes have a low concentration (Graybiel, 1990). The differential chemistry of the compartments is related to the functional innervation of corticostriatal and nigrostriatal inputs and the projections. Matrix neurons receive projections from deep cortical layers and in turn project mainly to the pallidum and the SNr while striosomal neurons are stimulated by projections from the superficial layer and mainly reciprocate SNc efferents (Graybiel, 1990;

Ralston, 2000; Packard and Knowlton, 2002). Corticostriatal neurons are mainly located in layer V and the layer III; projections from layers II, IV, and VI have also been reported (Cowan and Wilson, 1994). Dopamine neurotransmission from the VTA and SNc innervate the striosomes and matrix respectively (Packard and Knowlton, 2002). Neurons of the matrix mediate cortical processing while striosomes process dopaminergic input to the striatum (Graybiel, 1990). Within the matrix and striosomes there is preferential expression of ionotropic glutamate receptors. NMDA receptors and AMPA receptors are most highly expressed in the matrix whereas kainite is relatively increased in the striosomes (Dure *et al*, 1992).

3.3 *Corticistriatal and nigrostriatal afferents*

Medium spiny neurons receive convergent afferents from cortical, thalamic and dopaminergic nigrostriatal midbrain nuclei (Kocsis *et al*, 1977). Medium spiny neurons receiving thalamic inputs have lower density of dendritic spines compared to spiny neurons receiving cortical input (Smith and Bolam, 1990). The γ-aminobutyric acid (GABA) transmitting medium spiny neurons account for >95% of the total neuronal population in the striatum (Smith and Bolam, 1990; Smith *et al*, 1998; Yelnik, 2002; Venance and Glowinski, 2003). The rest of the neuronal population is comprised of small GABAergic interneurons and large aspiny cholinergic interneurons (Yelnik, 2002). Glutamatergic corticostriatal afferents make excitatory asymmetric contact (Gray's Type 1 synapses) on the heads of distal dendritic spines of the spiny neurons (Eccles, 1964; Smith and Bolam, 1990). Glutamate neurotransmission stimulates ionotropic receptors NMDA and AMPA in addition to mGluRs. The properties between the ionotropic receptors differ with respect to their affinity for glutamate and their channels kinetics. AMPA receptors have a low affinity for glutamate relative to NMDA receptors and also have fast, brief gating properties (Conti and Weinberg, 1999). These properties and the high Ca^{2+} permeability mean that NMDA receptors mediate much of dendritic excitation. Dendritic spikes are dependent on Ca^{2+} conductances (Llinás, 1988).

Though glutamate neurotransmission is the major source of input into the striatum, 21% of axon terminals in the striatum are dopaminergic (Kotter, 1994). The stimulatory glutamatergic effect on the spiny neurons is modulated by dopamine neurotransmission from neurons of the SNc and the VTA. Dopamine influence on the responsiveness of the medium spiny neurons cortical input, involves activation of a series of signal transduction pathways that interact with NMDA mediated

signaling pathways to induce changes in the properties of NMDA receptors and voltage gated channels to affect the firing activity of the neurons in response to cortical input (Reynolds and Wickens, 2002; Venance and Glowinski, 2003) (refer to Chapter 2).

The tyrosine hydroxylase (TH)* staining dopamine boutons, predominantly form symmetric contacts but asymmetric synapses also occur (Pickel *et al*, 1981; Kotter; 1994). Dopamine terminals converge onto the necks of dendritic spines that are also recipients of asymmetric, non-TH immunoreactive glutamate contacts (Groves, 1980; Pickel *et al*, 1981; Smith and Bolam, 1990). The length of the dendritic spine, ≈ 1-2 µm, means that the synaptic terminals on the head and on the neck are within close proximity to create an anatomical relationship through which dopamine may modulate the efficacy of glutamate stimulation to influence the neuronal response to cortical input (Kotter, 1994).

3.4 Basal Ganglia processing and the striatum

Information from the striatum is processed through pallidal and nigral structures and projected back to the cortical regions via the thalamus; completing the corticostriatocortical loops (Packard and Knowlton, 2002). Brainstem nuclei also receive basal ganglia afferents through which descending pathways are influenced (Albin *et al*, 1989; Alexander and Crutcher, 1990; Graybiel, 1990; Devan and White, 1999; Haber *et al*, 2000; Bar-Gad and Bergman, 2001; Gonzalo *et al*, 2002; Takakusaki *et al*, 2003). A model describing basal ganglia processing was developed from the functional anatomy of hyperkinetic and hypokinetic movement disorders associated with dysfunction of the basal ganglia e.g. ballism (subthalamic nucleus, STN, dysfunction), choreoathetosis, dystonia (striatal and pallidum disorder) and Parkinson's disease (Albin *et al*, 1989). In the model dopamine was proposed to be significant in basal ganglia processing as dopamine receptor antagonists or agonists were used in the treatment of basal ganglia associated hyperkinetic and hypokinetic disorders respectively (Albin *et al*, 1989).

The model proposes two segregated pathways, differentially regulated by striatal afferents that cause functionally opposite effects on basal ganglia output nuclei leading to the inhibition or

* Dopamine terminals in the striatum can be identified by their tyrosine hydroxylase immunoreactivity. TH is the dopamine synthesizing enzyme responsible for the conversion of DOPA to dopamine.

disinhibition of the thalamus that feeds back to cortical regions (Figure 3.1) (Albin *et al*, 1989). Basal ganglia output nuclei comprise the internal globus pallidus (GPi) and the SNr. Though anatomically distinct due to their separation by the fibers of the cerebral peduncles (Albin *et al*, 1989), these two nuclei are comprised of cytologically similar GABA transmitting neurons that project to the thalamus (Smith and Bolam, 1990). Henceforth the output nuclei shall be referred to as GPi/SNr. Distribution of peptides and selective expression of dopamine receptor subtypes, mediate activation of the direct monosynaptic and indirect multisynaptic pathways (Albin *et al*, 1989; Smith *et al*, 1998). Medium spiny neurons projecting directly to the GPi/SNr preferentially express D1 type receptors and are rich in substance P and dynorphin and those of the indirect pathway preferentially express D2 type receptors and are rich in enkephalin and neurotensin (Alexander and Crutcher, 1990; Graybiel, 1990, Smith *et al*, 1998). According to processing of the direct/indirect pathways, integration of cortical information is based on convergence of input from the nuclei with the greatest volume i.e. the striatum, to progressively smaller nuclei suggesting a funneling and convergence of information (Mink, 1999; Yelnik, 2002). The striatum is twenty times the size of the GPi/SNr (Yelnik, 2002).

Striatal neurons only increase their firing activity when activated by convergent input from many different cortical neurons (Smith *et al*, 1998). Under resting conditions, the activity of the medium spiny neurons is low whereas the output nuclei have high spontaneous activity resulting in continual tonic inhibition of the thalamic nuclei to which they project (Alexander and Crutcher, 1990; Marsden and Obeso, 1994; Smith *et al*, 1998). Individual GPi/SNr neurons receive projections from the striatum (direct pathway), STN (indirect pathway) and GPe (indirect pathway) (Smith *et al*, 1998). Phasic decreases through the direct pathway result in disinhibition of the thalamocortical connection to allow movement in the case of motor processing, whereas the indirect pathway by inducing phasic increases has the opposite effect (Alexander and Crutcher, 1990). Corticostriatal afferents stimulate neurotransmission of GABA from medium spiny neurons that project directly to GPi/SNr through the direct pathway to enable appropriate feedback to the cortical motor region to facilitate movement (Marsden and Obeso, 1994).

In the altemative indirect pathway, the medium spiny neurons projecting to the external globus pallidus (GPe) and ventral globus pallidus (VP) are activated causing the inhibition of the tonic discharge of the pallidal nuclei (Smith *et al*, 1998). This in turn reduces the tonic inhibitory

discharge of the pallidal nuclei (Smith *et al*, 1998). This in turn reduces the tonic inhibitory GABAergic transmission from the GPe/VP to the STN thereby disinhibiting the STN enabling it to stimulate GPi/SNr with its excitatory glutamatergic afferents. Stimulation of GPi/SNr projections increases inhibition of the thalamus (Albin *et al*, 1989; Marsden and Obeso, 1994, Smith *et al*, 1998). The indirect pathway prevents unwanted movement programs from interrupting the positive feedback through the inhibition of the thalamic nucleus (Marsden and Obeso, 1994). In Parkinson's disease the firing activity of medium spiny neurons is altered and this results in altered neuronal firing in other basal ganglia nuclei (Yelnik, 2002). Increased firing of the spiny neurons results in decreased firing of the GPe in the indirect pathway. This results in disinhibition of the STN which increases the activity of its GPi/SNr glutamatergic excitatory afferents resulting in increased firing activity of GPi/SNr neurons (Albin *et al*, 1989; Yelnik, 2002). This causes massive alteration of basal ganglia output.

3.5 The complexity of the basal ganglia circuitry

Though the classical direct/indirect pathways model has advanced the understanding of the basal ganglia processing, it offers a simplistic perspective regarding the complexity of neural connectivity. Firstly, the striatum is not the only direct recipient of cortical information; the fastest route of cortical neurotransmission into the basal ganglia is via the direct projections to the STN terminals (Smith *et al*, 1998). However, the greatest influence on the output nuclei is through the direct pathway, as 90% of the synaptic boutons are from medium spiny neuron projections while the STN only accounts for <10% (Yelnik, 2002). With respect to segregation of parallel pathways based on differential expression of D1 and D2 dopamine receptors on specific neurons, there is increasing evidence of co-localization of dopamine receptors on 'virtually all' spiny neurons within the striatum (Surmeier *et al*, 1999; Aizman *et al*, 2000). Furthermore, medium spiny neurons form extensive collaterals resulting in lateral inhibition between neurons within the striatum (Bar-Gad and Bergman, 2001; Plenz, 2003). Medium spiny neurons also project to thalamus and subcortical motor areas e.g. tegmentum and GPe (Smith and Bolam, 1990; Parent, 1990). Neuronal tracing studies have revealed more complex connections within the basal ganglia including dual projections to both pallidal nuclei from individual spiny neurons, massive projections from the GPe to the GPi/SNr (Smith *et al*, 1998; Bar-Gad and Bergman, 2001) and the centromedian parafascicular (CM-pf) thalamic complex direct projections to the striatum and the STN (Gonzalo *et al*, 2002). Extensive

extemal projections from striatal and SNr neurons innervate directly to the brain stem beyond the basal ganglia to influence postural muscle tone and locomotion (Bar-Gad and Bergman, 2001; Nandi *et al*, 2002; Takakusaki *et al*, 2003). Figure 3.2 illustrates the extensive connectivity between nuclei of the basal ganglia.

An interesting anomaly regarding processing within the basal ganglia through direct and indirect pathways has been the effectiveness of the stereotaxic surgical procedures in alleviating hypokinetic dysfunction seen in Parkinson's disease (Marsden and Obeso, 1994). SNc degeneration results in the activity of the output nuclei being increased causing prolonged inhibition of the thalamus. The result is lack of positive feedback to the cortex to allow movement to occur. One of the surgical approaches to arrest dysfunction of the basal ganglia nuclei in the treatment of Parkinson's disease, has been the lesioning of the thalamus (thalamotomy) and of the pallidum (pallidotomy) both of which are effective in alleviating the symptoms of tremor, rigidity and dyskinesia (Marsden and Obeso, 1994; Diederich and Alesoh, 1997; Bjorklund and Dunnett, 1999; Ghika *et al*, 1999). GPi lesions are effective against hyperkinesias and hypokinesia (Bar-Gad and Bergman, 2001). However, destruction of these two nuclei, according to the model of the direct and indirect pathways, would compromise normal voluntary movement. Lesioning of the thalamus should result in the destruction of pallidal outflow increasing excitation from thalamus to motor cortical regions theoretically causing dyskinesia. Paradoxically, this does not occur (Marsden and Obeso, 1994). In non-human primates (without parkinsonism), with bilateral thalamotomy, normal spontaneous movement is observed without motor deficits but learning of tasks was impaired. The paradox of surgical therapies in basal ganglia nuclei highlights the complexity of the basal ganglia circuitry and demonstrate that the classical model does not present complete understanding of the circuitries involved in information processing.

One aspect not considered within the direct/indirect model is the processing of information from non-motor cortices and the overlap of these with the motor regions. The striatum is delineated into topographic sectors related to their cortical innervation – sensorimotor (connected to primary motor cortex, SMA and pre-motor cortex), cognitive/associative (connected to dorsolateral prefrontal cortex and hippocampus) and limbic/motivational (connected to anterior cingulated and orbito-median

prefrontal cortex) (Smith and Bolam, 1990; Parent, 1990, Yelnik, 2002). However, the direct/indirect model only addresses processing of sensorimotor information within the dorsal striatum.

3.6 Striatonigrostriatal subcircuits

Functional and anatomical co-ordination of information systems between limbic, cognitive and motor regions within the dorsal and ventral striatum have been recently determined through anatomical tracing studies and this has led to a more extensive model of processing of inputs being proposed (Haber *et al*, 2000). The model proposes a series of spiralling striatonigrostriatal subcircuits in which the topographic organization of striatal information is maintained through subcircuits that are connected through midbrain spirals. The striatonigrostriatal model places more emphasis on reciprocal connectivity between the midbrain and the striatum, whereas the classical pathway focused on a one-way modulatory relationship only from the midbrain to the striatum (Figures 3.1 and 3.3). The striatonigral pathway was previously described by Smith and Bolam (1990) as a mechanism through which limbic striata could influence the dopaminergic modulation of dorsal striatal information. In this model striatal compartmentalization was considered as a necessary aspect of processing. The D2 expressing neurons of the striosomes were proposed to feedback to the SNc to influence dopamine modulation of D1 expressing spiny neurons of the matrix (Smith and Bolam, 1990).

Limbic information from the orbito – medial prefrontal cortex (OMPFC),dorsolateral prefrontal cortex and the hippocampus is similarly confined to the ventromedial aspects of both the striatum and the SN (VTA, and the dorsal SNc) (Haber *et al*, 2000). The ventromedial striatum has the largest projection to the midbrain but however receives relatively fewer projections in return. The associative / cognitive striatum innervated by the dorsolateral pre-frontal cortex, orbital prefrontal cortex and the pre-motor cortex is localized to the central striatum. There is overlap between the different functional centers within the striatum and the nigral projections are not evenly distributed (Haber *et al*, 2000). Nigral neurons projecting to this region from the ventral densocellular SN region lie between the ventromedial projection neurons and the ventrolateral neurons projecting to the motor centre in the dorsolateral striatum. The dorsolateral striatum sends the fewest projections to the SN, but receives the greatest nigral output.

Reciprocal pathways link common functional regions of the striatum with the SN while the non-reciprocal pathways feed-forward to relay to the adjacent region that differs in function. In this way the SN co-ordinates information between the striatal centres. There is overlap of cognitive function within the dorsal striatum mediating procedural and spatial learning, while the ventral striatum is also involved in spatial learning and Pavlovian conditioning (Voorn *et al*, 2004). Indeed, Albin *et al* (1989) in recognizing the limitations of the model of the direct/indirect pathways, proposed that '...one of the functions of the basal ganglia is to regulate sensorimotor interactions in a way that determines which sensory stimuli are used to initiate motor action and which are disregarded.'

The spiralling organization of the striatonigrostriatal pathways enables processing from the ventromedial striatum throughout the central striatum to the dorsolateral striatum to integrate limbic, cognitive and motor information. Limbic information from the ventromedial nucleus accumbens shell, projects to the VTA/dorsal SNc and the non-reciprocal pathway projects to the nucleus accumbens core which in turn projects to its own midbrain region to influence the projections directed towards the central associative striatum. The central striatum projects to its densocellular SNc region and from there projections are directed to the dorsolateral striatum. For an appropriate behavioural response to occur all inputs are required from the different regions (Haber *et al*, 2000). Rather than segregation of information, the striatonigrostriatal pathways facilitate information flow between limbic, cognitive and motor information. Furthermore, this model is suggestive of greater reciprocal modulation between glutamate and dopamine transmission within the medium spiny neurons.

3.7 Summary

The striatum plays a crucial role in basal ganglia processing. Despite the differences regarding the connectivity between the nuclei, the basal ganglia models have in common the emphasis of dopamine neurotransmission through the nigrostriatal pathway mediating the response of the medium spiny neurons to excitatory glutamate stimulation from the cortex. Previously dopamine was proposed to have a differential excitatory influence through the direct pathway and an inhibitory effect through the indirect pathway (Alexander and Crutcher, 1990). However, further studies have shown that the role of dopamine is more complex.

IMAGES

Figure 3.1 Classical modeling of Basal ganglia circuitry

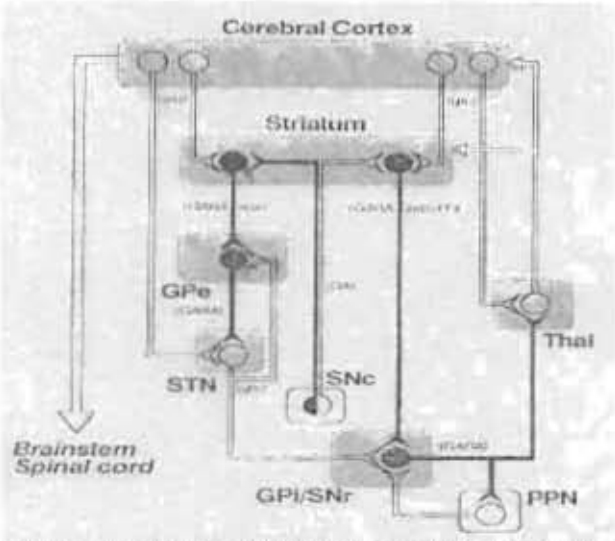

Schematic diagram of the circuitry and neurotransmitters of the basal ganglia indicating the parallel 'direct' and 'indirect' pathways from the striatum to the basal ganglia output nuclei. Image from Alexander and Crutcher (1990)

Figure 3.2 The complexity of basal ganglia circuitry

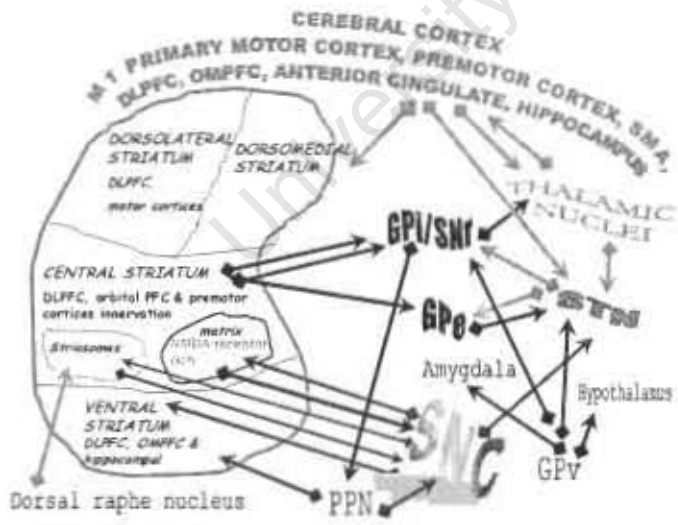

Illustration of some of the complex interconnectivity within the basal ganglia nuclei and other connections that influence basal ganglia processing but are not mentioned within the model of direct and indirect processing model in Figure 3.1.

Figure 3.3 Striatonigrostriatal subcircuits

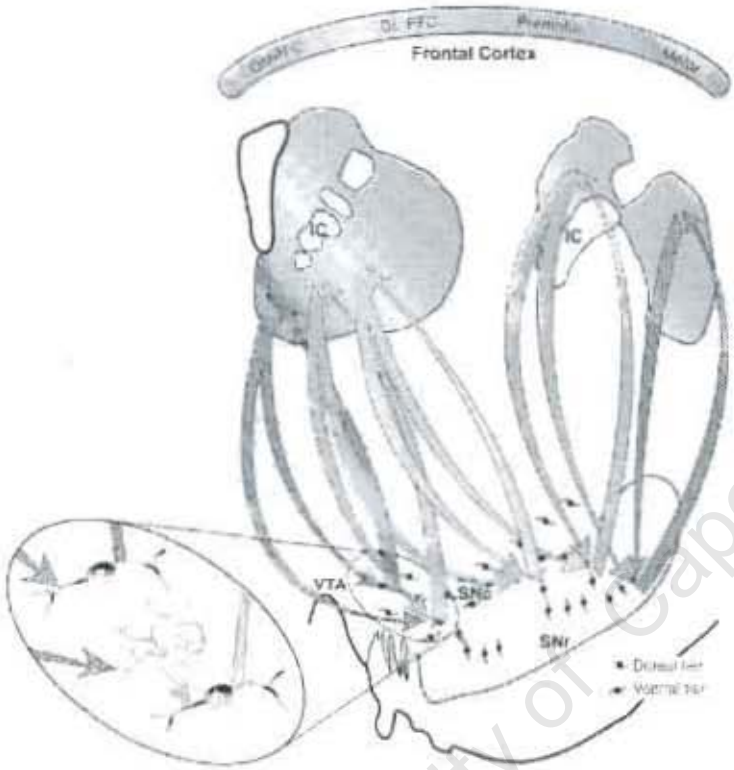

The ascending spiral pathways from the ventral striatum to dorsal striatum through the SN are illustrated. The innervation of different cortical regions is also shown. Image from Haber et al (2002)

STUDY PURPOSE

NMDA receptors are fundamental to the structural and functional integrity and efficiency of dendritic synapses. This feature of the receptors is attributed to the high Ca^{2+} ionic fluxes through the receptor channels in response to stimulation. NMDA receptor mediated influx of Ca^{2+} ions triggers a myriad of intracellular signalling cascades through which formation and architecture of dendritic spines are maintained and synaptic receptor expression and kinetics are regulated as discussed in Chapter 1. As a result NMDA receptors contribute significantly to synaptic modification. Such modification plays an important role in development and aging, consequently, the subunit composition and kinetics of NMDA receptors are altered. Specifically the activity of the receptors is reduced with age (Chapter 1). In the current study we tested the hypothesis that within the striatum, stimulation of NMDA receptors should result in a reduction in Ca^{2+} influx in older animals when compared with Ca^{2+} influx in younger animals. The age induced reduction of NMDA receptor function leading to reduced NMDA (100 μM) stimulated Ca^{2+} accumulation in vitro has not been described in young adult male Long Evans rats nor has it been previously described in any other strain.

Due to their role in synaptic location, the function and efficiency of NMDA receptors is critical to numerous synaptic activities. Efficiency of the receptor channels is highly regulated by their phosphorylation state (Conti and Weinberg,1999). Major changes in the phosphorylation state occur following dopamine depletion in animal models of Parkinson's disease such as increased phosphorylation of NR1 serine residues (Dunah *et al*, 2000), NR2 tyrosine residues (Oh *et al*, 1998, Dunah *et al*, 2000). Furthermore there are increases in NMDA receptor expression on the synaptic membrane in animal models and in Parkinson's disease patients (Lange *et al*, 1997). In addition to other abovementioned synaptic functions, NMDA receptors generate excitatory postsynaptic potentials and make a significant contribution to regulating neuronal excitability in response to glutamate stimulation by cortical and thalamic afferents. Changes of receptor phosphorylation state causes alterations in NMDA receptor channel open times and affects neuronal firing patterns (Yu *et al*, 1997). In parkinsonian animals, the membrane potential of striatal neurons is increased

(alleviating the Mg^{2+} block of receptor channels) and firing activity of striatal neurons is increased (Kish *et al*, 1999; Tseng *et al*, 2001; Wichmann and DeLong, 2003; Tseng *et al*, 2004).

The above evidence strongly suggests that there is increased NMDA receptor function in Parkinson's disease following dopamine depletion in the striatum. Indeed NMDA antagonists, attenuating receptor function, have been found to have similar beneficial anti-parkinsonian effects as dopamine replacement therapy in animals and are a used in the clinical treatment of Parkinson's disease (Lange *et al*, 1997; Oh et at, 1998). In the current study we tested the hypothesis that following dopamine depletion NMDA receptor upregulation should cause an increase in Ca^{2+} influx into striatal tissue following unilateral dopamine depletion in Long Evans rats.

STUDY ONE

Hypothesis

Aging will result in decreased NMDA stimulated Ca^{2+} uptake into striatal tissue in vitro of adult male rats compared to adolescent male rats.

Objective

To determine whether NMDA stimulated Ca^{2+} uptake into striatal slices is reduced with age by comparing male Long Evans rats aged 7 weeks and 16 weeks.

STUDY TWO

Hypothesis

Degeneration of the nigrostriatal pathway (6-OHDA induced) will result in increased NMDA stimulated Ca^{2+} uptake into striatal sections in vitro.

Objective

To determine whether NMDA stimulated Ca^{2+} uptake into striatal sections increases following degeneration of nigrostriatal dopamine pathway in a unilateral animal model of Parkinson's disease.

CHAPTER 4

EXPERIMENTAL PROCEDURES

4.1 Animals

A complete report of the rats used for the study is provided in Annex A.

The design of the current study and the use of animals were approved by the University of Cape Town Research Ethics Committee. Long Evans rats were obtained from the Faculty of Health Sciences Animal Unit where they were bred. The rats were housed in individual cages in the Department of Human Biology Anatomy Building animal house. The rats were maintained on a twelve-hour light/dark cycle and were provided with food pellets and water *ad libitum*. Male Long Evans rats (n=14) were used in a preliminary study to establish the technique of NMDA stimulated uptake of radioactive calcium-45 ($^{45}Ca^{2+}$) assay for the study. These rats were previously used to develop the 6-OHDA lesion technique. Of these rats, there were n=6 6-OHDA lesioned rats and a group of non 6-OHDA lesioned rats (n=8) which comprised of rats that were either untreated or had been injected with sterile saline (sham lesioned).

When the NMDA stimulated $^{45}Ca^{2+}$ uptake assay technique had been established, the effects of age on NMDA receptor function was investigated in male Long Evans rats aged 6 – 7 weeks, n=7 (106g – 210g) and 16 weeks, n=6 (482g – 556g); these rats did not receive pharmacological or surgical treatment prior to uptake assays being conducted. Male Long Evans rats (n=46) weighing 330g – 398g (aged 18 – 19 weeks at time of uptake assays) were used to investigate the effects of 6-OHDA lesion of the nigrostriatal pathway on NMDA receptor function. To identify the site of lesion in the medial forebrain bundle (MFB) using the method of cresyl violet staining, n=10 rats were used. The nigrostriatal pathway was lesioned with 6-OHDA in n=21 rats and n=15 rats were sham lesioned using sterile saline. Of the rats lesioned with 6-OHDA, n=3 were used to visually verify the extent of degeneration using tyrosine hydroxylase (TH) staining following behavioural assessment. From the sham lesioned group, n=1 rat, was used for the TH staining, in addition to n=1 unlesioned rat. NMDA stimulated uptake assays were conducted on n=12 of the 6-OHDA lesioned rats and on n=11 of the sham lesioned rats. Following surgery, there were infections resulting in n=9 treated rats being killed. Infections were reported to the department vet and tests were conducted at Groote

Schuur Hospital and by the state vet in Stellenbosch. It was established that *Pseudomonas aeruginosa* was the bacterium responsible for most of the infections reported.

4.2 NMDA stimulated $^{45}Ca^{2+}$ uptake assays

A comprehensive list and detail of the materials and solutions used to conduct the NMDA stimulated $^{45}Ca^{2+}$ uptake assays can be found in Annex A.

4.2.1 Tissue sectioning

Two studies involving NMDA stimulated calcium uptake assays were conducted as previously reported (Feldman *et al*, 1990; Lehohla *et al*, 2000; Lehohla *et al*, 2001). In the first study, the assay was conducted to determine the effects of ageing on NMDA receptor function in rats aged 6-7 weeks (n=7) and 16 weeks (n=6). Each rat was deeply anaesthetized with halothane and decapitated. The brain was rapidly removed and cooled for 5 min in continuously oxygenated, ice-cold incubation HEPES buffer (120 mM NaCl, 1 mM $MgCl_2$, 3.36 mM KCl, 10 mM D-Glucose, 20 mM HEPES buffer pH 7.4, 1.2 mM $CaCl_2$). After 5 min, the brain was placed onto a dampened filter paper in a petri dish kept on ice. The purpose of the dampened filter paper was to prevent the brain from sliding while the posterior end of the brain, ≈ 2 mm anterior to the cerebellum, was cut. The posterior brain surface of the block was glued onto the vibratome cutting stage using Loctite 406 glue. Prior to use, the vibratome bath was filled with continuously oxygenated ice-cold HEPES buffer slush made from frozen buffer. A new blade was cleaned with absolute ethanol and fitted into the vibratome holder in preparation for cutting. The blade inclination was 20°. The cutting stage was inserted into the chuck within the vibratome bath and clamped into position in preparation for sectioning of the brain.

4.2.2 Dissection of striata

The first few slices from the anterior end were of variable size and were cut to straighten the block. Thereafter, serial coronal sections of 350 µm thickness containing the anterior, intermediate and posterior striata were cut. The ventral striata were obtained from slices corresponding approximately to antero-posterior co-ordinates 11.20 mm to 10.00 mm with reference to the interaural line (Paxinos and Watson, 1986). The serial sections containing the dorsal striata were cut from slices corresponding approximately to antero-posterior co-ordinates 10.20 mm to 8.74 mm with reference to the interaural line (Paxinos and Watson, 1986). Consequently, the anterior dorsal striatal sections were obtained from either the same slice from which the posterior ventral striatal sections were

obtained or from consecutive slices. A nick was made in the left cerebrum to enable differentiation of the left hemisphere from the right hemisphere. As each slice was cut, it was immediately transferred from the vibratome bath into a perforated Perspex tissue container immersed in a glass container and filled with continuously oxygenated ice-cold HEPES buffer. The glass container was kept on ice to maintain the temperature of the HEPES buffer solution at 4°C. Oxygen was bubbled through plastic tubing attached to the glass container beneath the Perspex tissue container. The base of the Perspex tissue container comprised small-drilled holes to allow oxygen to reach the slices. Each slice was placed onto a cold glass slide and the striata were carefully dissected from each hemisphere using a curved blade. The striatal sections were transferred to individual Teflon vials with nylon mesh stretched across the base and held firmly to the bottom with a rubber o-ring fitted to a groove near the base of the tube. The vials were marked to indicate the slice number and hemisphere (right or left) of the striatum. The vials were held firmly in a rack that was used to facilitate the simultaneous transfer of all the striatal sections between sets of polyethylene wells containing different buffers in subsequent phases of the assay.

4.2.3 Incubation phases

In the first phase, dissected striata were incubated in 10 ml continuously oxygenated HEPES buffer contained in individual wells and equilibrated to room temperature for 45 min. The sections were then transferred to 35°C continuously oxygenated HEPES buffer and incubated for 5 min. NMDA stimulated uptake of $^{45}Ca^{2+}$ was determined by incubating dissected striatal sections in HEPES buffer containing 100 µM NMDA and comparing the $^{45}Ca^{2+}$ accumulation with striatal sections incubated in control buffer to which NMDA was not added. The incubation period was for 2 min at 35°C. Dissected striatal sections from the anterior (1L and 1R) and posterior (3L and 3R) slices were used as the test sections incubated in stimulation buffer and the striatal sections dissected from the intermediate (2L and 2R) slice served as the controls. 'L' and 'R' represent striatal sections dissected from the left and right hemispheres respectively. The experiment was concluded with a series of lanthanum washes at 4°C to remove excess $^{45}Ca^{2+}$ from the surfaces of the striatal sections. The buffered lanthanum chloride ($LaCl_3$) solution had similar composition to the normal HEPES buffer solution except that $CaCl_2$ was replaced by 10 mM $LaCl_3$. The first wash was a rapid wash for 10 sec followed by a 15 min wash. These washes were conducted in individual wells containing 10 ml $LaCl_3$. The final 15 min wash was in flat petri dishes containing 10 ml $LaCl_3$

solution. During this wash, the striatal sections were carefully freed from the nylon mesh. The sections were transferred to individual Eppendorf vials containing 1 ml ice-cold distilled water.

The striatal sections were sonicated in 1 ml ice-cold distilled water to rupture the cells and release accumulated $^{45}Ca^{2+}$. A 600 µl aliquot of the sonicate was mixed thoroughly with 3.4 ml of scintillation fluid (Zinsser Analytic, UK) and the counts per minute (CPMs) from the sample were measured using a liquid scintillation counter (Packard Tri-Carb 2100TR). A standard quench curve was constructed for each experiment using NMDA containing and non-NMDA containing incubation buffer. The purpose of the quench curve was to determine the amount of quenching in the samples by comparison with the standards whose quench is known. Varying volumes of distilled water 0 ml, 50 µl, 250 µl, 600 µl, 1.0 ml, 1.5 ml and 2.0 ml were added to 5 ml Teflon vials. Using a Finn pipette, 20 µl of the test incubation buffer containing $^{45}Ca^{2+}$ was added into each of the vials. A separate standard curve was constructed for the control incubation buffer. Scintillation fluid (3.4 ml) was added to the vials and mixed thoroughly. The vials were placed into larger 20 ml polyethylene vials and taken to the liquid scintillation counter. From the counts per minute (CPMs) recorded for the quenched standards, a curve of percentage efficiency (this had to be calculated) was plotted against tSIE (amount of quench calculated by the counter)

4.2.4 Protein determination

The remaining sonicate was used to determine the protein content using the Miller method of protein determination. Protein dilutions using 1 mg/ml bovine serum albumin (BSA) were made to construct a standard curve. Different volumes of BSA (0 µl, 10 µl, 20 µl, 40 µl and 80 µl) were made up to 1 ml with distilled water. For each dilution a duplicate dilution was made in a separate test tube. Samples of the sonicate were made in duplicate using volumes of 80 µl (for dorsal striatal samples) and 160 µl (for ventral striatal samples) and these were made up to 1 ml with distilled water. 1 ml of freshly prepared Reagent A was added to all the test tubes using a Finn pipette and mixed thoroughly on the vortex. The samples were allowed to stand at room temperature for 10 min. Folin acid reagent (3 ml) was forcefully added to each test tube using a Finn pipette and mixed thoroughly on the vortex. The test tubes were incubated in a 50°C water bath for 10 min. After 10 min the samples were cooled to room temperature, before being transferred to cuvettes for the absorbance measurement at 650 nm in the spectrophotometer (UV-9100, Laboratory & Scientific Equipment

Company). The absorbance of the BSA solutions were used to construct a standard curve from which the dilutions of the sonicate were read to obtain the amount of protein in 80 µl and 160 µl of sonicate. The amount of $^{45}Ca^{2+}$ accumulated in the tissue samples was expressed as nanomoles of $^{45}Ca^{2+}$ accumulation per milligram of protein (nmol $^{45}Ca^{2+}$/mg protein) in 2 min. In the second study, the assay was used to determine whether unilateral nigrostriatal degeneration altered NMDA receptor function in the lesioned striatum. Calcium uptake assays were conducted as described above following the surgical treatment and behavioral studies of the rats as described below (refer to Sections 4.4 and 4.5).

4.3 Calculations and statistical analysis

The data for NMDA stimulated $^{45}Ca^{2+}$ uptake were analysed with Student t-tests (dependent samples) for within factor comparison with Bonferroni correction for multiple comparisons (while $pi \leq \alpha/n$ reject Hi, otherwise accept Hi. Where n is equal to the number of null hypotheses that are simultaneously tested) (García *et al*, 2004) of uptake into left (lesioned) vs. right (unlesioned) hemispheres. One-way ANOVA was used for comparison between 6-OHDA lesioned and sham lesioned rats and for comparison between rats aged 6-7 weeks and 16 weeks. In all the statistical analyses, statistical significance was taken as $p< 0.05$. Statistica 7 software package was used for all analyses. Results are given as the mean ± standard error of the mean (SEM) and uptake was calculated as nmol $^{45}Ca^{2+}$ /mg protein / 2 min.

4.4 Surgical Procedure

A comprehensive list and detail of the materials and solutions used to conduct the surgical procedures can be found in Annex A.

Surgery was conducted to lesion the nigrostriatal pathway on n=21 rats and in n=10 animals, surgery was undertaken to obtain a histological representation of the site of lesion. All surgical lesioning procedures were conducted under semi-sterile conditions on rats weighing 330g – 398g (aged 13 - 14 weeks).

In preparation for surgery, each rat was deeply anaesthetized with halothane inhalation anaesthetic (Safeline Pharmaceuticals, South Africa) placed in a stereotaxic apparatus. The rat was positioned with its upper incisors over the incisor bar and the head was held in position with ear bars.

Throughout the surgery, 3% halothane/oxygen anaesthesia was administered using a Blease vaporizer via a specifically designed and constructed nose cone that fitted over the incisor bar and the nose of the rat. Proper positioning of the ear bars in the rat's ears and positioning of the head centrally in the stereotaxic apparatus enabled calculation of the co-ordinates from the interaural line. The co-ordinates of the MFB were determined using the stereotaxic rat atlas of Paxinos & Watson (1986). Co-ordinates were: anterior-posterior with reference to the interaural line - 4.7 mm and lateral relative to the midline - 1.6 mm. A midline incision of the skin overlying the skull was made to expose the dura mater above the MFB target site in the left hemisphere. The dura was carefully lifted using the bent tip of a 20Gx1½ needle and a 0.3 mm stainless steel infusion needle was lowered 8.4 mm from dura to the MFB. The needle was left in place for five minutes before being withdrawn slowly. The rats used to obtain histological representations of the site of lesion were immediately killed by the method of transcardial perfusion.

The above surgical technique was used to infuse 6-hydroxydopamine hydrochloride, 6-OHDA, (Sigma, USA) into the MFB of n=21 rats and to sham lesion n=15 rats with infusion of sterile saline. Prior to surgery, the fur above the skull was clipped to minimize possible infection during the operation and post-operatively around the sutures. Each rat was injected intraperitoneally (i.p.) with desipramine hydrochloride (25mg/kg) (Sigma, USA) at least 25 min prior 6-OHDA or saline infusion into the MFB (Magill *et al*, 2001). The rat was deeply anaesthetized and placed on the stereotaxic apparatus. The method of lowering the infusion needle to the MFB was conducted as described above.

A syringe pump connected to the infusion needle regulated the rate of infusion of 13.5 µg/4.5 µl dose of 6-OHDA into the left hemisphere (Magill *et al*, 2001). 6-OHDA solution was prepared with sterile saline and 0.02% L-ascorbic acid (Merck, Germany) just before use. At the end of the infusion period, 5 min was allowed for the toxin to diffuse before the needle was withdrawn slowly from the brain. The burr hole was sealed with bone wax and the skin incision was sutured with silk suture and sterilized with 70% alcohol and iodine. Sham-operated control rats underwent the same surgical procedure receiving only 4.5 µl of the vehicle (sterile saline with 0.02% ascorbic acid). Following the surgery, animals were carefully monitored for weight loss and any signs of stress. In response to postoperative weight loss, wetted Epol pellets were placed in the cages of the animals in

addition to the ad libitum availability of the dry pellets for 2 weeks following surgery to minimize weight loss. The animals responded well to the wet pellet feeding.

4.5 Behavioral assessment of lesion

A complete list and detail of the materials and solutions used to conduct the behavioural assessments can be found in Annex A.

Fourteen days after surgery, n=17 6-OHDA lesioned and n=14 sham lesioned rats underwent behavioural assessment to determine the extent of degeneration of dopamine neurons innervating the striatum. An established technique of apomorphine-induced rotations was used (Ungerstedt and Arbuthnott, 1970; Tillerson *et al*, 2001). The rats were placed in rotameter drums and the rotameter recorded the number of quarter rotations made by the rat over a period of 90 min using the Automatic Rodent Monitor programme. The first 30 min of the recording session was used to acclimatize the rats to the new environment and to record the baseline rotational movement. After 30 min, the rats were removed from the drums and were subcutaneously injected with 0.5 mg/kg apomorphine (apomorphine hydrochloride hemihydrate, Sigma, USA). The rats were returned to the drums immediately following the injection and the rotational response to apomorphine was recorded. 6-OHDA lesioned rats (n=3) exhibiting less than 400 contraversive quarter rotations i.e. 100 complete rotations were removed from further analysis involving NMDA stimulated $^{45}Ca^{2+}$ assays. More than 100 complete contralateral rotations has been established to represent a loss of >90% of dopamine in the striatum (Ungerstedt, 1971). On the basis of this criterion, n=14 6-OHDA lesioned rats, completing >100 contralateral rotations were selected for further study. Sham lesioned rats did not exhibit contralateral turning in response to apomorphine, but rather conducted predominantly ipsilateral rotations. At the end of the recording session, the rats were returned to their individual cages and transported to the animal house.

4.6 Histology

A comprehensive list and detail of the materials and solutions used to conduct all histology studies can be found in Annex A.

4.6.1 Transcardial perfusion

To conduct the histology on brain tissue to obtain a representation of the site of lesion using cresyl violet staining and to obtain a visual record of the extent of lesion using tyrosine hydroxylase staining, n=14 rats were transcardially perfused. The rats, which had undergone lesioning operations, were perfused five weeks following 6-OHDA injection i.e. 21 days after behavioural assessment (section 4.5). The method of transcardial perfusion was employed as it was the only method that allowed the efficient clearing of blood from the brain tissue and the complete perfusion of the brain with paraformaldehyde fixative. For this to occur it was necessary that the rat's heart was still beating during perfusion.

The operation was conducted as humanely as possible with each rat being deeply anaesthetized by placing it in a halothane filled airtight chamber. Under deep anaesthesia, the thorax of the rat was opened to expose the heart. The rat was perfused with 150 ml 0.15 M phosphate buffer saline (PBS) solution p.H 7.4 through a 20Gx1½ perfusion needle inserted into the left atrium. Perfusion with saline was followed by fixation with 300 ml solution of 4% paraformaldehyde (PFA) in 0.15 M PBS p.H 7.4 solution. 50 ml syringes were used for perfusion as they facilitated the most accurate measurement of the volume administered. Following the perfusion procedure, the brain was removed from the cranium and was placed in a glass vial containing 20% sucrose for cryoprotection overnight. In most cases the tissue only required overnight cryoprotection, however, if the brain did not sink it was left in the sucrose for an additional 24 hrs. The brain was removed from the sucrose solution and was embedded in tissue freezing medium within tin foil moulds, frozen over liquid nitrogen vapour and stored at -80°C wrapped in parafilm until removed for sectioning. Using a cryostat, 20 µm sections of brain containing the striatum and the midbrain (SN and VTA) were cut at -20°C and placed on gelatinized glass slides in preparation for cresyl violet and tyrosine hydroxylase staining.

4.6.2 *Cresyl violet Nissl staining*

Sections used for cresyl violet staining were air-dried overnight prior to use. The 20 µm sections on the slides were placed on staining racks and rinsed briefly in distilled water. They were incubated in the cresyl violet solution for 20 min. Following cresyl violet incubation the sections were cleared in distilled water for 1 min and subjected to a series of dehydration steps in 90% alcohol (1 min), 95% alcohol (1 min) and 100% alcohol (1 min x3) followed by clearing in xylene. The slides were then mounted with Entellan.

4.6.3 *Tyrosine hydroxylase staining*

Sections of the brain tissue containing the midbrain (SNc and VTA) and the striatum were stained for the dopamine synthesis regulating enzyme, tyrosine hydroxylase, to confirm whether degeneration had occurred. Tyrosine hydroxylase staining was conducted on the brain from n=2 6-OHDA lesioned rats completing >100 complete rotations and n=1 rat completing <100 rotations. The brains from n=1 sham lesioned rat and from n=1 unlesioned animal were also stained for tyrosine hydroxylase.

Prior to processing for immunohistochemistry, the sections had to reach room temperature. Each section on each slide was encircled with a grease pap pen. The purpose was to ensure that during the incubations, the reagent would not run off and would be concentrated in the area of the section. Following encircling with pap pen the slides were immersed in 0.15 M PBS p.H. 7.4 if found to have reduced in moisture during encircling. The brain sections were prepared for staining by initially quenching their endogenous peroxidase activity to reduce background staining. The sections were incubated with hydrogen peroxide solution in a humidifying chamber for 30 min at room temperature followed by a series of 3 washes of 10 min each in 0.15 M PBS p.H 7.4. Blocking serum was prepared and immediately applied to each slice; the sections were incubated for 30 min at room temperature in the humidifying incubation chamber. After 30 min, the blocking solution was blotted from the sections. This involved gently tapping each slide onto absorbing paper towels to remove excess solution. Primary anti-monoclonal anti-tyrosine hydroxylase antibody solution was prepared just before use. The primary antibody solution was applied onto each slice and the sections were incubated overnight in the humidifying chamber kept in a fridge at 4°C.

The overnight incubation was terminated with a series of x5 10 min washes in 0.15M PBS pH 7.4. The sections were then incubated with biotinylated secondary antibody in the humidifying chamber for 1hour at room temperature. The biotinylated secondary antibody solution was prepared just before use. The sections were washed 4 times with 0.15M PBS pH 7.4 with each wash lasting 10 min. Avidin-Biotin-Peroxidase Complex (ABC) reagent (Elite kit, Vector Laboratories, USA) was used to visualise the staining. This had to be prepared thirty minutes before use as per kit instructions. The sections were incubated with ABC reagent for 30 min at room temperature in a humidifying chamber. This was followed by x2 5 min washes in 0.15 M PBS pH7.4.

3,3'-diaminobenzidine (DAB) peroxidase (Vector Laboratories, USA) was used to obtain a dark blue stain. Precautions were necessary as DAB is noxious and needs to be handled with care. The slides were removed from the 0.15M PBS pH 7.4 wash and laid out onto absorbing paper in a demarcated area of the work bench. DAB solution was prepared as per kit instructions and was applied to the sections. The sections were incubated at room temperature until a dark blue stain had developed. The sections were washed for 15 min in running distilled water. In addition to demarcating a work area, a large beaker of diluted bleach solution was placed within the work area and all the equipment that came in contact with the DAB solution was incubated for a week within the solution before being further processed with normal washing or being disposed of. A plastic bag was also placed nearby within the work area to allow gloves and used absorbing paper to be disposed of immediately after use. The sections were then dehydrated in alcohol, cleared in xylene and mounted with Entellan.

CHAPTER 5
RESULTS

5.1 *PRELIMINARY STUDY*
NMDA stimulates $^{45}Ca^{2+}$ uptake into striatal sections

Preliminary data was acquired to determine whether 100μM NMDA could stimulate $^{45}Ca^{2+}$ uptake into dorsal striatal sections following 2 mins incubation *in vitro*. NMDA stimulated $^{45}Ca^{2+}$ uptake into striatal tissue was measured from untreated rats and rats that were used to develop the 6-OHDA lesioning technique (n=14). The results from the untreated rats and sham lesioned rats were not significant and are reported as one group, non 6-OHDA lesioned rats (n=8). Results for the complete statistical analyses are reported in Annex B. A copy of a spreadsheet used for calculation of nmol $^{45}Ca^{2+}$ in striata from each rat is provided in Annex B. Measurement of total $^{45}Ca^{2+}$ uptake into striatal sections from non lesioned rats, showed that within both hemispheres, total $^{45}Ca^{2+}$ uptake into the anterior (1L and 1R) and posterior (3L and 3R) striata incubated in buffer containing NMDA (100μM) was significantly increased (student t-test, $p<0.05$) above basal (unstimulated) $^{45}Ca^{2+}$ uptake into intermediate sections (2L and 2R) (Table 5.1a, Figure 5.1a). Results from 6-OHDA lesioned rats (n=6) were similar with levels of $^{45}Ca^{2+}$ uptake into anterior and posterior striata being significantly greater than basal levels (Table 5.1a, Figure 5.1b). NMDA significantly increased $^{45}Ca^{2+}$ uptake into striatal sections obtained from non lesioned rats and 6-OHDA lesioned rats (student t-test, $p<0.05$).

Table 5.1a Total $^{45}Ca^{2+}$ uptake into anterior (1L and 1R) and posterior (3L and 3R) striatal sections following 2 min incubation in buffer containing NMDA (100 μM) and basal $^{45}Ca^{2+}$ uptake into intermediate striata (2L and 2R) in the absence of NMDA.

		$^{45}Ca^{2+}$ uptake into striatal sections (nmol $^{45}Ca^{2+}$ /mg protein)							
GROUP		1L	1R		2L	2R		3L	3R
NON LESIONED RAT	n=8	13.22 ± 1.31 *	14.03 ± 1.35 *		7.09 ± 0.86	6.40 ± 0.70		11.73 ± 1.27 *	12.57 ± 1.38 *
6-OHDA LESIONED RAT	n=6	9.14 ± 1.12 *	10.41 ± 1.74 *		5.28 ± 0.88	5.14 ± 0.97		8.11 ± 0.98 *	10.14 ± 1.68 *

***NMDA stimulated significant increases in $^{45}Ca^{2+}$ uptake into anterior and posterior striata compared to basal (unstimulated) uptake in both groups (Student t-test ($p<0.05$) plus Bonferroni correction $p<0.025$). Data are reported as mean ± sem (nmol $^{45}Ca^{2+}$ /mg protein).**

PRELIMINARY RESULTS

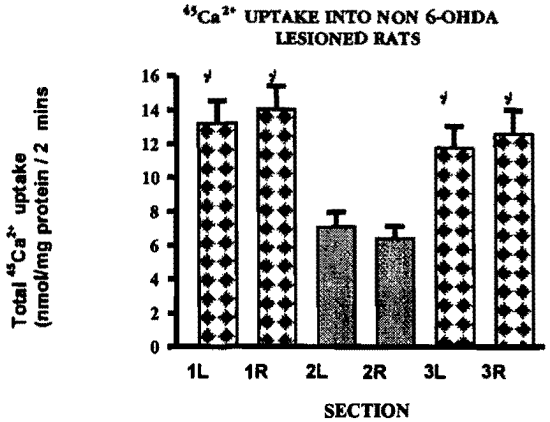

Figure 5.1a Preliminary results from non lesioned rats (n=8). *NMDA (100 μM) stimulated significant increases in $^{45}Ca^{2+}$ uptake into the anterior (1L and 1R) and posterior (3L and 3R) dorsal striata in the left and right hemispheres relative to basal non-stimulated uptake (2L and 2R) (Student t-test ($p<0.05$) plus Bonferroni correction $p<0.025$). Data are reported as mean ± sem (nmol $^{45}Ca^{2+}$ /mg protein). Data are reported in Table 5.1a.

PRELIMINARY RESULTS

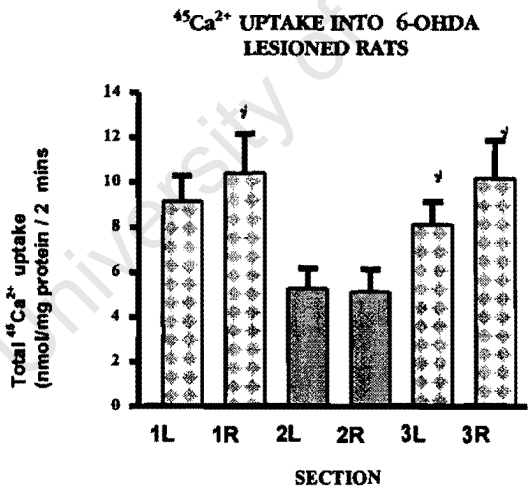

Figure 5.1b Preliminary results from 6-OHDA lesioned rats (n=6). * NMDA (100 μM) stimulated significant increases in $^{45}Ca^{2+}$ uptake into the anterior (1L and 1R) and posterior (3L and 3R) dorsal striata in the left and right hemispheres from basal non-stimulated uptake (2L and 2R) (Student t-test ($p<0.05$) plus Bonferroni correction $p<0.025$). Data are reported as mean ± sem (nmol $^{45}Ca^{2+}$ /mg protein). Data are reported in Table 5.1a.

5.2 *AGE EFFECTS ON NMDA STIMULATED $^{45}Ca^{2+}$ UPTAKE*

NMDA receptors are critical in the regulation of pre-natal and post-natal synaptic development. A group of rats (n=13) was studied to determine whether there were age-dependent differences in $^{45}Ca^{2+}$ uptake into the dorsal and ventral striata of adolescent and adult rats (aged 7 week and 16 week old) following NMDA (100μM) stimulation. The rats in this group did not receive any prior treatment. Results for the complete statistical analyses reported below are reported in Annex B.

5.2.1 NMDA stimulated $^{45}Ca^{2+}$ uptake in rats aged 7 weeks

5.2.1.1 Dorsal Striatum – 7 week old rats

In the 7 week old rats (n=7), the total $^{45}Ca^{2+}$ uptake into dorsal striatal sections incubated in NMDA (100μM) (1L, 1R, 3L and 3R) showed significant increase above basal $^{45}Ca^{2+}$ accumulated in non-stimulated striatal sections (2L and 2R) (Table 5.2a). The results show that NMDA evoked a significant increase of $^{45}Ca^{2+}$ uptake into striatal sections above control levels.

To determine the level of effect of NMDA stimulation, a measure of the NMDA effect on $^{45}Ca^{2+}$ uptake was calculated by subtracting basal $^{45}Ca^{2+}$ uptake derived from intermediate unstimulated striatal sections (2L and 2R) from total $^{45}Ca^{2+}$ uptake into the anterior (1L and 1R) and posterior (3L and 3R) striatal sections. NMDA stimulated $^{45}Ca^{2+}$ uptake is presented as 1L-2L (left anterior striatum), 1R-2R (right anterior striatum), 3L-2L (left posterior striatum) and 3R-2R (right posterior striatum). NMDA stimulated $^{45}Ca^{2+}$ uptake into striatal sections was compared within the left hemisphere i.e. 1L-2L vs. 3L-2L and within the right hemisphere i.e. 1R-2R vs. 3R-2R. Within the left hemisphere, NMDA stimulated $^{45}Ca^{2+}$ uptake into the anterior dorsal striatum (1L-2L) was not different from stimulated uptake into the posterior dorsal striatum (3L-2L) (Table 5.2b, Figure 5.2a). Within the right hemisphere, NMDA stimulated $^{45}Ca^{2+}$ uptake in the anterior dorsal striatal section (1R-2R) was also not different from the posterior dorsal striata (3R-2R) (Table 5.2b, Figure 5.2a). There were no significant differences in $^{45}Ca^{2+}$ uptake stimulated by NMDA between anterior and posterior dorsal striata within either the left or the right hemisphere.

The response to NMDA stimulation was compared across the hemispheres using Bonferroni correction for multiple comparisons. There were no differences in NMDA

stimulated $^{45}Ca^{2+}$ uptake into the anterior dorsal striatum of the left hemisphere and into the anterior dorsal striatum of the right hemisphere i.e. 1L-2L vs. 1R-2R (Figure 5.2b). There were also no differences in $^{45}Ca^{2+}$ uptake into the posterior dorsal striata i.e. 3L-2L vs. 3R-2R (Figure 5.2b).

Table 5.2a **Total $^{45}Ca^{2+}$ uptake into the dorsal and ventral striata of rats aged 7 weeks (n=7).**

	Total $^{45}Ca^{2+}$ uptake into striatal sections (nmol $^{45}Ca^{2+}$ /mg protein)							
STRIATAL REGION		**1L**	**1R**		**2L**	**2R**	**3L**	**3R**
DORSAL STRIATUM	n=7	11.42 ± 0.75 *	10.01 ± 0.89 *		4.69 ± 0.39	4.70 ± 0.47	9.05 ± 0.82 *	10.44 ± 0.64 *
VENTRAL STRIATUM	n=7	12.80 ± 1.64 *	10.65 ± 1.45 *		4.48 ± 0.36	4.80 ± 0.55	11.27 ± 1.38 *	10.32 ± 1.02 *

*** NMDA (100μM) evoked significant increases in $^{45}Ca^{2+}$ uptake into NMDA incubated sections (1L, 1R, 3L and 3R) compared to basal (unstimulated) uptake into dorsal and ventral striatal sections not incubated in NMDA (2L and 2R) (Student t-test ($p<0.05$) plus Bonferroni correction $p<0.025$). Data are reported as mean ± sem (nmol $^{45}Ca^{2+}$ /mg protein).**

Table 5.2b **NMDA (100μM) stimulated $^{45}Ca^{2+}$ uptake into the dorsal and ventral striata of rats aged 7 weeks (n=7).**

	$^{45}Ca^{2+}$ uptake into striatal sections (nmol $^{45}Ca^{2+}$ /mg protein)					
STRIATAL REGION		**1L-2L**	**± sem**		**1R-2R**	**± sem**
DORSAL STRIATUM	n=7	6.73	0.81		5.30	0.86
VENTRAL STRIATUM	n=7	6.89	1.41		5.85	1.49
		3L-2L	**± sem**		**3R-2R**	**± sem**
DORSAL STRIATUM	n=7	4.35	0.61		5.73	0.72
VENTRAL STRIATUM	n=7	7.34	1.43		5.52	1.10

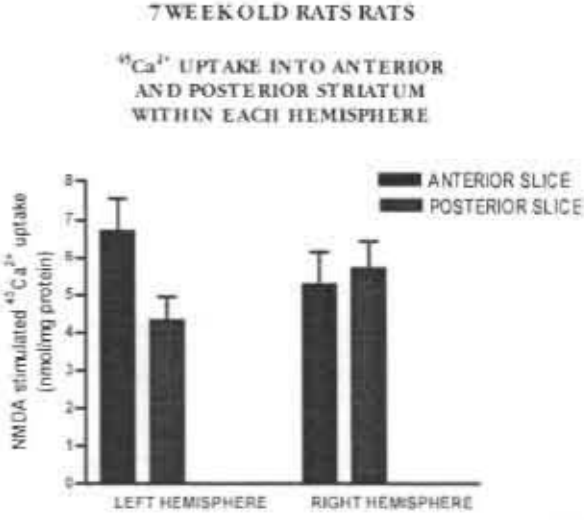

Figure 5.2a NMDA stimulated $^{45}Ca^{2+}$ uptake into anterior dorsal striata and posterior dorsal striata within each hemisphere of 7 week old rats (n=7). No significant difference in uptake between the anterior striatum and the posterior striatum within either the left or right hemisphere (Student t-test ($p>0.05$) plus Bonferroni correction $p>0.025$). Data are reported as mean ± sem (nmol $^{45}Ca^{2+}$ /mg protein). Data are reported in Table 5.2b.

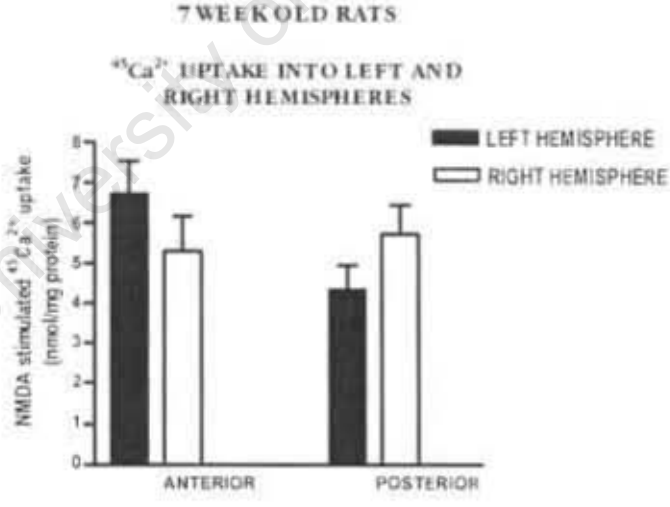

Figure 5.2b NMDA stimulated $^{45}Ca^{2+}$ uptake into dorsal striata of left vs. right hemispheres of 7 week old rats. No significant difference in uptake between the left and right hemispheres (Student t-test ($p>0.05$) plus Bonferroni correction $p>0.025$). Data are reported as mean ± sem (nmol $^{45}Ca^{2+}$ /mg protein). Data are reported in Table 5.2b and also in Figure 5.2a.

5.2.1.2 *Ventral Striata – 7 week old rats*

Results from the measurement of $^{45}Ca^{2+}$ uptake into the ventral striata of the 7 week old rats, show that total uptake into ventral striatal sections 1L, 1R, 3L and 3R incubated in buffer containing NMDA (100μM) was significantly increased above basal uptake into non-stimulated striata (2L, 2R). NMDA was effective in inducing significant $^{45}Ca^{2+}$ uptake above basal levels into ventral striata (Table 2a). Comparison of NMDA stimulated $^{45}Ca^{2+}$ uptake into the anterior (1L-2L and 1R-2R) and the posterior (3L-2L and 3R-2R) striata, showed that there were no differences in $^{45}Ca^{2+}$ accumulation within either the left or the right hemispheres (Table 5.2b). Across the hemispheres, there were also no differences in NMDA stimulated uptake into the anterior ventral striata of the left (1L-2L) and the right (1R-2R) hemispheres, neither were there any differences in uptake between the posterior (3L-2L and 3R-2R) ventral striata (Table 5.2b).

5.2.1.3 *NMDA stimulated $^{45}Ca^{2+}$ uptake into dorsal vs. ventral striata – 7 week old rats*

To determine whether there were any differences in NMDA stimulated $^{45}Ca^{2+}$ accumulation in the dorsal and the ventral striata, uptake into striatal tissue from these regions was compared. NMDA stimulated $^{45}Ca^{2+}$ uptake into dorsal anterior striata (1L-2L and 1R-2R) was compared with uptake into the ventral posterior striata (3L-2LV and 3R-2RV) as these were derived either from the same slice or from consecutive serial slices during dissection (see Experimental Procedures, section 4.2.2). There were no differences in uptake into the dorsal and ventral striata within either the left hemisphere (1L-2L vs. 3L-2L) or the right hemisphere (1R-2R vs. 3R-2R) (student t-test, $p>0.05$) (Figure 5.2c).

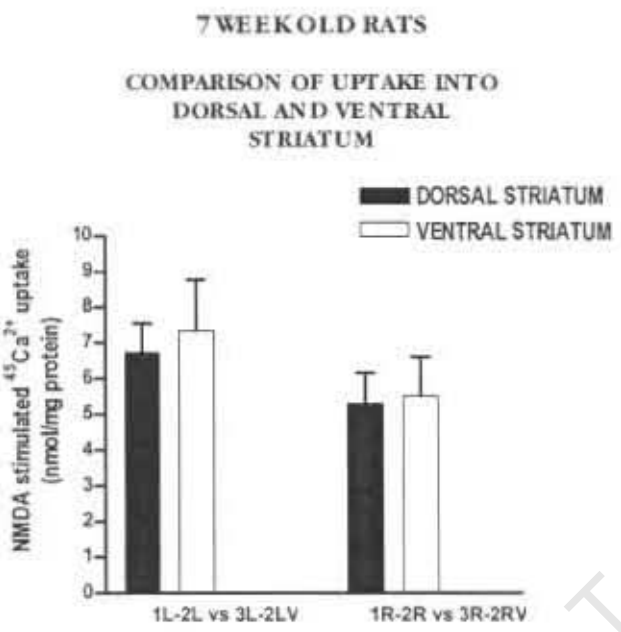

Figure 5.2c NMDA (100µM) stimulated $^{45}Ca^{2+}$ uptake into dorsal and ventral striata in the 7 week old rat. Results show stimulated $^{45}Ca^{2+}$ uptake into anterior dorsal striata and uptake into posterior ventral striata (1L-2L vs. 3L-2LV) from left hemisphere and uptake into striata from the right hemisphere (1R-2R vs. 3R-2RV). There were no differences in stimulated $^{45}Ca^{2+}$ uptake between the dorsal and ventral striata (ANOVA). Results are reported as mean ± sem nmol $^{45}Ca^{2+}$ /mg protein. Data are reported in Table 5.2b.

5.2.2 *NMDA Stimulated $^{45}Ca^{2+}$ Uptake into striata of 16 week old rats*

5.2.2.1 Dorsal Striata – 16 week old rats

Results for the complete statistical analyses reported below are reported in Annex B. Comparison of total $^{45}Ca^{2+}$ uptake into dorsal striatal sections (1L, 1R, 3L and 3R) incubated in NMDA (100µM) with non-stimulated striatal sections (2L and 2R) showed that NMDA evoked a significant increase of $^{45}Ca^{2+}$ uptake above basal levels into striatal sections obtained from rats aged 16 weeks (Table 5.3a). Measurement of NMDA stimulated $^{45}Ca^{2+}$ uptake (calculated as described above, section 5.1) showed that within the left hemisphere, $^{45}Ca^{2+}$ uptake into the anterior striatal sections (1L-2L) was not different from $^{45}Ca^{2+}$ uptake into the posterior striatal sections (3L-2L) (Table 5.3b, Figure 5.3a). In the right hemisphere there was no difference between $^{45}Ca^{2+}$ uptake into the anterior striatal section (1R-2R) and $^{45}Ca^{2+}$ uptake into the posterior striatum (3R-2R) (Table 5.3b, Figure 5.3a). Comparison of $^{45}Ca^{2+}$ uptake into striatal sections in the left hemisphere with uptake into striata in the right hemisphere showed there were no

differences in $^{45}Ca^{2+}$ uptake between the anterior striata (1L-2L vs. 1R-2R) and posterior striata (3L-2L vs. 3R-2R) (Table 5.3b, Figure 5.3b).

Table 5.3a Total $^{45}Ca^{2+}$ uptake into the dorsal and ventral striata of rats aged 16 weeks (n=6).

	$^{45}Ca^{2+}$ uptake into striatal sections (nmol $^{45}Ca^{2+}$ /mg protein)							
STRIATAL REGION		1L	1R		2L	2R	3L	3R
DORSAL STRIATUM	n=6	5.94 ± 0.71 *	6.93 ± 0.81 *		3.88 ± 0.65	4.06 ± 0.51	5.37 ± 0.69 *	6.20 ± 0.54 *
VENTRAL STRIATUM	N=6	8.09 ± 0.65 *	8.54 ± 0.70 *		4.56 ± 0.55	4.55 ± 0.68	7.11 ± 0.68 *	7.79 ± 0.81 *

*NMDA (100µM) evoked significant increases in $^{45}Ca^{2+}$ into NMDA incubated striatal sections (1L, 1R, 3L and 3R) compared to basal uptake into non-stimulated striatal sections (2L and 2R) (Student t-test ($p<0.05$) plus Bonferroni correction $p<0.025$). Data are reported as mean ± sem (nmol $^{45}Ca^{2+}$ /mg protein).

Table 5.3b NMDA (100µM) stimulated $^{45}Ca^{2+}$ uptake into the dorsal and ventral striata of rats aged 16 weeks (n=6).

	$^{45}Ca^{2+}$ uptake into striatal sections (nmol $^{45}Ca^{2+}$ /mg protein)					
STRIATAL REGION		1L-2L	± sem		1R-2R	± sem
DORSAL STRIATUM	n=6	2.07	0.86		2.86	0.57
VENTRAL STRIATUM	n=6	3.53	0.62		3.99	0.75
		3L-2L	± sem		3R-2R	± sem
DORSAL STRIATUM	n=6	1.49	0.62		2.14	0.46
VENTRAL STRIATUM	n=6	2.55	0.66		3.24	1.21

Data are reported as the mean ± sem (nmol $^{45}Ca^{2+}$ /mg protein).

16 WEEK OLD RATS RATS

$^{45}Ca^{2+}$ UPTAKE INTO ANTERIOR AND POSTERIOR STRIATUM WITHIN EACH HEMISPHERE

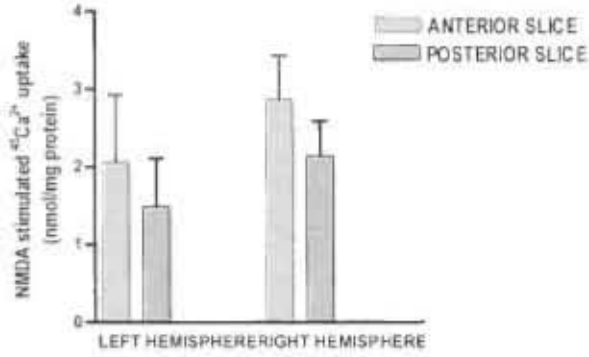

Figure 5.3a NMDA (100 µM) stimulated $^{45}Ca^{2+}$ uptake into anterior and posterior dorsal striata of 16 week old rats (n=6). No significant difference in uptake into the anterior and posterior striata within the left and the right hemisphere (Student t-test ($p<0.05$) plus Bonferroni correction $p<0.025$). Data are reported as mean ± sem (nmol $^{45}Ca^{2+}$ /mg protein). Data are reported in Table 5.3b.

16 WEEK OLD RATS

$^{45}Ca^{2+}$ UPTAKE INTO LEFT AND RIGHT HEMISPHERES

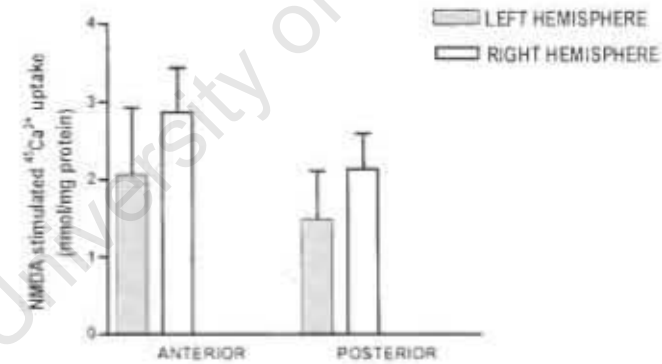

Figure 5.3b NMDA (100 µM) stimulated $^{45}Ca^{2+}$ uptake into the dorsal striata of the left vs. right hemispheres of 16 week old rats (n=6). No significant difference in uptake between the left and right hemispheres. (Student t-test ($p>0.05$) plus Bonferroni correction $p>0.025$). Data are reported as mean ± sem (nmol $^{45}Ca^{2+}$ /mg protein). Data are reported in Table 5.3b and Figure 5.3a.

5.2.2.2 Ventral Striata

$^{45}Ca^{2+}$ uptake was measured in the ventral striata of the 16 week old rats (n=6). NMDA (100 µM) stimulated significant increases in $^{45}Ca^{2+}$ uptake into the anterior (1L, 1R) and posterior (3L, 3R) striata relative to basal levels measured in non-stimulated striatal sections (2L, 2R) (Table 5.3a). Results of the stimulated effect showed that there were no differences in $^{45}Ca^{2+}$ uptake into anterior (1L-2L) and posterior (3L-2L) striata in the left hemisphere, nor were there any differences in uptake into anterior (1R-2R) and posterior (3R-2R) striata in the right hemisphere (Table 5.3b). Results comparing $^{45}Ca^{2+}$ uptake across the hemispheres were similar. There were no differences in stimulated $^{45}Ca^{2+}$ uptake into ventral striata between the left and right hemisphere (Table 5.3b).

5.2.2.3 NMDA Stimulated $^{45}Ca^{2+}$ uptake into dorsal vs. ventral striata

Stimulated $^{45}Ca^{2+}$ uptake into the anterior dorsal striata (1L-2L and 1R-2R) was compared with $^{45}Ca^{2+}$ uptake into the posterior ventral striata (3L-2LV and 3R-2RV) within each hemisphere i.e.1L-2L vs. 3L-2LV and 1R-2R vs. 3R-2RV as previously described (refer to section 5.2.1.3). There were no significant differences in $^{45}Ca^{2+}$ uptake levels between the dorsal and ventral striata into either the left or the right hemispheres of 16 week old rats (Table 5.3b, Figure 5.3c).

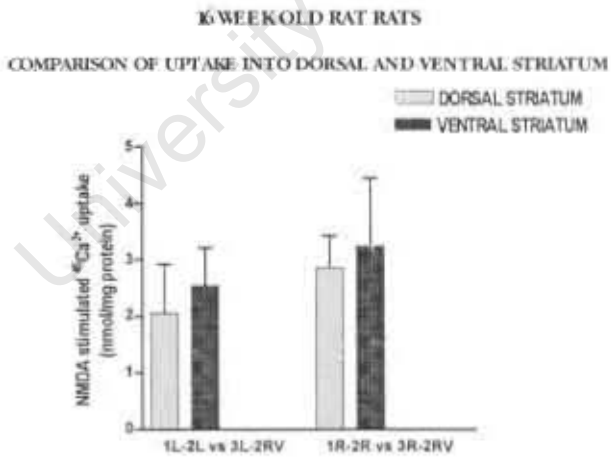

Figure 5.3c NMDA (100µM) stimulated $^{45}Ca^{2+}$ uptake into the dorsal and ventral striata of 16 week old rats (n=6). Stimulated $^{45}Ca^{2+}$ uptake into anterior dorsal and posterior ventral striata from the left hemisphere (1L-2L vs. 3L-2LV) and right hemisphere (1R-2R vs. 3R-2RV). There were no differences in stimulated $^{45}Ca^{2+}$ uptake between the dorsal and ventral striata (Student t-test ($p>0.05$) plus Bonferroni correction $p>0.025$). Data are reported as mean ± sem (nmol $^{45}Ca^{2+}$ /mg protein). Data are reported in Table 5.3b.

5.2.3 *Age effects on NMDA stimulated $^{45}Ca^{2+}$ uptake - 7 week vs. 16 week old rats*

To determine whether there were any age dependent changes in NMDA stimulated $^{45}Ca^{2+}$ uptake into striata, stimulated uptake into striata from rats aged 7 weeks (n=7) was compared with uptake into striata from rats aged 16 weeks (n=6). Results for the complete statistical analyses reported below are reported in Annex B.

5.2.3.1 Dorsal Striata – 7 week vs. 16 week old rats

In both the left and right hemispheres, stimulated $^{45}Ca^{2+}$ uptake into the anterior dorsal striata (1L-2L and 1R-2R) was significantly greater in 7 week old rats than in 16 week old rats (Table 5.4a, Figure 5.4a). In the posterior striata (3L-2L and 3R-2R), levels of stimulated $^{45}Ca^{2+}$ accumulation were also significantly higher in 7 week old rats than in 16 week old rats (Table 5.4a, Figure 5.4a). Results demonstrate that NMDA evoked significantly greater $^{45}Ca^{2+}$ uptake levels into dorsal striata of 7 week old rats compared with 16 week old rats. In addition to comparing stimulated uptake between the two age groups, basal unstimulated uptake was compared. In the left hemisphere mean uptake of 7 week old rats was 4.69 ± 0.39 nmol $^{45}Ca^{2+}$ /mg protein and 16 week old rats was 3.88 ± 0.65 nmol $^{45}Ca^{2+}$ /mg protein (Tables 5.2a and 5.3a, Figure 5.4b). In the right hemisphere the uptake for the 7 week and 16 week old rats was 4.7 ± 0.47 nmol $^{45}Ca^{2+}$ /mg protein and 4.06 ± 0.51 nmol $^{45}Ca^{2+}$ /mg protein respectively (Tables 5.2a and 5.3a, Figure 5.4b). Comparison of basal uptake into the dorsal striatum showed there was no significant difference between the two ages.

Table 5.4a NMDA (100μM) stimulated $^{45}Ca^{2+}$ into the dorsal striata of rats aged 7 weeks (n=7) and 16 weeks (n=6).

		$^{45}Ca^{2+}$ uptake into dorsal striatal sections (nmol $^{45}Ca^{2+}$ /mg protein)				
GROUP		1L-2L	± sem		1R-2R	± sem
7 WEEK OLD RATS	n=7	6.73 *	0.81		5.30 *	0.86
16 WEEK OLD RATS	n=6	2.07	0.86		2.86	0.57
		3L-2L	± sem		3R-2R	± sem
7 WEEK OLD RATS	n=7	4.35 *	0.61		5.73 *	0.72
16 WEEK OLD RATS	n=6	1.49	0.62		2.14	0.46

***Stimulated $^{45}Ca^{2+}$ uptake into striatal sections from 7 week old rats was significantly greater than stimulated $^{45}Ca^{2+}$ uptake into 16 week old rats (ANOVA, $p<0.05$). Data are reported as mean ± sem (nmol $^{45}Ca^{2+}$ /mg protein). Data are reported from Tables 5.2b and 5.3b.**

EFFECTS OF AGE ON NMDA STIMULATED $^{45}Ca^{2+}$ UPTAKE INTO DORSAL STRIATUM

UPTAKE OF 16 WEEK OLD RATS AND 7 WEEK OLD RATS

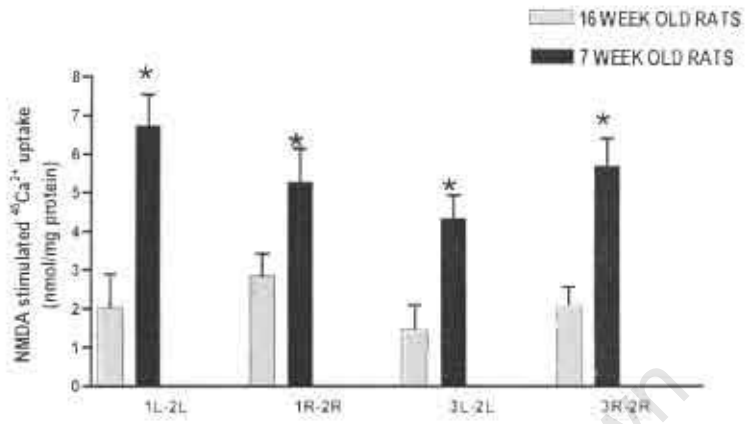

Figure 5.4a Comparison of the age effect on NMDA stimulated $^{45}Ca^{2+}$ uptake in the dorsal striata of 7 week (n=7) and 16 week old rats (n=6). There was significantly higher uptake measured in 7 week old rats when compared with 16 week old rats (ANOVA, $p<0.05$). Results are mean ± sem nmol $^{45}Ca^{2+}$ /mg protein. Data are reported in Table 5.4a.

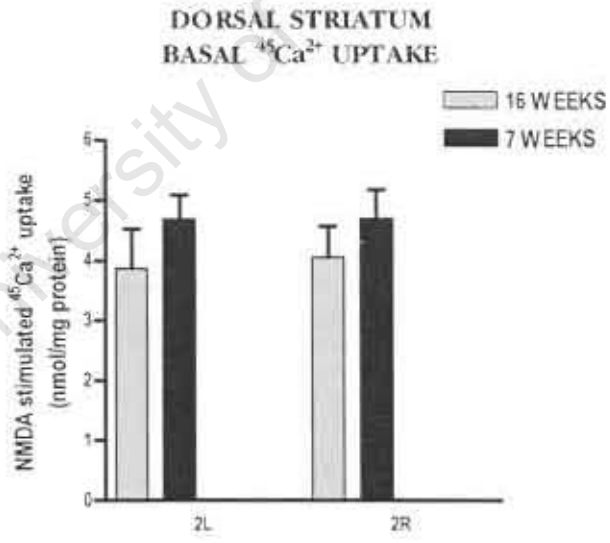

Figure 5.4b Basal $^{45}Ca^{2+}$ uptake into the dorsal striata from the left hemisphere (2L) and the right hemisphere (2R) of the 16 week and 7 week old rat was not significantly different (ANOVA, $p>0.05$). Results are mean ± sem nmol $^{45}Ca^{2+}$ /mg protein. Data are reported in Tables 5.2a and 5.3a.

5.2.3.1 Ventral Striata – 7 week and 16 week old rats

When the effect of age on NMDA stimulated $^{45}Ca^{2+}$ uptake was examined in the ventral striata for uptake into the anterior striata in both hemispheres, there was no significant difference in uptake into striata of 7 week old rats compared to uptake into striata of 16 week old rats (Table 5.4b, Figure 5.4c). The results of the uptake into right posterior ventral striata were similar as there was no difference between the two age groups (Table 5.4b, Figure 5.4c). However, there was significantly greater stimulated uptake into the left posterior striata of 7 week old rats compared to stimulated uptake in 16 week old rats (Table 5.4b, Figure 5.4c). Basal $^{45}Ca^{2+}$ uptake into the ventral striata was also compared. In the non-stimulated striata in the left hemisphere (2L), mean basal uptake into striata from a 7 week old rat was 4.48 ± 0.36 nmol $^{45}Ca^{2+}$ /mg protein and was 4.56 ± 0.55 nmol $^{45}Ca^{2+}$ /mg protein into striata from 16 week old rat. The results show that in the left hemisphere, there was no difference in basal uptake (Tables 5.2a and 5.3a, Figure 5.4d). In the right hemisphere the basal uptake for the 7 week and 16 week old rats was 4.80 ± 0.55 nmol $^{45}Ca^{2+}$ /mg protein and 4.55 ± 0.68 nmol $^{45}Ca^{2+}$ /mg protein respectively (Tables 5.2a and 5.3a, Figure 5.4d). In both hemispheres there was no significant difference in basal uptake into the ventral striata between the two ages.

Table 5.4b NMDA (100µM) stimulated $^{45}Ca^{2+}$ uptake into the ventral striata of rats aged 7 weeks (n=7) and 16 weeks (n=6).

GROUP		1L-2L Means	SEM		1R-2R Means	SEM
7 WEEK OLD	n=7	6.89	1.41		5.85	1.49
16 WEEK OLD	n=6	3.53	0.62		3.99	0.75
		3L-2L Means	SEM		3R-2R Means	SEM
7 WEEK OLD	n=7	7.34 *	1.43		5.52	1.10
16 WEEK OLD	n=6	2.55	0.66		3.24	1.21

There was no significant difference in uptake measured between the two groups except in the posterior striata of the left hemisphere where uptake from 7 week old rats was significantly greater than uptake into 16 week old rats (*) (ANOVA, $p<0.05$). Results are mean ± sem nmol $^{45}Ca^{2+}$ /mg protein. Data are reported from Tables 5.2b and 5.3b.

EFFECTS OF AGE ON NMDA STIMULATED $^{45}Ca^{2+}$ UPTAKE INTO VENTRAL STRIATUM

UPTAKE OF 16 WEEK OLD RATS AND 7 WEEK OLD RATS

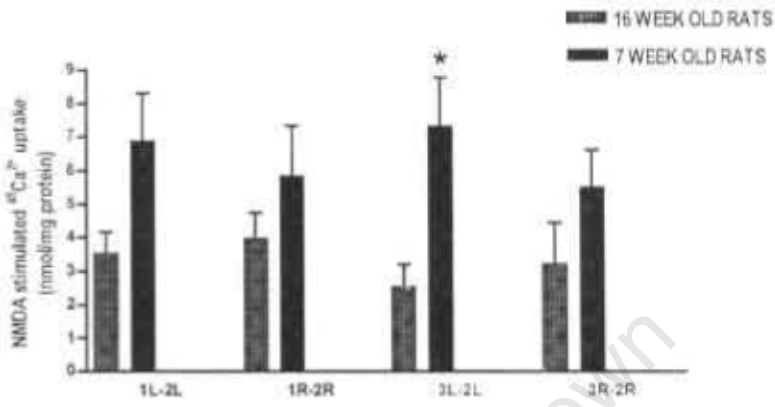

Figure 5.4c Age effect on stimulated $^{45}Ca^{2+}$ uptake into the ventral striata. 7 week old rats were compared with 16 week old rats. There was significantly higher uptake measured into the posterior striatum of the left hemisphere in 7 week old rats compared to the 16 week old rats (*)(ANOVA, $p<0.05$). Results are mean ± sem nmol $^{45}Ca^{2+}$ /mg protein. Data are reported in Table 5.4b.

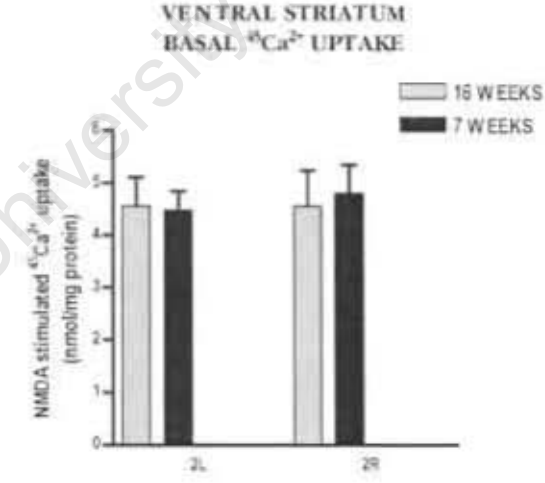

Figure 5.4d Basal $^{45}Ca^{2+}$ uptake into ventral striata of 7 week and 16 week old rats. Basal $^{45}Ca^{2+}$ uptake into the ventral striata from the left hemisphere (2L) or the right hemisphere (2R) between the 16 week and 7 week old rat was not significantly different (ANOVA, $p>0.05$). Results are mean ± sem nmol $^{45}Ca^{2+}$ /mg protein. Data are reported in Tables 5.2a and 5.3a.

5.3 EFFECTS OF DOPAMINE DEPLETION BY 6-OHDA LESIONING ON $^{45}Ca^{2+}$ UPTAKE

5.3.1 Verification of position of infusion needle at target lesion site

To obtain a visual representation of the position of the infusion needle at the MFB target lesion site during surgery, histology of the infusion needle at the target site was obtained from cresyl violet stained coronal sections. The slides were used to map the position of the needle tip onto Paxinos and Watson atlas (2004) diagrams as presented below. Table 5.5a shows the co-ordinates used to map the position of the needle infusion within each rat. Data are presented from n=8 rats as sections from n=2 rats were washed from slides during the cresyl violet staining procedure. Figure 5.5a shows half the atlas diagram of a coronal section of a rat brain with the MFB 4.70 mm relative to the interaural line (Paxinos and Watson, 1986) juxtaposed with half a cresyl violet stained coronal section that corresponds approximately with the anterior posterior region and shows the position of the needle tip. The needle tip position appears medial to the target MFB site. Figures 5.5b and 5.5c show that in half of the rats (n=4), the needle tips were positioned ≈ 0.06 - 0.14 mm posterior to the intended target site that lies 4.70 mm anterior to the interaural line (Paxinos and Watson, 1986).* The needle tip was placed at AP 4.56 mm in n=2 rats (rat M13 and rat O20) and at AP 4.64 mm in n=2 rats (rat O17 and O19). The position of the needle in n=4 rats was = 0.1 – 0.46 mm anterior to AP 4.70 mm relative to the interaural line (Figures 5.5d-5.5g). Data obtained from the cresyl violet stained sections show that the needle was placed at variable anterior posterior positions from the target co-ordinates of the MFB.

Table 5.5a Co-ordinates used for mapping the position of the infusion needle targeting of the medial forebrain bundle (MFB).

		CO-ORDINATES		
RAT	WEIGHT	**ANTERIOR POSTERIOR** Relative to the interaural line **(AP) (mm)**	**MEDIO-LATERAL** Relative to the midline **(ML) (mm)**	**DORSO-VENTRAL** From dura **(DV) (mm)**
M13	310g	4.56 mm	1.6	7.8
M15	368g	4.92 mm	1.5	78
N13	372g	4.80 mm	1.4	8.0
N14	357g	5.16 mm	1.4	7.8
N15	338g	5.04 mm	1.3	8.0
O17	353g	4.64 mm	1.5	9.0
O18	349g	4.92 mm	1.2	7.8
O19	330g	4.64 mm	1.0	7.9

* The lesion co-ordinates were obtained using Paxinos and Watson (1986). However, diagrams from Paxinos and Watson (2004) contain better representation of serial sections containing the MFB and were more suitable for purposes of mapping.

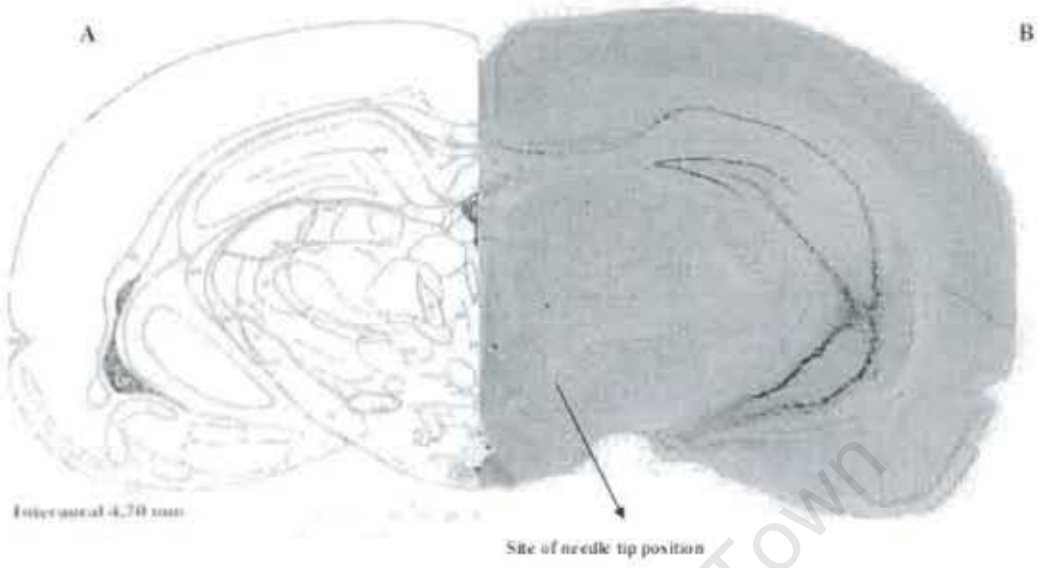

Figure 5.5a (A) shows the MFB (encircled in red) 4.70 mm anterior to the interaural line (Paxinos & Watson, 1986). (B) Part of cresyl violet stained section = 4.70 mm anterior to the interaural line. Position of the needle tip from this section appears medial to the intended MFB target site within the left hemisphere.

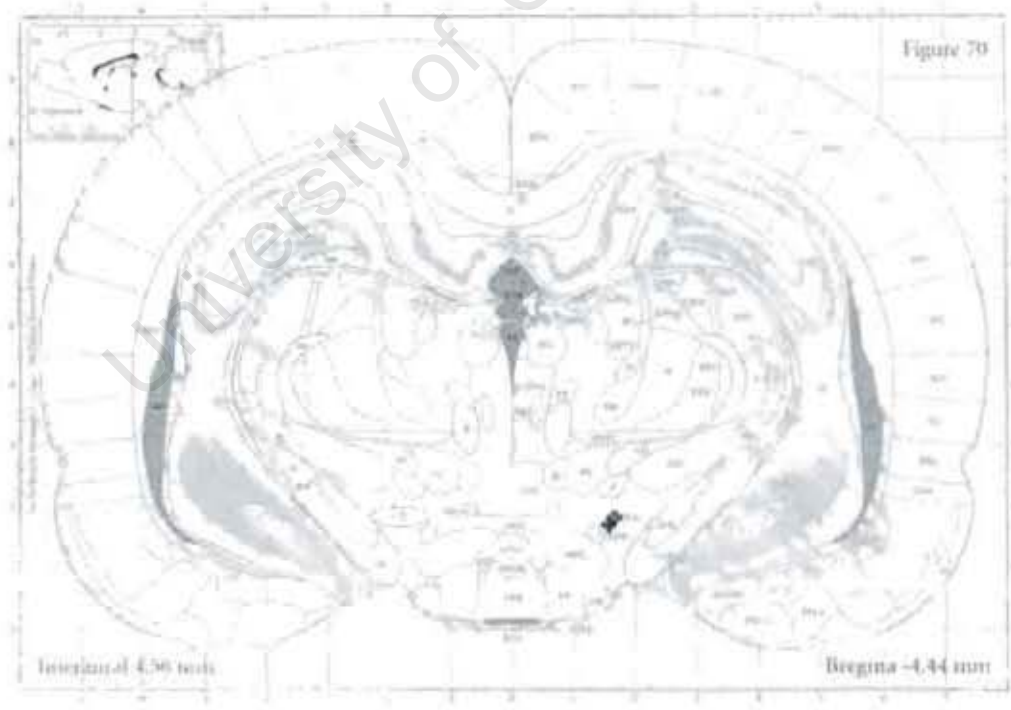

Figure 5.5b. Mapping of the position of the infusion needle targeting the MFB (Paxinos and Watson, 2004). Diagram shows MFB 4.56 mm anterior to the interaural line. Position of the needle tip is mapped onto the right hemisphere to allow comparison with the left hemisphere as the MFB (encircled in red ring) is identified in the left hemisphere on the atlas diagram. Positions of the needle tips are presented by quad arrows coloured blue (rat M13) and red (rat O20).

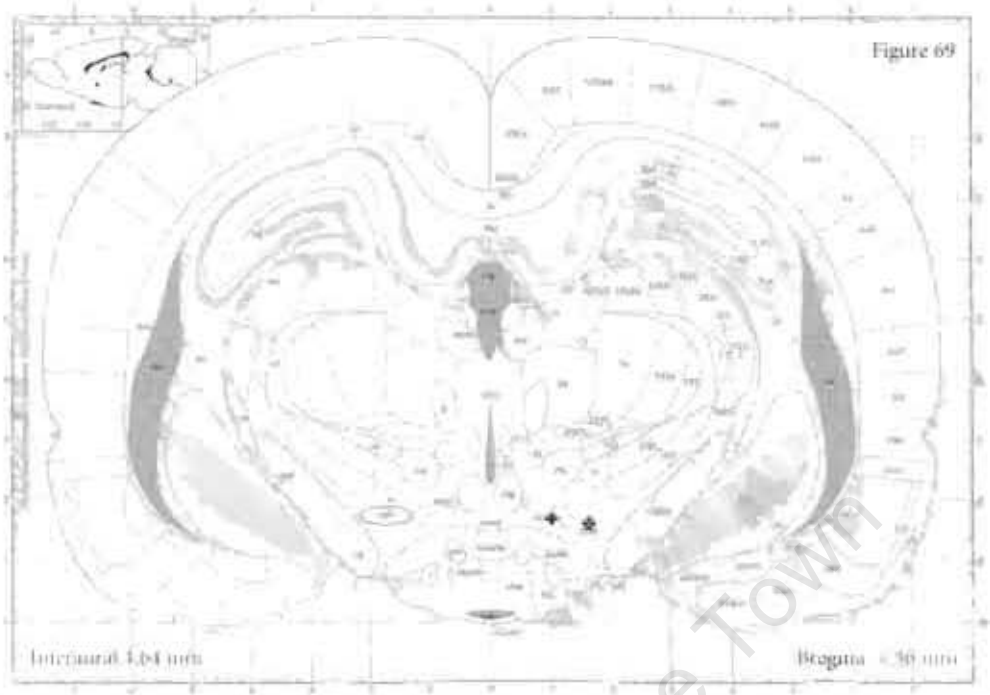

Figure 5.5c. Mapping of the position of the infusion needle targeting the MFB (Paxinos and Watson, 2004). Diagram shows MFB 4.64 mm anterior to the interaural line. Position of the needle tip is mapped onto the right hemisphere to allow comparison with the left hemisphere as the MFB (encircled in red ring) is identified in the left hemisphere on the atlas diagram. Positions of the needle tips are presented by quad arrows coloured blue (rat O19) and red (rat O17).

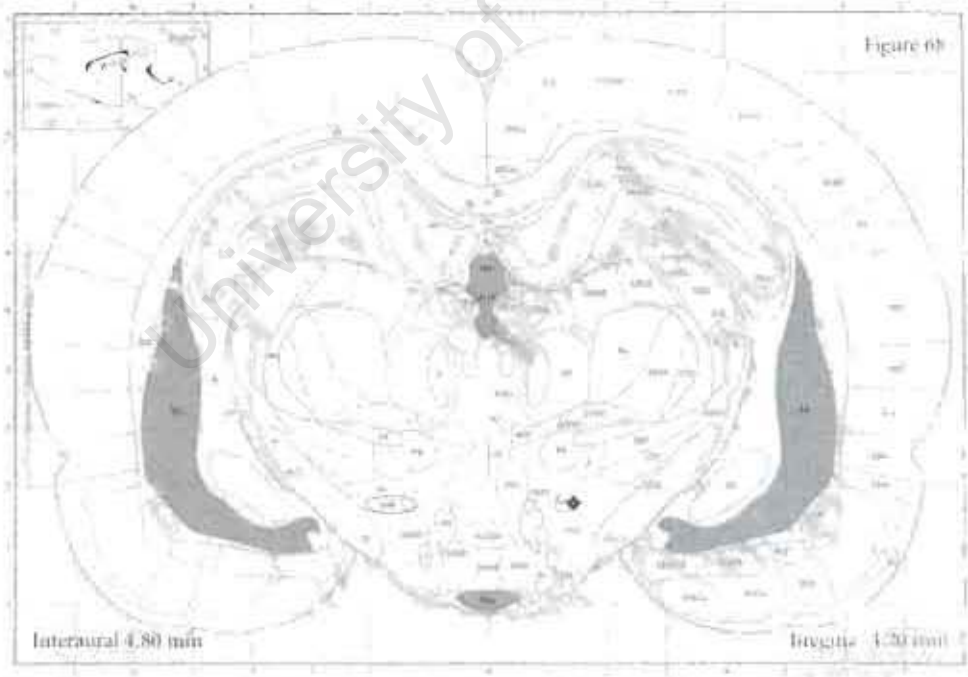

Figure 5.5d. Mapping of the position of the infusion needle targeting the MFB (Paxinos and Watson, 2004). Diagram shows MFB 4.80 mm anterior to the interaural line. Position of the needle tip is mapped onto the right hemisphere to allow comparison with the left hemisphere as the MFB (encircled in red ring) is identified in the left hemisphere on the atlas diagrams. Position of the needle tip is presented by quad arrow coloured red (rat N13).

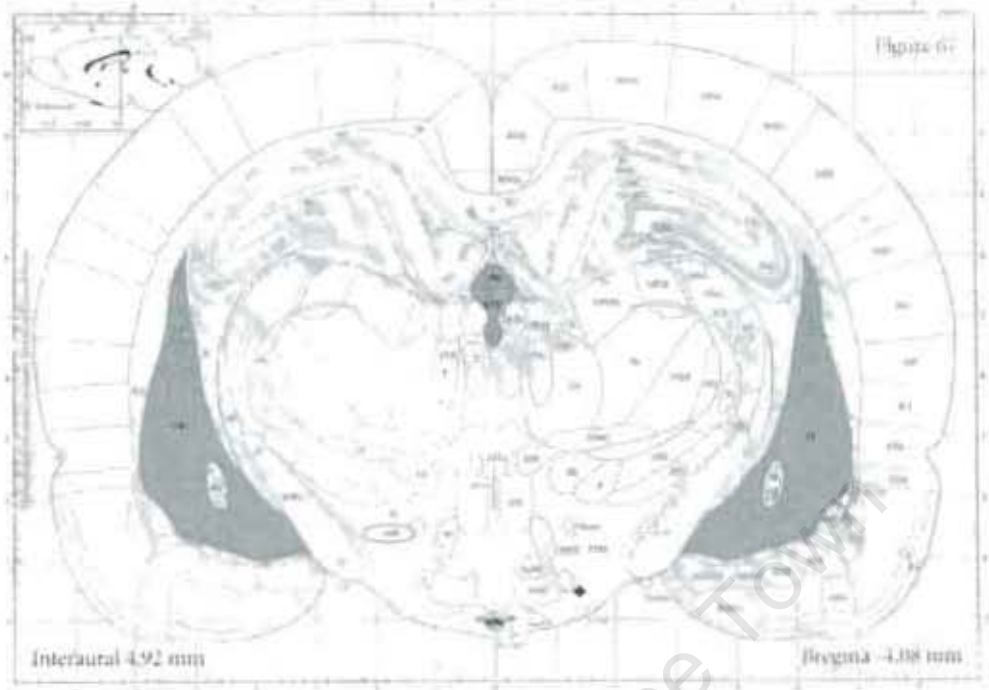

Figure 5.5e. Mapping of the position of the infusion needle targeting the MFB (Paxinos and Watson, 2004). Diagram shows MFB 4.92 mm anterior to the interaural line. Position of the needle tip is mapped onto the right hemisphere to allow comparison with the left hemisphere as the MFB (encircled in red ring) is identified in the left hemisphere on the atlas diagram. Position of the needle tip is presented by red coloured quad arrow (rat O18).

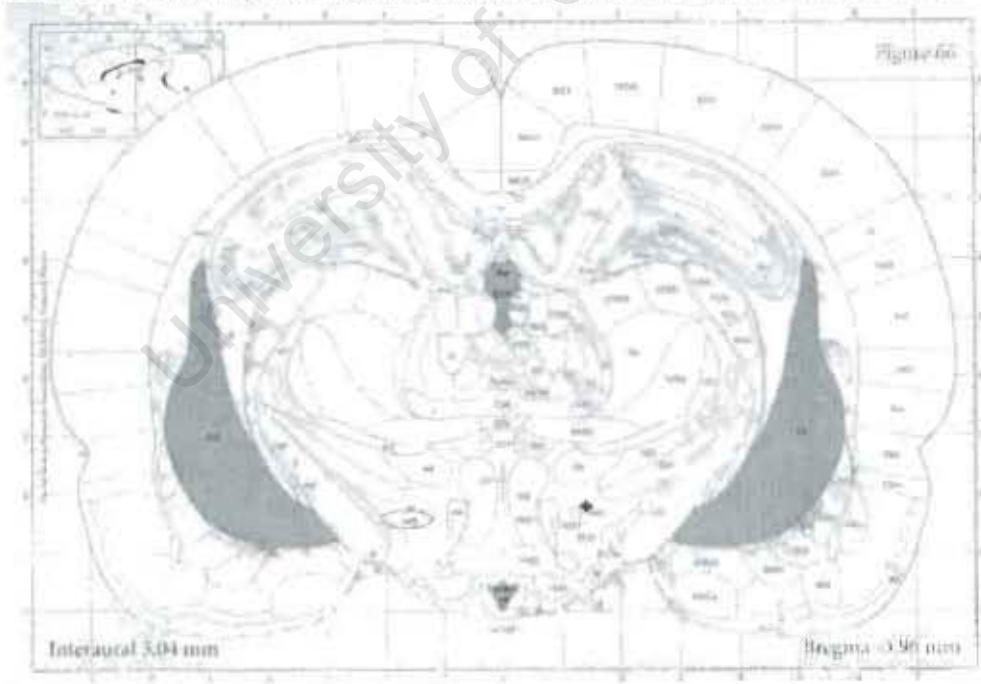

Figure 5.5f. Mapping of the position of the infusion needle targeting the MFB (Paxinos and Watson, 2004). Diagram shows MFB 5.04 mm anterior to the interaural line. Position of the needle tip is mapped onto the right hemisphere to allow comparison with the left hemisphere as the MFB (encircled in red ring) is identified in the left hemisphere on the atlas diagram. Position of the needle tip is presented by red coloured quad arrow (rat N15).

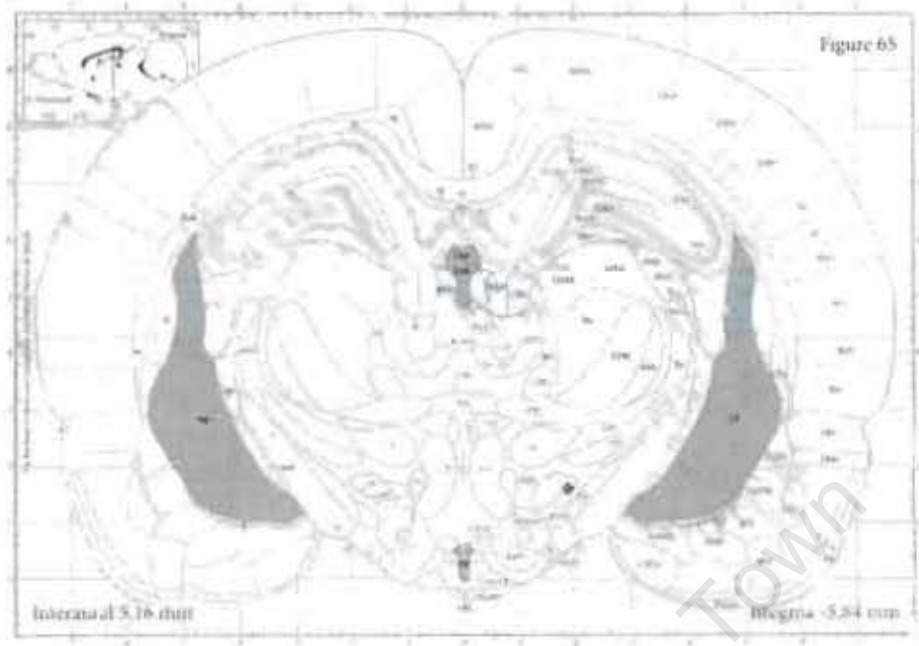

Figure 5.5g. Mapping of the position of the infusion needle targeting the MFB (Paxinos and Watson, 2004). Diagram shows MFB 5.16 mm anterior to the interaural line. Position of the needle tip is mapped onto the right hemisphere to allow comparison with the left hemisphere as the MFB (encircled in red ring) is identified in the left hemisphere on the atlas diagram. Position of the needle tip is presented by red coloured quad arrow (rat N14).

5.3.2 *Behavioural Assessment – Apomorphine induced rotations*

Results for the complete statistical analyses reported below are reported in Annex B. Tables 5.6a and 5.6b show the number of rotations conducted in response to apomorphine by sham lesioned (n=14) and 6-OHDA lesioned (n=17) rats respectively. From Table 5.6a, n=9 sham lesioned rats conducted <100 ipsilateral rotations while n=5 rats conducted <50 contralateral rotations. All sham lesioned rats were selected for further study. Apomorphine induced >100 complete contralateral* rotations in n=14 rats lesioned with 6-OHDA, with n=1 rat conducting <100 contralateral rotations. Ipsilateral rotations were conducted by n=2 6-OHDA lesioned rats (Table 5.6b). 6-OHDA lesioned rats, conducting >100 contralateral rotations (n=12) were selected for NMDA stimulated $^{45}Ca^{2+}$ uptake study while n=2 were selected for tyrosine hydroxylase study. One 6-OHDA lesioned rat conducting ipsilateral rotations was selected for tyrosine hydroxylase study. The remaining 2 rats not conducting >100 contralateral rotations were removed from further study. Figure 5.6 shows the average number of rotations made by 6-OHDA lesioned (n=14) and sham lesioned (n=14) rats selected for further study in the calcium uptake assay.

Table 5.6a Table shows the number of apomorphine (0.5 mg / kg) induced rotations conducted by individual sham lesioned rats (n=14).

RAT	LESION TYPE	1/4 ROTATIONS	COMPLETE ROTATIONS	SELECTED FOR $^{45}Ca^{2+}$ UPTAKE STUDY
K6	sham	+16	+4	selected
K7	sham	+0	+0	selected
K8	sham	+45	+11	selected
M8	sham	-220	-55	selected
M9	sham	-303	-75	selected
M10	sham	+26	+0.5	selected
M11	sham	-278	-69	selected
M12	sham	-22	-6	selected
O11	sham	-91	-23	selected
O12	sham	127	+32	selected
O13	sham	-134	-34	selected
O14	sham	-157	-39	selected
O15	sham	-12	-3	selected
O16	sham	-80	-20	selected

(-) rotations represent ipsilateral rotations and (+) rotations represent contralateral rotations. Sham lesioned rats exhibited predominantly complete ipsilateral rotations, however; n=3 rats conducted <100 contralateral rotations. All sham lesioned rats were selected for further study.

* Contralateral indicates the rats were turning to the right away from their left lesioned hemisphere. Turning towards the lesioned hemisphere is referred to as ipsilateral rotational movement.

Table 5.6b Table showing the number of apomorphine (0.5 mg / kg) induced rotations conducted by individual 6-OHDA lesioned rats (n=17).

RAT	LESION TYPE	1/4 ROTATIONS	COMPLETE ROTATIONS	SELECTED FOR $^{45}Ca^{2+}$ UPTAKE ASSAY STUDY
K1	6-OHDA	+ 1419	+ 355	selected
K2	6-OHDA	+ 1950	+ 488	selected
K3	6-OHDA	+ 1341	+ 335	selected
K4	6-OHDA	+ 453	+ 113	selected
K5	6-OHDA	+ 760	+ 190	selected
M1	6-OHDA	+ 1104	+ 276	selected
M2	6-OHDA	+ 595	+ 149	selected
M3	6-OHDA	-402	-101	*not selected*
M4	6-OHDA	+ 208	+ 52	*not selected*
M5	6-OHDA	+ 1700	+ 425	selected
M6	6-OHDA	+ 707	+ 176	selected
O1	6-OHDA	+ 705	+ 176	selected
O2	6-OHDA	+ 1977	+ 494	selected
O4	6-OHDA	-197	-49	*not selected*
O5	6-OHDA	+ 1022	+ 256	selected
O7	6-OHDA	+ 648	+ 162	selected
O10	6-OHDA	+ 1872	+ 468	selected

(-) rotations represent ipsilateral rotations and (+) rotations represent contralateral rotations. 6-OHDA lesioned rats conducted predominantly contralateral rotations though n=2 rats conducted ipsilateral rotations. Table shows the rats selected for further study on the basis of completing >100 complete rotations.

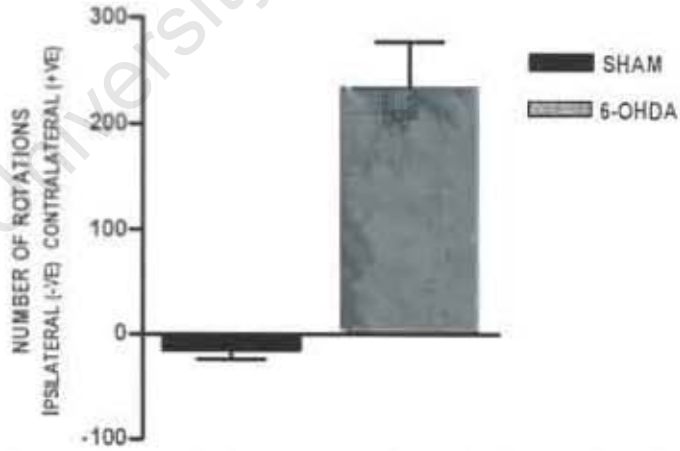

Figure 5.6 Apomorphine (0.5 mg / kg) induced rotations exhibited by 6-OHDA lesioned and sham lesioned rats that were selected for further study. Contralateral rotations are positive on the y-axis and ipsilateral rotations are negative. Sham lesioned rats conducted 19 ± 8 ipsilateral rotations. Selected 6-OHDA lesioned rats conducted 233 ± 43 contralateral rotations. Results are mean ± sem rotations. Data are reported in Tables 5.6a and 5.6b.

5.3.3 Extent of degeneration – *Immunocytochemistry*

Immunocytochemistry conducted on a sagittal section of the brain stained for the dopamine synthesis - regulating enzyme, tyrosine hydroxylase, highlights the dopamine concentrated areas of the basal ganglia. The dopamine fibres originate from the neurons of the midbrain and traverse the MFB to the striatum (Figure 5.7a). Figure 5.7b shows sections obtained from rats that had undergone apomorphine - induced rotations. The sham lesioned rat conducted 55 ipsilateral rotations and stained positive for tyrosine hydroxylase in the midbrain (SNc/VTA) and in the striatum in both hemispheres (Figure 5.7bi). 6-OHDA induced degeneration of dopamine producing neurons of the midbrain in the left lesioned hemisphere, resulting in lack of tyrosine hydroxylase (Figure 5.7bii). The 6-OHDA lesioned rat conducted 381 complete contralateral rotations. Figure 5.7biii shows tyrosine hydroxylase in 6-OHDA lesioned rat with partial degeneration of the left medial midbrain. The lesioned rat conducted 104 complete ipsilateral rotations. Degeneration of neurons in the midbrain SNc and the VTA (Figure 5.7b) from infusion of 6-OHDA into the MFB demonstrates retrograde degeneration. Lack of tyrosine hydroxylase staining in the striatum (Figures 5.7c and 5.7d) demonstrates anterograde degeneration.

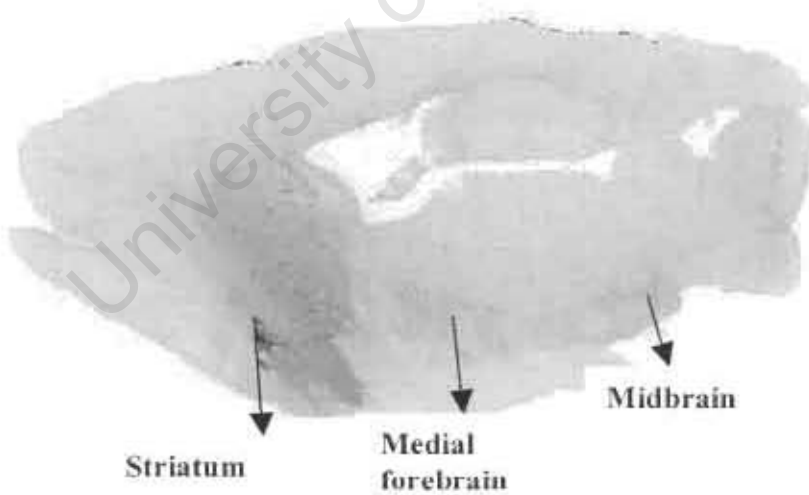

Figure 5.7a Sagittal section of Long Evans rat brain stained for tyrosine hydroxylase highlights the dopamine concentrated areas within the basal ganglia: the midbrain, medial forebrain bundle (MFB) and the striatum. Section corresponds approximately to 2.40mm relative to the midline Paxinos & Watson (1986).

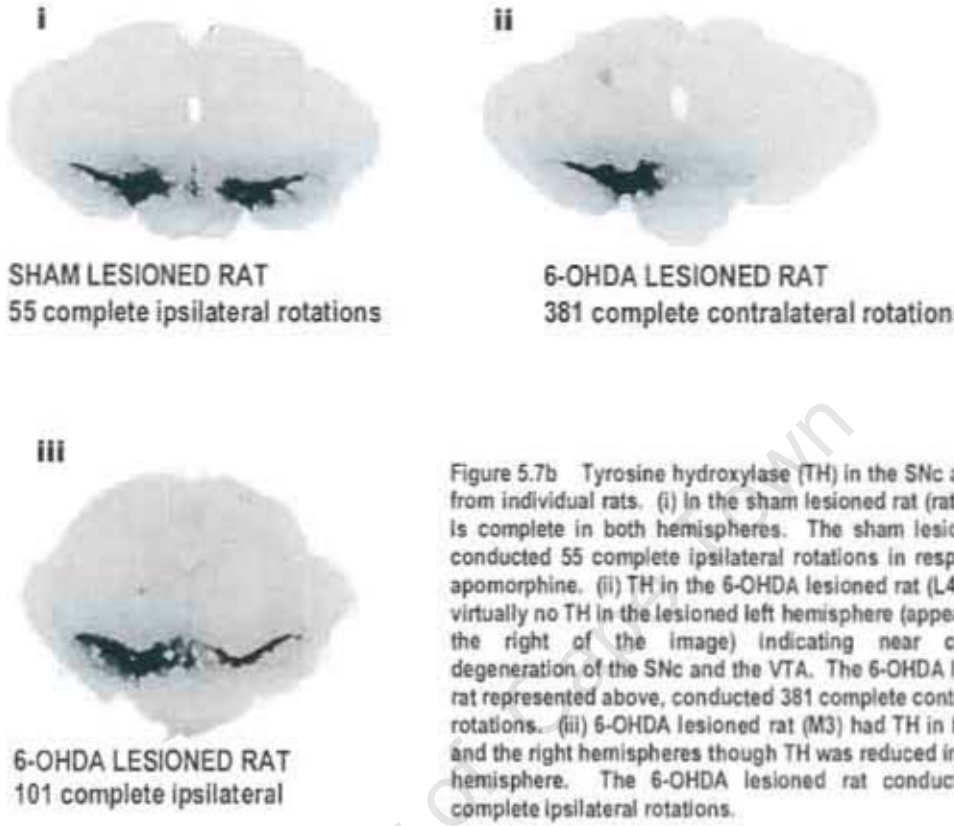

Figure 5.7b Tyrosine hydroxylase (TH) in the SNc and VTA from individual rats. (i) In the sham lesioned rat (rat M8) TH is complete in both hemispheres. The sham lesioned rat conducted 55 complete ipsilateral rotations in response to apomorphine. (ii) TH in the 6-OHDA lesioned rat (L4) shows virtually no TH in the lesioned left hemisphere (appearing on the right of the image) indicating near complete degeneration of the SNc and the VTA. The 6-OHDA lesioned rat represented above, conducted 381 complete contralateral rotations. (iii) 6-OHDA lesioned rat (M3) had TH in both left and the right hemispheres though TH was reduced in the left hemisphere. The 6-OHDA lesioned rat conducted 101 complete ipsilateral rotations.

Tyrosine hydroxylase staining of the striatum, 5 weeks post surgery confirmed degeneration to have been complete within the striatum at the time that the $^{45}Ca^{2+}$ uptake assays were conducted. Figures 5.7c and 5.7d show stained coronal sections representative of the anterior (1L and 1R), intermediate (2L and 2R) and posterior (3L and 3R) striata of sham and 6-OHDA lesioned rats used for the NMDA stimulated $^{45}Ca^{2+}$ uptake assay. In the sham lesioned rats, tyrosine hydroxylase was complete in both the sham lesioned left and the right hemispheres. Following complete 6-OHDA lesions, dopamine loss was uniform throughout the dorsal and ventral striata from anterior to posterior regions in rats that had completed >100 complete contralateral rotations. In 6-OHDA lesioned rat that had conducted <100 complete contralateral rotations, tyrosine hydroxylase is partially reduced in the ventral striatum and in the dorsomedial striatum (Figures 5.7c and 5.d).

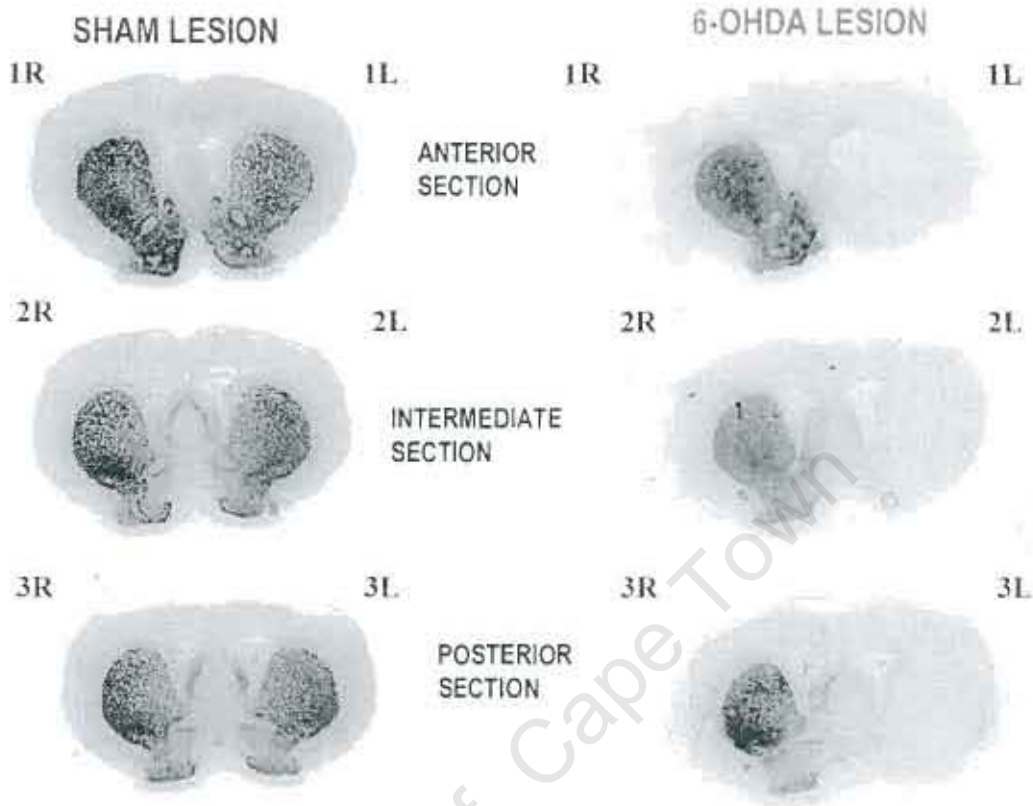

Figure 5.7c Representative serial coronal sections of rat brain showing dopamine terminals stained for tyrosine hydroxylase within striata. The serial sections were from sham lesioned (on the left) and 6-OHDA lesioned rats (on the right). Lack of tyrosine hydroxylase staining in the left hemisphere of the 6-OHDA lesioned rats (1L, 2L, 3L) confirms near complete dopamine loss following 6-OHDA injection into the MFB. These sections show that in the 6-OHDA lesioned rats dopamine loss in the left hemisphere was uniform from the anterior to the posterior striatum. These sections are representative of the sections of the anterior, intermediate and posterior striata from which the dorsal striata were dissected for NMDA stimulated $^{45}Ca^{2+}$ uptake studies. Below are serial coronal sections from a 6-OHDA lesioned rat with partial striatal degeneration. Tyrosine hydroxylase is partially reduced in the dorsal medial striatum of the lesioned left hemisphere.

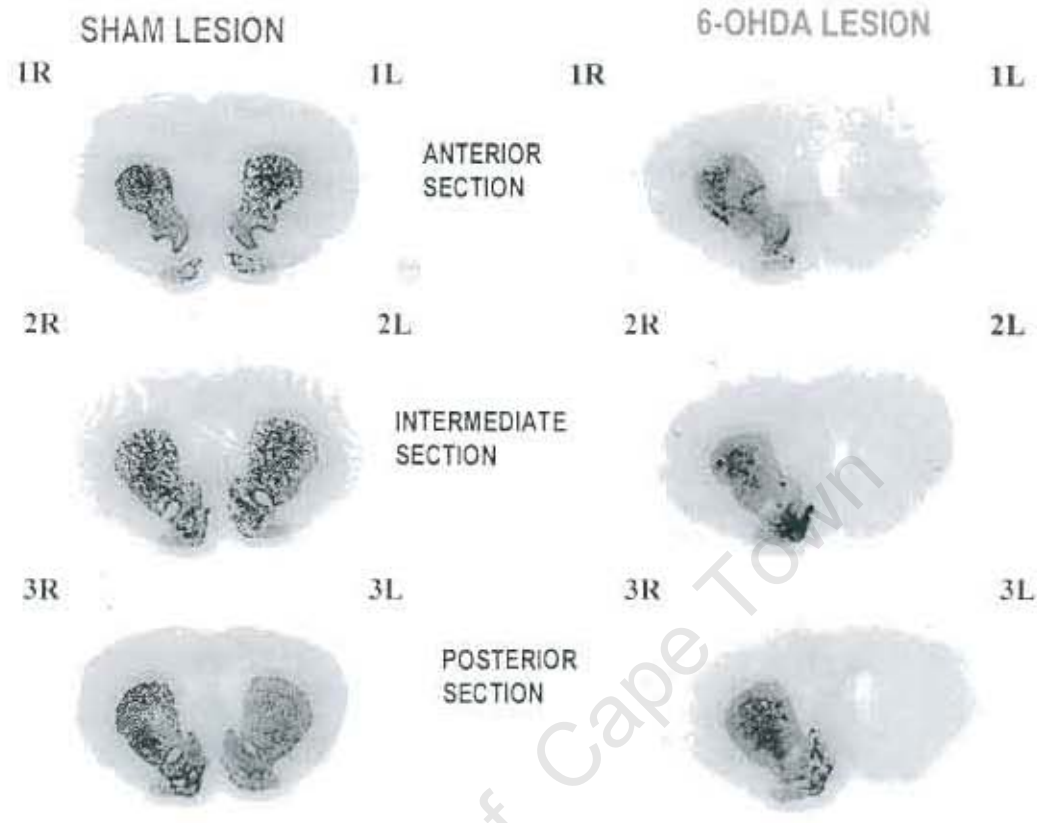

Figure 5.7d Representative serial coronal sections of rat brain showing dopamine terminals stained for tyrosine hydroxylase within ventral striata. The serial sections were from sham lesioned rat M8 (on the left) and 6-OHDA lesioned rats (on the right). Lack of tyrosine hydroxylase staining in the left hemisphere of the 6-OHDA lesioned rats (1L, 2L, 3L) confirms near complete dopamine loss following 6-OHDA injection into the MFB. These sections show that in the 6-OHDA lesioned rats dopamine loss in the left hemisphere was uniform from the anterior to the posterior striatum. These sections are representative of the sections of the anterior, intermediate and posterior ventral striata from which ventral striata were dissected for NMDA stimulated $^{45}Ca^{2+}$ uptake studies. Below are serial coronal sections from a 6-OHDA lesioned rat with partial striatal degeneration. Tyrosine hydroxylase in the ventral striata is partially reduced in the left striatum.

5.3.4 NMDA STIMULATED $^{45}Ca^{2+}$ UPTAKE

5.3.4.1 *NMDA stimulation increases $^{45}Ca^{2+}$ uptake into SHAM lesioned rats*

5.3.4.1.1 Dorsal striatum – SHAM lesioned rats

Results for the complete statistical analyses reported below are reported in Annex B. In the sham lesioned rats, the anterior (1L and 1R) and posterior (3L and 3R) striatal sections incubated in NMDA (100µM) had significantly greater $^{45}Ca^{2+}$ accumulation above the basal $^{45}Ca^{2+}$ accumulation in non-stimulated striatal section (2L and 2R) (Table 5.7a, Figure 5.8a). The basal $^{45}Ca^{2+}$ uptake into the anterior striatum of the left hemisphere (2L) was not different from basal $^{45}Ca^{2+}$ uptake into the striata of the right hemisphere (2R) (Table 5.7a, Figure 5.8a). NMDA (100 µM) significantly increased $^{45}Ca^{2+}$ uptake dorsal striatal sections in sham lesioned rats.

Table 5.7a Total $^{45}Ca^{2+}$ uptake into dorsal and ventral striata of SHAM lesioned rats (n=9).

		$^{45}Ca^{2+}$ uptake into striatal sections (nmol $^{45}Ca^{2+}$ /mg protein)					
STRIATAL REGION		1L	1R	2L	2R	3L	3R
DORSAL STRIATUM	n=9	10.10 ± 0.93 *	9.38 ± 0.97 *	6.56 ± 0.61	5.89 ± 0.63	9.69 ± 0.89 *	10.09 ± 1.12 *
VENTRAL STRIATUM	n=5	8.22 ± 1.11 *	7.95 ± 1.59 *	3.29 ± 0.59	3.29 ± 0.69	7.78 ± 1.48 *	8.11 ± 1.13 *

*NMDA significantly increased total $^{45}Ca^{2+}$ uptake into anterior and posterior striata compared to basal uptake (Student t-test ($p<0.05$) plus Bonferroni correction $p<0.025$). Data are reported as mean ± sem (nmol $^{45}Ca^{2+}$ /mg protein).

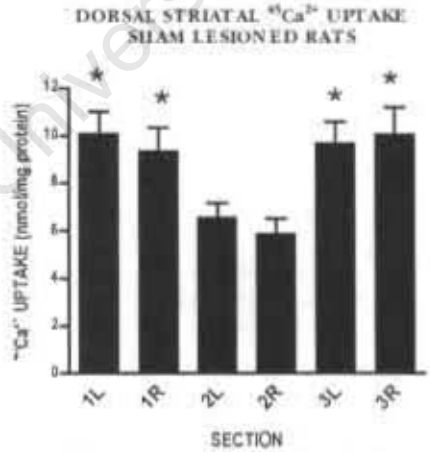

Figure 5.8a In the SHAM lesioned rats (n=9), the NMDA (100µM) stimulated slices, anterior slices (1L and 1R) and posterior slices (3L and 3R) showed significantly greater $^{45}Ca^{2+}$ uptake in dorsal striatum than the basal uptake of control sections (2L and 2R) incubated in normal buffered ACSF (Student t-test ($p<0.05$) plus Bonferroni correction $p<0.025$)Results are mean ± sem nmol $^{45}Ca^{2+}$ /mg protein. Data are reported in Table 5.7a.

NMDA stimulated $^{45}Ca^{2+}$ uptake was calculated as previously described (section 6.1) by subtracting the basal uptake from the total uptake. Stimulated $^{45}Ca^{2+}$ uptake into the anterior striata (1L-2L) and uptake into the posterior striata (3L-2L) of the left hemisphere showed no statistical difference (Table 5.7b, Figure 5.8b). Results of stimulated $^{45}Ca^{2+}$ uptake in the right hemisphere between the anterior and posterior striata were similar; there was no statistical difference between uptake in the anterior (1R-2R) and in the posterior (3R-2R) striata (Table 5.6b, Figure 5.6b). Analysis of stimulated uptake between hemispheres, showed that stimulated $^{45}Ca^{2+}$ uptake into the anterior striata of the left hemisphere (1L-2L) was not different from uptake into the anterior striata of the right hemisphere (1R-2R) (Table 5.7b, Figure 5.8c). Similarly, stimulated $^{45}Ca^{2+}$ uptake into the posterior striata (3L-2L and 3R-2R) was not different (Table 5.7b, Figure 5.8c).

Table 5.7b NMDA stimulated $^{45}Ca^{2+}$ uptake into dorsal and ventral striata of SHAM lesioned rats.

	$^{45}Ca^{2+}$ uptake into striatal sections (nmol $^{45}Ca^{2+}$ /mg protein)				
SHAM		1L-2L	± sem	1R-2R	± sem
DORSAL STRIATA	n=9	3.54	0.66	3.49	0.57
VENTRAL STRIATA	n=5	4.93	0.71	4.66	1.28
SHAM		3L-2L	± sem	3R-2R	± sem
DORSAL STRIATA	n=9	3.12	0.57	4.20	0.93
VENTRAL STRIATA	n=5	4.49	1.18	4.82	0.61

Measurements of NMDA stimulated $^{45}Ca^{2+}$ uptake into anterior sections from the left (1L-2L) and right (1R-2R) hemispheres and into posterior striatal sections from the left (3L-2L) and right (3R-2R) hemispheres. There were no significant differences in uptake measured between the two groups. (Student t-test ($p>0.05$) plus Bonferroni correction $p>0.025$). Data are reported as mean ± sem (nmol $^{45}Ca^{2+}$ /mg protein).

SHAM LESIONED RATS

$^{45}Ca^{2+}$ UPTAKE ANTERIOR AND POSTERIOR STRIATUM WITHIN EACH HEMISPHERE

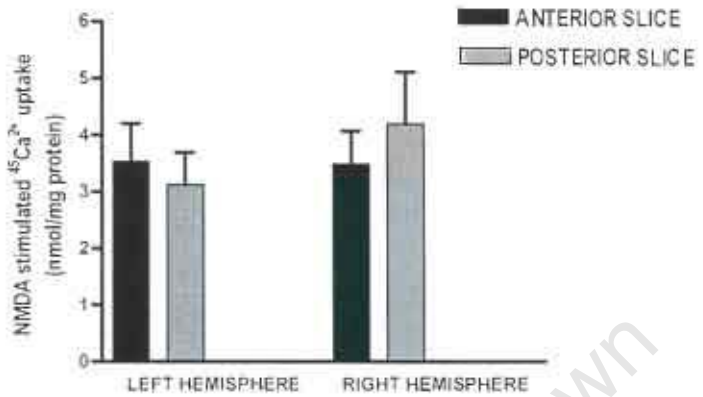

Figure 5.8b Within each hemisphere of the SHAM lesioned rat NMDA stimulated uptake was compared between the anterior and posterior dorsal striatum. There was no significant difference in uptake between the anterior striatum and the posterior striatum in both hemispheres (student t-test, $p>0.05$). Results are mean ± sem nmol $^{45}Ca^{2+}$ /mg protein (n=9). Data are reported in Table 5.7b.

SHAM LESIONED RATS

$^{45}Ca^{2+}$ UPTAKE INTO LEFT AND RIGHT HEMISPHERES

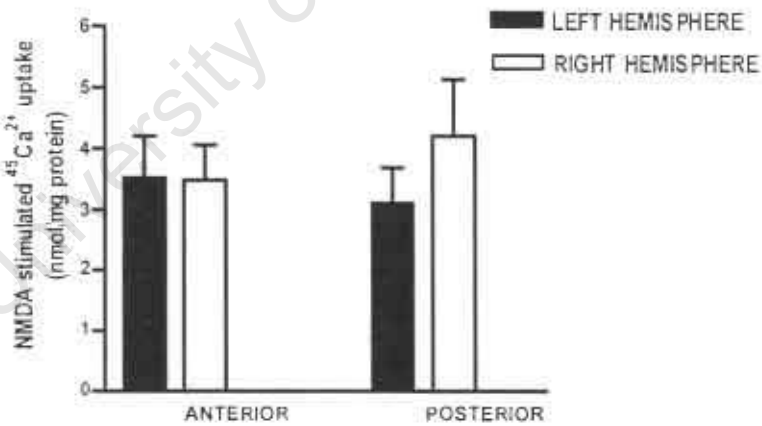

Figure 5.8c NMDA stimulated $^{45}Ca^{2+}$ uptake into the dorsal striata comparing the left lesioned vs. right unlesioned hemisphere SHAM lesioned rats (n=9). There was no significant difference in uptake between the lesioned and unlesioned hemisphere (student t-test, $p<0.05$). Results are mean ± sem nmol $^{45}Ca^{2+}$ /mg protein. Data are reported in Table 5.7b and represented in Figure 5.8b.

5.3.4.1.2 *Ventral striatum – SHAM lesioned rats*

Total uptake into the ventral striata of SHAM lesioned rats was measured in n=5 rats. In the left and the right hemispheres of the sham lesioned rats, total $^{45}Ca^{2+}$ uptake into anterior (1L and 1R) and posterior (3L and 3R) ventral striata was significantly greater than basal uptake (2L and 2R) (Table 5.8a, Figure 5.8d). Stimulated $^{45}Ca^{2+}$ uptake into the anterior (1L-2L) and posterior (3L-2L) ventral striata showed no significant difference within the left hemisphere nor was there a significant difference between the anterior (1R-2R) and posterior (3R-2R) striata of the right hemisphere (Table 5.6b). The stimulated $^{45}Ca^{2+}$ uptake into the anterior striata of the left (1L-2L) and right (1R-2R) hemispheres was not different (Table 5.7b). Stimulated $^{45}Ca^{2+}$ uptake into the posterior striata (3L-2L and 3R-2R) was also not different (Table 5.7b).

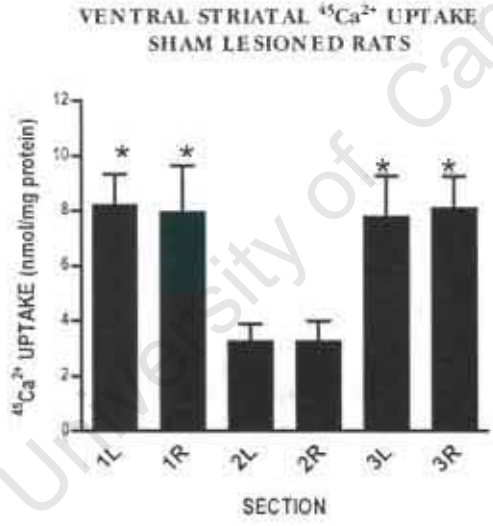

Figure 5.8d Total $^{45}Ca^{2+}$ uptake into ventral striata of SHAM lesioned rats (n=5). *NMDA (100μM) stimulated significant uptake into anterior (1L and 1R) and posterior striata (3L and 3R) above basal $^{45}Ca^{2+}$ uptake into non-stimulated striata (2L and 2R). Results are mean ± sem nmol $^{45}Ca^{2+}$ /mg protein. Data are reported in Table 5.7a.

5.3.4.1.3 *NMDA Stimulated $^{45}Ca^{2+}$ uptake into dorsal and ventral striata – SHAM lesioned rats*

The results comparing stimulated $^{45}Ca^{2+}$ uptake into dorsal and ventral striata are provided here as mean ± standard deviation of the mean. Stimulated $^{45}Ca^{2+}$ uptake of dorsal (1L-2L and 1R-2R) and ventral (3L-2L*V* and 3R-2R*V*) striata obtained from the same slice or from consecutive slices, showed that uptake into the dorsal striata 1L-2L, 3.43 ± 1.89 nmol $^{45}Ca^{2+}$ /mg protein, was not significantly different from uptake into the ventral striatum (3L-2L*V*) measured to be 4.49 ± 2.63 nmol $^{45}Ca^{2+}$ /mg protein (Table 5.7b, Figure 5.8e) in the left hemisphere. In the right hemisphere, uptake into the dorsal striatum (1R-2R), 2.89 ± 1.54 nmol $^{45}Ca^{2+}$ /mg protein was significantly less than uptake into the ventral striatum (3R-2R*V*), 4.82 ± 1.37 nmol $^{45}Ca^{2+}$ /mg protein (student t-test, $p<0.05$) (Table 5.7b, Figure 5.8e).

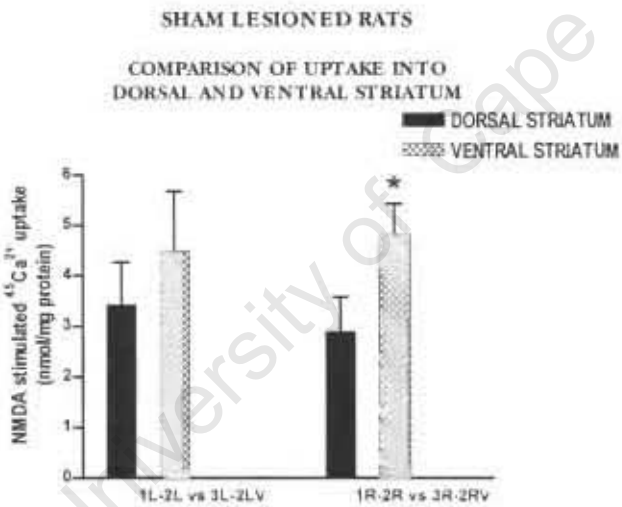

Figure 5.8e NMDA (100μM) stimulated $^{45}Ca^{2+}$ uptake from the dorsal and ventral striata in (n=5) SHAM lesioned rats. In the left hemisphere stimulated uptake was not significantly different into the dorsal and ventral striata. * Ventral striatal uptake in the right hemisphere was significantly greater than dorsal striatal uptake. Results are mean ± sem nmol $^{45}Ca^{2+}$ /mg protein. Data are reported in Table 5.7b.

5.3.4.2 *NMDA stimulation increases $^{45}Ca^{2+}$ uptake into 6-OHDA lesioned rats*

5.3.4.2.1 Dorsal striatum – 6-OHDA lesioned rats

Results for the complete statistical analyses reported below are reported in Annex B. Measurement of total $^{45}Ca^{2+}$ uptake into dorsal striatal sections of 6-OHDA lesioned rats (n=10), showed that the total $^{45}Ca^{2+}$ accumulation of the anterior (1L and 1R) and posterior (3L and 3R) sections was significantly different ($p < 0.05$) from the basal uptake of the control sections (2L and 2R) (Table 5.8a, Figure 5.9a). NMDA (100 μM) stimulated a significant increase of $^{45}Ca^{2+}$ uptake into dorsal striatal sections in 6-OHDA lesioned rats. Measurements of basal $^{45}Ca^{2+}$ uptake into the striata of the left lesioned hemisphere (2L) and the right unlesioned (2R) were not significantly different (Table 5.8a, Figure 5.9a).

Table 5.8a Total $^{45}Ca^{2+}$ uptake into dorsal and ventral striata of 6-OHDA lesioned rats (n=10).

		$^{45}Ca^{2+}$ uptake into striatal sections (nmol $^{45}Ca^{2+}$ /mg protein)					
STRIATAL REGION		1L	1R	2L	2R	3L	3R
DORSAL STRIATUM	n=10	8.74 ± 0.78 *	8.89 ± 0.83 *	4.92 ± 0.65	4.98 ± 0.55	9.50 ± 1.00 *	9.49 ± 1.11 *
VENTRAL STRIATUM	n=4	9.69 ± 0.74 *	10.97 ± 1.19 *	4.49 ± 0.15	4.12 ± 0.62	9.88 ± 0.85 *	9.99 ± 1.66 *

*NMDA stimulated significant increases in total $^{45}Ca^{2+}$ uptake into anterior (1L and 1R) and posterior (3L and 3R) striata from basal uptake into non-stimulated intermediate striata (2L and 2R) (student t-test $p<0.05$).

DORSAL STRIATAL $^{45}Ca^{2+}$ UPTAKE 6-OHDA LESIONED RATS

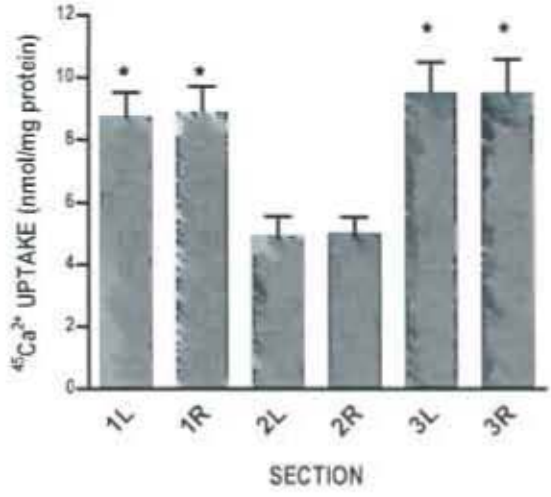

Figure 5.9a Total $^{45}Ca^{2+}$ uptake into dorsal striata from 6-OHDA lesioned rats (n=10). *NMDA (100μM) stimulated significantly greater $^{45}Ca^{2+}$ uptake into dorsal anterior striata (IL and 1R) and posterior striata (3L and 3R) than basal uptake into non-stimulated striatal sections (2L and 2R) incubated in normal buffer (student t-test, $p<0.05$). Results are mean ± sem nmol $^{45}Ca^{2+}$/mg protein (n=10). Data are reported in Table 5.8a.

Measurement of stimulated $^{45}Ca^{2+}$ uptake was used to determine whether there were any differences in uptake of anterior and posterior striata within each hemisphere, and to determine whether there were any differences in uptake in the left hemisphere and the right hemisphere. There was no difference in stimulated $^{45}Ca^{2+}$ uptake into the anterior striata of the left lesioned hemisphere (1L-2L) and the posterior striata (3L-2L) neither was there any difference in stimulated $^{45}Ca^{2+}$ uptake into the anterior striata of the right hemisphere (1R-2R) and the posterior striata (3R-2R) (Table 5.7b, Figure 5.7b). The results of the difference of stimulated $^{45}Ca^{2+}$ uptake into the left lesioned hemisphere and into the right lesioned hemisphere show that there was no difference in $^{45}Ca^{2+}$ uptake into the anterior striata, nor was there any difference into posterior striata (Table 5.8b, Figure 5.9c). There was no significant difference in stimulated $^{45}Ca^{2+}$ uptake into the left 6-OHDA lesioned hemisphere from stimulated $^{45}Ca^{2+}$ uptake into the right unlesioned hemisphere.

Table 5.8b NMDA (100 µM) stimulated $^{45}Ca^{2+}$ uptake into dorsal and ventral striata of 6-OHDA lesioned rats.

	$^{45}Ca^{2+}$ uptake into striatal sections (nmol $^{45}Ca^{2+}$ /mg protein)					
STRIATAL REGION		1L-2L	± sem		1R-2R	± sem
DORSAL STRIATA	n=10	3.83	0.64		3.90	0.80
VENTRAL STRIATA	n=4	5.20	0.63		6.85	1.14
STRIATAL REGION		3L-2L	± sem		3R-2R	± sem
DORSAL STRIATA	n=10	4.58	0.69		4.51	0.89
VENTRAL STRIATA	n=4	5.39	0.76		5.87	1.32

Measurements of NMDA stimulated $^{45}Ca^{2+}$ uptake into anterior sections from the left (1L-2L) and right (1R-2R) hemispheres and into posterior striatal sections from the left (3L-2L) and right (3R-2R) hemispheres. NMDA stimulated $^{45}Ca^{2+}$ uptake is reported as the mean ± sem nmol $^{45}Ca^{2+}$ /mg protein.

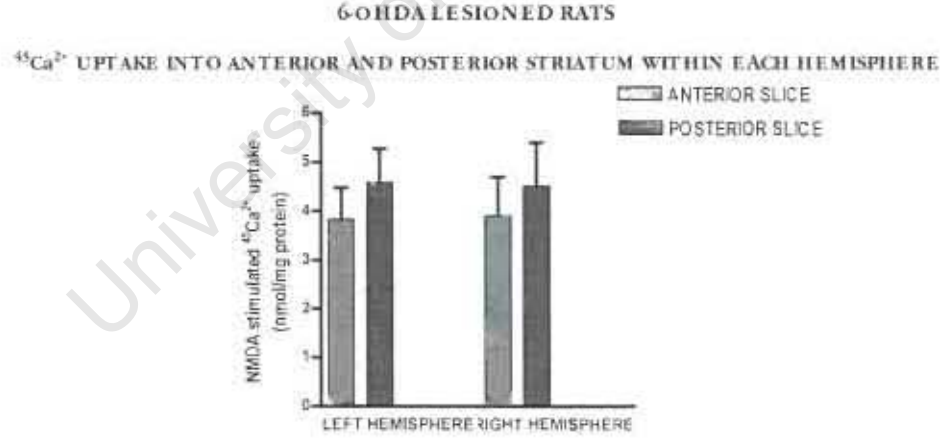

Figure 5.9b NMDA stimulated $^{45}Ca^{2+}$ uptake into dorsal striata within each hemisphere of the 6-OHDA lesioned rats (n=10). Stimulated uptake was compared between the anterior and posterior dorsal striata in the left and right hemispheres. No significant difference in uptake between the anterior striatum and the posterior striatum in both hemispheres. Results are reported as mean ± sem nmol $^{45}Ca^{2+}$ /mg protein. Data are reported in Table 5.8b.

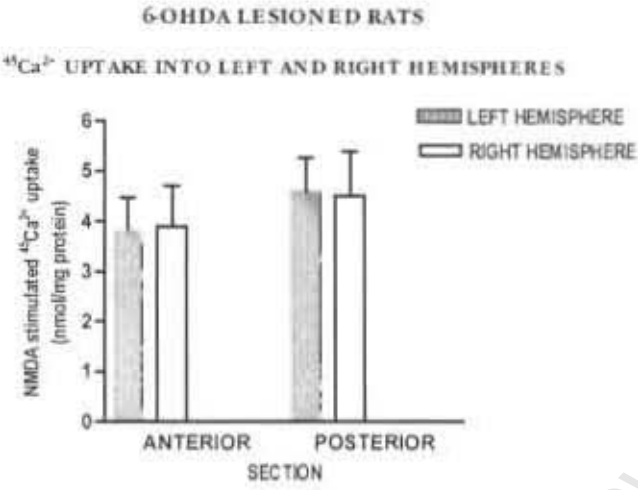

Figure 5.9c NMDA stimulated $^{45}Ca^{2+}$ uptake into dorsal striata comparing the left lesioned vs. right unlesioned hemisphere 6-OHDA lesioned rats (n=10). No significant difference in uptake between the lesioned and unlesioned hemisphere (student t-test, $p>0.05$). Results are reported as mean ± sem nmol $^{45}Ca^{2+}$ /mg protein. Data are reported in Table 5.8b.

5.3.4.2.2 Ventral striatum – 6-OHDA lesioned rats

Total uptake into the ventral striata of 6-OHDA lesioned rats was measured in n=4 rats. Anterior and posterior striata from the left (1L and 3L) and right hemisphere (1R and 3R) had significantly increased $^{45}Ca^{2+}$ accumulation from intermediate striata (2L and 2R). NMDA (100 µM) stimulated significant increase in $^{45}Ca^{2+}$ uptake above basal levels (Table 5.8a, Figure 5.9d). However, the results of the NMDA stimulated $^{45}Ca^{2+}$ uptake show that there was no significant difference of uptake into anterior striata and posterior striata within both hemispheres. Furthermore, there was not significant difference in NMDA stimulated $^{45}Ca^{2+}$ into the striata of the left 6-OHDA lesioned hemisphere and into the striata of the right unlesioned hemisphere (Table 5.8b).

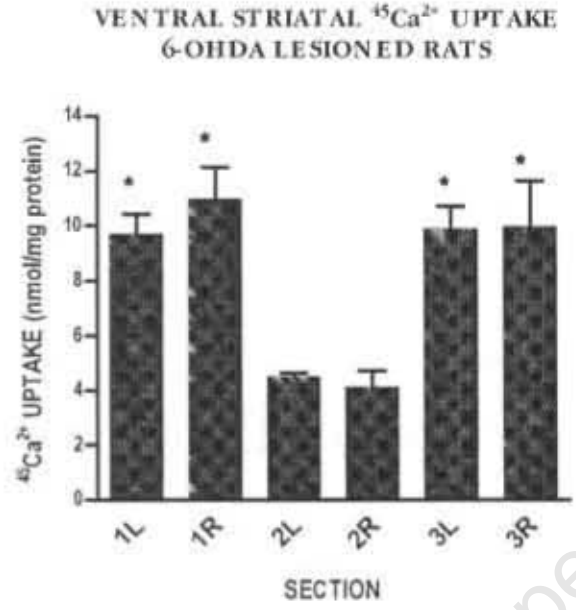

Figure 5.9d Total $^{45}Ca^{2+}$ uptake into ventral striata of 6-OHDA lesioned rats (n=4). *Anterior (1L and 1R) and posterior (3L and 3R) striata had significant uptake in response to NMDA stimulation from basal levels (2L and 2R) (student t-test, $p>0.05$). Results are reported as mean ± sem nmol $^{45}Ca^{2+}$ /mg protein. Data are reported in Table 5.8a.

5.3.4.2.3 NMDA Stimulated $^{45}Ca^{2+}$ uptake into dorsal and ventral striata – 6-OHDA lesioned rats

The results comparing stimulated $^{45}Ca^{2+}$ uptake into dorsal and ventral striata are provided here as mean ± standard deviation of the mean. Stimulated $^{45}Ca^{2+}$ uptake of dorsal (1L-2L and 1R-2R) and ventral (3L-2L*V* and 3R-2R*V*) striata obtained from the same slice showed stimulated $^{45}Ca^{2+}$ uptake, 2.66 ± 2.53 nmol $^{45}Ca^{2+}$ /mg protein into the dorsal striatum (1L-2L) was not significantly different from uptake into the ventral striatum (3L-2L*V*) measured to be 5.39 ± 1.52 nmol $^{45}Ca^{2+}$ /mg protein (Table 5.8b, Figure 5.9e) in the left hemisphere. In the right hemisphere, uptake into the dorsal striatum (1R-2R), 2.74 ± 3.13 nmol $^{45}Ca^{2+}$ /mg protein was significantly less than uptake into the ventral striatum (3R-2R*V*), 5.87 ± 2.63 nmol $^{45}Ca^{2+}$ /mg protein (student t-test, $p<0.05$) (Table 5.8b, Figure 5.9e). Based on the

measurements of n=4 6-OHDA lesioned rats, there was no statistical significance between dorsal and ventral striatal stimulated $^{45}Ca^{2+}$ uptake.

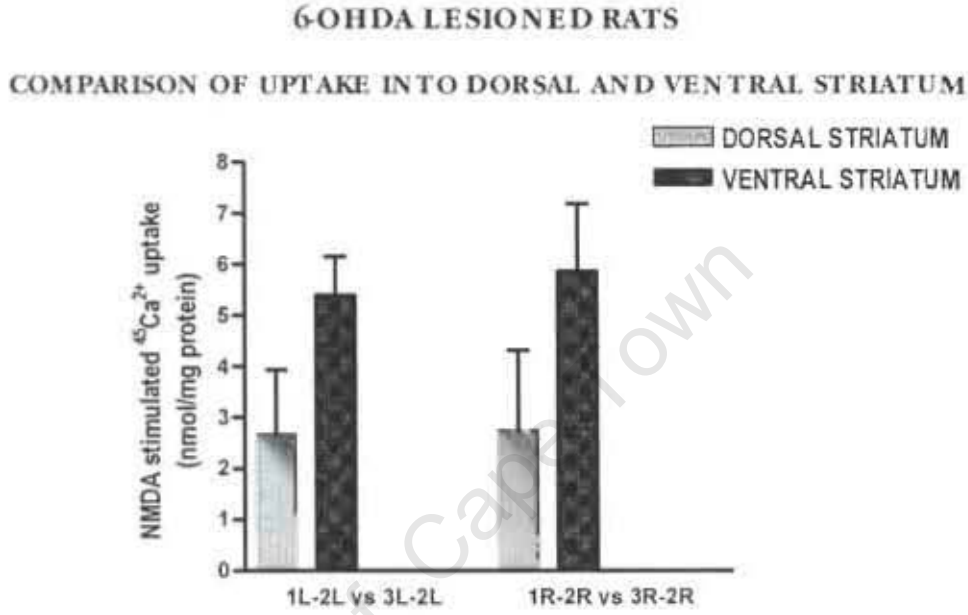

Figure 5.9e Analysis of stimulated uptake comparing the dorsal and ventral striata in the 6-OHDA lesioned rats (n=4). There was no statistical significant difference between the dorsal and ventral striatum. Results are reported as mean ± sem nmol $^{45}Ca^{2+}$ /mg protein. Data are reported in Table 5.8b.

5.3.4.3 *NMDA Stimulated $^{45}Ca^{2+}$ Uptake – 6-OHDA lesioned vs. SHAM lesioned rats*

Results for the complete statistical analyses reported below are reported in Annex B. NMDA (100 μM) stimulated $^{45}Ca^{2+}$ uptake into dopamine depleted striata into sham lesioned rats and following 6-OHDA lesions showed that $^{45}Ca^{2+}$ uptake measured into anterior (1L-2L and 1R-2R) striata was not statistically different, neither was uptake into the posterior (3L-2L and 3R-2R) striata (ANOVA, $p>0.05$) (Table 5.9a, Figure 5.10a). Data suggest that dopamine depletion induced by 6-OHDA lesions did not cause significant changes in $^{45}Ca^{2+}$ influx in response to NMDA stimulation relative to sham lesions. As stimulated $^{45}Ca^{2+}$ uptake was measured relative to basal uptake into striata, basal $^{45}Ca^{2+}$ uptake into striata (2L and 2R) from sham lesioned and 6-OHDA lesioned rats were compared to determine whether differences in basal $^{45}Ca^{2+}$ uptake may have masked the response to NMDA stimulation.

There was no significant difference in basal uptake into striata of the left (2L) and right (2R) hemispheres (ANOVA, $p>0.05$) (Table 5.9a, Figure 5.10b). Within the ventral striata, stimulated $^{45}Ca^{2+}$ uptake into striata of sham lesioned rats and 6-OHDA lesioned rats, was also not significantly different neither was basal uptake (Table 5.9b, Figures 5.10c).

Table 5.9a Basal (2L and 2R) and NMDA stimulated $^{45}Ca^{2+}$ uptake into dorsal striata of SHAM and 6-OHDA lesioned rats.

		$^{45}Ca^{2+}$ uptake into dorsal striatal sections (nmol $^{45}Ca^{2+}$ /mg protein)					
GROUP		1L-2L	1R-2R	3L-2L	3R-2R	2L	2R
SHAM	n=9	3.54 ± 0.66	3.49 ± 0.57	3.12 ± 0.57	4.20 ± 0.93	6.56 ± 0.61	5.89 ± 0.63
6-OHDA	n=10	3.83 ± 0.64	3.90 ± 0.80	4.58 ± 0.69	4.51 ± 0.89	4.92 ± 0.65	4.98 ± 0.55

Measurements of NMDA stimulated $^{45}Ca^{2+}$ uptake into anterior sections from the left (1L-2L) and right (1R-2R) hemispheres and into posterior striatal sections from the left (3L-2L) and right (3R-2R) hemispheres. There was no significant difference in stimulated uptake between the two treatment groups. NMDA stimulated $^{45}Ca^{2+}$ uptake is reported as the mean ± sem nmol $^{45}Ca^{2+}$ /mg protein. These results are duplicated from Tables 5.7a, 5.7b, 5.8a and 5.8b.

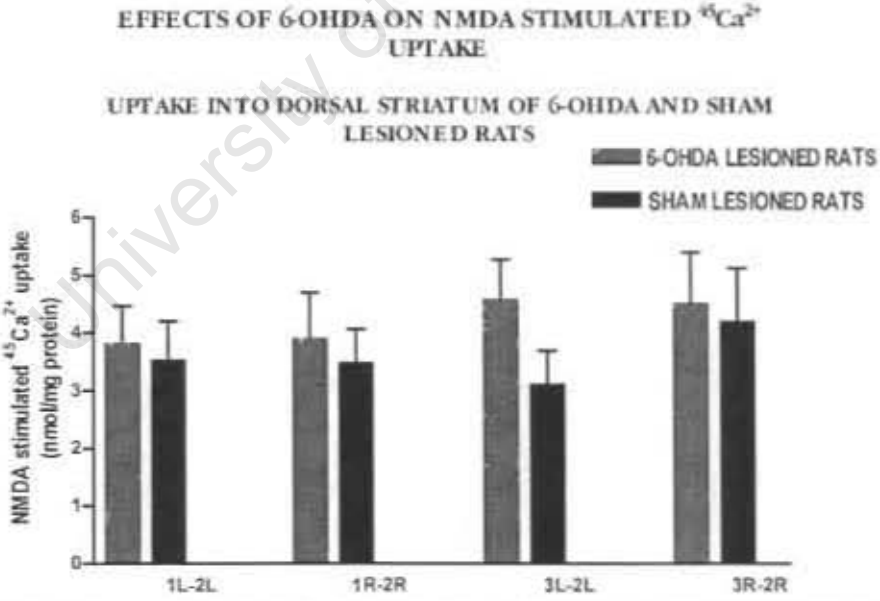

Figure 5.10a Comparison of NMDA stimulated uptake in the dorsal striata of 6-OHDA lesioned (n=10) and sham lesioned (n=9) showed no significant difference in stimulated $^{45}Ca^{2+}$ uptake (ANOVA, $p>0.05$). Results are mean ± sem nmol $^{45}Ca^{2+}$ /mg protein. Data are reported in Tables 5.7b, 5.8b and 5.9a

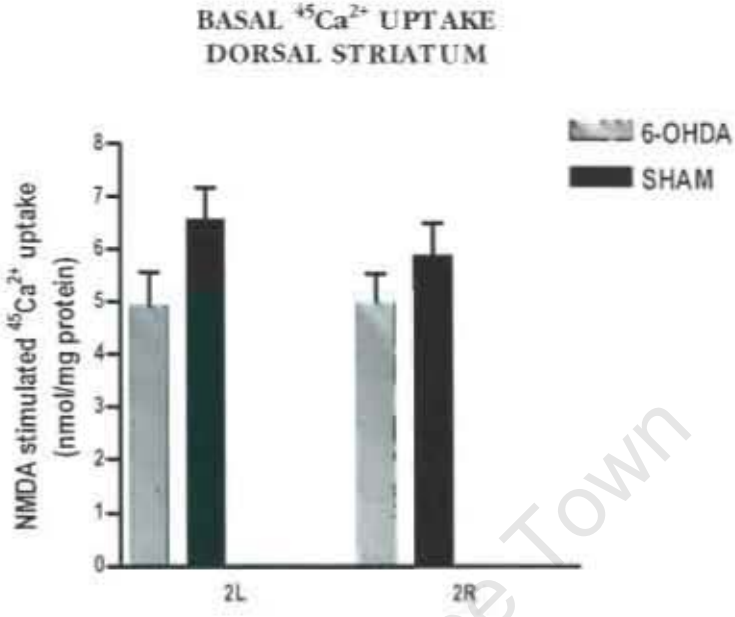

Figure 5.10b Basal $^{45}Ca^{2+}$ uptake into dorsal striatal sections obtained from the left lesioned hemisphere (2L) and the right unlesioned hemisphere (2R) of sham (n=9) and 6-OHDA (n=10) lesioned rats. Basal $^{45}Ca^{2+}$ uptake into striata of 6-OHDA lesioned rats was not significantly different from basal uptake into striata of the sham lesioned rats (ANOVA, $p>0.05$). Results are reported as mean ± sem nmol $^{45}Ca^{2+}$ /mg protein. Data are reported in Table 5.9a.

Table 5.9b Basal (2L and 2R) and NMDA stimulated $^{45}Ca^{2+}$ uptake into ventral striata of SHAM and 6-OHDA lesioned rats.

		$^{45}Ca^{2+}$ uptake into ventral striatal sections (nmol $^{45}Ca^{2+}$ /mg protein)					
GROUP		1L-2L	1R-2R	3L-2L	3R-2R	2L	2R
SHAM	n=5	4.93 ± 0.71	4.66 ± 1.28	4.49 ± 1.18	4.82 ± 0.61	3.29 ± 0.59	3.29 ± 0.69
6-OHDA	n=4	5.20 ± 0.63	6.85 ± 1.14	5.39 ± 0.76	5.87 ± 1.32	4.49 ± 0.15	4.12 ± 0.62

Measurements of NMDA stimulated $^{45}Ca^{2+}$ uptake into anterior sections from the left (1L-2L) and right (1R-2R) hemispheres and into posterior striatal sections from the left (3L-2L) and right (3R-2R) hemispheres. There was no significant difference in stimulated uptake between the two treatment groups. NMDA stimulated $^{45}Ca^{2+}$ uptake is reported as the mean ± sem nmol $^{45}Ca^{2+}$ /mg protein. These results are duplicated from Tables 5.7a, 5.7b, 5.8a and 5.8b.

EFFECTS OF 6-OHDA ON NMDA STIMULATED $^{45}Ca^{2+}$ UPTAKE

UPTAKE INTO VENTRAL STRIATUM OF 6-OHDA AND SHAM LESIONED RATS

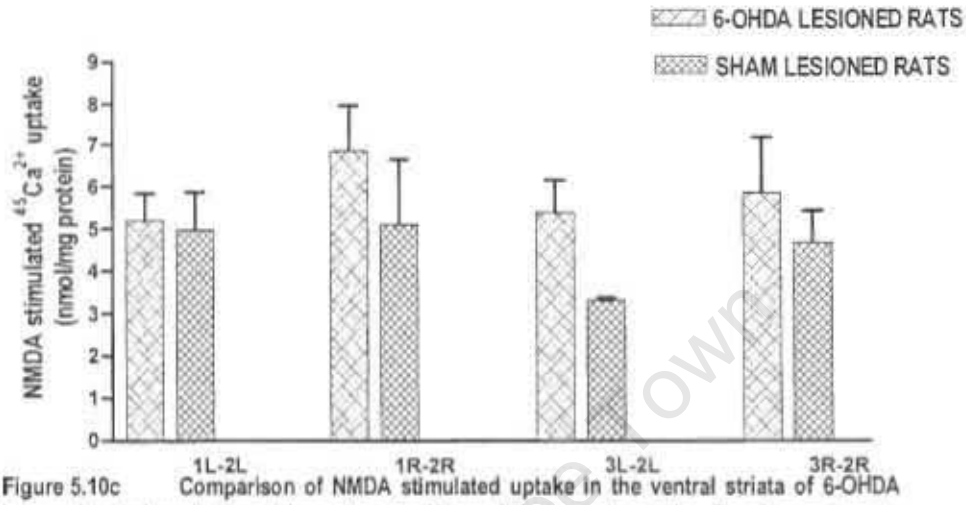

Figure 5.10c Comparison of NMDA stimulated uptake in the ventral striata of 6-OHDA lesioned and sham lesioned showed no significant differences in uptake. Results are mean ± sem nmol $^{45}Ca^{2+}$ /mg protein.

CHAPTER 6

DISCUSSION

6.1 NMDA (100 µM) stimulated $^{45}Ca^{2+}$ uptake response in striatal sections

In this study we were able to demonstrate that NMDA receptor-mediated Ca^{2+} influx can be measured in striatal tissue in vitro using the assay as described by Lehohla *et al* (2000). To our knowledge, these are the first such measurements to be made in striatal tissue using this method. Preliminary experiments were conducted to determine whether 100 µM NMDA was effective in stimulating significant levels of $^{45}Ca^{2+}$ uptake into 350 µm thick striatal sections and to confirm the reproducibility of the assay (Table 5.1a, Figure 5.1). Measurement of $^{45}Ca^{2+}$ uptake into striatal tissue from 7 week old rats, n=7, (Table 5.2a), 16 week old rats, n=6, (Table 5.3a), sham lesioned, n=9, (Table 5.7a, Figure 5.8a) and 6-OHDA lesioned rats, n=10, (Table 5.8a, Figure 5.9a) confirmed that NMDA (100 µM) was effective in stimulating significant $^{45}Ca^{2+}$ influx into dorsal striatal and ventral striatal sections.

Lehohla *et al* (2000) reported NMDA stimulated $^{45}Ca^{2+}$ uptake into Long Evans rat barrel cortex was 28 - 31% above basal $^{45}Ca^{2+}$ uptake levels. The results of the current study show that NMDA (100 µM) evoked a greater response in the striatum than in the barrel cortex. Results from 7 week old rats show that NMDA stimulated $^{45}Ca^{2+}$ uptake was 117 – 156% above basal levels (Tables 5.2a and 5.2b). In 16 week old rats NMDA stimulated increases of 38 – 70% above basal $^{45}Ca^{2+}$ uptake levels (Tables 5.3a and 5.3b). These results suggest that a two to three fold decrease in NMDA stimulated response occurs over 9 weeks of growth. The results from the ventral striata were similarly increased in both 7 week and 16 week old rats (Tables 5.2a, 5.2b, 5.3a and 5.3b). In the lesioned rats, the NMDA stimulated $^{45}Ca^{2+}$ uptake response above basal levels was also higher than the levels reported by Lehohla *et al* (2000). NMDA stimulated increased $^{45}Ca^{2+}$ uptake in the sham lesioned rats by 54 – 71% above basal $^{45}Ca^{2+}$ uptake levels (Tables 5.7a and 5.7b, Figure 5.8a) while in the 6-OHDA lesioned rats, increases of $^{45}Ca^{2+}$ uptake were 78 – 93% above basal $^{45}Ca^{2+}$ uptake levels in response to NMDA stimulation (Tables 5.8a, 5.8b, Figure 5.9a).

6.2 *Effect of age on NMDA stimulated $^{45}Ca^{2+}$ uptake response*

6.2.1 *Dorsal Uptake*

When the NMDA stimulated $^{45}Ca^{2+}$ uptake in anterior dorsal striata of 7 week old rats was compared with uptake in 16 week old rats, uptake into anterior striata of 16 week old rats showed a 69% and 46% reduction in the left and right hemispheres below uptake of 7 week old rats (Table 5.4a, Figure 5.4a). In the posterior striata of 16 week old rats, NMDA stimulated $^{45}Ca^{2+}$ uptake was decreased 66% and 63% in the left and right striata below NMDA stimulated $^{45}Ca^{2+}$ uptake of 7 week old rats (Table 5.4a, Figure 5.4a). These results show a significant decrease in stimulated uptake of 16 week old rats compared to 7 week old rats and suggests that during 9 weeks of growth from juvenile to young adult development, there is an average decrease of ≈ 60% in dorsal striatal NMDA mediated Ca^{2+} influx.

6.2.2 *Ventral uptake*

Results comparing ventral striatal $^{45}Ca^{2+}$ uptake in 7 week and 16 week old rats also indicate a tendency for $^{45}Ca^{2+}$ uptake in the older animals to exhibit a reduction in NMDA mediated $^{45}Ca^{2+}$ influx in all striatal sections. In 16 week old rats, NMDA stimulated $^{45}Ca^{2+}$ uptake into ventral anterior striata of the left and right hemispheres was 49% and 32% below NMDA stimulated $^{45}Ca^{2+}$ uptake into anterior ventral striata of 7 week old rats (Table 5.4b, Figure 5.4c). In the posterior ventral striata of the right hemisphere in 16 week old rats, the NMDA stimulated $^{45}Ca^{2+}$ uptake was 41% less than in NMDA stimulated $^{45}Ca^{2+}$ uptake in 7 week old rats (Table 5.4b, Figure 5.4c). Whereas NMDA stimulated $^{45}Ca^{2+}$ uptake in the posterior striata of the left hemisphere of 16 week old rats was reduced by 65% compared to NMDA stimulated $^{45}Ca^{2+}$ uptake in 7 week old rats. Surprisingly, the only significant difference in NMDA stimulated ventral striatal $^{45}Ca^{2+}$ uptake between 7 week and 16 week old rats was in the posterior section of the left hemisphere were the reduction during 9 weeks of growth was greater than 50%.

The above results showing significant reduction in NMDA receptor mediated $^{45}Ca^{2+}$ influx with increasing age from 7 weeks to 16 weeks concur with reported age dependent attenuation of NMDA receptor activity attributed to reduction of NMDA receptor density that occurs in rats (Mitchell and Anderson, 1998; Wenk and Barnes, 2000, Bai *et al*, 2004). There are major changes of dendritic spines that occur, including shrinkage and loss and these undoubtedly contribute to the reduction of

NMDA receptor density (Levine *et al*, 1988; Dunia *et al*, 1996; Segovia *et al*, 2001). Owing to this, the results from the ventral striatal $^{45}Ca^{2+}$ uptake showing lack of significant difference were indeed surprising.

6.2.3 Striatal Ca^{2+} homeostasis and age

Basal uptake was compared to determine whether differences in NMDA stimulated $^{45}Ca^{2+}$ uptake between 7 week and 16 week old rats could be a factor influencing the levels of $^{45}Ca^{2+}$ influx. There was no significant difference in basal $^{45}Ca^{2+}$ uptake into dorsal or ventral striata between adolescent 7 week old rats and young adult 16 week old rats (Tables 5.2a and 5.3a, Figures 5.4b and 5.4d). These results are consistent with the findings of Griffith *et al* (2000) that intracellular Ca^{2+} concentrations are unchanged and that Ca^{2+} homeostasis is not compromised with age.

6.3 6-OHDA lesion technique and extent of degeneration

6.3.1 MFB lesioning and apomorphine induced rotations

In the current study the 6-OHDA model of Parkinson's disease was established by conducting histological mappings of the needle tip positions around the MFB and by conducting behavioural assessments of the lesion followed by immunocytochemistry. In targeting the MFB, the mappings shown on the atlas diagrams, show variability of the needle tip position (Figures 5.5a – 5.5g). In n=1 rat, the needle was positioned too ventral from the intended target suggesting possible error in lesion technique (Figure 5.5e). The main factor influencing variability in the study may be attributed to natural variability of rat brain sizes and shape. In n=14 sham lesioned rats and n=17 6-OHDA lesioned rats, apomorphine induced rotations were used to assess extent of dopamine depletion. Results from sham lesioned rats in the current study show that 19 ± 8 rotations ipsilateral to the lesion were conducted (Table 5.6a, Figure 5.6a). The mean number of rotations conducted by 6-OHDA lesioned rats was 233 ± 43 complete contralateral rotations (Table 5.6b, Figure 5.6a). This is consistent with Hudson *et al* (1993) who showed that apomorphine injection did not produce a significant number of rotations in non-lesioned rats. Moore *et al* (2001) found that a contralateral rotational bias in response to apomorphine only occurred when >70 – 80% degeneration of midbrain dopamine neurons and striatal dopamine fibres had occurred in rats infused with 6-OHDA into the MFB. This suggests that in the current study, >70% degeneration was achieved in 6-OHDA lesioned rats selected for NMDA stimulated $^{45}Ca^{2+}$ uptake assays.

6.3.2 *Tyrosine hydroxylase immunoreactivity*

Tyrosine hydroxylase staining of the midbrain and the striatum confirmed that degeneration, shown by TH staining, was minimal in sham lesioned rats; there was complete staining in the striatum and midbrain of both hemispheres (Figures 5.7b – 5.7d). In a 6-OHDA lesioned rat that had conducted 381 contralateral rotations, there was near complete loss of TH ipsilateral to the site of 6-OHDA injection (Figures 5.7b – 5.7d). Immunocytochemistry was conducted on a 6-OHDA lesioned rats that had exhibited 101 ipsilateral rotations in response to apomorphine. There was a reduced TH in the midbrain and in the medial dorsal and medial ventral striata but the reduction was not as extensive as the degeneration observed in 6-OHDA rat conducting >100 contralateral rotations (Figures 5.7biii, 5.7c and 5.7d). These results confirm the findings by Carman *et al* (1991) that the number of TH immunoreactive neurons that remain unlesioned is correlated to the number of contralateral rotations conducted in response to apomorphine; the fewer the number of degenerated neurons the fewer the number of contralateral rotations. Apomorphine induced rotations are a useful predicator of the extent of midbrain degeneration of dopamine neurons and dopamine terminals in the striatum (Carman *et al*, 1991). The results of TH immunocytochemistry obtained from the serial sections confirmed that 5 weeks post surgery, there was near complete depletion of dopamine neurons in the entire striatum of the lesioned left hemisphere in 6-OHDA lesioned rats selected for NMDA stimulated $^{45}Ca^{2+}$ uptake assay and that in selected sham lesioned rats, dopamine innervation remained intact within both hemispheres.

6.4 *Effects of dopamine depletion on NMDA $^{45}Ca^{2+}$ uptake response*

6.4.1 *NMDA stimulated $^{45}Ca^{2+}$ uptake in lesioned vs. unlesioned hemisphere*

Having confirmed through TH immunoreactivity that there was near complete depletion of dopamine in the left striatum, ipsilateral to the 6-OHDA lesion, it was expected that there would be increases in NMDA receptor mediated $^{45}Ca^{2+}$ influx in the left striatum relative to NMDA stimulated $^{45}Ca^{2+}$ uptake in the striatum of the right hemisphere that had intact TH immunoreactivity. NMDA stimulated $^{45}Ca^{2+}$ uptake into the anterior striatum of the left hemisphere was 2% less than NMDA stimulated $^{45}Ca^{2+}$ uptake into the anterior striatum of the right hemisphere whereas in the posterior striata NMDA stimulated $^{45}Ca^{2+}$ uptake into the striatum of the left lesioned hemisphere was 2% more than uptake into the striatum of the right hemisphere (Table 5.8b, Figure 5.9c). These differences in NMDA stimulated $^{45}Ca^{2+}$ uptake between striata of the 6-OHDA lesioned left hemisphere and the

unlesioned right hemisphere were marginal and not significant (Table 5.8b, Figure 5.9c). These results from 6-OHDA lesioned rats were similar to the results of NMDA stimulated $^{45}Ca^{2+}$ uptake measured in sham lesioned rats. In the sham lesioned rats there was a 2% difference in NMDA stimulated $^{45}Ca^{2+}$ uptake between the anterior striata of the left and right hemispheres. In the posterior striata NMDA stimulated $^{45}Ca^{2+}$ uptake levels in the right hemisphere were 17% higher than NMDA stimulated $^{45}Ca^{2+}$ uptake levels in posterior striatum of the left hemisphere (Table 5.7a, Figure 5.8c). There was no significant difference in NMDA stimulated $^{45}Ca^{2+}$ uptake between the sham operated left hemisphere and the unlesioned right hemisphere. These results suggest that mechanical stress induced by the surgical procedure did not disturb NMDA mediated $^{45}Ca^{2+}$ influx.

6.4.2 Comparing sham lesioned and dopamine depleted striatal uptake

NMDA stimulated $^{45}Ca^{2+}$ uptake into the anterior dorsal striata of 6-OHDA lesioned rats showed increases of 8% and 11% in the left and right hemispheres respectively above NMDA stimulated $^{45}Ca^{2+}$ uptake in sham lesioned rats (Table 9a, Figure 5.10a). In the posterior striata of 6-OHDA lesioned rats, NMDA stimulated $^{45}Ca^{2+}$ uptake in the left and right hemispheres showed 32% and 7% increases respectively above NMDA stimulated $^{45}Ca^{2+}$ uptake levels of sham lesioned rats (Table 9a, Figure 5.10a). There was no significant difference in NMDA stimulated $^{45}Ca^{2+}$ uptake between 6-OHDA lesioned and sham lesioned rats. It is of interest that while the measurement of the left posterior striatum was the highest measurement in the 6-OHDA lesioned rats, the measurement from the same striatal section was the lowest measurement in sham lesioned rats. While these findings could suggest that NMDA receptor function in the posterior striata of the lesioned hemisphere was attenuated in response to sham operations and enhanced in 6-OHDA lesioned rats, this does not seem likely as there were no significant differences between the left lesioned and the right unlesioned hemispheres in either sham lesioned or 6-OHDA lesioned rats.

To determine whether changes in basal uptake may have masked upregulation of NMDA receptor mediated $^{45}Ca^{2+}$ influx in dopamine depleted animals, basal uptake between striata of sham lesioned and 6-OHDA lesioned rats was analyzed. Although there was a tendency for basal $^{45}Ca^{2+}$ uptake to be lower in striatal sections obtained from 6-OHDA lesioned rats compared to sham lesioned rats, there was no significant difference between the two groups (Figure 10b). Sham operated rats had 25% greater uptake in the left hemisphere and 15% greater basal uptake in the right hemisphere

than 6-OHDA lesioned rats. Our investigations examining the differences in NMDA receptor function in the dopamine depleted striatum do not support the original hypothesis that reported upregulation of NMDA receptors would translate into increased ionic flux of $^{45}Ca^{2+}$ in response to NMDA stimulation.

6.4.3 Dorso-ventral differences

NMDA stimulation seemed to evoke a higher $^{45}Ca^{2+}$ influx response in ventral striata than in dorsal striata but there was no significant difference in NMDA stimulated $^{45}Ca^{2+}$ uptake between the dorsal and ventral striatal $^{45}Ca^{2+}$ uptake in either sham lesioned or 6-OHDA lesioned rats (Tables 5.7b, 5.8b and Figures 5.8e and 5.9e). The lack of statistical significance in these results may be attributed to the small number of rats (n=4 in 6-OHDA lesioned rats and n=5 in sham lesioned rats) used in the analysis which could also account for the large standard deviation from the mean.

6.5 NMDA stimulated $^{45}Ca^{2+}$ uptake into anterior and posterior striatal regions

Lehohla *et al* (2001) reported differences in $^{45}Ca^{2+}$ uptake between rostral, middle and caudal barrel cortices. In our study we sought to identify whether similar regional differences between anterior and posterior striatal regions existed. In the 7 week old rats, anterior dorsal striata showed 35% increase above posterior dorsal striatal uptake in the left hemisphere but showed an 8% decrease below uptake in the posterior dorsal uptake in the right hemisphere (Table 5.2b, Figure 5.2a). There were no significant differences between anterior and posterior dorsal uptake in either hemisphere in 7 week old rats. In 16 week old rats, anterior dorsal uptake levels were 28% higher than uptake levels in the posterior striatum in the left hemisphere and were 25% higher than posterior striatal $^{45}Ca^{2+}$ uptake in the right hemisphere (Table 5.3b, Figure 5.3a). However, there were no significant differences in anterior-posterior $^{45}Ca^{2+}$ uptake in either hemisphere. In 6-OHDA lesioned rats, the trend was reversed with NMDA stimulated $^{45}Ca^{2+}$ uptake levels into the posterior striata showing a tendency to be higher than levels in the anterior striata. In the left hemisphere, NMDA stimulated $^{45}Ca^{2+}$ uptake into the anterior striatum was 17% less than uptake into the posterior striatum. In the right hemisphere, NMDA stimulated $^{45}Ca^{2+}$ uptake into the anterior striatum was 14% less than uptake into the posterior striatum. These differences between anterior and posterior NMDA stimulated $^{45}Ca^{2+}$ uptake in 6-OHDA lesioned rats were not significant. In the sham lesioned rats anterior striatal uptake in the left hemisphere was 1% higher than uptake into the posterior striatum

though in the right hemisphere the anterior striatal uptake was 17% below posterior striatal uptake (Table 5.7b, Figure 5.8b). In all the animals studied there were no significant differences in NMDA stimulated uptake between anterior and posterior striata and that there was variability in anterior-posterior NMDA stimulated $^{45}Ca^{2+}$ uptake.

6.6 Conclusion

6.6.1 Findings on striatal NMDA receptor function

In the current study we set out to determine whether aging would result in decreased NMDA stimulated $^{45}Ca^{2+}$ uptake into the striatum and whether dopamine depletion induced by degeneration of the nigrostriatal pathway increases NMDA stimulated $^{45}Ca^{2+}$ uptake. We were able to demonstrate that 9 weeks of growth from adolescence to young adulthood in male Long Evans rats, results in reduction of NMDA receptor mediated $^{45}Ca^{2+}$ influx of up to 69%. These results support the findings that striatal glutamate innervation and NMDA receptor responsiveness hence neuronal excitability are reduced with age (Cepeda *et al*, 1989; Cepeda *et al*, 1996; Segovia *et al*, 2001). To our knowledge, this is the first study to demonstrate such a significant reduction of NMDA receptor function in the dorsal striatum using the in vitro NMDA stimulated $^{45}Ca^{2+}$ uptake assay.

The second hypothesis we tested was that degeneration of the nigrostriatal pathway would result in increased NMDA stimulated $^{45}Ca^{2+}$ uptake. The results from the study did not concur with this stated hypothesis. Instead we found that there are no differences in NMDA stimulated $^{45}Ca^{2+}$ uptake between 6-OHDA lesioned and sham lesioned rats and neither are there any differences in NMDA stimulated $^{45}Ca^{2+}$ uptake within the 6-OHDA lesioned rats comparing the striatal $^{45}Ca^{2+}$ uptake from the lesioned and the unlesioned hemispheres. These results rather suggest that reported modifications of NMDA synaptic expression and phosphorylation state in parkinsonian rats may serve a different function from altering receptor mediated Ca^{2+} influx. Dunah *et al* (2000) described changes in subunit composition on the synaptic membrane attributed to internalization.

6.6.2 Functional mechanisms for consideration

A factor that could have masked any upregulation of NMDA receptor function may have been the morphological changes that occur i.e. dendritic spine atrophy following dopamine depletion (Ingham *et al*, 1998; Meshul *et al*, 1999; Arbuthnott *et al*, 2000). This would influence the number of

functional NMDA receptors stimulated in the assay. The morphological changes could be attributed to increased Ca^{2+} influx which causes a reduction in the binding affinity of NMDA receptor subunits for crosslinking structural proteins resulting in depolymerisation of cytoskeletal proteins (Krupp *et al*, 1999; van Rossum and Hanisch, 1999). As a result, despite their necessary role in synaptic function and modification, Ca^{2+} influxes are tightly regulated in neurons as they can also induce neuropathological disturbances that cause cell death (Hardingham and Bading, 2003). One could speculate that to counter possible collapse following dopamine depletion, homeostatic mechanisms in surviving spines would be increased in response to increased NMDA receptor mediated Ca^{2+} influx. Ca^{2+} influx is substantially influenced by homeostatic regulation of intracellular Ca^{2+} levels that occurs to counter changes in neuronal excitability (Yeung *et al*, 2004). Increases of the membrane potential of the medium spiny neurons that follow dopamine depletion would also increase NMDA receptor mediated influx of Ca^{2+} ions (as the Mg^{2+} block is removed) *and* in addition the opening of voltage gated Ca^{2+} channels would increase Ca^{2+} intracellular levels (Tseng *et al*, 2001). It would be necessary to study whether the activity of Ca^{2+}-ATPase is enhanced following dopamine depletion in the striatum to understand some of the mechanisms involved in regulating levels of intracellular Ca^{2+}.

6.6.3 Sensitivity of the NMDA stimulated $^{45}Ca^{2+}$ uptake assay

The issue of sensitivity of the NMDA stimulated $^{45}Ca^{2+}$ uptake assay was considered particularly as NMDA receptor mediated currents are maximal at depolarised potentials and with glycine co-stimulation; two conditions not included in the assay. To induce membrane depolarization in the study would have skewed our measurements of the NMDA mediated $^{45}Ca^{2+}$ uptake response as a consequence of the invariable activation of other channels including L-type voltage activated Ca^{2+} channels. Though as mentioned above, previous studies have found that membrane potential of spiny neurons does become less negative in response to dopamine loss and this was not a variable we could control easily in our preparation. Co-stimulation of NMDA receptors with glycine increases the open probability of receptor channels hence the number of open NMDA receptors and this influences the amplitude of Ca^{2+} currents (Jahr, 1992). Lehohla *et al* (2000) in developing the assay found that addition of 1mM glycine to the assay did not result in a significant difference in NMDA stimulated $^{45}Ca^{2+}$ uptake into the barrel cortex and it was deemed unnecessary to add glycine to the assays used in the current study. A further factor that may have influenced activation of the NMDA

receptors is the use of halothane anaesthetic prior to killing the rats for the assay. Halothane reduces the amplitude of NMDA receptor mediated excitatory postsynaptic potentials (Nishikawa *et al*, 2000). Finally, the conclusive results of the effects of age on NMDA stimulated $^{45}Ca^{2+}$ uptake serve as a strong indication that the assay was indeed sufficiently sensitive to in measuring NMDA mediated Ca^{2+} influx into the striatum.

REFERENCES

Aizman, O., Brismar, H., Uhlén, P., Zettergren, E., Levey, A.I., Forssberg, H., Greengard, P. and Aperia, A. (2000) Anatomical and physiological evidence for D1 and D2 dopamine receptor colocalization in neostriatal neurons. *Nature Neuroscience* **3(3):** 226 - 230

Albin, R.L., Young, A.B. and Penney, J.B. (1989) The functional anatomy of basal ganglia disorders. *Trends in Neurosciences* **12(10)**: 366 – 375

Alexander, G.E. and Crutcher, M.D. (1990) Functional architecture of basal ganglia circuits: neural substrates of parallel processing. *Trends in Neurosciences* **13(7):** 266 - 271

Allen, P.B. (2004) Functional plasticity in the organization of signalling complexes in the striatum. *Parkinsonism and Related Disorders* **10:** 287 - 292

Arbuthnott, G.W., Ingham, C.A. and Wickens, J.R. (2000) Dopamine and synaptic plasticity in the neostriatum. *Journal of Anatomy* **196(4):** 587 - 596

Awad, H., Hubert, G.W, Smith, Y., Levey, A.I. (2000) Activation of metabotropic glutamate receptor 5 has direct excitatory effects and potentiates NMDA receptor currents in neurons of the subthalamic nucleus. *The Journal of Neuroscience* **20(21):** 7871-7879

Bai, L., Hof, P.R., Standaert, D.G., Xing, Y., Nelson, S.E., Young, A.B. and Magnusson, K.R. (2004) Changes in the expression of the NR2B subunit during aging in macaque monkeys. *Neurobiology of Aging* **25(2):** 201- 208

Bar-Gad, I. and Bergman, H. (2001) Stepping out of the box: information processing in the neural networks of the basal ganglia. *Current Opinion in Neurobiology* **11:** 689 – 695

Barria, A. and Malinow, R. (2002) Subunit specific NMDA receptor trafficking to synapses. *Neuron* **35:** 345-353

Berger, A.J., Dieudonne, S. and Ascher, P. (1998) Glycine uptake governs glycine site occupancy at NMDA receptors of excitatory synapses. *Journal of Neurophysiology* **80(6):** 3336 - 3340

Bergman, H. and Deuschl, G. (2002) Pathophysiology of Parkinson's disease: From clinical neurology to basic neuroscience and back. *Movement Disorders* **17(Suppl 3):** S28 – S40

Blackstone, C. and Sheng, M. (1999) Protein targeting and calcium signalling microdomains in neuronal cells. *Cell Calcium* **26(5):** 181 - 192

Blank, T., Nijholt, I., Teichert, U., Kugler, H., Behrsing, H., Fienberg, A., Greengard, P. and Spiess J. (1997) The phosphoprotein DARPP-32 mediates cAMP-dependent potentiation of striatal N-methyl-D-aspartate responses. *Proceedings of the National Academy of Sciences USA* **94(26):**14859 – 14864

Bliss, T.V.P. and Collingridge, G.L. (1993) A synaptic model of memory: long-term potentiation in the hippocampus. *Nature* ***361:*** 31 - 38

Bourne, H.R. and Nicoll, R. (1993) Molecular machines integrate coincident synaptic signals. *Neuron* **10 (Suppl):** 65-75

Burnashev, N., Schoepfer, R., Monyer, H., Ruppersberg, J.P., Gunther, W., Seeburg, P.H. and Sakmann, B. (1992) Control by asparagine residues of calcium permeability and magnesium blockade in the NMDA receptor. *Science* **257:** 1415 – 1419

Calabresi, P., Mercuri, N.B., Stefani, A. and Bernardi, G. (1990) Synaptic and intrinsic control of membrane excitability of neostriatal neurons. 1. An in vivo analysis. *Journal of Neurophysiology* **63(4):** 651- 662

Calabresi, P., Mercuri, N.B. and Bernardi, G. (1990) Synaptic and intrinsic control of membrane excitability of neostriatal neurons. II. An in vitro analysis. *Journal of Neurophysiology* **63(4):** 663 - 675

Carlisle, H.J. and Kennedy, M.B. (2005) Spine architecture and synaptic plasticity. *Trends in Neurosciences* **28(4):** 182 – 187

Carman, L.S., Gage, F.H. and Shults, C.W. (1991) Partial lesion of the substantia nigra: relation between extent of lesion and rotational behavior. *Brain Research* **553(2):** 275 – 283

Carroll, R.C. and Zukin, R.S. (2002) NMDA receptor trafficking and targeting: implications for synaptic transmission and plasticity. *Trends in Neurosciences* **25(11):** 571 – 577

Carter, A.G. and Sabatini, B.L. (2004) State-dependent calcium signalling in dendritic spines of striatal medium spiny neurons. *Neuron* **44:** 483 – 493

Cavazzini, M., Bliss, T. and Emptage, N. (2005) Ca^{2+} and synaptic plasticity. *Cell Calcium* **38 (3-4):** 355 – 367

Cepeda, C., Walsh, J.P., Hull, C.D., Buchwald, N.A. and Levine, M.S. (1989) Intracellular neurophysiological analysis reveals alterations in excitation in striatal neurons in aged rats. *Brain Research* **494(4):** 215 – 226

Cepeda, C., Li, Z. ad Levine, M.S. (1996) Aging reduces neostriatal responsiveness to N-methyl- D-aspartate and dopamine: An in vitro electrophysiological study. *Neuroscience* **73(3):** 733 – 750

Cepeda, C., Colwell, C.S., Itri, J.N., Chandler, S.H. and Levine, M.S. (1998) Dopaminergic modulation of NMDA-induced whole cell currents in neostriatal neurons in slices: contribution of calcium conductances. *Journal of Neurophysiology* **79:** 82 – 94

Charpier, S., Mahon, S. and Deniau, J.M. (1999) In vivo induction of striatal long-term potentiation by low-frequency stimulation of the cerebral cortex. *Neuroscience* **91(4):** 1209 - 1222

Chase T.N., Oh J.D. and Blanchet P.J. (1998) Neostriatal mechanisms in Parkinson's disease. *Neurology* **51 (Suppl 2):** S30 – S35

Chase, T.N. and Oh, J.D. (2000) Striatal dopamine- and glutamate-mediated dysregulation in experimental parkinsonism. *Trends in Neurosciences* **23(10 Suppl 1):** S86 – S91

Chen, Q. and Reiner, A. (1996) Cellular distribution of the NMDA receptor NR2A/2B subunits in the rat striatum. *Brain Research* **743(1-2):** 346 – 352

Chung, H.J., Huang, Y.H., Lau, L.F. and Huganir, R.L. (2004) Regulation of the NMDA receptor complex and trafficking by activity-dependent phosphorylation of the NR2B subunit PDZ ligand. *The Journal of Neuroscience* **24(45):** 10248 – 10259

Clements, JD. (1996) Transmitter timecourse in the synaptic cleft: its role in central synaptic function. *Trends in Neurosciences* **19(5):** 163 - 171

Coghlan, V.M., Perrino, B.A., Howard, M., Langeberg, L.K., Hicks, J.B., Gallatin, W.M. and Scott, J.D. (1995) Association of protein kinase A and protein phosphatase 2B with a common anchoring protein. *Science* **267:** 108 – 111

Cohen-Cory S. (2002) The developing synapse: construction and modulation of synaptic structures and circuits. *Science* **298:** 770 – 776

Colledge, M., Dean, R.A., Scott, G.K., Langeberg, L.K., Huganir, R.L. and Scott, J.D. (2000) Targeting of PKA to glutamate receptors through a MAGUK-AKAP complex. *Neuron* **27(1):** 107 – 119

Colwell, C. S. and Levine, M. S. (1995) Excitatory synaptic transmission in neostriatal neurons: regulation by cyclic AMP-dependent mechanisms. *The Journal of Neuroscience* **15(3):** 1704 – 1713

Conti, F. and Weinberg, R.J. (1999) Shaping excitation at glutamatergic synapses. *Trends in Neurosciences* **22(10):** 451 – 458

Cowan, R.L. and Wilson, C.J. (1994) Spontaneous firing patterns and axonal projections of single corticostriatal neurons in the rat medial agranular cortex. *Journal of Neurophysiology* **71(1):** 17 – 32

Cull-Candy S., Brickley S. and Farrant M. (2001) NMDA receptor subunits: diversity, development and disease. *Current Opinion in Neurobiology* **11(3):** 327 – 335

Devan, B.D. and White, N.M. (1999) Parallel information processing in the dorsal striatum: relation to hippocampal function. *The Journal of Neuroscience*: **19(7):** 2789 – 2798

Dostrovsky, J.O. and Lozano, A.M (2002) Mechanisms of deep brain stimulation. *Movement Disorders* **17(Suppl 3):** S63 - S68

Dunah, A.W., Wang Y, Yasuda, R.P., Kameyama, K., Huganir, R.L., Wolfe, B.B. and Standaert, D.G. (2000) Alterations in subunit expression, composition, and phosphorylation of striatal N-methyl-D-aspartate glutamate receptors in a rat 6-hydroxydopamine model of Parkinson's disease. *Molecular Pharmacology* **57(2):** 342 – 352

Dunah A.W. and Standaert D.G. (2001) Dopamine D1 receptor-dependent trafficking of striatal NMDA glutamate receptors to the postsynaptic membrane. *The Journal of Neuroscience* **21(15):** 5546 – 5558

Dunah A.W. and Standaert D.G. (2003) Subcellular segregation of distinct heteromeric NMDA glutamate receptors in the striatum. *Journal of Neurochemistry* **85(4):** 935 – 943

Dunah, A.W., Sirianni, A.C., Fienberg, A.A., Bastia, E., Schwarzschild, M.A. and Standaert, D.G. (2004) Dopamine D1-dependent trafficking of striatal N-methyl-D-aspartate glutamate receptors requires Fyn protein tyrosine kinase but not DARPP-32. *Molecular Pharmacology* **65(1):** 121 – 129

Dunia, R., Buckwalter, G., Defazio, T., Villar, F.D., McNeill, T.H. and Walsh, J.P. (1996) Decreased duration of Ca^{2+}-mediated plateau potentials in striatal neurons from aged rats. *Journal of Neurophysiology* **76(4):** 2353 – 2363

Dunnett, S.B. and Bjorklund, A. (1999) Prospects for new restorative and neuroprotective treatments in Parkinson's disease. *Nature* **399 (Suppl):** A32 – A39

Dure, L.S., Young, A.B/, Penney, J.B. (1992) Compartmentalization of excitatory amino acid receptors in human striatum. *Proceedings of the National Academy of Sciences USA* **89(16):** 7688 – 7692

Eccles, J.C. (1964) *The Physiology of Synapses.* New York, Academic Press

Ehlers, M.D., Zhang, S., Bernhadt, J.P. and Huganir, R.L. (1996) Inactivation of NMDA receptors by direct interaction of calmodulin with the NR1 subunit. *Cell* **84(5):** 745 – 755

Erreger, K., Dravid, S.M., Banke, T.G., Wyllie, D.J. and Traynelis, S.F. (2005) Subunit-specific gating controls rat NR1/NR2A and NR1/NR2B NMDA channel kinetics and synaptic signalling profiles. *The Journal of Physiology* **563 (2):** 345 – 358

Feldman, D., Sherin, J.E., Press, W.A. and Bear, M.F. (1990) N-methyl-D-aspartate-evoked calcium uptake by kitten visual cortex maintained in vitro. *Experimental Brain Research* **80:** 252 – 259

Flores-Hernández, J., Cepeda, C., Hernández-Echeagaray, E., Calvert, C.R., Jokel, E.S., Fienberg, A.A., Greengard, P. and Levine, M.S. (2002) Dopamine enhancement of NMDA currents in dissociated medium sized striatal neurons: role of D1 receptors and DARPP-32. *Journal of Neurophysiology* **88:** 3010 – 3020

Forsythe, I.D. and Westbrook, G.L. (1988) Slow excitatory postsynaptic currents mediated by N-methyl-D-aspartate receptors on cultured mouse central neurons. *Journal of Physiology* **396:** 515 – 533

Gabel, L.A. and Nisenbaum, E.S. (1998) Biophysical characterization and functional consequences of a slowly inactivating potassium current in neostriatal neurons. *Journal of Neurophysiology* **79:** 1989 – 2002

Gardoni, F., Bellone, C., Cattabeni, F. and Di Luca, M. (2001) Protein kinase C activation modulates alpha-calmodulin kinase II binding to NR2A subunit of N-methyl-D-aspartate receptor complex. *The Journal of Biological Chemistry* **276(10):** 7609 – 7613

Ghika, J., Ghika-Schmid, F., Fankhauser, H., Assal, G., Vingerhoets, F., Albanese, A., Bogousslavsky, J. and Favre, J. (1999) Bilateral contemporaneous posteroventral pallidotomy for the treatment of Parkinson's disease: neuropsychological and neurological side effects. Report of four cases and review of the literature. *Journal of Neurosurgery* **91(2):** 313 – 321

Girault J.A., Barbeito L., Spampinato U., Gozlan H., Glowinski J. and Besson M.J. (1986) In vivo release of endogenous amino acids from the rat striatum: further evidence for a role of glutamate and aspartate in corticostriatal neurotransmission. *Journal of Neurochemistry* **47(1):** 98 – 106

Gonzalo, N., Lanciego, J.L., Castle, M., Vázquez, A., Erro, E. and Obeso, J.A. (2002) The parafascicular thalamic complex and basal ganglia circuitry: further complexity to the basal ganglia model. *Thalamus and Related Systems* **1:** 341 – 348

Götz T., Kraushaar U., Geiger J., Lubke J., Berger T. and Jonas P. (1997) Functional properties of AMPA and NMDA receptors expressed in identified types of basal ganglia neurons. *The Journal of Neuroscience* **17**(1): 204 - 215

Graybiel, A.M. (1990) Neurotransmitters and neuromodulators in the basal ganglia. *Trends in Neurosciences* **13(7):** 244 – 253

Griffith, W.H., Jasek, M.C., Bain, S.H. and Murchison, D. (2000) Modification of ion channels and calcium homeostasis of basal forebrain neuron during aging. *Behavioural Brain Research* **115:** 219 – 233

Groves, P.M. (1980) Synaptic endings and their postsynaptic targets in neostriatum: synaptic specializations revealed from analysis of serial sections. *Proceedings of the National Academy of Sciences USA* **77(11):** 6926 - 6929

Haber, S.N., Fudge, J.L. and McFarland, N.R. (2000) Striatonigrostriatal pathways in primates form an ascending spiral from the shell to the dorsolateral striatum. *The Journal of Neuroscience* **20(6):** 2369 – 2382

Håkansson, K., Lindskog, M., Pozzi, L., Usiello, A. and Fisone, G. (2004) DARPP-32 and modulation of cAMP signalling: involvement in motor control and levodopa-induced dyskinesia. *Parkinsonism and Related Disorders* **10:** 281 – 286

Hardingham, G.E., Cruzalegui, F.H., Chawla, S. and Bading, H. (1998) Mechanisms controlling gene expression by nuclear calcium signals. *Cell Calcium* **23(2/3):** 131 – 134

Hardingham, G.E. and Bading, H. (2003) The Yin and Yang of NMDA receptor signalling. *Trends in Neurosciences* **26(2):** 81 – 89

Hernández-López, S., Bargas, J., Surmeier, D.J., Reyes, A. and Galarraga, E. (1997) D1 receptor activation enhances evoked discharge in neostriatal medium spiny neurons by modulating an L-type Ca^{2+} conductance. *The Journal of Neuroscience* **17(9):** 3334 – 3342

Hernández-López, S., Tkatch, T., Perez-Garci, E., Galarraga, E., Bargas, J., Hamm H. and Surmeier, D.J. (2000) D2 dopamine receptors in striatal medium spiny neurons reduce L-type Ca^{2+} currents and excitability via a novel PLC β1-IP3-Calcineurin-signalling cascade. *The Journal of Neuroscience* **20(24):** 8987 – 8995

Heynen, A.J., Quinlan, E.M., Bae, D.C. and Bear, M.F. (2000) Bidirectional activity dependent regulation of glutamate receptors in the adult hippocampus in vivo. *Neuorn* **28:** 527 – 536

Hille, B. (2001) *Ionic channels of excitable membranes*. 3rd Edition. Sunderland – USA:, Sinauer Associates.

Hisatsune, C., Umemori, H., Inoue, T., Michikawa, T., Kohda, K., Mikoshiba, K. and Yamamoto, T. (1997) Phosphorylation-dependent regulation of N-methyl-D-aspartate receptors by calmodulin. *The Journal of Biological Chemistry* **272(33):** 20805 – 20810

Hudson, J.L., van Horne, C.G., Stromberg, I., Brock, S., Clayton, J., Masserano, J., Hoffer, B.J. and Gerhardt, G.A. (1993) Correlation of apomorphine- and amphetamine-induced turning with nigrostriatal dopamine content in unilateral 6-hydroxydopamine lesioned rats. *Brain Research* **626(1-2):** 167- 174

Ingham, C.A., Hood, S.H., Taggart, P. and Arbuthnott, G.W. (1998) Plasticity of synapses in the rat neostriatum after unilateral lesion of the nigrostriatal dopaminergic pathway. *The Journal of Neuroscience* **18(12):** 4732 – 4743

Jahr, C.E. (1992) High probability opening of NMDA receptor channels by L-glutamate. *Science* **255:** 470 – 472

Johnson J.W. and Ascher P. (1987) Glycine potentiates the NMDA response in cultured mouse brain neurons. *Nature* **325:** 529 - 531

Jontes, J.D. and Smith S.J. (2000) Filopodia, spines, and the generation of synaptic diversity. *Neuron* **27:** 11 – 14

Kasai, H., Matsuzaki, M., Noguchi, J., Yasumatsu, N. and Nakahara, H. (2003) Structure-stability-function relationships of dendritic spines. *Trends in Neurosciences* **26(7):** 360 – 368

Kennedy, M.B. (1997) The postsynaptic density at glutamatergic synapses. *Trends in Neurosciences* **20(6):** 264 – 268

Kerr, J.N.D. and Plenz, D. (2002) Dendritic calcium encodes striatal neuron output during up-states. *The Journal of Neuroscience* **22(5):** 1499 – 1512

Kerr, J.N.D. and Plenz, D. (2004) Action potential timing determines dendritic calcium during striatal up-states. *The Journal of Neuroscience* **24(4):** 877 – 885

Kish, L.J., Palmer, M.R., Gerhardt, G.A. (1999) Multiple single-unit recordings in the striatum of freely moving animals: effects of apomorphine and D-amphetamine in normal and unilateral 6-hydroxydopamine-lesioned rats. *Brain Research* **833(1):** 58 – 70

Kiyatkin, E.A. and Rebec, G.V. (1996) Dopaminergic modulation of glutamate-induced excitations of neurons in the neostriatum and nucleus accumbens of awake, unrestrained rats. *Journal of Neurophysiology* **75(1):** 142 – 153

Klauck, T. M., Faux, M. C., Labudda, K., Langeberg, L. K., Jaken, S. and Scott, J. D. (1996) Coordination of three signaling enzymes by AKAP79, a mammalian scaffold protein. *Science* **271:** 1589 – 1592

Kocsis, J.D., Sugimori, M and Kitai, S.T. (1977) Convergence of excitatory synaptic inputs to caudate spiny neurons. *Brain Research* **124:** 403 – 413

Konradi, C., Leveque, J-C. and Hyman, S.E. (1996) Amphetamine and dopamine-induced immediate early gene expression in striatl neurons depends on postsynaptic NMDA receptors and calcium. The *Journal of Neuroscience* **16(13):** 4231-4239

Korkotian, E. and Segal, M. (2001) Spike-associated fast contraction of dendritic spines in cultured hippocampal neurons. *Neuron* **30**: 751 - 758

Kornhauser, J.M., Cowan, C.W., Shaywitz, A.J., Dolmetsch, R.E., Griffith, E.C., Hu, L.S., Haddad, C., Xia, Z. and Greenberg, M.E. (2002) CREB Transcriptional activity in neurons is regulated by multiple calcium specific phosphorylation events. *Neuron* **34:** 221 – 233

Kotter, R. (1994) Postsynaptic integration of glutamatergic and dopaminergic signals in the striatum. *Progress in Neurobiology* **44:** 163 – 196

Krupp, J.J., Vissel, B., Heinemann, S.F. and Westbrook, G.L. (1998) N-terminal domains in the NR2 subunit control desensitization of NMDA receptors. *Neuron* **20:** 317 – 327

Krupp, J. J., Vissel, B., Thomas, C. G., Heinemann, S. F. and Westbrook, G. L. (1999) Interactions of calmodulin and alpha-actinin with the NR1 subunit modulate Ca2+-dependent inactivation of NMDA receptors. *The Journal of Neuroscience* **19(4):** 1165 – 1178

Krupp, J.J., Vissel, B., Thomas, C.G., Heinemann, S.F. and Westbrook, G.L. (2002) Calcineurin acts via the C-terminus of NR2A to modulate desensitization of NMDA receptors. *Neuro Pharmacology* **42:** 593 – 602

Lange, K.W., Kornhuber, J. and Riederer, P. (1997) Dopamine/Glutamate Interactions in Parkinson's disease. *Neuroscience and Biobehavioural Reviews* **21(4):** 393 – 400

Lehohla, M., Russell, V., Kellaway, L. and Govender, A. (2000) Development of a method to evaluate glutamate receptor function in rat barrel cortex slices. *Metabolic Brain disease* **15(4):** 305 – 314

Lehohla, M., Russell, V., Kellaway, L. (2001) NMDA-stimulated Ca^{2+} uptake into barrel cortex slices of spontaneously hypertensive rats. *Metabolic Brain Disease* **16(3/4):** 135 – 143

Leonard, A.S., Lim, I.A., Hemsworth, D.E., Horne, M.C. and Hell, J.W. (1999) Calcium/calmodulin-dependent protein kinase II is associated with the N-methyl-D-aspartate receptor. *Proceedings of the National Academy of Sciences USA* **96(6):** 3239 – 3244

Levine, M.S/, Adinolfi, A.M., Fisher, R.S., Hull, C.D., Guthrie, D. and Buchwald, N.A. (1988) Ultrastructural alterations in caudate nucleus in aged cats. *Brain Research* **440(2):** 267 – 279

Li, B., Murphy, T.H., Raymond, L.A (2003) Developmental decrease in NMDA receptor desensitization associated with shift to synapse and interaction with postsynaptic density 95. The *Journal of Neuroscience* **23(35):** 11244 – 11254

Lieberman, D. N. and Mody, I. (1994) Regulation of NMDA channel function by endogenous Ca(2+)-dependent phosphatase. *Nature* **369:** 235 – 239

Lieberman, D.N. and Mody, I. (1999) Casein kinase II regulates NMDA channel function in hippocampal neurons. *Nature Neuroscience* **2(2):** 125 – 132

Lin, J.Y., Dubey, R., Funk, G.D. and Lipski, J. (2003) Receptor subtype-specific modulation by dopamine of glutamatergic responses in striatal medium spiny neurons. *Brain Research* **959:** 251 – 262

Lin, Y., Skeberdis, V.A., Francesconi, A., Bennett, M.V. and Zukin, R.S. (2004) Postsynaptic density protein-95 regulates NMDA channel gating and surface expression. *The Journal of Neuroscience* **24(45):** 10138 – 10148

Lisman, J., Schulman, H. and Cline, H. (2002) The molecular basis of CaMKII function in synaptic and behavioural memory. *Nature Reviews Neuroscience* **3(3):** 175 – 190

Llinás, R.R. (1988) The intrinsic electrophysiological properties of mammalian neurons: Insights into central nervous system function. *Science* **242:** 1654 – 1655

Loftis, J.M. and Janowsky, A. (2003) The N-methyl-D-aspartate receptor subunit NR2B: localization, functional properties, regulation, and clinical implications. *Pharmacology and Therapeutics* **97(1):** 55 – 85

Luo,J., Wang, Y., Yasuda, R.P., Dunah, A.W., Wolfe, B.B (1997) The majority of N-methyl-D-aspartate receptor complexes in adult rat cerebral cortex contain at least three different subunits (NR1/NR2A/NR2B). *Molecular Pharmacology* **51**: 79 – 86

MacDermott, A.B., Mayer, M.L., Westbrook, G.L., Smith, S.J. and Barker, J.L.(1986) NMDA receptor activation increases cytoplasmic calcium concentration in cultured spinal cord neurones. *Nature* **321:** 519 - 522

Mahon, S., Deniau, J-M. and Charpier, S. (2003a) Various synaptic activities and firing patterns in cortico-striatal and striatal neurons in vivo. *Journal of Physiology (Paris)* **97:** 557- 566

Mahon, S., Casassus, G., Mulle, C. and Chapier, S. (2003b) Spike-dependent intrinsic plasticity increases firing probability in rat striatal neurons in vivo. *Journal of Physiology* **550(3):** 947 - 959

Matsuda, K., Fletcher, M., Kamiya, Y. and Yuzaki, M. (2003) Specific assembly with the NMDA receptor 3B subunit controls surface expression and calcium permeability of NMDA receptors. *The Journal of Neuroscience* **23(31):** 10064 - 10073

Marsden, C.D. and Obeso, J.A. (1994) The functions of the basal ganglia and the paradox of stereotaxic surgery in Parkinson's disease. *Brain* **117:** 877 – 897

Meshul, C. K., Emre, N., Nakamura, C. M., Allen, C., Donohue, M. K. and Buckman, J. F. (1999) Time-dependent changes in striatal glutamate synapses following a 6-hydroxydopamine lesion. *Neuroscience* **88(1):** 1 - 16

Mink, J.W. (1999) The Basal Ganglia. In Zigmond, M.J., Bloom, F.E., Landis, S.C., Roberts, J.L. and Squire, L.R. (Eds) *Fundamental Neuroscience.* USA, Academic Press – Elsevier Science

Mitchell, J.J. and Anderson, K.J. (1998) Age-related changes in [^{3}H]MK-801 binding in the Fischer 344 rat brain. *Neurobiology of Aging* **19(3):** 259 - 265

Montastruc, J.L., Rascol, O. and Senard, J.M. (1997) Glutamate antagonists and Parkinson's disease: a review of clinical data. *Neuroscience and biobehavioural reviews* **21(4):** 477 – 480

Monyer, H., Sprengel, R., Schoepfer, R., Herb A., Higuchi, M., Lomeli, H., Burnashev, N., Sakmann, B. and Seeburg, P.H. Heteromeric NMDA receptors molecular and functional distinction of subtypes, *Science* **256:** 1217 – 1221

Moore, A.E., Cicchetti, F., Hennen, J. and Isacson, O. (2001) Parkinsonian motor deficits are reflected by proportional A9/A10 dopamine neuron degeneration in the rat. *Experimental Neurology* **172(2):** 363 – 376

Morari, M., O'Connor, W.T., Ungerstedt, U., Bianchi, C. and Fuxe, K. (1996) Functional neuroanatomy of the nigrostriatal and striatonigral pathways as studied with dual probe microdialysis in the awake rat--II. Evidence for striatal N-methyl-D-aspartate receptor regulation of striatonigral GABAergic transmission and motor function. *Neuroscience* **72(1):** 89 – 97

Mori H. and Mishina M. (1995) Structure and function of the NMDA receptor channel. *Neuropharmacology* **34(10):** 1219 – 1237

Mothet, J.P., Parent, A.T., Wolosker, H., Brady, R.O. Jr, Linden, D.J., Ferris, C.D., Rogawski, M.A. and Snyder, S.H. (2000) D-serine is an endogenous ligand for the glycine site of the N-methyl-D-aspartate receptor. *Proceedings of the National Academy of Sciences USA* **97(9):** 4926 – 4931

Nakanishi, S. (1992) Molecular diversity of glutamate receptors and implications for brain function. *Science* **258:** 597 – 603

Nakanishi, S. (1994) Metabotropic glutamate receptors: synaptic transmission, modulation, and plasticity. *Neuron* **13:**1031 – 1037

Nash, J.E. and Brotchie, J.M. (2002) Characterisation of striatal NMDA receptors involved in the generation of parkinsonian symptoms: intrastriatal microinjection studies in the 6-OHDA-lesioned rat. *Movement Disorders* **17(3):** 455 – 466

Nisenbaum, E.S. and Wilson, C.J. (1995) Potassium currents responsible for inward and outward rectification in rat neostriatal spiny projection neurons. *The Journal of Neurosciences* **15(6):** 4449 – 4463

Nishi, A., Wanatabe, Y., Higashi, H., Tanaka, M., Nairn, A.C. and Greengard, P. (2005) Glutamate regulation of DARPP-32 phosphorylation in neostriatal neurons involves activation of multiple signalling cascades. *Proceedings of the National Academy of Sciences USA* **102 (4):** 1199 – 1204

Nishikawa, K. and MacIver, M.B. (2000) Excitatory synaptic transmission mediated by NMDA receptors is more sensitive to isoflurane than are non-NMDA receptor mediated responses. *Anethesiology* **92(1):** 228-236

Nowak, L., Bregestovski, P., Ascher, P., Herbet, A. and Prochiantz, A. (1984) Magnesium gates glutamate-activated channels in mouse central neurones. *Nature* **307:**462 – 465

Oh, J. D., Russell, D. S., Vaughan, C. L. and Chase, T. N. (1998) Enhanced tyrosine phosphorylation of striatal NMDA receptor subunits: effect of dopaminergic denervation and L-DOPA administration. *Brain Research* **813(1):** 150 – 159

Oh, J.D. and Chase, T.N. (2002) Glutamate-mediated striatal dysregulation and the pathogenesis of motor response complications in Parkinson's disease. *Amino acids* **23:** 133 – 139

Olanow, C.W. and Tatton, W.G. (1999) Etiology and pathogenesis of Parkinson's disease. *Annual Review of Neuroscience* **22:** 123 – 144

Packard, M.G. and Knowlton, B.J. (2002) Learning and memory functions of the basal ganglia. *Annual Review of Neuroscience* **25:** 563 – 593

Parent, A. (1990) Extrinsic connections of the basal ganglia. *Trends in Neurosciences* **13(7):** 254 – 258

Pauly, T., Schlicksupp, A., Neugebauer, R. and Kuhse, J. (2005) Synaptic targeting of N-methyl-D-aspartate receptor splice variants is regulated differentially by receptor activity. *Neuroscience* **131(1):** 99 – 111

Pawson, T. and Scott, J.D. (1997) Signaling through scaffold, anchoring, and adaptor proteins. *Science* **278:** 2075 – 2080

Pei, L., Lee, F.J., Moszczynska, A., Vukusic, B. and Liu, F. (2004) Regulation of dopamine D1 receptor function by physical interaction with the NMDA receptors. *The Journal of Neuroscience* **24(5):** 1149 – 1158

Pickel, V.M., Beckley, S.C., Joh, T.H. and Reis, D.J. (1981) Ultrastructural immunocytochemical localization of tyrosine hydroxylase in the neostriatum. *Brain Research* **225(2):** 373 – 385

Plenz, D. (2003) When inhibition goes *incognito*: feedback interaction between spiny projection neurons in striatal function. *Trends in Neurosciences* **26(8):** 436 – 443

Qian, A. and Johnson, J.W. (2002) Channel gating of NMDA receptors. *Physiology and Behaviour* **77(4-5):** 577 – 582

Raman, I.M., Tong, G. and Jahr, C.E. (1996) Beta-adrenergic regulation of synaptic NMDA receptors by cAMP-dependent protein kinase. *Neuron* **16(2):** 415 – 421

Reynolds, J.N. and Wickens, J.R. (2002) Dopamine-dependent plasticity of corticostriatal synapses. *Neural Networks* **15(4-6):** 507 – 521

Rosenmund, C., Feltz, A. and Westbrook, G.L. (1995) Synaptic NMDA receptor channels have a low open probability. *The Journal of Neuroscience* **15(4):** 2788 – 2795

Rumbaugh, G. and Vicini, S. (1999) Distinct synaptic and extrasynaptic NMDA receptors in developing cerebellar granule neurons. *The Journal of Neuroscience* **19(24):** 10603 – 10610

Rycroft, B.K. and Gibb, A.J. (2004) Inhibitory interactions of calcineurin (phosphatase 2B) and calmodulin on rat hippocampal NMDA receptors. *Neuro Pharmacology* **47:** 505 – 514

Sairni, Y. and Kung, C (2002) Calmodulin as an ion channel subunit. *Annual Review of Physiology* **64:** 289 – 311

Salter, M.W. (2003) D1 and NMDA receptors hook up: expanding on an emerging theme. *Trends in Neurosciences.* **26(5):** 235 – 237

Salter, M. W. and Kalia, L. V. (2004) Src kinases: a hub for NMDA receptor regulation. *Nature Reviews Neuroscience* **5(4):** 317 – 328

Sandstrom, M.I. and Rebec, G.V. (2003) Characterization of striatal activity in conscious rats: contribution of NMDA and AMPA/kainate receptors to both spontaneous and glutamate-driven firing. *Synapse* **47(2):** 91 – 100

Saper, C.B. (1999) 'Like a thief in the night': the selectivity of degeneration in Parkinson's disease. *Brain* **122(8):** 1401 – 1402

Scannevin, R.H. and Huganir, R.L. (2000) Postsynaptic organization and regulation of excitatory synapses. *Nature Reviews Neuroscience* **1**: 133 – 141

Schultz, W. (2000) Multiple reward signals in the brain. *Nature Reviews Neuroscience* **1:** 199 – 207

Schmidt, W.J. and Kretschmer, B.D. (1997) Behavioural pharmacology of glutamate receptors in the basal ganglia. *Neuroscience and biobehavioural reviews* **21(4):** 381 – 392

Scott, D.B., Blanpied, T.A., and Ehlers, M.D. (2003) Coordinated PKA and PKC phosphorylation suppresses RXR-mediated ER retention and regulates the surface delivery of NMDA receptors. *Neuropharmacology* **45:** 755 – 767

Segal, M., Korkotian, E. and Murphy, D.D. (2000) Dendritic spine formation and pruning: common cellular mechanisms? *Trends in Neurosciences* **23(2):** 53 – 57

Segovia, G., Porras, A., Arco, A.D. and Mora, F. (2001) Glutamatergic neurotransmission in aging: a critical perspective. *Mechanisms of Ageing and Development* **122:** 1 – 29

Segovia, G. and Mora, F. (2005) Dopamine and GABA increases produced by activation of glutamate receptors in the nucleus accumbens are decreased during aging. *Neurobiology of Aging* **26:** 91 – 101

Sheng, M. and Kim M.J. (2002) Postsynaptic signaling and plasticity mechanisms. *Science* **298:** 776 – 80

Shulman, H. and Hyman (1999) Intracellular Signaling. In Zigmond, M.J., Bloom, F.E., Landis, S.C., Roberts, J.L. and Squire, L.R. (Eds) *Fundamental Neuroscience.* USA, Academic Press – Elsevier Science

Sim, A. T. and Scott, J. D. (1999) Targeting of PKA, PKC and protein phosphatases to cellular microdomains. *Cell Calcium* **26(5):** 209 – 17

Smart, T.G. (1997) Regulation of excitatory and inhibitory neurotransmitter-gated ion channels by protein phosphorylation. *Current Opinion in Neurobiology* **7(3):** 358 – 367

Smith, A.D. and Bolam, J.P. (1990) The neural network of the basal ganglia as revealed by the study of synaptic connections of identified neurons. *Trends in Neurosciences* **13(7):** 259 – 265

Smith, Y., Bevan, M.D., Shink, E. and Bolam, J.P. (1998) Microcircuitry of the direct and indirect pathways of the basal ganglia. *Neuroscience* **86(2):** 353 – 387

Snyder, G.L., Fienberg, A.A., Huganir, R.L. and Greengard, P. (1998) A dopamine / D1 receptor / Protein Kinase A / dopamine-and cAMP – regulated phosphoprotein (Mr 32kDa) / Protein phosphatase -1 pathway regulates dephosphorylation of the NMDA receptor. *The Journal of Neuroscience*. **18(24):** 10297 – 10303

Stern, E.A., Jaeger, D. and Wilson, C.J. (1998) Membrane potential synchrony of simultaneously recorded striatal spiny neurons in vivo. *Nature* **394:** 475 – 478

Strack, S., McNeill, R. B. and Colbran, R. J. (2000) Mechanism and regulation of calcium/calmodulin-dependent protein kinase II targeting to the NR2B subunit of the N-methyl-D-aspartate receptor. *The Journal of Biological Chemistry* **275(31):** 23798 – 23806

Surmeier, D.J., Song, W-J. and Yan, Z. (1996) Coordinated expression of dopamine receptors in neostriatal medium spiny neurons. *The Journal of Neuroscience* **16(20):** 6579 – 6591

Svenningsson, P., Nishi, A.., Fisone, G., Girault, J-A.; Nairn, A.C. and Greengard, P. (2004) DARPP-32: An integrator of neurotransmission. *Annual Review of Pharmacology and Toxicology* **44:** 269 – 296

Takakusaki, K., Habaguchi, T., Ohtinata-Sugimoto, J., Saitoh, K. and Sakamoto, T. (2003) Basal ganglia efferents to the brainstem centers controlling postural muscle tone and locomotion: a new concept for understanding motor disorders in basal ganglia dysfunction. *Neuroscience* **119:** 293 – 308

Tao-Cheng, J. H., Vinade, L., Smith, C., Winters, C. A., Ward, R., Brightman, M. W., Reese, T. S. and Dosemeci, A. (2001) Sustained elevation of calcium induces Ca(2+)/calmodulin-dependent protein kinase II clusters in hippocampal neurons. *Neuroscience* **106(1):** 69 – 78

Tao-Cheng, J. H., Vinade, L., Winters, C.A., Reese, T.S. and Dosemeci, A. (2005) Inhibition of phosphatase activity facilitates the formation and maintenance of NMDA-induced Calcium/Calmodulin-dependent protein kinase II clusters in hippocampal neurons. *Neuroscience* **130:** 651 – 656

Tingley, W. G., Ehlers, M. D., Kameyama, K., Doherty, C., Ptak, J. B., Riley, C. T. and Huganir, R. L. (1997) Characterization of protein kinase A and protein kinase C phosphorylation of the N-methyl-D-aspartate receptor NR1 subunit using phosphorylation site-specific antibodies. *The Journal of Biological Chemistry* **272(8):** 5157 – 5166

Trovar, K.R. and Westbrook, G.L (2002) Mobile NMDA receptors at hippocampal synapses. *Neuron* **34:** 255 – 264

Tseng, K.Y., Kasanetz, F., Kargieman, L., Riquelme, L.A. and Murer, M.G. (2001) Cortical slow oscillatory activity is reflected in the membrane potential and spike trains of striatal neurons in rats with chronic nigrostriatal lesions. *The Journal of Neuroscience* **21(16):** 6430 – 6439

Valjent,E., Pascoli, V., Svennigsson, P., Paul, S., Corvol, J-C., Stippanovich, A., Caboche, J., Lombroso, P.J., Naim, A.C., Greengard, P., Herve, D. and Girault, J-A. (2005) Regulation of a protein phosphatase cascade allows convergent dopamine and gluatamet signals to activate ERK in the striatum. *Proceedings of the National Academy of Sciences USA* **102(2):** 491 – 496

van Rossum, D. and Hanisch, U-K. (1999) Cytoskeletal dynamics in dendritic spines: direct modulation by glutamate receptors? *Trends in Neurosciences* **22(7):** 290 – 295

van Zundert B., Yoshii A. and Constantine-Paton M. (2004) Receptor compartmentalization and trafficking at glutamate synapses: a developmental proposal. *Trends in Neurosciences* **27(7):** 428 – 437

Venance, L. and Glowinski, J. (2003) Heterogeneity of spike frequency adaptation among medium spiny neurons from the rat striatum. *Neuroscience* **122:** 77 – 92

Voorn, P., Vanderschuren, L.J.M.J., Groenewegen, H.J., Robbins, T.W. and Pennartz, C.M.A (2004) Putting a spin on the dorsal-ventral divide of the striatum. *Trends in Neurosciences* **27(8):** 468 – 474

Wang, Y.T., Yu, X-M. and Salter, M.W. (1996) Ca^{2+} independent reduction of NMDA channel activity by tyrosine phosphorylation. *Proceedings of the National Academy of Sciences USA* **93:** 1721 – 1725

Wang, W.W., Cao, R., Rao, Z.R. and Chen, L.W. (2004) Differential expression of NMDA and AMPA receptor subunits in DARPP-32-containing neurons of the cerebral cortex, hippocampus and neostriatum of rats. *Brain Research* **998(2):** 174 – 183

Wenk, G.L. and Barnes, C.A. (2000) Regional changes in the hippocampal density of AMPA and NMDA receptors across the lifespan of the rat. *Brain Research* ***885*:** 1 – 5

West, A.R. and Grace, A.A. (2002) Opposite influences of endogenous dopamine D1 and D2 receptor activation on activity states and electrophysiological properties of striatal neurons: studies combining in vivo intracellular recordings and reverse microdialysis. *The Journal of Neuroscience* **22(1):** 294 – 304

Wichmann, T. and DeLong, M.R. (2003) Pathophysiology of Parkinson's disease: The MPTP primate model of the human disorder. *Annals of the New York Academy of Sciences* **991:** 199 – 213

Wickens, J.R., Reynolds, J.N.J. and Hyland, B.I. (2003) Neural mechanisms of reward-related motor learning. *Current Opinion in Neurobiology* **13:** 685 – 690

Wickens, J.R., and Wilson, C.J. (1998) Regulation of action potential firing in spiny neurons of the rat neostriatum in vivo. *Journal of Neurophysiology* **79:** 2358 – 2364

Wroblewski, J.T., Fadda, E., Mazzetta, J., Lazarewicz, J.W. and Costa, E. (1989) Glycine and D-serine act as positive modulators of signal transduction at N-methyl-D-aspartate sensitive glutamate receptors in cultured cerebellar granule cells. *Neuropharmacology* **28(5):** 447 – 452

Xin, W-K., Kwan, C.L., Zhao, X-H., Xu, J., Ellen, R.P., McCulloch, C.A.G. and Yu, X-M. (2005) A functional interaction of sodium and calcium in the regulation of NMDA receptor activity by remote NMDA receptors. *The Journal of Neuroscience* **25(1):** 139 – 148

Yang L, Mao L, Tang Q, Samdani S, Liu Z, Wang JQ. (2004) A novel Ca2+-independent signaling pathway to extracellular signal-regulated protein kinase by coactivation of NMDA receptors and metabotropic glutamate receptor 5 in neurons. *The Journal of Neuroscience* **24(48):** 10846 – 10857

Yasumoto, S., Tanaka, E., Hattori, G., Maeda, H., and Higashi, H. (2002) Direct and indirect actions of dopamine on the membrane potential in medium spiny neurons of the mouse neostriatum. *Journal of Neurophysiology* **87:** 1234 – 1243

Yelnik, J. (2002) Functional anatomy of the basal ganglia. *Movement Disorders* **17(Suppl 3):** S15 – S21

Yeung, L.C., Shouval, H.Z., Blais, B.S. and Cooper, L.N. (2004) Synaptic homeostasis and input selectivity follow from a calcium-dependent plasticity model. *Proceedings of the National Academy of Sciences USA* **101(41):** 14943 – 14948

Zigmond, M.J., Bloom, F.E., Landis, S.C., Roberts, J.L. and Squire, L.R. (1999) *Fundamental Neuroscience*. USA, Academic Press – Elsevier Science

ANNEX A REPORT OF RATS USED FOR STUDY

K GROUP lesioned RAT	WEIGHT week pre-lesion (g)	5/10/04 & WEIGHT at lesion (g)	6/10/2004 WEIGHT CHANGE (g)	WEIGHT day 2 post lesion (g)	WEIGHT CHANGE (g)	WEIGHT week 1 post lesion (g)	WEIGHT week 2 post lesion (g)
K1	317	352	35	316	-36	278	264
K2	302	343	41	314	-29	305	312
K3	305	341	36	310	-31	276	275
K4	304	336	32	314	-22	273	263
K5	297	331	34	298	-33	259	286
K6	304	331	27	306	-25	277	278
K7	303	330	27	309	-21	301	313
K8	297	329	32	315	-14	300	317
K9	298	336 unlesioned	0	341		365	380

M GROUP lesioned RAT	WEIGHT week pre-lesion (g)	5/10/04 & WEIGHT at lesion (g)	6/10/2004 WEIGHT CHANGE (g)	WEIGHT day 2 post lesion (g)	WEIGHT CHANGE (g)	WEIGHT week 1 post lesion (g)	WEIGHT week 2 post lesion (g)
M1	330	360	30	336	-24	293	297
M2	290	325	35	297	-28	258	253
M3	330	365	35	337	-28	312	320
M4	340	365	25	346	-19	306	297
M5	320	358	38	328	-30	303	318
M6	329	365	36	336	-29	303	302
M7	315	366	51	333	-33	346	356

K GROUP RAT	WEIGHT CHANGE from date of lesion (g)	Type of lesion	Number apomorphine rotations	Post lesion treatment
K1	-88	6-OHDA	1419	TH staining
K2	-31	6-OHDA	1950	Ca UPTAKE ASSAY
K3	-66	6-OHDA	1341	Ca UPTAKE ASSAY
K4	-73	6-OHDA	453	Ca UPTAKE ASSAY
K5	-45	6-OHDA	760	Ca UPTAKE ASSAY
K6	-53	sham	16	Ca UPTAKE ASSAY
K7	-17	sham	0	Ca UPTAKE ASSAY
K8	-12	sham	45	Ca UPTAKE ASSAY
K9	82	unlesioned	93	Ca UPTAKE ASSAY

M GROUP RAT	WEIGHT CHANGE from date of lesion (g)	Type of lesion	Number apomorphine rotations	Post lesion treatment
M1	-63	6-OHDA	1104	Ca UPTAKE ASSAY
M2	-72	6-OHDA	595	Ca UPTAKE ASSAY
M3	-45	6-OHDA	-402	TH staining sacrificed 2/11/04 cyst infection
M4	-68	6-OHDA	208	died in cage 20/10/04 suspected urinary tract infection (blood filled erect genetalia)
M5	-40	6-OHDA	1700	Ca UPTAKE ASSAY
M6	-63	6-OHDA	707	TH staining sacrificed 2/11/04 cyst infection
M7	-10	sham	not rotated	sacrificed 20/10/04 stitch infection and cyst

M8	329	364	35	338	-26	324	330

ANNEX A REPORT OF RATS USED FOR STUDY

M9	322	359	37	325	-34	350	392
M10	292	336	44	309	-27	317	344
M11	310	365	55	325	-40	328	367
M12	306	357	51	324	-33	326	369
M13	310g						
M14	350g						
M15	380g						

N GROUP RAT	lesioned WEIGHT week pre-lesion (g)	16/10/04 & WEIGHT at lesion (g)	17/10/04 WEIGHT CHANGE (g)	WEIGHT day 2 post lesion (g)	WEIGHT CHANGE (g)	WEIGHT week 1 post lesion (g)	WEIGHT week 2 post lesion (g)
N1	301g	381	80	349	-32	324	366
N2	291g	349	58	not survive surgery			
N3	327g	387	60	359	28	310	290
N4	320g	396	76	359	37	333	370
N5	292g	360	68	342	-18	334	380
N6	294g	355	61	326	-29	319	348
N7	330g	379	49	351	-28	306	344
N8	303g	361	58	336	-25	354	385
N9	290g	338	48	324	-14	345	360
N10	305g	358	53	334	-24	308 cyst	
N11	322g	385	63	371	-14	368 cyst	

M8	-34	sham	-220	TH staining
				sacrificed 2/11/04
				cyst infection
M9	33	sham	-303	Ca UPTAKE ASSAY
M10	8	sham	26	Ca UPTAKE ASSAY
M11	2	sham	-278	Ca UPTAKE ASSAY
M12	12	sham	-22	
M13		Needle placement		TH staining and cresyl violet staining
M14		Needle placement		
M15		Needle placement		

N GROUP RAT	WEIGHT CHANGE from date of lesion (g)	Type of lesion	Number apomorphine rotations	Post lesion treatment
N1	-15	6-OHDA		sacrificed 9/11/04
				cyst infection
N2				
N3	-97	6-OHDA	661	sacrificed 2/11/04
				suspected urinary tract infection
				bladder from autopsy shows
				thickish yellow urine and blood
N4	-26	6-OHDA		sacrificed 2/11/04
				cyst infection
N5	20	6-OHDA		sacrificed 9/11/04
				cyst infection
N6	-7	6-OHDA		sacrificed 9/11/04
				cyst infection
N7	-35	sham	-67	sacrificed not used in study
N8	24	sham	-83	sacrificed not used in study
N9	22	sham	-98	sacrificed not used in study
N10		sham		sacrificed 27/10/04
				cyst infection
				organs to Stellenbosch
N11		sham		taken to Stellenbosch alive 27/10/04

N12	307g		355	48	332	-23	328	350

ANNEX A REPORT OF RATS USED FOR STUDY

N13	368g
N14	372g
N15	357g
N16	390g

O GROUP RAT	lesioned WEIGHT week pre-lesion (g)	4/11/04 & WEIGHT at lesion (g)	5/11/2004 WEIGHT CHANGE (g)	WEIGHT day 2 post lesion (g)	WEIGHT CHANGE (g)	WEIGHT week 1 post lesion (g)	WEIGHT week 2 post lesion (g)
O1	364	390	26	353	-37	302	300
O2	346	359	13	333	-26	316	284
O3	310	335	25	320	-15	346	
O4	345	370	25	335	-35	330	398
O5	333	356	23	322	-34	301	333
O6	343	362	19	317	-45		
O7	307	340	33	300	-40	263	212
O8	345	370	25	336	-34		
O9	358	379	21	342	-37		
O10	335	355	20	319	-36	297	322
O11	366	391	25	367	-24	355	372
O12	351	388	37	350	-38	330	360
O13	347	398	51	362	-36	364	382
O14	346	385	39	355	-30	328	340
O15	375	410	35	385	-25		
O16	330	390	60	342	-48	384	404
O17	338g						
O18	353g						

				cyst infection
N12	-5	sham		sacrificed 2/11/04
				cyst infection
N13		Needle placement		
N14		Needle placement		
N15		Needle placement		
N16		Needle placement		

O GROUP RAT	WEIGHT CHANGE from date of lesion (g)	Type of lesion	Number apomorphine rotations	Post lesion treatment
O1	-90	6-OHDA	705	Ca UPTAKE ASSAY
O2	-75	6-OHDA	1977	Ca UPTAKE ASSAY
O3		6-OHDA		sacrificed 13/11/04
				cyst infection
O4	28	6-OHDA	-197	sacrificed not used in study
O5	-23	6-OHDA	1022	Ca UPTAKE ASSAY
O6		6-OHDA		sacrificed 9/11/04
				Paws with blood from scratching nose
				stitches untouched
O7	-128	6-OHDA	648	Ca UPTAKE ASSAY
O8		6-OHDA		died in cage 9/11/04
				Nostrils red
				eyes filled with red fluid
O9		6-OHDA		sacrificed 9/11/04
				cyst infection
O10	-33	6-OHDA	1872	Ca UPTAKE ASSAY
O11	-19	sham	-91	Ca UPTAKE ASSAY
O12	-28	sham	127	Ca UPTAKE ASSAY
O13	-16	sham	-134	Ca UPTAKE ASSAY
O14	-45	sham	-157	Ca UPTAKE ASSAY
O15		sham	-12	Ca UPTAKE ASSAY
O16	14	sham	-80	sacrificed not used in study
O17		Needle placement		
O18		Needle placement		

O19	349g
O20	330g

O19 Needle placement
O20

ANNEX A

2.1 MATERIALS

2.1.1 SURGICAL LESION PROCEDURE

- Airtight container
- Blease vaporisor (Clinical & Medical Services, 4 Stanley Road, Observatory, South Africa)
- 2-bromo-2-chloro 1:1:1 trifluoroethane with 0.01% thymol (Halothane) (Safeline Pharmaceuticals LTD, 1 Manchester Road, Wadeville, South Africa)
- Desipramine hydrochloride

  Desipramine hydrochloride No D-3900 (Sigma Chemical Company, St Louis MO 63178, USA).

  Desipramine hydrochloride USP grade D-125 (Research Biochemicals Incorporated, 1 Strathmore Road, Natick, MA 01760 USA).
- Hamilton Syringe (Hamilton Bonaduz AG, OH-7402 Bonaduz, Switzerland)
- L-Ascorbic Acid (Merck, 64271 Darmstadt, Germany)
- Medical Oxygen (Air Liquide, Cape Town, South Africa)
- Silk suturing thread (CliniSilk 3/0) CliniSut, Sasurel (Pty)LTD 21 McHardy Avenue, Holland Park, Port Elizabeth 6001, South Africa
- Stereotaxic apparatus
- Syringe Pump (Model 341A, Sage Instruments, Division of Orion Research Incorporated, 840 Memorial Drive Cambridge, MA 02139, USA)
- 2,4,5-Trihydroxyphenethylamine (6-hydroxydopamine) Hydrochloride (6-OHDA) (Sigma Aldrich Company, St Louis MO 63178, USA).

2.1.2 BEHAVIOURAL ASSESSMENT OF 6-OHDA LESIONING

- Apomorphine hydrochloride hemihydrate (Sigma Chemical Company, St Louis MO 63178, USA)
- Automatic Rodent Monitor V2.02β (Software by Andrē Skarzynski, April 1992)
- Plastic rotameter drums

2.1.3 NMDA STIMULATED CALCIUM UPTAKE ASSAY

- Airtight container
- Branson Sonifier 250 (Branson Sonic Power Company, Danbury, CT 06810, USA)
- Calcium Chloride ($CaCl_2.2H_2O$) (Merck NT Laboratory Supplies, Unit 11, Fedsure Park, Midrand, South Africa)
- D-Glucose (Merck NT Laboratory Supplies, Unit 11, Fedsure Park, Midrand, South Africa)
- Eppendorf vials
- Lanthanum Chloride ($LaCl_3.7H_2O$) (Merck, 64271 Darmstadt, Germany)
- Liquid Scintillation Analyzer (Tri-Carb 2100TR, Packard Bioscience Company)
- Loctite 406 glue
- Magnesium Chloride ($MgCl_2.6H_2O$) (Merck NT Laboratory Supplies, Unit 11, Fedsure Park, Midrand, South Africa)
- Medical Oxygen (Air Liquide, Cape Town, South Africa)
- (N-[2-Hydroxyethyl]piperazine-N'-[2ethanesulfonic acid]) HEPES (Sigma Chemical Company, St Louis MO 63178, USA)
- N-Methyl-D-Aspartic Acid (NMDA) (Sigma Chemical Company, St Louis MO 63178, USA)
- Nylon
- O-rings
- Paint brushes
- Perspex multiwell container
- Perspex tissue container
- Phase flow heater (FH16-D, Grant Instruments (Cambridge) Ltd, Shepreth, Cambridgeshire, SG8 6GB, England)
- Plastic Water bath
- Polyethylene vials (20ml)
- Polystyrene containers

- Potassium Chloride (KCl) (Merck NT Laboratory Supplies, Unit 11, Fedsure Park, Midrand, South Africa)
- PVC Manifold tubing (0.25mm, Watson-Marlow Ltd, Falmouth, Cornwall, TR11 4RU, England)
- Radioactive $^{45}Ca^{2+}$ (PerkinElmer Life & Analytical Sciences, 549 Albany Street, Boston, MA 02118, USA)
  26.93 mCi/ml (23rd January 2004)
  69.62 mCi/ml (14th May 2004)
- Scintillation fluid (Zinsser Analytic, Aquasafe 500 Plus, Howarth Road, Maidenhead, Berkshire SL6 1AP, UK)
- Sodium Chloride (NaCl) Merck Chemicals, 259 Davidson Road, Wadeville 1428, South Africa)
- Staining glass dish
- Surgical instruments (forceps, scalpel, blades etc)
- Teflon vials (5ml)
- Vibrotome (Series 1000 Sectioning system, ARH Horwell)

2.1.4 PROTEIN DETERMINATION

- Bovine Serum Albumin (BSA) (Miles Laboratories, South Africa)
- Copper Sulphate ($CuSO_45H_2O$) (Merck Chemicals,259 Davidson Road, Wadeville, South Africa)
- Cuvettes
- Finnipipette (Thermo Electron Corporation, P.O. Box 100, FIN-01621 Vantaa, Finland)
- Folin-Ciocalteu's Phenol Reagent Acid (Merck, 64271 Darmstadt, Germany)
- Sodium Carbonate (Na_2CO_3) (Merck NT Laboratory Supplies, Unit 11, Fedsure Park, Midrand, South Africa)
- Sodium Potassium Tartrate (Na^+K^+-Tartrate) (BDH Chemicals LTD, Poole, England)

- Test tubes
- UV-VIS Spectrophotometer (UV-9100, Laboratory & Scientific Equipment Company (Lasec), Cape Town, South Africa)
- Water bath (Techne Cambridge Ltd, Duxford, Cambridge, England)

2.1.5 TRANSCARDIAL PERFUSION

- Airtight container
- 2-bromo-2-chloro 1:1:1 trifluoroethane with 0.01% thymol (Halothane) (Safeline Pharmaceuticals LTD, 1 Manchester Road, Wadeville, South Africa)
- Gelatine (Davis Gelatine Industries (Pty) LTD, 25 Verster Street, Delporton, West Krugersdorp, South Africa)
- JungTissue Freezing Medium (Leica, Instruments, GmbH, Postfach 1120, Heidelberger Street, Nussloda, Germany)
- Leica CM 1850 Cryostat (Leica, Instruments, GmbH, Postfach 1120, Heidelberger Street, Nussloda, Germany)
- Liquid nitrogen (Air Liquide, Cape Town, South Africa)
- Microscope slides & cover slips (Labstar 100, Laboratory & Scientific Equipment Company (Lasec), Cape Town, South Africa)
- Paraformaldehyde (Merck-Schuchardt, Schuchardt 85662 Hohenbrum, Germany)
- Phosphate Buffer Solution (0.15M) PBS
- Syringes(50ml)
- Sucrose (Merck Chemicals,259 Davidson Road, Wadeville, South Africa)
- Surgical instruments

2.1.6 TYROSINE HYDROXYLASE IMMUNOSTAINING

- Biotinylated secondary antibody (Sigma Chemical Company, St Louis MO 63178, USA)

- Cy3 Conjugated Affinipure F(ab')2 Fragment Donkey Antimouse IgG (Lot 51344) Jackson ImmunoResearch Laboratories, 872 West Baltimore Pike, PA 19390, USA)
- 3,3'-diaminobenzidine (DAB) Peroxidase Substrate Kit SK 4100 (Vector Laboratories, Inc, Burlingame, CA 94010, USA)
  Buffer Stock Solution
  DAB Stock Solution
  Hydrogen Peroxide Solution
  Nickel Solution
- 4,6 Diamidino-2-Phenylindole dihydrochloride (DAPI)(Lot D-9542 Sigma Chemical Company, St Louis MO 63178, USA)
- Dehydrating alcohol solutions
- Entellan Mounting Medium (Merck, 64271 Darmstadt, Germany)
- Grease pap pen (Science Services, Postfach 190949, Munchen, Germany)
- Horse serum blocking solution (Sigma Chemical Company, St Louis MO 63178, USA)
- Humidifying incubation chamber (The chamber was constructed from Tupperware plastic containers into which removable Perspex frame specially constructed by UCT Department of Human Biology Workshop)
- Hydrogen Peroxide (0.3%) H_2O_2
- Mouse monoclonal anti-tyrosine hydroxylase Clone TH-16 (Sigma Chemical Company, St Louis MO 63178, USA)
- Mowiol Mounting Medium (Hoechst Chemical Company, Germany)
- Phosphate Buffer Solution (0.15M) PBS
- Technical Methanol
- Triton X-100 (BDH Chemicals, Poole, England)
- VECTASTAIN Elite ABC (Avidin-Biotin-Peroxidase Complex) Kit (Vector Laboratories, Inc, Burlingame, CA 94010, USA)
  Reagent A
  Reagent B
- Xylene

2.1.7 CRESYL VIOLET NISSL STAINING

- Acetic Acid (Associated Chemical Enterprises, Gauteng, South Africa)
- Cresyl Violet (BDH Chemicals, Poole, England)
- Sodium Acetate (Hopkin & Williams LTD, Essex, England)

  Thionin (BDH Chemicals, Poole, England)

ANNEX A

2.2 PREPARATION OF SOLUTIONS

2.2.1 SURGICAL LESIONS PROCEDURE

Ascorbate Stock Solution

0.2mg of L-ascorbate was diluted with 1ml sterile saline solution to give a concentration of 0.2%. This solution was only used for one day. However, due to the low concentrations and to enable ease of weighing the ascorbate, a stock solution was made.

6-OHDA Solution

6-Hydroxydopamine hydrochloride (3 mg/ml) was dissolved immediately before use in ice-cold sterile saline containing 0.02% ascorbate to prevent autoxidation of the 6-OHDA. The total volume made varied with each operation depending on the amount weighed.

2.2.2 BEHAVIOURAL ASSESSMENT OF 6-OHDA LESIONING

Apomorphine Solution

Apomorphine (0.5mg/kg) was dissolved in sterile saline solution immediately before use. The amount weighed depended on the weight and number of rats assessed. The apomorphine solution was freshly prepared on the day of assessment.

2.2.3 NMDA STIMULATED CALCIUM UPTAKE ASSAY

The following *stock solutions* were made up and used as described below:

$CaCl_2.2H_2O$ (12mM)

1.76 grams of $CaCl_2.2H_2O$ (147.02 g/mol) were dissolved in one litre of distilled water.

D-Glucose (100mM)

18.02 grams of D-Glucose (180.1 g/mol) were dissolved in one litre of distilled water.

HEPES (200mM)

47.66 grams of HEPES (238.3 g/mol) were dissolved in ≈800ml of distilled water. The solution was adjusted to pH to 7.4 by adding 5M NaOH drop by drop. The solution was then made up to one litre with distilled water.

KCl (33.6mM)

2.52 grams of KCl (74.56g/mol) were dissolved in one litre of distilled water

$LaCl_3.7H_2O$ (100mM)

37.14 grams of $LaCl_3.7H_2O$ (371.37 g/mol) were dissolved in one litre of distilled water.

$MgCl_2.6H_2O$ (10mM)

2.03 grams of $MgCl_2.6H_2O$ (203.3 g/mol) were dissolved in one litre of distilled water.

NaCl (1.2M)

70.12 grams of NaCl (58.44g/mol) were dissolved in one litre of distilled water.

NMDA (100mM)

1.47 grams of NMDA (147.1 g/mol) were dissolved in 90µl of distilled water. The pH was adjusted to 7 by mixing with 10µl 5M NaOH. The solution was wrapped in foil to avoid exposure to light and was stored at 4°C. The solution was used within two weeks.

Working solutions

HEPES Buffer Solution

The solution was freshly prepared in a 500ml volumetric flask. To the volumetric flask, 50ml of each of the abovementioned stock solutions was added to the volumetric flask and the final volume was made up to the mark with distilled water. The solution was comprised of the following concentrations: 120mM NaCl, 1mM $MgCl_2$, 3.36mM KCl, 10mM D-Glucose, 20mM HEPES buffer pH 7.4 and 1.2mM $CaCl_2$.

Lanthanum Chloride Washing Buffer

The solution was made from the abovementioned stock solutions with the exception of $CaCl_2$ which was substituted with $LaCl_3$. 20ml of the stock solutions was added to a 250ml volumetric flask and the final volume made up with distilled water to the mark.

Test Incubation Solutions

The test solutions were prepared as follows. In a glass vial 0.22µl of $^{45}Ca^{2+}$ was added to 2.2ml of 12mM $CaCl_2$ stock solution, to give a solution of cold and hot calcium with a final concentration of 1µCi/µl. Into two 10ml volumetric flasks, 1ml of each of the stock solutions, used to make up the HEPES buffer excluding $CaCl_2$, was added. 1ml of the solution of cold and hot calcium was aliquoted to each of the two 10ml volumetric flasks. This gave a final concentration of 1.2mM of $CaCl_2$ in both the test and control solutions, each containing the same amount of radioactivity. One of the volumetric flasks was designated to contain the test stimulation solution and to this 10µl of 100mM NMDA stock solution was added. The final concentration of NMDA in the test stimulation

solution was 10mM. Distilled water was added to both the volumetric flasks to make the final volume up to 10ml.

2.2.4 PROTEIN DETERMINATION

The following solutions were made up and used as described below:

Bovine Serum Albumin (BSA)

50ml solution of 1mg/ml was made up by carefully dissolving 50mg of BSA with distilled water.

$CuSO_45H_2O$ (1% w/v)

2.5 grams $CuSO_45H_2O$ (249.68 g/mol) was dissolved in distilled water to a total volume of 250ml.

Folin Acid Reagent

A dilution of Folin Reagent was made with distilled water to a ratio of 1:10. The solution was freshly prepared before use.

Na_2CO_3 (10% w/v)

50 grams Na_2CO_3 (105 g/mol) were dissolved in 0.5M NaOH to a total volume of 500ml.

NaOH (0.5M)

20 grams NaOH (40 g/mol) were dissolved in 1 litre of distilled water.

Na^+K^+-Tartrate (2% w/v)

5 grams Na^+K^+-Tartrate (282.22 g/mol) were dissolved in distilled water to a total volume of 250ml.

Reagent A

1% $CuSO_45H_2O$ was mixed with 2% Na^+K^+-Tartrate to a ratio of 1:1.

2.2.5 TRANSCARDIAL PERFUSION

Gelatinized solution and slide preparation

Gelatinized solution was made by mixing 10 grams gelatine with 500ml distilled water in an Erlenmeyer flask. The solution was mixed in a 50°C water bath until the gelatine had fully dissolved. Microscope slides were washed by placing on slide racks and immersing in staining glass dishes filled with 2% Deconex detergent (Borer Chemie, Zuchmil, Switzerland). The slides on the racks were rinsed thoroughly in running tap water followed by rinsing in distilled water before being dried in the oven set at 50°C. Once the slides were dried, they were placed in previously warmed staining glass dishes filled with the gelatine solution and dipped into the solution 30 times. The slides were removed from the solution and returned to dry overnight in the oven set at 50°C.

1.5M Phophate Buffer Stock Solution (PBS)

The x10 Stock solution was made by dissolving 80 grams NaCl, 2 grams KCl, 14.4 grams of Na2HPO4 and 2.4 grams KH2PO4 in 800ml of distilled water. The pH was adjusted to 7.4 with 5M NaOH. Distilled water was added to make up the solution to 1litre.

A 0.15M PBS working solution was made by mixing the stock solution with distilled water to a ration of 1:10.

4% Paraformaldehyde Solution

40 grams of paraformaldehyde were mixed in 800ml 0.15M PBS made from the stock solution. The mixture was covered and mixed on a stirring magnetic plate with the heat set at 40°C.

20% Sucrose solution

200 grams of sucrose were mixed with 0.15M PBS working solution to make the solution to 1litre.

2.2.6 TYROSINE HYDROXYLASE

Avidin-biotin-peroxidase complex (ABC) Reagent

All reagents were contained in the SIGMA ABC VECTA KIT and were mixed as directed by the instructions enclosed. Exactly two drops of Reagent A were added to 5ml PBS buffer and was mixed thoroughly. To this solution, two drops of Reagent B were added and mixed thoroughly. The ABC Reagent was prepared and allowed to stand for thirty minutes before use.

Biotinylated Secondary Antibody

The antibody was diluted in freshly prepared blocking solution as described above to a dilution of 1:400. At least 5ml total volume was required for 25 slides ∴13µl antibody in 5.2ml blocking solution.

Blocking Serum (For Initial Blocking and for dissolving primary monoclonal antibody).

3 drops (150µl) of horse blocking serum (yellow label) was added to 10ml of 0.15M PBS solution containing 0.2% (20µl) Triton X-100.

Blocking Serum (For secondary antibody)

3 drops (150µl) of horse blocking serum (yellow label) was added to 10ml of 0.15M PBS solution. This solution did <u>not</u> contain Triton X-100.

DAB Solution

All reagents were contained in the SIGMA DAB KIT and were mixed as directed by the instructions enclosed. To 5ml dH_2O, two drops of Buffer Stock solution were added and mixed well. To this

solution, four drops of DAB Stock solution were added and mixed well. Two drops of hydrogen peroxide solution were then added and mixed well. Two drops of nickel solution were also added to obtain a grey-black stain desired.

0.3% Hydrogen Peroxide Solution

0.4ml of 30% H_2O_2 was dissolved in 40ml technical methanol just before use.

Mouse monoclonal anti-tyrosine hydroxylase

Monoclonal antibody was diluted in freshly prepare blocking solution as described above to a dilution of 1:8000. The monoclonal antibody was stored as aliquots containing 50% glycerol. Glycerol was added to the aliquots to enable refreezing for storage purposes. For this reason, a 1:8000 dilution was a measurement of 2µl of monoclonal antibody aliquot in 8000µl blocking serum solution.

1.5M Phophate Buffer Stock Solution (PBS)

As described above (section 2.2.1.5).

2.2.7 CRESYL VIOLET NISSL STAINING

Cresyl Violet Working Solution

100ml of each of the buffer solutions and the pH was adjusted to 3.5. The solution was mixed with 10ml of the thionin solution. 0.2 grams of Cresyl violet were dissolved in the solution to make up the working solution.

0.1M Glacial Acetic Acid

6ml acetic acid was mixed with 800ml distilled water. The solution was made up to 1L.

0.1M Sodium Acetate Buffer Solution (pH 3.5)

13.6 grams of sodium acetate (82.03 g/mol) was mixed with 800ml distilled water. The solution was made up to 1L.

1% Thionin solution

1 gram of thionin was dissolved in 100ml distilled water.

ANNEX B CALCULATIONS OF Ca2+ UPTAKE

nmol of radioactive calcium were calculated from amount of protein per striatal sample

SECTION	PROTEIN µg in 80µl sample	PROTEIN µg in 600µl	CPM in 600µl	CPM std per 24 nmol Ca	nmol Ca2+ per 600µl	nmol Ca / mg protein
1L	18.10	135.77	2378.10	29000.00	1.97	14.50
1R	21.43	160.76	2669.20	29000.00	2.21	13.74
2L	28.89	216.67	1104.30	29000.00	0.91	4.22
2R	35.71	267.82	1640.00	29000.00	1.36	5.07
3L	23.02	172.65	2751.40	29000.00	2.28	13.19
3R	46.02	345.15	3081.10	29000.00	2.55	7.39
Cont 80ul	40.31					
Cont 120ul	54.585					

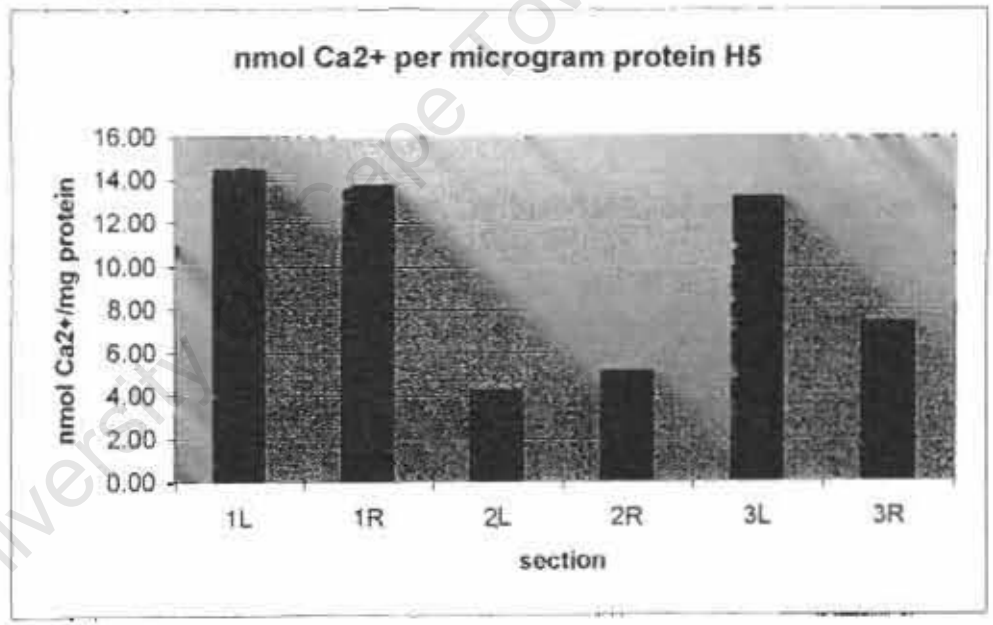

	tSIE	cpm
45 Ca stds	315	29763.7
on 30/1/04	299	27712.8
	273	30570.8
	255	28803.1
	238	26250.8
	158	30113.1
	144	26642.1
NMDA std:	315	21660.3
on 30/4/04	294	29602.8
	272	28661.6
	251	28547.5
	236	29554.5
	167	27105.9
	137	27785.7

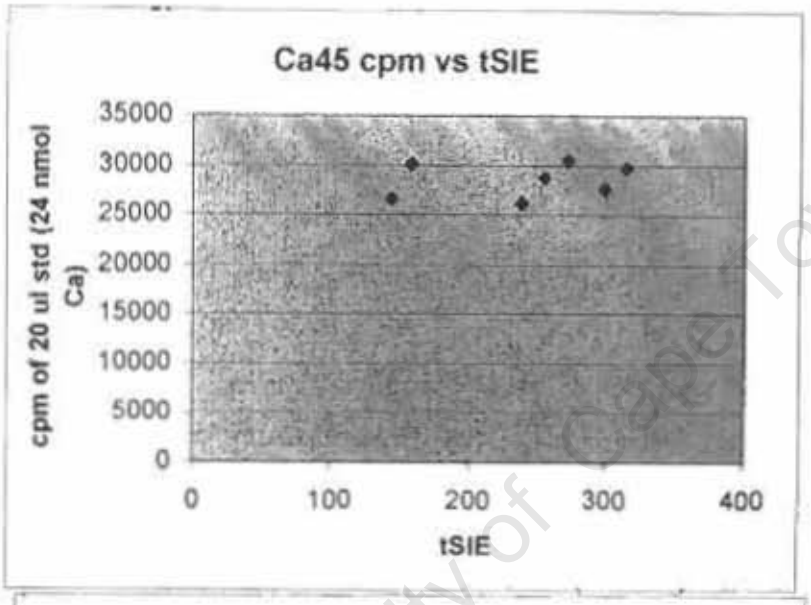

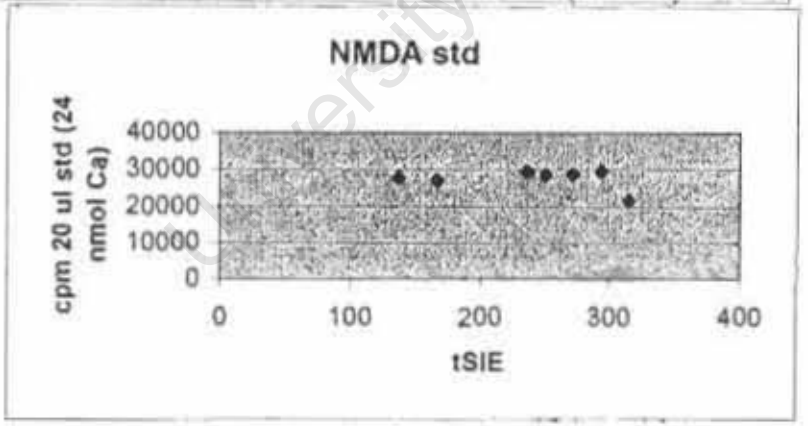

NON-6OHDA LESIONED RATS PRELIMINARY DATA

PRELIMINARY RESULTS
CONTROL GROUP

$^{45}Ca^{2+}$ UPTAKE IN NON 6-OHDA LESIONED RATS

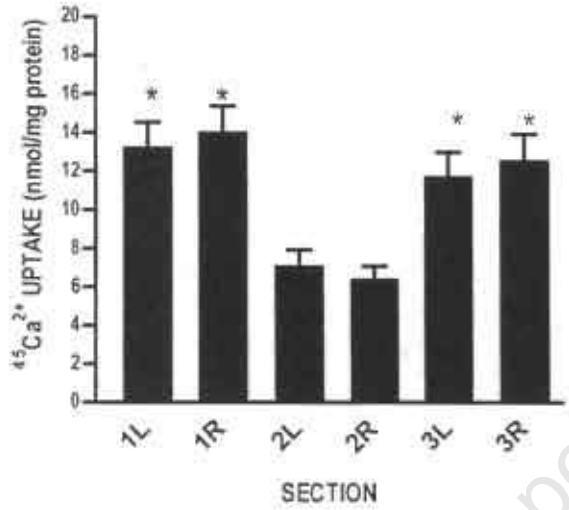

SPREADSHEET

	LESION GROUP	1L	2L	3L	1R	2R	3R	1L-2L	3L-2L	1R-2R	3R-2R
H5	2	14.5	4.22	13.19	13.74	5.07	7.39	10.28	8.97	8.67	2.32
H6	2	7.19	4.87	6.46	6.17	4.02	9.94	2.32	1.59	2.15	5.92
I6	2	13.44	8.98	15.75	19.22	8.18	15.75	4.46	6.77	11.04	7.57
J7	2	11.38	8.42	10.34	16.05	4.95	13.77	2.96	1.92	11.1	8.82
J8	2	10.39	6.12	9.77	14.9	7.09	12.15	4.27	3.65	7.81	5.06
I3	2	18.23	6.35	17.5	13.14	5.13	14.74	11.88	11.15	8.01	9.61
J9	2	12.77	6.19	9.5	12.56	6.82	8.15	6.58	3.31	5.74	1.33
J10	2	17.88	11.58	11.34	16.43	9.94	18.7	6.3	-0.24	6.49	8.76

DESCRIPTIVE STATISTICS

	Valid N	Mean	Minimum	Maximum	Std.Dev.	Standard Error
1L	8	13.22250	7.190000	18.23000	3.712149	1.312443
2L	8	7.09125	4.220000	11.58000	2.419117	0.855287
3L	8	11.73125	6.460000	17.50000	3.590792	1.269537
1R	8	14.02625	6.170000	19.22000	3.823797	1.351917

2R	8	6.40000	4.020000	9.94000	1.982106	0.700780
3R	8	12.57375	7.390000	18.70000	3.915175	1.384224
1L-2L	8	6.13125	2.320000	11.88000	3.408600	1.205122
3L-2L	8	4.64000	-0.240000	11.15000	3.944801	1.394698
1R-2R	8	7.62625	2.150000	11.10000	2.923535	1.033626
3R-2R	8	6.17375	1.330000	9.61000	3.095314	1.094359

STUDENT T-TESTS

	Mean	Std.Dv.	N	Diff.	Std.Dv. Diff.	t	df	p
1L	13.22250	3.712149						
2L	7.09125	2.419117	8	6.131250	3.408600	5.087659	7	0.001419
3L	11.73125	3.590792						
2L	7.09125	2.419117	8	4.640000	3.944801	3.326885	7	0.012645

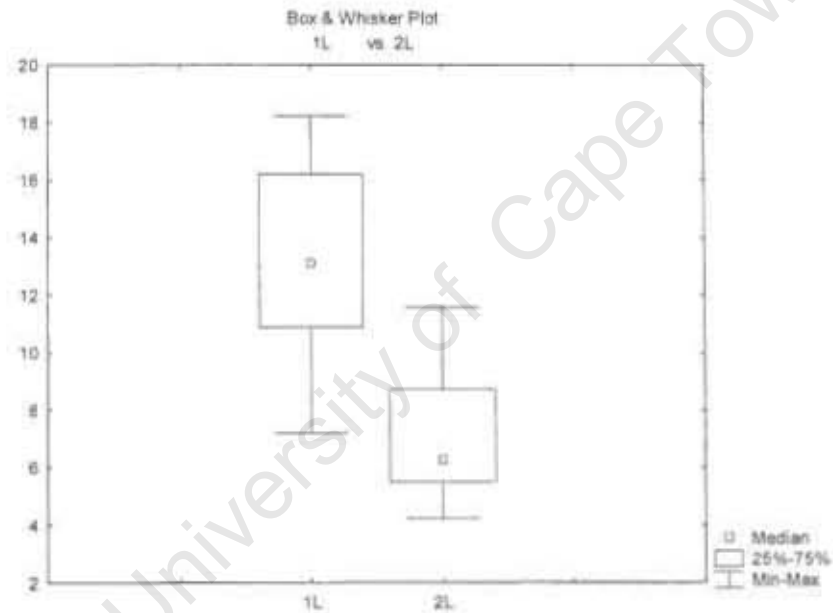

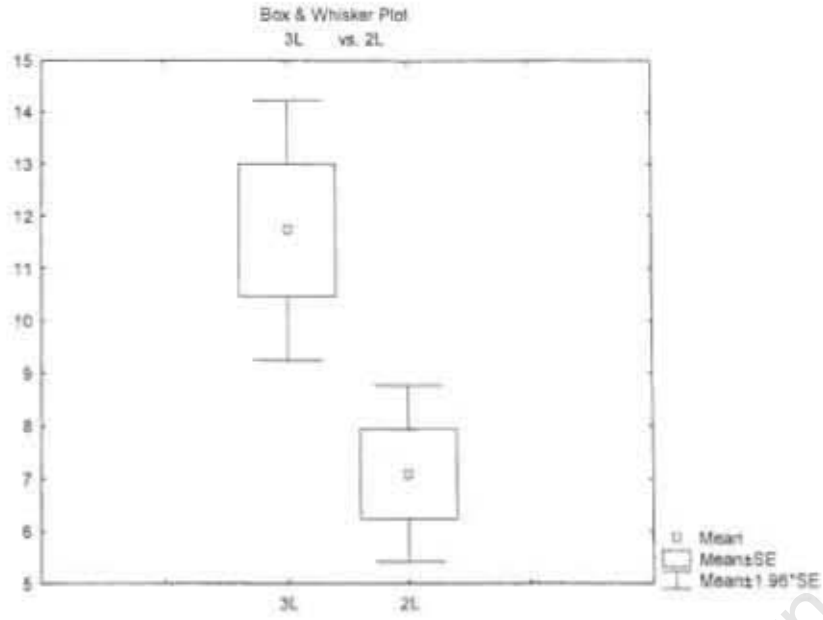

	Mean	Std.Dv.	N	Diff.	Std.Dv. Diff.	t	df	p
1R	14.02625	3.823797						
2R	6.40000	1.982106	8	7.626250	2.923535	7.378155	7	0.000152
3R	12.57375	3.915175						
2R	6.40000	1.982106	8	6.173750	3.095314	5.641431	7	0.000781

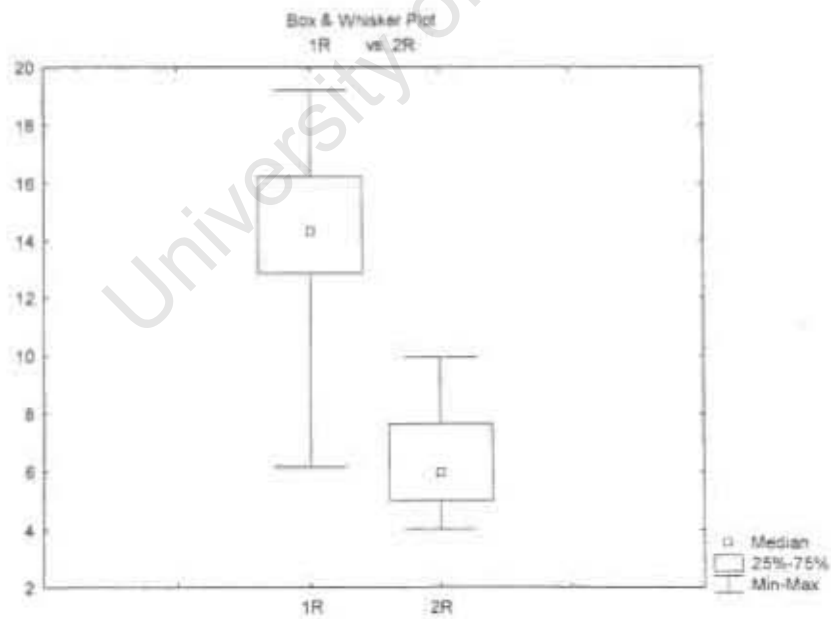

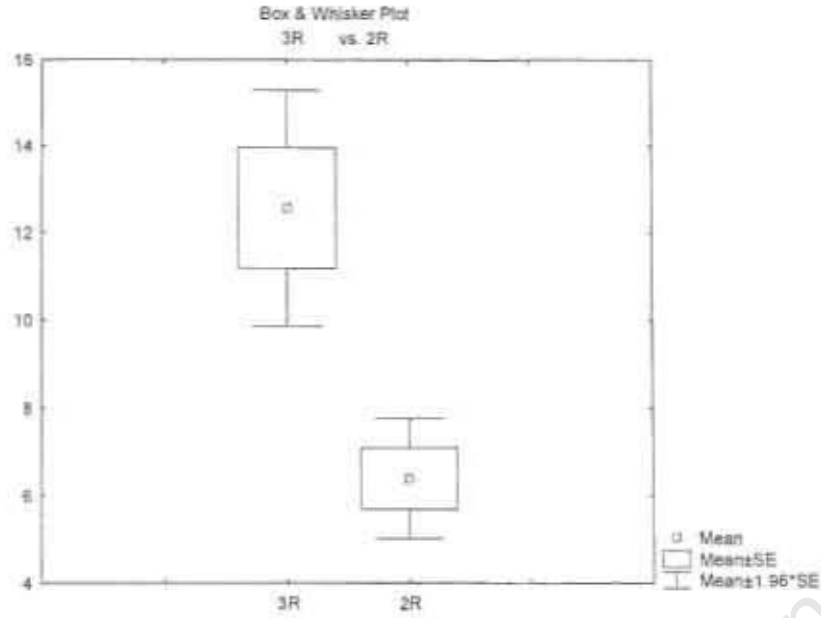

	Mean	Std.Dv.	N	Diff.	Std Dv. Diff.	t	df	p
1L-2L	6.131250	3.408600						
1R-2R	7.626250	2.923535	8	-1.49500	4.184103	-1.01061	7	0.345853

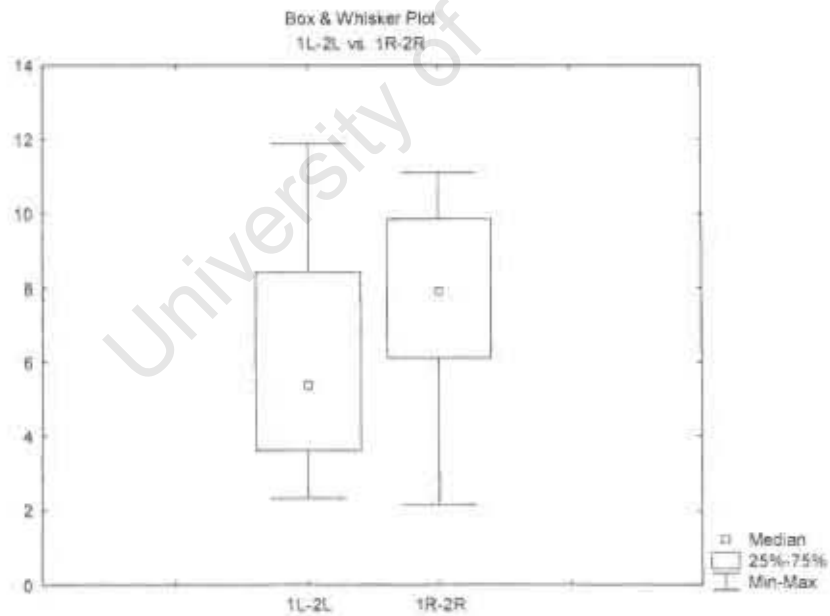

	Mean	Std.Dv.	N	Diff.	Std.Dv.	t	df	p

					Diff.			
3L-2L	4.640000	3.944801						
3R-2R	6.173750	3.095314	8	-1.53375	5.094568	-0.851515	7	0.422654

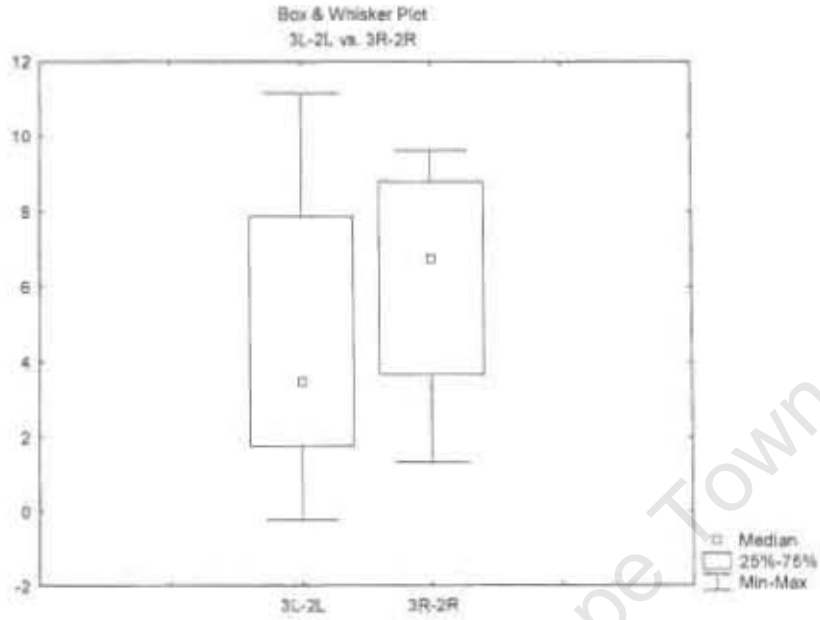

6-OHDA LESIONED PRELIMINARY DATA

PRELIMINARY RESULTS
6-OHDA LESIONED GROUP

$^{45}Ca^{2+}$ UPTAKE IN 6-OHDA LESIONED RATS

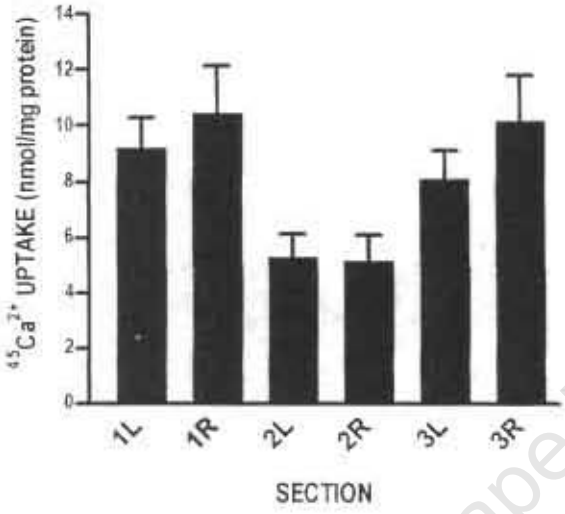

SPREADSHEET

	LESION GROUP	1L	2L	3L	1R	2R	3R	1L-2L	3L-2L	1R-2R	3R-2R
H3	1	8.22	4.45	7.46	9.66	4.16	7.61	3.77	3.01	5.5	3.45
H4	1	6.54	3.16	4.49	6.45	3.04	4.01	3.38	1.33	3.41	0.97
I1	1	13.59	4.41	11.36	10.58	5.05	12.97	9.18	6.95	5.53	7.92
I5	1	6.25	3.76	6.93	9.55	2.74	11.47	2.49	3.17	6.81	8.73
J2	1	10.34	7.3	9.83	18.54	8.8	15.64	3.04	2.53	9.74	6.84
J4	1	9.91	8.57	8.6	7.67	7.04	9.14	1.34	0.03	0.63	2.1

DESCRIPTIVE STATISTICS

	Valid N	Mean	Minimum	Maximum	Std Dev	Standard Error
1L	6	9.14167	6.250000	13.59000	2.749323	1.122406
2L	6	5.27500	3.160000	8.57000	2.151974	0.878540
3L	6	8.11167	4.490000	11.36000	2.395007	0.977757
1R	6	10.40833	6.450000	18.54000	4.257161	1.737979
2R	6	5.13833	2.740000	8.80000	2.372513	0.968574
3R	6	10.14000	4.010000	15.64000	4.123241	1.683306

1L-2L	6	3.86667	1.340000	9.18000	2.736433	1.117144
3L-2L	6	2.83667	0.030000	6.95000	2.336756	0.953976
1R-2R	6	5.27000	0.630000	9.74000	3.080980	1.257805
3R-2R	6	5.00167	0.970000	8.73000	3.252023	1.327633

STUDENT T-TESTS

	Mean	Std.Dv.	N	Diff.	Std.Dv. Diff.	t	df	p
1L	9.141667	2.749323						
2L	5.275000	2.151974	6	3.866667	2.736433	3.461206	5	0.018019
3L	8.111667	2.395007						
2L	5.275000	2.151974	6	2.836667	2.336756	2.973518	5	0.031031

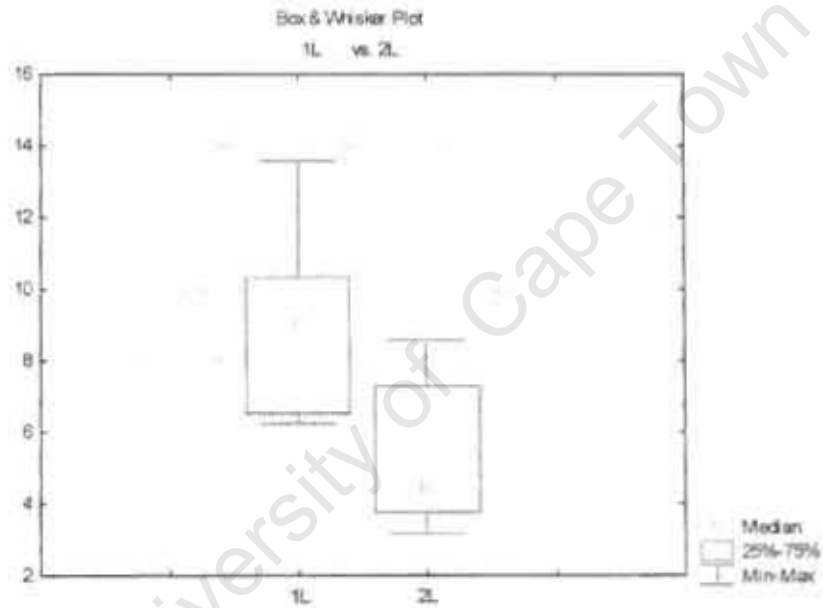

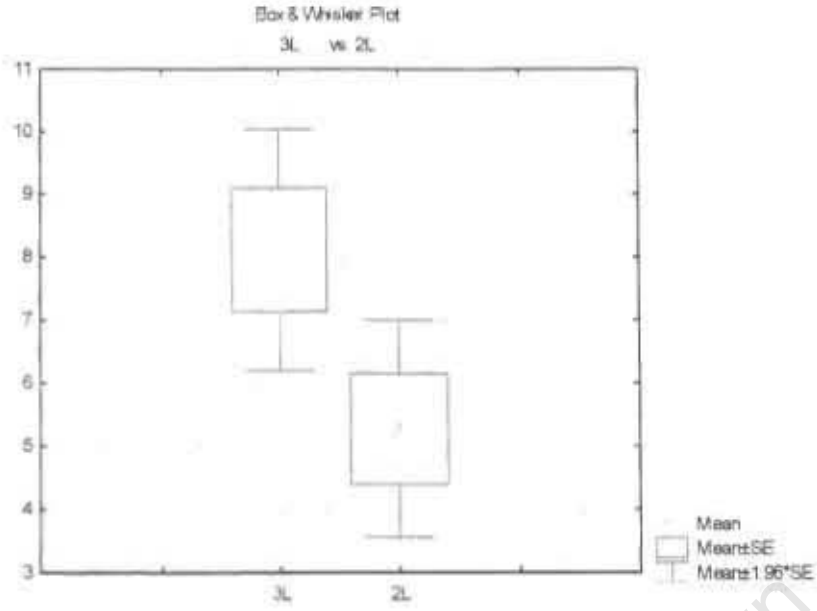

	Mean	Std.Dv.	N	Diff.	Std.Dv. Diff.	t	df	p
1R	10.40833	4.257161						
2R	5.13833	2.372513	6	5.270000	3.080980	4.189839	5	0.008573
3R	10.14000	4.123241						
2R	5.13833	2.372513	6	5.001667	3.252023	3.767356	5	0.013058

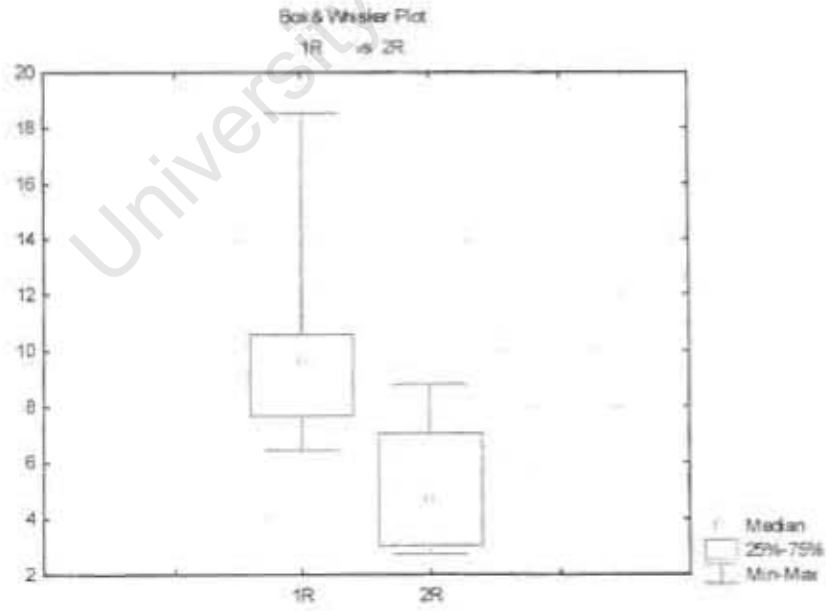

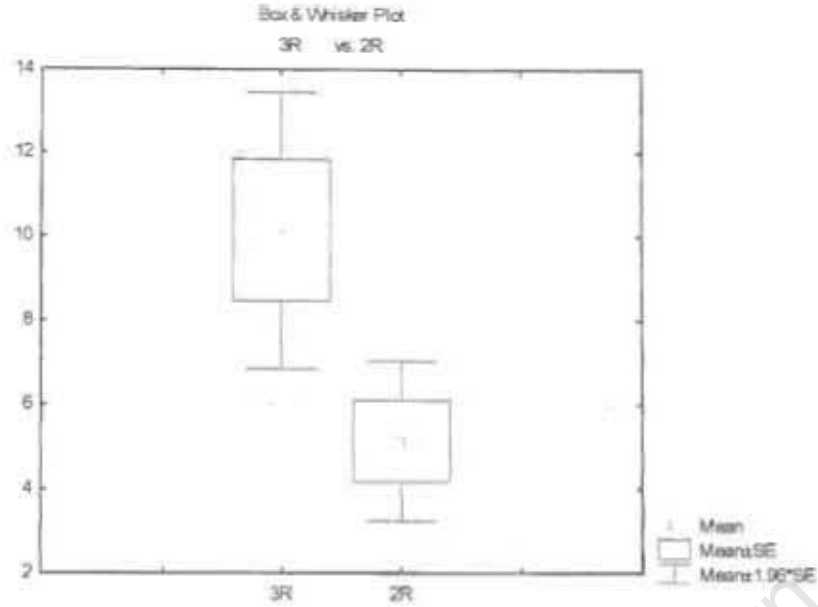

	Mean	Std.Dv.	N	Diff.	Std.Dv. Diff.	t	df	p
1L-2L	3.866667	2.736433						
1R-2R	5.270000	3.080980	6	-1.40333	3.702884	-0.928317	5	0.395849

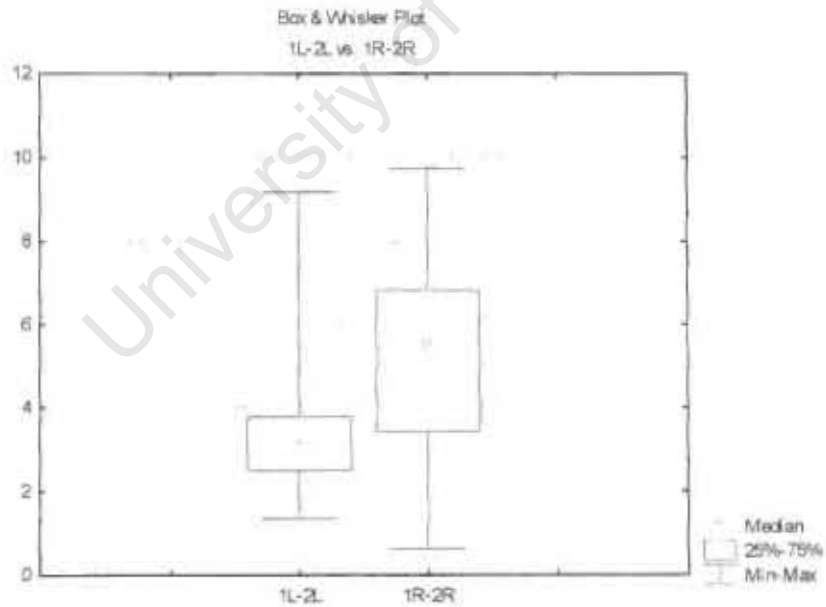

	Mean	Std.Dv.	N	Diff.	Std.Dv. Diff.	t	df	p

3L-2L	2.836667	2.336756						
3R-2R	5.001667	3.252023	6	-2.16500	2.320144	-2.28570	5	0.071030

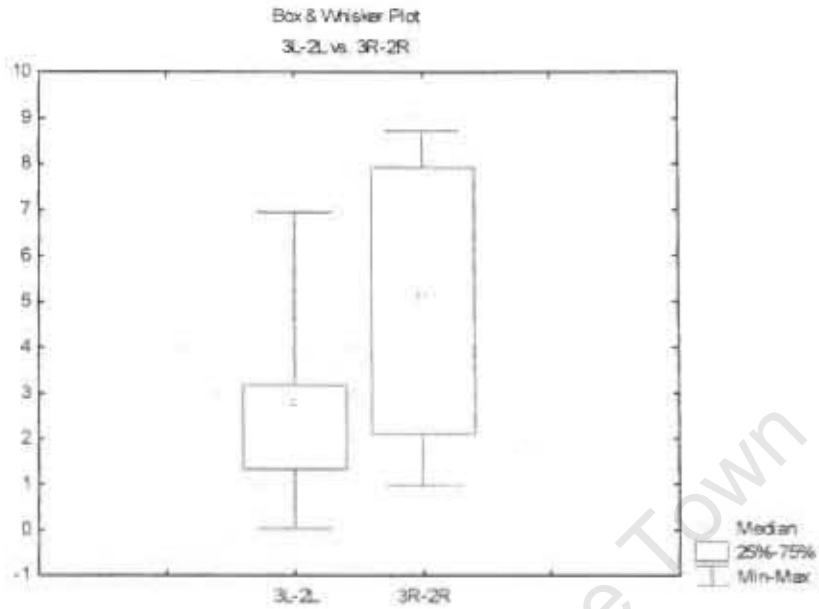

PRELIMINARY DATA STATS REPORT II

	LESION GROUP	1L	2L	3L	1R	2R	3R	1L-2L	3L-2L	1R-2R	3R-2R
I1	1	13.59	4.41	11.36	10.58	5.05	12.97	9.18	6.95	5.53	7.92
I5	1	6.25	3.76	6.93	9.55	2.74	11.47	2.49	3.17	6.81	8.73
J2	1	10.34	7.3	9.83	18.54	8.8	15.64	3.04	2.53	9.74	6.84
J4	1	9.91	8.57	8.6	7.67	7.04	9.14	1.34	0.03	0.63	2.1
H3	1	8.22	4.45	7.46	9.66	4.16	7.61	3.77	3.01	5.5	3.45
H4	1	6.54	3.16	4.49	6.45	3.04	4.01	3.38	1.33	3.41	0.97
I6	2	13.44	8.98	15.75	19.22	8.18	15.75	4.46	6.77	11.04	7.57
J7	2	11.38	8.42	10.34	16.05	4.95	13.77	2.96	1.92	11.1	8.82
J8	2	10.39	6.12	9.77	14.9	7.09	12.15	4.27	3.65	7.81	5.06
I3	3	18.23	6.35	17.5	13.14	5.13	14.74	11.88	11.15	8.01	9.61
J9	3	12.77	6.19	9.5	12.56	6.82	8.15	6.58	3.31	5.74	1.33
J10	3	17.88	11.58	11.34	16.43	9.94	18.7	6.3	-0.24	6.49	8.76
H5	2	14.5	4.22	13.19	13.74	5.07	7.39	10.28	8.97	8.67	2.32
H6	2	7.19	4.87	6.46	6.17	4.02	9.94	2.32	1.59	2.15	5.92

DESCRIPTIVE

	Valid N	Mean	Minimum	Maximum	Std.Dev.	Standard Error
LESION GROUP	14	1.78571	1.000000	3.00000	0.801784	0.214286
1L	14	11.47357	6.250000	18.23000	3.836574	1.025368
2L	14	6.31286	3.160000	11.58000	2.408796	0.643778
3L	14	10.18000	4.490000	17.50000	3.550252	0.948845
1R	14	12.47571	6.170000	19.22000	4.277353	1.143171
2R	14	5.85929	2.740000	9.94000	2.168000	0.579422
3R	14	11.53071	4.010000	18.70000	4.044119	1.080836
1L-2L	14	5.16071	1.340000	11.88000	3.238626	0.865559
3L-2L	14	3.86714	-0.240000	11.15000	3.367059	0.899884
1R-2R	14	6.61643	0.630000	11.10000	3.117281	0.833128
3R-2R	14	5.67143	0.970000	9.61000	3.096588	0.827598

STUDENT T-TESTS

	Mean	Std.Dv.	N	Diff.	Std.Dv. Diff.	t	df	p
1L	11.47357	3.836574						

2L	6.31286	2.408796	14	5.160714	3.238626	5.962289	13	0.000047
3L	10.18000	3.550252						
2L	6.31286	2.408796	14	3.867143	3.367059	4.297378	13	0.000867

	Mean	Std.Dv	N	Diff.	Std.Dv. Diff.	t	df	p
1R	12.47571	4.277353						
2R	5.85929	2.168000	14	6.616429	3.117281	7.941668	13	0.000002
3R	11.53071	4.044119						
2R	5.85929	2.168000	14	5.671429	3.096588	6.852878	13	0.000012

ANALYSIS OF VARIANCE

	SS Effect	df Effect	MS Effect	SS Error	df Error	MS Error	F	p
1L	102.3608	2	51.18039	88.9902	11	8.09001	6.326366	0.014836
2L	15.6307	2	7.81533	59.7992	11	5.43629	1.437621	0.278828
3L	50.1984	2	25.09922	113.6574	11	10.33249	2.429155	0.133735
1R	44.8791	2	22.43954	192.9657	11	17.54233	1.279165	0.316611
2R	9.3169	2	4.65843	51.7860	11	4.70782	0.989509	0.402559
3R	28.2904	2	14.14521	184.3233	11	16.75666	0.844155	0.455973
1L-2L	39.1984	2	19.59921	97.1547	11	8.83224	2.219052	0.155022
3L-2L	11.1978	2	5.59888	136.1843	11	12.38039	0.452237	0.647520
1R-2R	22.7487	2	11.37437	103.5780	11	9.41618	1.207960	0.335542
3R-2R	5.4511	2	2.72557	119.2040	11	10.83673	0.251512	0.781976

ADULT RATS AGED 7 WEEKS ANALYSIS REPORT (WITHIN GROUP ANALYSIS)

SPREADSHEET

	LESION GROUP	1L	2L	3L	1R	2R	3R	1L-2L	3L-2L	1R-2R	3R-2R
RAT 1	3	12.46	4.5	10.04	7.44	4.35	10.74	7.96	5.54	3.09	6.39
RAT 2	3	13.98	6.61	10.81	13.37	6.29	10.06	7.37	4.2	7.08	3.77
RAT 3	3	12.77	3.31	4.23	11.1	2.84	8.38	9.46	0.92	8.26	5.54
RAT 4	3	9.9	4.98	9.4	7.74	5.67	11.73	4.92	4.42	2.07	6.06
RAT 5	3	8.75	4.58	9.42	7.79	3.81	9.28	4.17	4.84	3.98	5.47
RAT 6	3	9.58	5.01	9.87	12	5.84	9.45	4.57	4.86	6.16	3.61
RAT 7	3	12.52	3.85	9.55	10.62	4.13	13.41	8.67	5.7	6.49	9.28

DESCRIPTIVE STATISTICS

	Valid N	Mean	Minimum	Maximum	Std.Dev.	Standard Error
1L	7	11.42286	8.750000	13.98000	1.978743	0.747895
2L	7	4.69143	3.310000	6.61000	1.043319	0.394337
3L	7	9.04571	4.230000	10.81000	2.179135	0.823636
1R	7	10.00857	7.440000	13.37000	2.362770	0.893043
2R	7	4.70429	2.840000	6.29000	1.256156	0.474782
3R	7	10.43571	8.380000	13.41000	1.697477	0.641586
1L-2L	7	6.73143	4.170000	9.46000	2.146093	0.811147
3L-2L	7	4.35429	0.920000	5.70000	1.608880	0.608100
1R-2R	7	5.30429	2.070000	8.26000	2.278339	0.861131
3R-2R	7	5.73143	3.610000	9.28000	1.896782	0.716916

STUDENT T-TEST

	Mean	Std.Dv.	N	Diff.	Std.Dv. Diff.	t	df	p
1L	11.42286	1.978743						
1R	10.00857	2.362770	7	1.414286	2.214105	1.690005	6	0.141985
	Mean	**Std.Dv.**	**N**	**Diff.**	**Std.Dv. Diff.**	**t**	**df**	**p**
2L	4.691429	1.043319						
2R	4.704286	1.256156	7	-0.012857	0.602902	-0.056422	6	0.956838
	Mean	**Std.Dv.**	**N**	**Diff.**	**Std.Dv. Diff.**	**t**	**df**	**p**
3L	9.04571	2.179135						
3R	10.43571	1.697477	7	-1.39000	2.052429	-1.79182	6	0.123341

	Mean	Std.Dv.	N	Diff.	Std.Dv. Diff.	t	df	p
1L	11.42286	1.978743						
2L	4.69143	1.043319	7	6.731429	2.146093	8.298656	6	*0.000166*

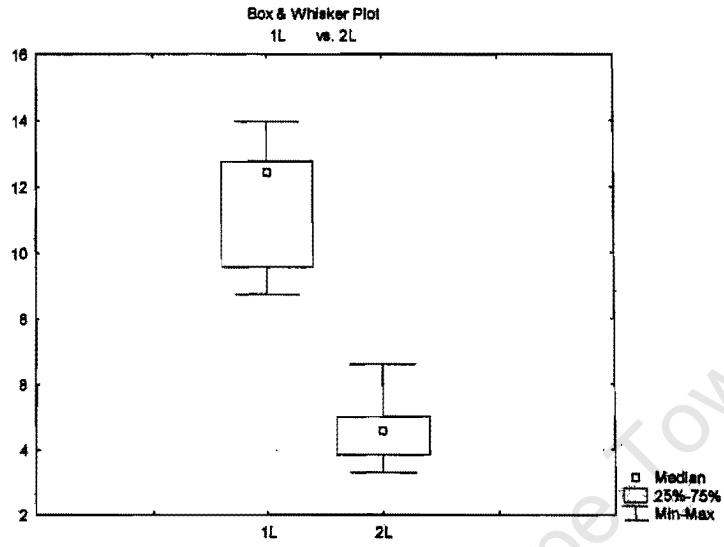

	Mean	Std.Dv.	N	Diff.	Std.Dv. Diff.	t	df	p
3L	9.045714	2.179135						
2L	4.691429	1.043319	7	4.354286	1.608880	7.160482	6	*0.000374*

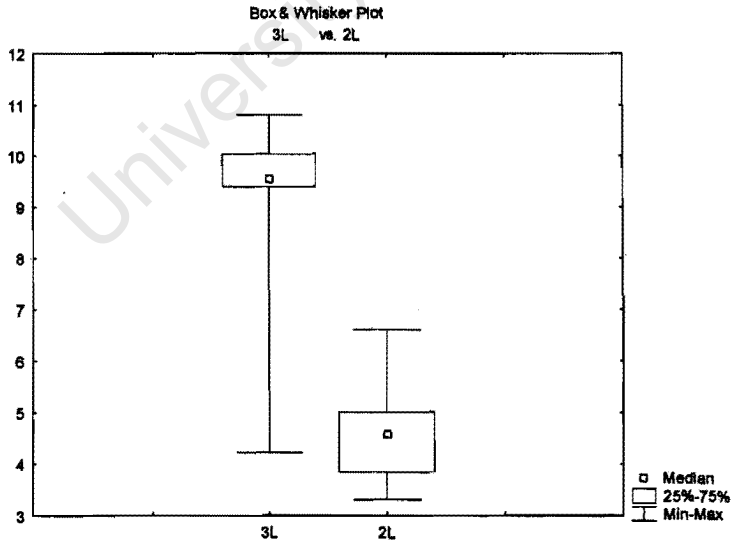

	Mean	Std.Dv.	N	Diff.	Std.Dv. Diff.	t	df	p
1R	10.00857	2.362770						
2R	4.70429	1.256156	7	5.304286	2.278339	6.159672	6	***0.000840***

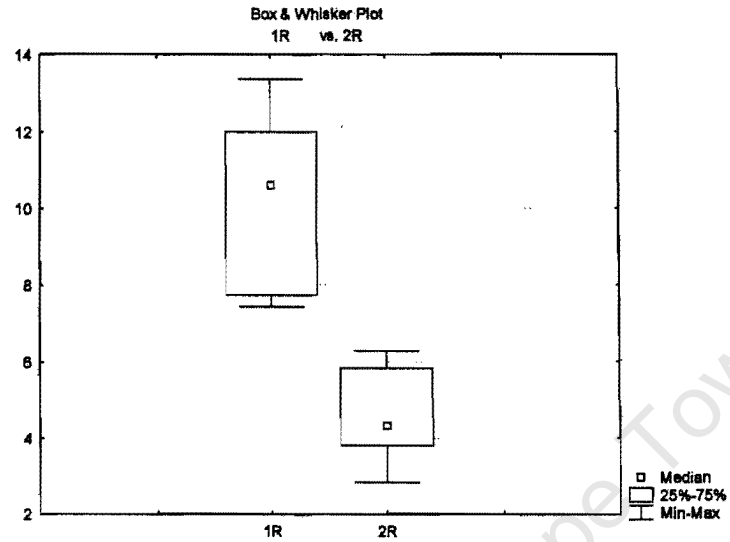

	Mean	Std.Dv.	N	Diff.	Std.Dv. Diff.	t	df	p
3R	10.43571	1.697477						
2R	4.70429	1.256156	7	5.731429	1.896782	7.994560	6	***0.000204***

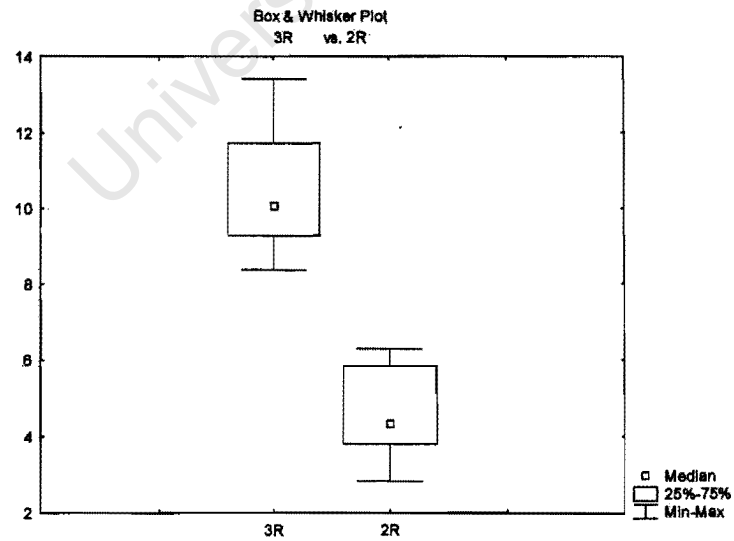

	Mean	Std.Dv.	N	Diff.	Std.Dv. Diff.	t	df	p
1L-2L	6.731429	2.146093						
3L-2L	4.354286	1.608880	7	2.377143	3.132761	2.007599	6	0.091458

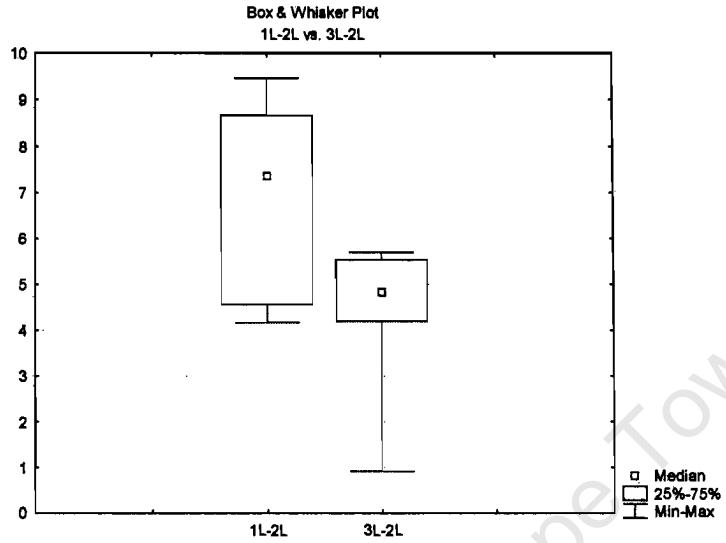

	Mean	Std.Dv.	N	Diff.	Std.Dv. Diff.	t	df	p
1R-2R	5.304286	2.278339						
3R-2R	5.731429	1.896782	7	-0.427143	3.172647	-0.356205	6	0.733877

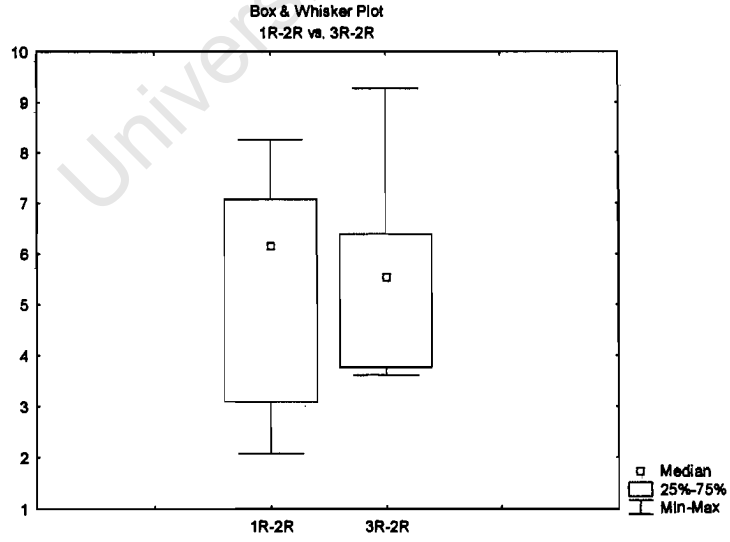

	Mean	Std.Dv.	N	Diff.	Std.Dv. Diff.	t	df	p
1L-2L	6.731429	2.146093						
1R-2R	5.304286	2.278339	7	1.427143	2.098529	1.799291	6	0.122072

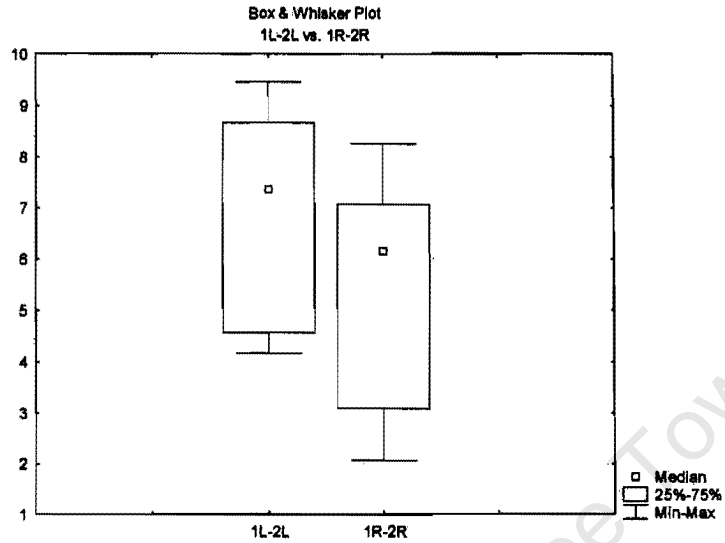

	Mean	Std.Dv.	N	Diff.	Std.Dv. Diff.	t	df	p
3L-2L	4.354286	1.608880						
3R-2R	5.731429	1.896782	7	-1.37714	2.099267	-1.73564	6	0.133311

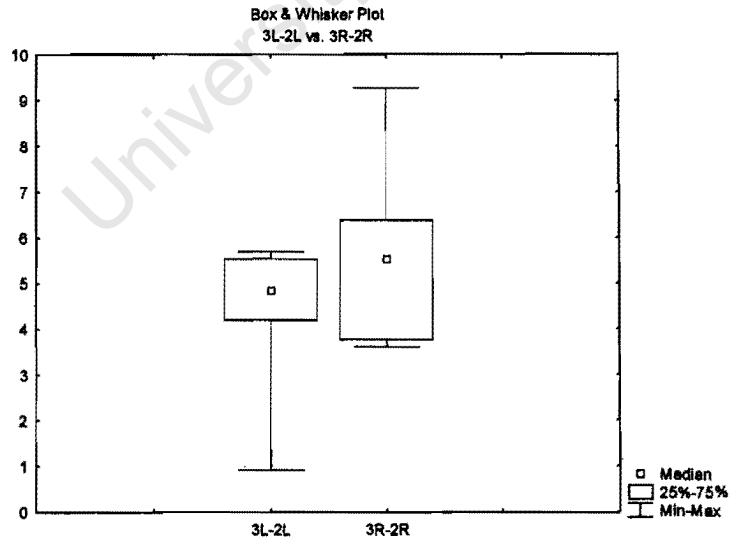

ADULT RATS AGED 7 WEEKS VENTRAL STRIATUM ANALYSIS REPORT (WITHIN GROUP ANALYSIS)

SPREADSHEET

	LESION GROUP	1L	2L	3L	1R	2R	3R	1L-2L	3L-2L	1R-2R	3R-2R
RAT 1	3	10.16	5.34	12.44	12.71	6.72	10.57	4.82	7.1	5.99	3.85
RAT 2	3	6.29	3.95	5.46	7.19	3.49	5.74	2.34	1.51	3.7	2.25
RAT 3	3	13.04	3.25	9.4	12.84	3.94	8.26	9.79	6.15	8.9	4.32
RAT 4	3	9.45	4.6	11.41	8.73	6.72	9.84	4.85	6.81	2.01	3.12
RAT 5	3	17.19	4.75	17.66	6.85	3.32	13.64	12.44	12.91	3.53	10.32
RAT 6	3	15.69	5.93	11.51	8.83	5.2	12.86	9.76	5.58	3.63	7.66
RAT 7	3	17.79	3.55	11.04	17.41	4.21	11.32	4.21	11.32	13.2	7.11

DESCRIPTIVE STATISTICS

	Valid N	Mean	Minimum	Maximum	Std.Dev.	Standard Error
1L	7	12.80143	6.290000	17.79000	4.342697	1.641385
2L	7	4.48143	3.250000	5.93000	0.965064	0.364760
3L	7	11.27429	5.460000	17.66000	3.641977	1.376538
1R	7	10.65143	6.850000	17.41000	3.832921	1.448708
2R	7	4.80000	3.320000	6.72000	1.444934	0.546134
3R	7	10.31857	5.740000	13.64000	2.707609	1.023380
1L-2L	7	6.88714	2.340000	12.44000	3.736771	1.412367
3L-2L	7	7.34000	1.510000	12.91000	3.779471	1.428506
1R-2R	7	5.85143	2.010000	13.20000	3.937501	1.488235
3R-2R	7	5.51857	2.250000	10.32000	2.910598	1.100103

STUDENT T-TEST

	Mean	Std.Dv.	N	Diff.	Std.Dv. Diff.	t	df	p
1L	12.80143	4.342697						
1R	10.65143	3.832921	7	2.150000	4.648172	1.223786	6	0.266906
	Mean	**Std.Dv.**	**N**	**Diff.**	**Std.Dv. Diff.**	**t**	**df**	**p**
2L	4.481429	0.965064						
2R	4.800000	1.444934	7	-0.318571	1.250965	-0.673768	6	0.525549
	Mean	**Std.Dv.**	**N**	**Diff.**	**Std.Dv. Diff.**	**t**	**df**	**p**
3L	11.27429	3.641977						
3R	10.31857	2.707609	7	0.955714	1.779858	1.420665	6	0.205234

	Mean	Std.Dv.	N	Diff.	Std.Dv. Diff.	t	df	p
1L	12.80143	4.342697						
2L	4.48143	0.965064	7	8.320000	4.402776	4.999721	6	***0.002453***

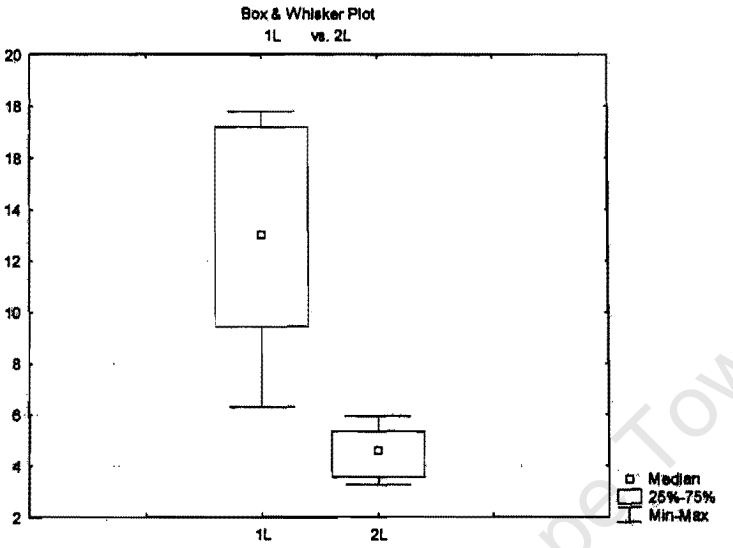

	Mean	Std.Dv.	N	Diff.	Std.Dv. Diff.	t	df	p
3L	11.27429	3.641977						
2L	4.48143	0.965064	7	6.792857	3.361372	5.346689	6	***0.001750***

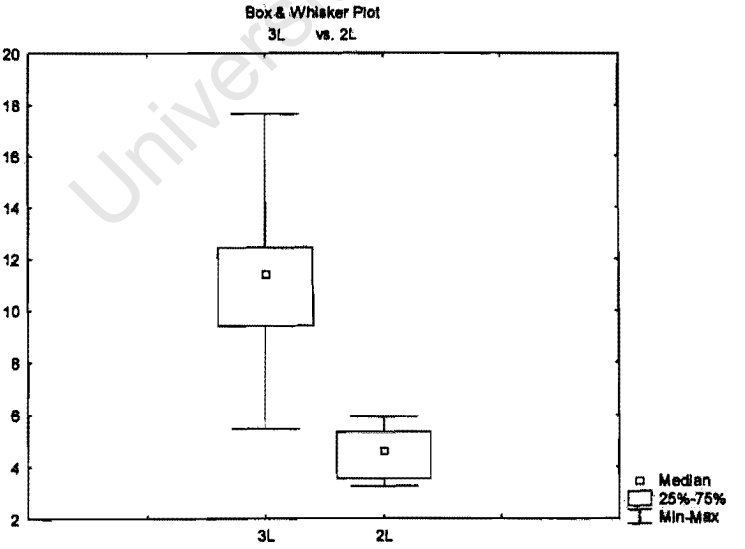

	Mean	Std.Dv.	N	Diff.	Std.Dv. Diff.	t	df	p
1R	10.65143	3.832921						
2R	4.80000	1.444934	7	5.851429	3.937501	3.931789	6	***0.007697***

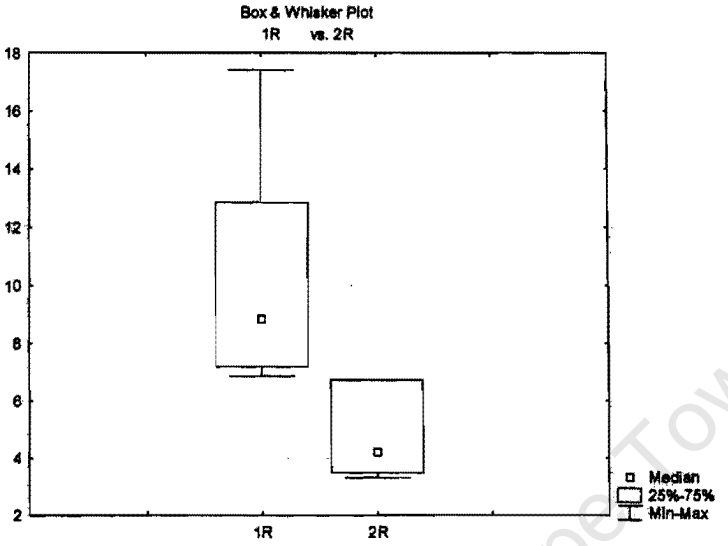

	Mean	Std.Dv.	N	Diff.	Std.Dv. Diff.	t	df	p
3R	10.31857	2.707609						
2R	4.80000	1.444934	7	5.518571	2.910598	5.016415	6	***0.002413***

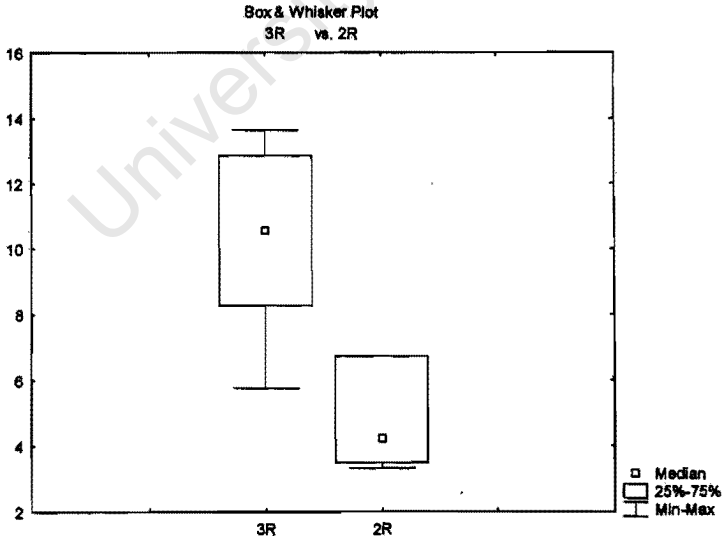

	Mean	Std.Dv.	N	Diff.	Std.Dv. Diff.	t	df	p
1L-2L	6.887143	3.736771						
3L-2L	7.340000	3.779471	7	-0.452857	3.868427	-0.309725	6	0.767245

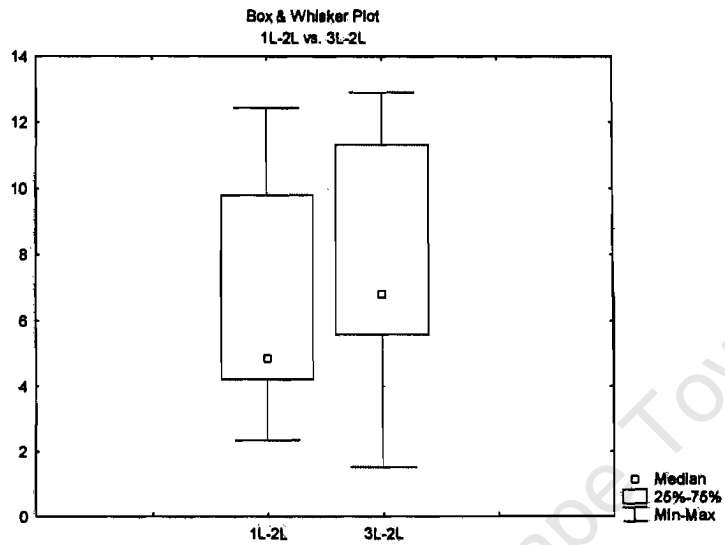

	Mean	Std.Dv.	N	Diff.	Std.Dv. Diff.	t	df	p
3L-2L	7.340000	3.779471						
3R-2R	5.518571	2.910598	7	1.821429	2.366801	2.036101	6	0.087918

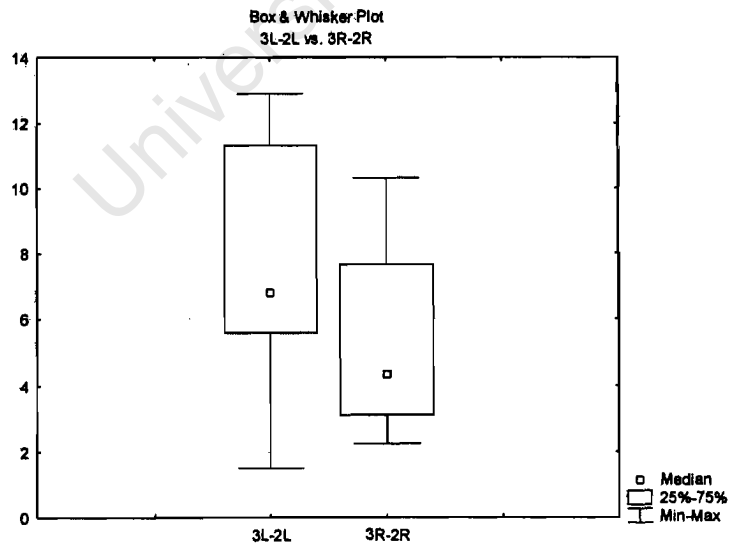

	Mean	Std.Dv.	N	Diff.	Std.Dv. Diff.	t	df	p
1L-2L	6.887143	3.736771						
1R-2R	5.851429	3.937501	7	1.035714	5.807357	0.471857	6	0.653700

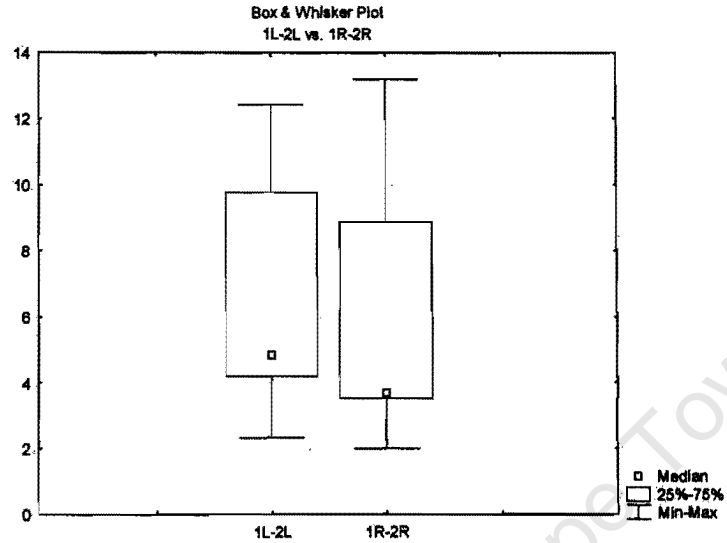

	Mean	Std.Dv.	N	Diff.	Std.Dv. Diff.	t	df	p
3L-2L	7.340000	3.779471						
3R-2R	5.518571	2.910598	7	1.821429	2.366801	2.036101	6	0.087918

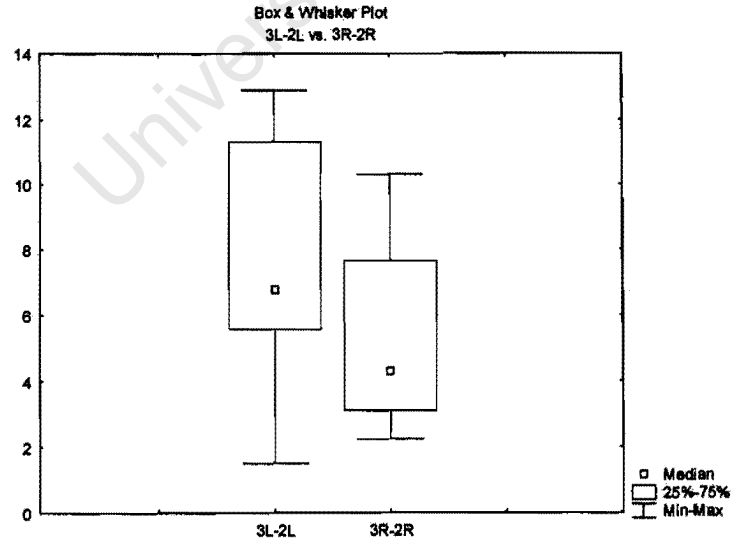

ADULT RATS AGED 16 WEEKS ANALYSIS REPORT (WITHIN GROUP ANALYSIS)

SPREADSHEET

	NUCLEI GROUP	1L	2L	3L	1R	2R	3R	1L-2L	3L-2L	1R-2R	3R-2R
Z1	1	4.24	2	4.03	6.13	3.18	5.68	2.24	2.03	2.95	2.5
Z2	1	5.48	5.99	4.82	7.55	4.26	7.18	-0.51	-1.17	3.29	2.92
Z3	1	4.62	2.98	3.48	3.39	3.01	6.23	1.64	0.5	0.38	3.22
Z4	1	5.17	4.04	6.66	8.19	3.58	6.12	1.13	2.62	4.61	2.54
Z5	1	7.47	5.46	7.97	9.05	6.46	7.92	2.01	2.51	2.59	1.46
Z6	1	8.67	2.79	5.26	7.25	3.89	4.08	5.88	2.47	3.36	0.19

DESCRIPTIVE STATISTICS

	Valid N	Mean	Minimum	Maximum	Std.Dev.	Standard Error
1L	6	5.941667	4.24000	8.670000	1.745319	0.712523
2L	6	3.876667	2.00000	5.990000	1.581552	0.645666
3L	6	5.370000	3.48000	7.970000	1.679667	0.685721
1R	6	6.926667	3.39000	9.050000	1.986974	0.811179
2R	6	4.063333	3.01000	6.460000	1.259852	0.514332
3R	6	6.201667	4.08000	7.920000	1.318399	0.538234
1L-2L	6	2.065000	-0.51000	5.880000	2.110609	0.861652
3L-2L	6	1.493333	-1.17000	2.620000	1.524791	0.622493
1R-2R	6	2.863333	0.38000	4.610000	1.394900	0.569466
3R-2R	6	2.138333	0.19000	3.220000	1.125103	0.459321

STUDENT T-TESTS

	Mean	Std.Dv.	N	Diff.	Std.Dv. Diff.	t	df	p
1L	5.941667	1.745319						
1R	6.926667	1.986974	6	-0.985000	1.853739	-1.30156	5	0.249808
	Mean	Std.Dv.	N	Diff.	Std.Dv. Diff.	t	df	p
2L	3.876667	1.581552						
2R	4.063333	1.259852	6	-0.186667	1.148802	-0.398013	5	0.707046
	Mean	Std.Dv.	N	Diff.	Std.Dv. Diff.	t	df	p
3L	5.370000	1.679667						
3R	6.201667	1.318399	6	-0.831667	1.636526	-1.24481	5	0.268365

	Mean	Std.Dv.	N	Diff.	Std.Dv. Diff.	t	df	p
1L	5.941667	1.745319						
2L	3.876667	1.581552	6	2.065000	2.110609	2.396558	5	0.061884

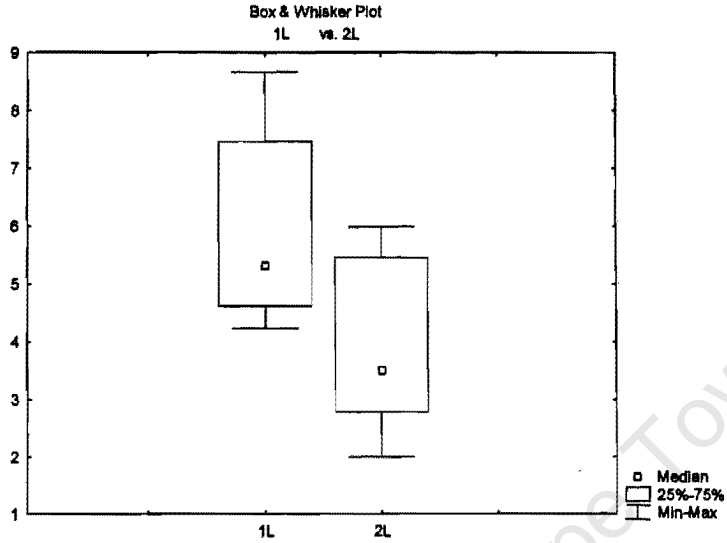

	Mean	Std.Dv.	N	Diff.	Std.Dv. Diff.	t	df	p
3L	5.370000	1.679667						
2L	3.876667	1.581552	6	1.493333	1.524791	2.398955	5	0.061700

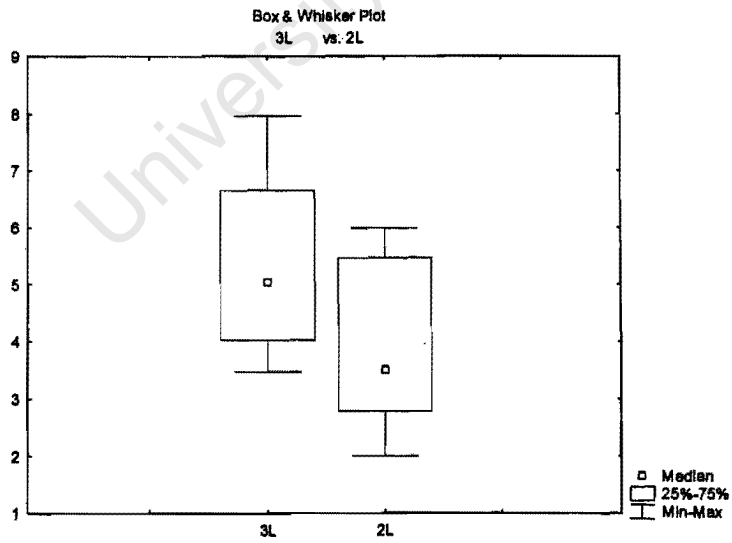

	Mean	Std.Dv.	N	Diff.	Std.Dv. Diff.	t	df	p
1R	6.926667	1.986974						
2R	4.063333	1.259852	6	2.863333	1.394900	5.028106	5	***0.004007***

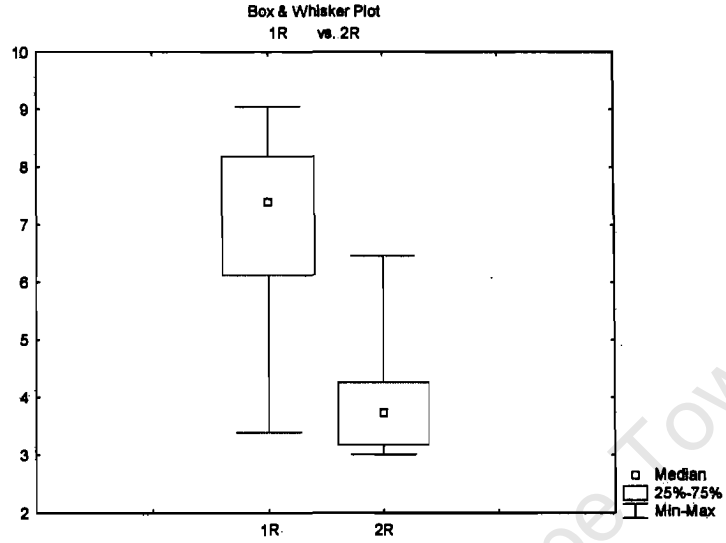

	Mean	Std.Dv.	N	Diff.	Std.Dv. Diff.	t	df	p
3R	6.201667	1.318399						
2R	4.063333	1.259852	6	2.138333	1.125103	4.655419	5	***0.005555***

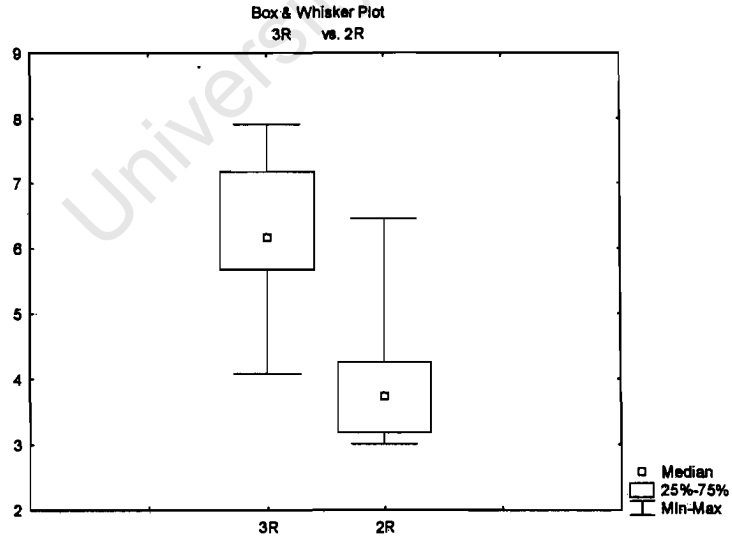

	Mean	Std.Dv.	N	Diff.	Std.Dv. Diff.	t	df	p
1L-2L	2.065000	2.110609						
3L-2L	1.493333	1.524791	6	0.571667	1.668333	0.839336	5	0.439555

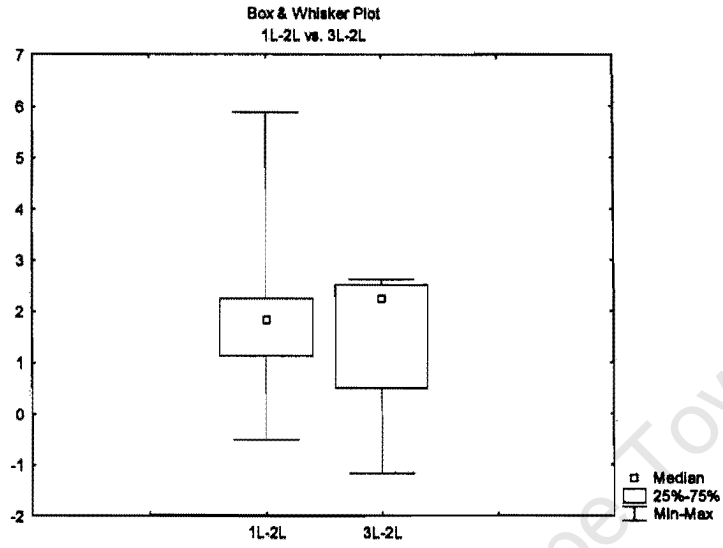

	Mean	Std.Dv.	N	Diff.	Std.Dv. Diff.	t	df	p
1R-2R	2.863333	1.394900						
3R-2R	2.138333	1.125103	6	0.725000	2.042643	0.869403	5	0.424387

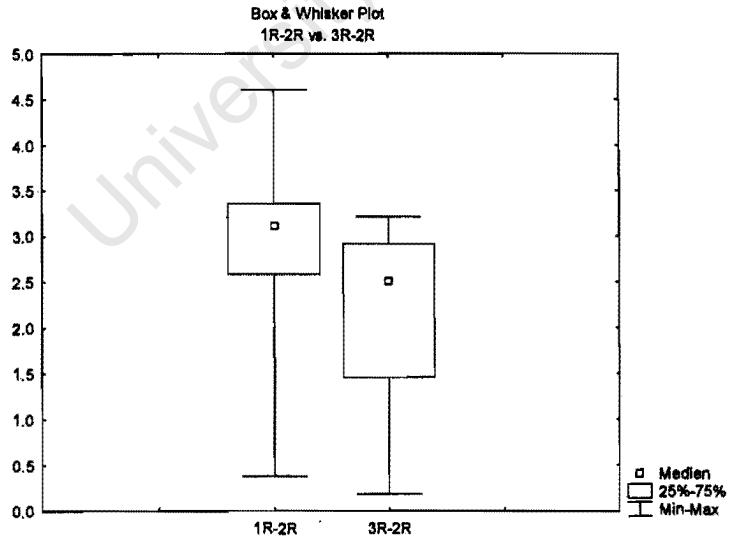

	Mean	Std.Dv.	N	Diff.	Std.Dv. Diff.	t	df	p
1L-2L	2.065000	2.110609						
1R-2R	2.863333	1.394900	6	-0.798333	2.510175	-0.779033	5	0.471204

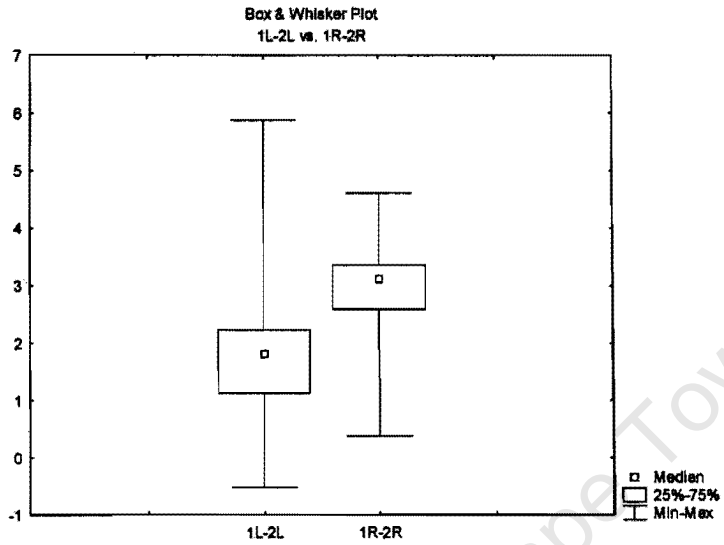

	Mean	Std.Dv.	N	Diff.	Std.Dv. Diff.	t	df	p
3L-2L	1.493333	1.524791						
3R-2R	2.138333	1.125103	6	-0.645000	2.373122	-0.665756	5	0.535045

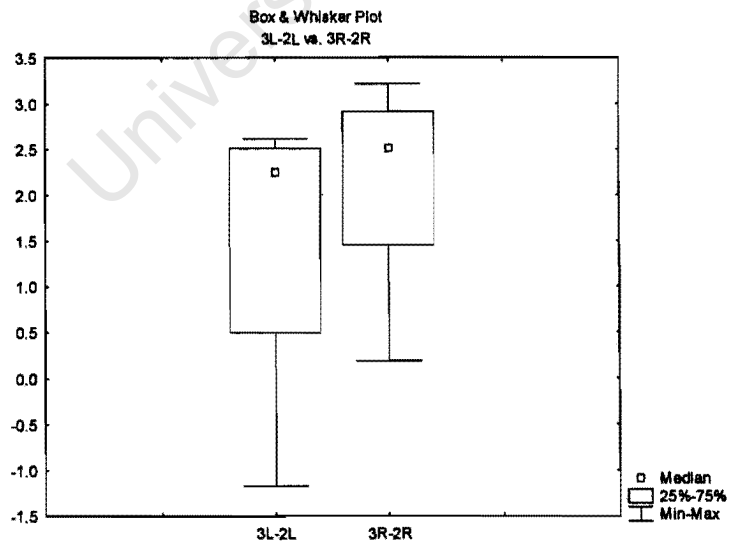

ADULT RATS AGED 16 WEEKS VENTRAL STRIATUM ANALYSIS REPORT (WITHIN GROUP ANALYSIS)

SPREADSHEET

	NUCLEI GROUP	1L	2L	3L	1R	2R	3R	1L-2L	3L-2L	1R-2R	3R-2R
Z1	2	7.63	3.04	6.85	6.41	2.39	7.08	4.59	3.81	4.02	4.69
Z2	2	6.96	6.05	9.61	8.35	4.85	7.9	0.91	3.56	3.5	3.05
Z3	2	6.79	3.62	5.57	6.97	3.67	7.09	3.17	1.95	3.3	3.42
Z4	2	9.97	4.64	8.71	10.86	4.1	8.92	5.33	4.07	6.76	4.82
Z5	2	10.24	6.3	6.1	10.03	4.93	10.82	3.94	-0.2	5.1	5.89
Z6	2	6.97	3.71	5.81	8.63	7.37	4.93	3.26	2.1	1.26	-2.44

DESCRIPTIVE STATISTICS

	Valid N	Mean	Minimum	Maximum	Std.Dev.	Standard Error
NUCLEI GROUP	6	2.000000	2.00000	2.00000	0.000000	0.000000
1L	6	8.093333	6.79000	10.24000	1.586804	0.647810
2L	6	4.560000	3.04000	6.30000	1.354297	0.552889
3L	6	7.108333	5.57000	9.61000	1.670885	0.682136
1R	6	8.541667	6.41000	10.86000	1.711636	0.698772
2R	6	4.551667	2.39000	7.37000	1.663086	0.678952
3R	6	7.790000	4.93000	10.82000	1.982100	0.809189
1L-2L	6	3.533333	0.91000	5.33000	1.523058	0.621786
3L-2L	6	2.548333	-0.20000	4.07000	1.615121	0.659370
1R-2R	6	3.990000	1.26000	6.76000	1.847972	0.754431
3R-2R	6	3.238333	-2.44000	5.89000	2.964870	1.210403

STUDENT T-TEST

	Mean	Std.Dv.	N	Diff.	Std.Dv. Diff.	t	df	p
1L	8.093333	1.586804						
1R	8.541667	1.711636	6	-0.448333	1.080619	-1.01626	5	0.356132
	Mean	**Std.Dv.**	**N**	**Diff.**	**Std.Dv. Diff.**	**t**	**df**	**p**
2L	4.560000	1.354297						
2R	4.551667	1.663086	6	0.008333	1.867013	0.010933	5	0.991700
	Mean	**Std.Dv.**	**N**	**Diff.**	**Std.Dv. Diff.**	**t**	**df**	**p**
3L	7.108333	1.670885						
3R	7.790000	1.982100	6	-0.681667	2.262577	-0.737979	5	0.493685

	Mean	Std.Dv.	N	Diff.	Std.Dv. Diff.	t	df	p
1L	8.093333	1.586804						
2L	4.560000	1.354297	6	3.533333	1.523058	5.682556	5	***0.002351***

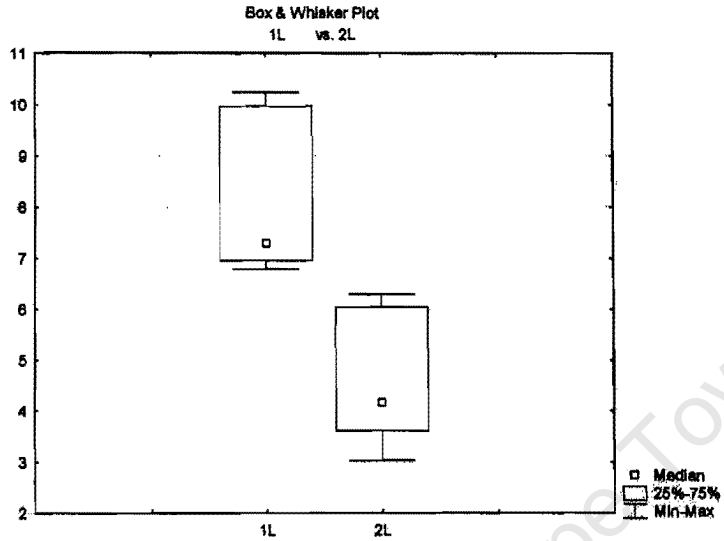

	Mean	Std.Dv.	N	Diff.	Std.Dv. Diff.	t	df	p
3L	7.108333	1.670885						
2L	4.560000	1.354297	6	2.548333	1.615121	3.864797	5	***0.011822***

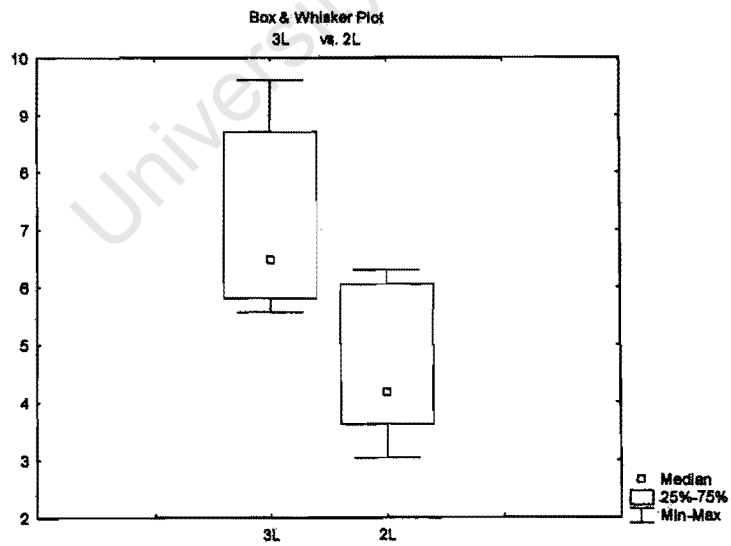

	Mean	Std.Dv.	N	Diff.	Std.Dv. Diff.	t	df	p
1R	8.541667	1.711636						
2R	4.551667	1.663086	6	3.990000	1.847972	5.288752	5	***0.003222***

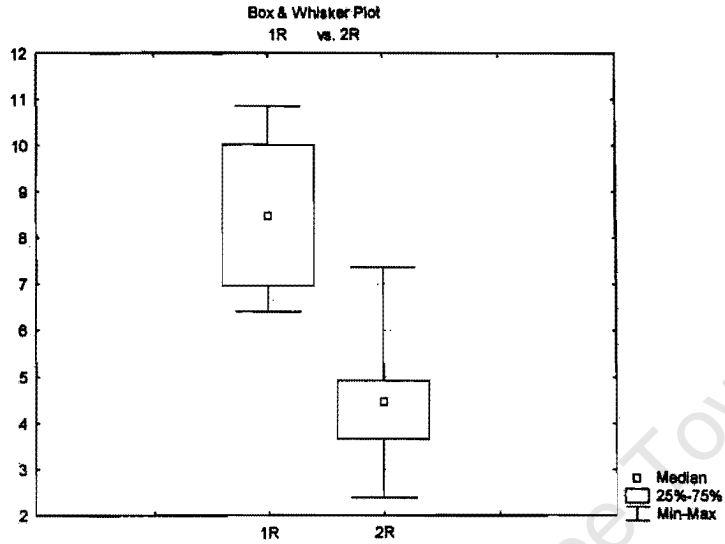

	Mean	Std.Dv.	N	Diff.	Std.Dv. Diff.	t	df	p
3R	7.790000	1.982100						
2R	4.551667	1.663086	6	3.238333	2.964870	2.675417	5	***0.044061***

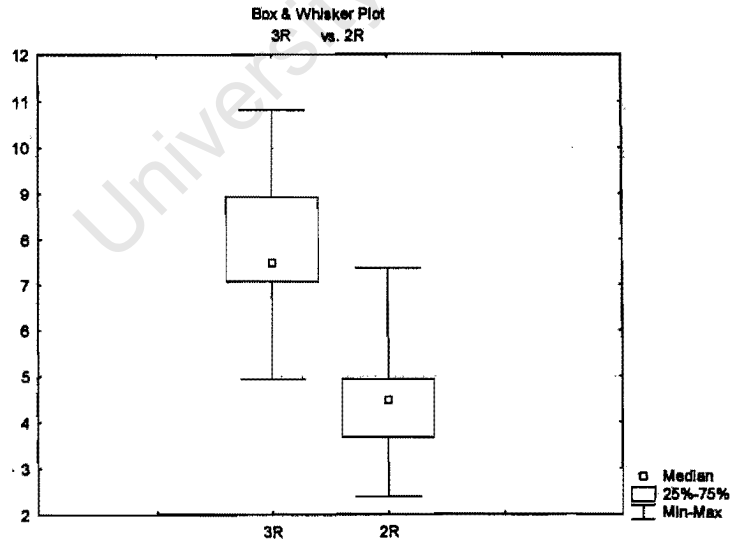

	Mean	Std.Dv.	N	Diff.	Std.Dv. Diff.	t	df	p
1L-2L	3.533333	1.523058						
3L-2L	2.548333	1.615121	6	0.985000	2.161978	1.115991	5	0.315168

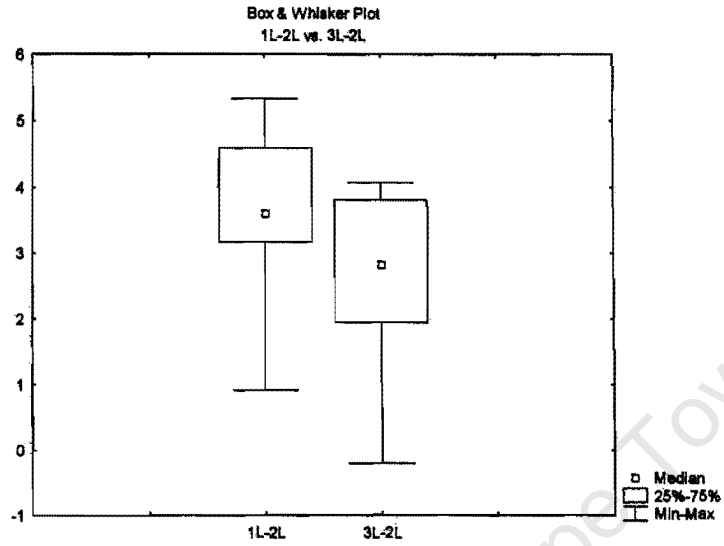

	Mean	Std.Dv.	N	Diff.	Std.Dv. Diff.	t	df	p
1R-2R	3.990000	1.847972						
3R-2R	3.238333	2.964870	6	0.751667	1.752340	1.050709	5	0.341499

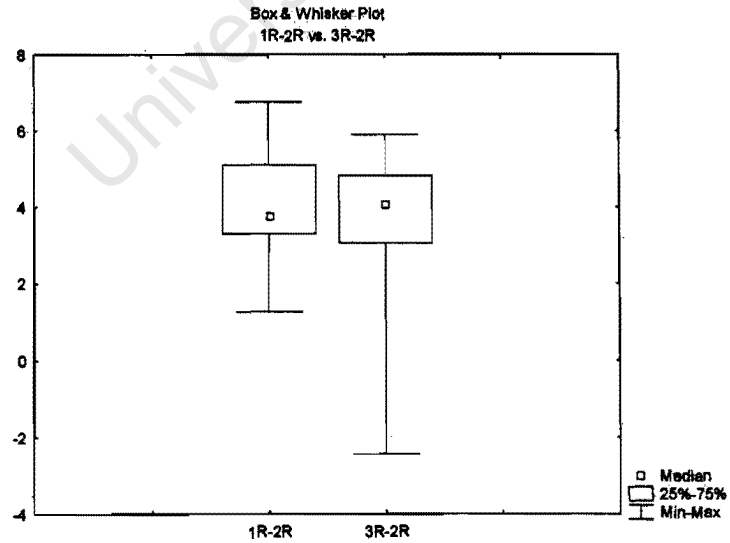

	Mean	Std.Dv.	N	Diff.	Std.Dv. Diff.	t	df	p
1L-2L	3.533333	1.523058						
1R-2R	3.990000	1.847972	6	-0.456667	1.624139	-0.688734	5	0.521638

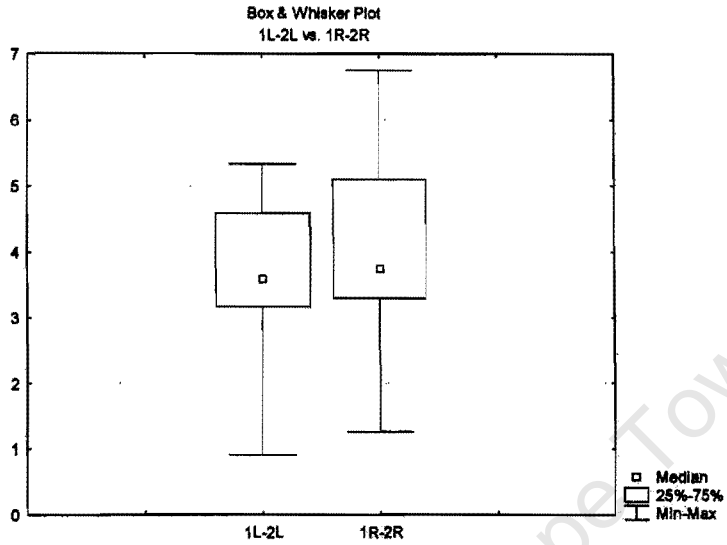

	Mean	Std.Dv.	N	Diff.	Std.Dv. Diff.	t	df	p
3L-2L	2.548333	1.615121						
3R-2R	3.238333	2.964870	6	-0.690000	3.423478	-0.493693	5	0.642442

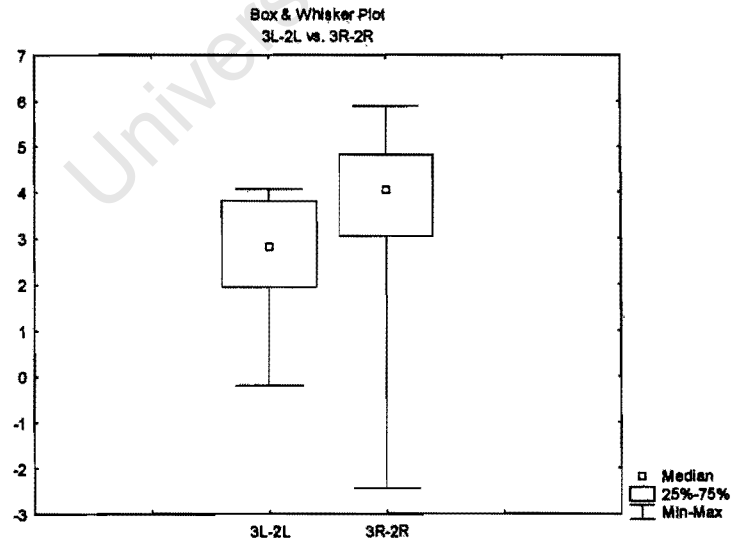

ANALYSIS OF STIMULATED UPTAKE IN DORSAL STRIATUM OF 7 WEEK OLD AND 16 WEEK OLD UNTREATED RATS

SPREADSHEET

	AGE GROUP	1L	2L	3L	1R	2R	3R	1L-2L	3L-2L	1R-2R	3R-2R
Z1	3	4.24	2	4.03	6.13	3.18	5.68	2.24	2.03	2.95	2.5
Z2	3	5.48	5.99	4.82	7.55	4.26	7.18	-0.51	-1.17	3.29	2.92
Z3	3	4.62	2.98	3.48	3.39	3.01	6.23	1.64	0.5	0.38	3.22
Z4	3	5.17	4.04	6.66	8.19	3.58	6.12	1.13	2.62	4.61	2.54
Z5	3	7.47	5.46	7.97	9.05	6.46	7.92	2.01	2.51	2.59	1.46
Z6	3	8.67	2.79	5.26	7.25	3.89	4.08	5.88	2.47	3.36	0.19
RAT 1	2	12.46	4.5	10.04	7.44	4.35	10.74	7.96	5.54	3.09	6.39
RAT 2	2	13.98	6.61	10.81	13.37	6.29	10.06	7.37	4.2	7.08	3.77
RAT 3	2	12.77	3.31	4.23	11.1	2.84	8.38	9.46	0.92	8.26	5.54
RAT 4	2	9.9	4.98	9.4	7.74	5.67	11.73	4.92	4.42	2.07	6.06
RAT 5	2	8.75	4.58	9.42	7.79	3.81	9.28	4.17	4.84	3.98	5.47
RAT 6	2	9.58	5.01	9.87	12	5.84	9.45	4.57	4.86	6.16	3.61
RAT 7	2	12.52	3.85	9.55	10.62	4.13	13.41	8.67	5.7	6.49	9.28

BREAKDOWN STATISTICS

AGE GROUP	1L Means	1L N	1L Std.Dev.	1L Std.Err.
2	11.42286	7	1.978743	0.747895
3	5.94167	6	1.745319	0.712523
All Grps	8.89308	13	3.363860	0.932967

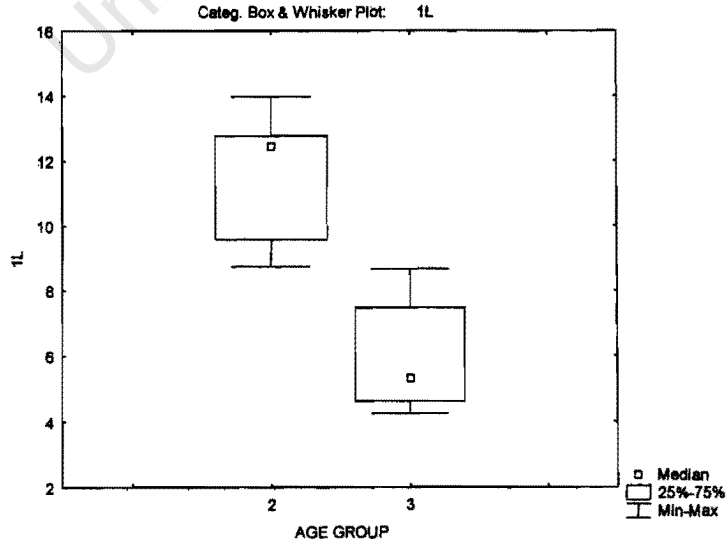

AGE GROUP	2L Means	2L N	2L Std.Dev.	2L Std.Err.
2	4.691429	7	1.043319	0.394337
3	3.876667	6	1.581552	0.645666
All Grps	4.315385	13	1.328606	0.368489

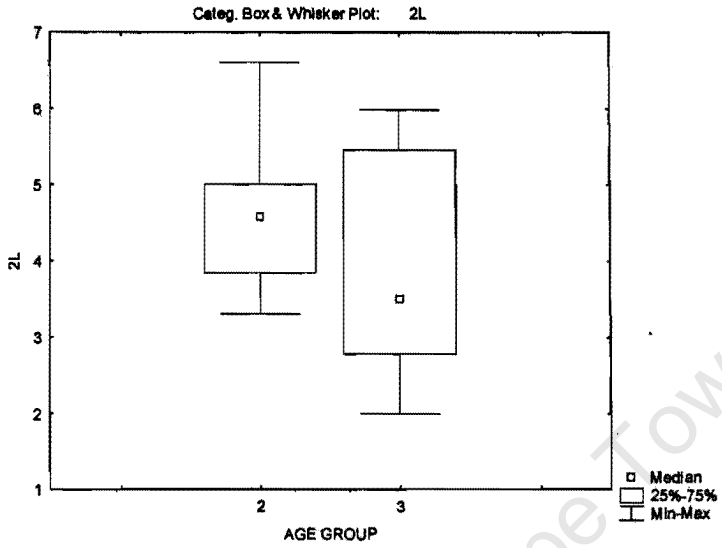

AGE GROUP	3L Means	3L N	3L Std.Dev.	3L Std.Err.
2	9.045714	7	2.179135	0.823636
3	5.370000	6	1.679667	0.685721
All Grps	7.349231	13	2.680931	0.743556

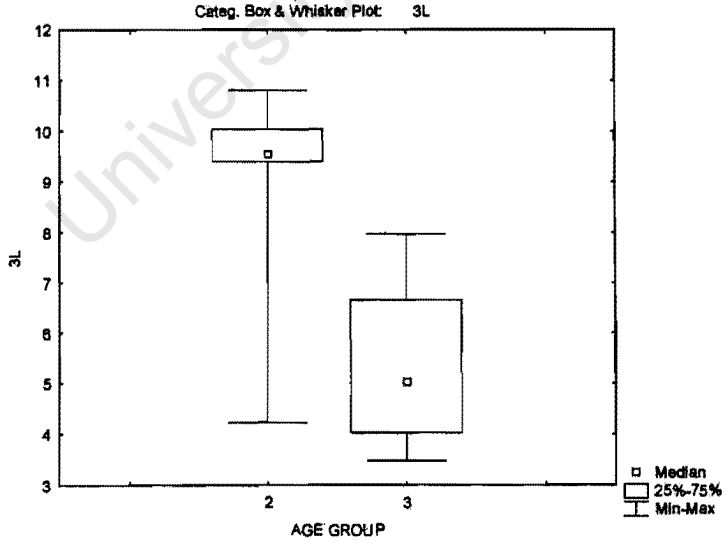

AGE GROUP	1R Means	1R N	1R Std.Dev.	1R Std.Err.
2	10.00857	7	2.362770	0.893043
3	6.92667	6	1.986974	0.811179
All Grps	8.58615	13	2.644534	0.733462

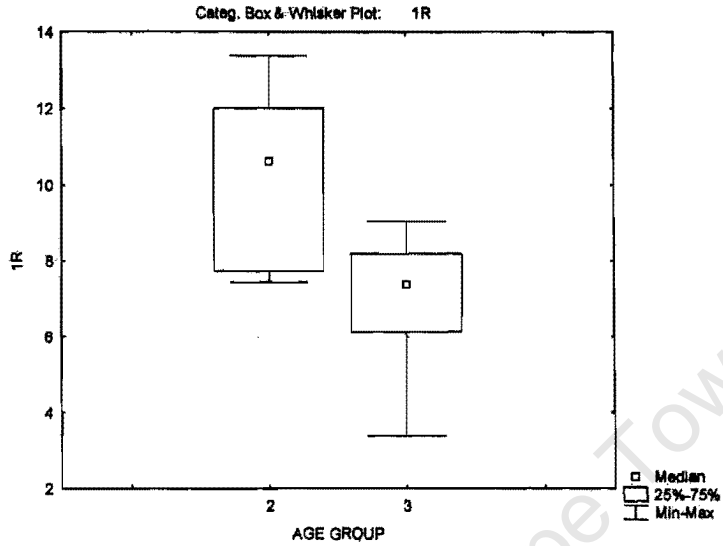

AGE GROUP	2R Means	2R N	2R Std.Dev.	2R Std.Err.
2	4.704286	7	1.256156	0.474782
3	4.063333	6	1.259852	0.514332
All Grps	4.408462	13	1.249365	0.346512

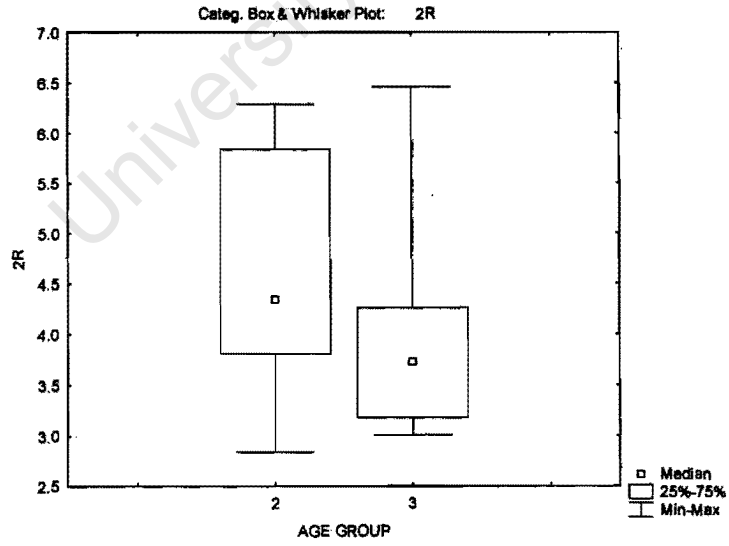

AGE GROUP	3R Means	3R N	3R Std.Dev.	3R Std.Err.
2	10.43571	7	1.697477	0.641586
3	6.20167	6	1.318399	0.538234
All Grps	8.48154	13	2.644144	0.733354

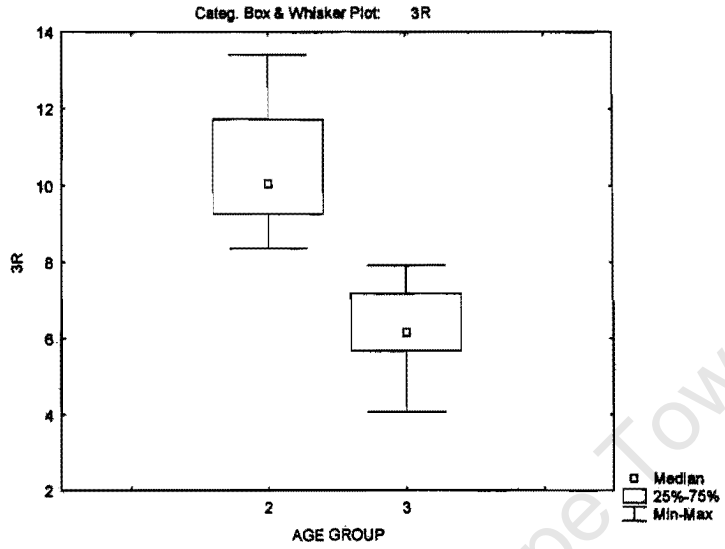

AGE GROUP	1L-2L Means	1L-2L N	1L-2L Std.Dev.	1L-2L Std.Err.
2	6.731429	7	2.146093	0.811147
3	2.065000	6	2.110609	0.861652
All Grps	4.577692	13	3.165694	0.878006

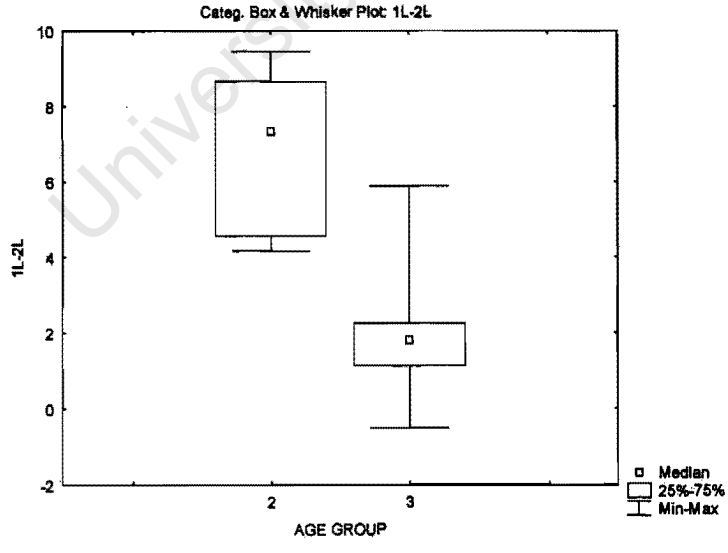

AGE GROUP	3L-2L Means	3L-2L N	3L-2L Std.Dev.	3L-2L Std.Err.
2	4.354286	7	1.608880	0.608100
3	1.493333	6	1.524791	0.622493
All Grps	3.033846	13	2.113447	0.586165

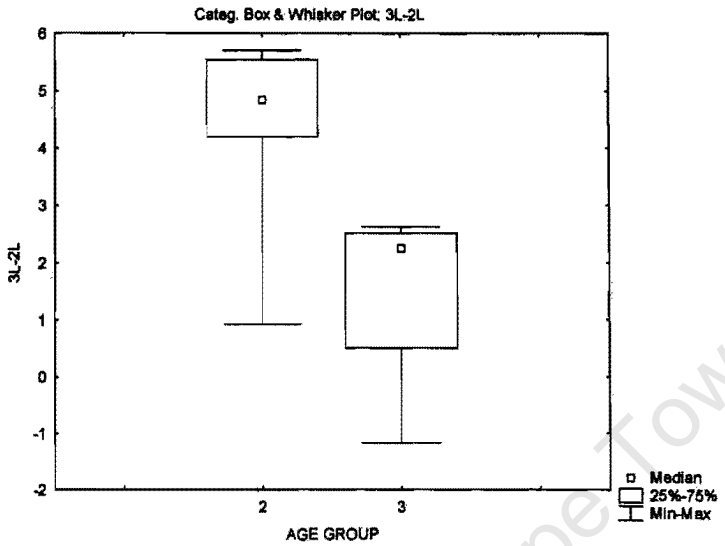

AGE GROUP	1R-2R Means	1R-2R N	1R-2R Std.Dev.	1R-2R Std.Err.
2	5.304286	7	2.278339	0.861131
3	2.863333	6	1.394900	0.569466
All Grps	4.177692	13	2.238367	0.620811

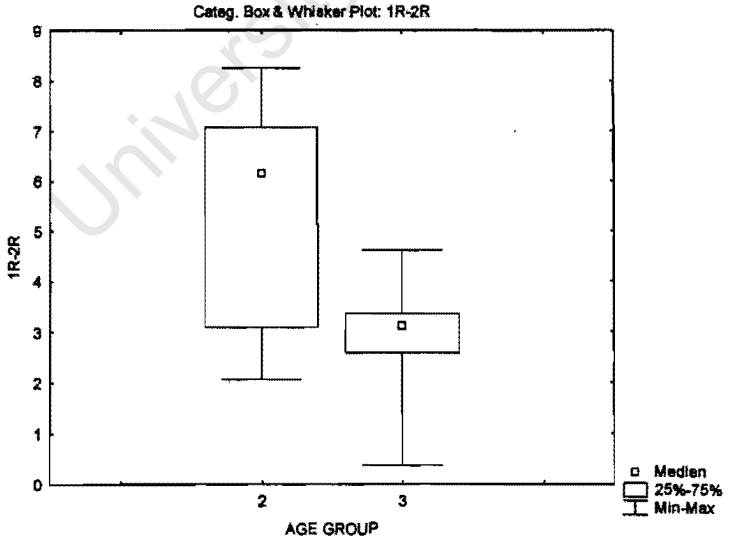

AGE GROUP	3R-2R Means	3R-2R N	3R-2R Std.Dev.	3R-2R Std.Err.
2	5.731429	7	1.896782	0.716916
3	2.138333	6	1.125103	0.459321
All Grps	4.073077	13	2.408773	0.668074

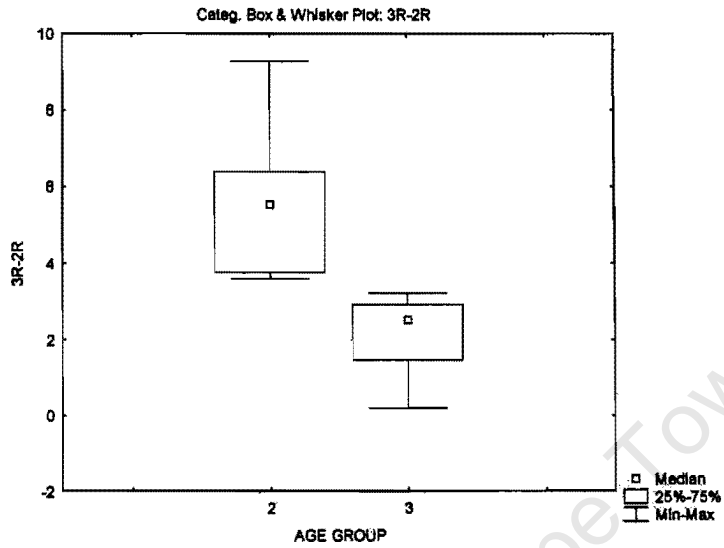

ANALYSIS OF VARIANCE

	SS Effect	df Effect	MS Effect	SS Error	df Error	MS Error	F	p
1L	97.06345	1	97.06345	38.72323	11	3.520293	27.57255	***0.000272***
2L	2.14470	1	2.14470	19.03762	11	1.730693	1.23922	0.289357
3L	43.65052	1	43.65052	42.59817	11	3.872561	11.27175	***0.006394***
1R	30.68629	1	30.68629	53.23642	11	4.839674	6.34057	***0.028575***
2R	1.32726	1	1.32726	17.40370	11	1.582155	0.83890	0.379354
3R	57.91851	1	57.91851	25.97945	11	2.361769	24.52337	***0.000434***
1L-2L	70.35180	1	70.35180	49.90764	11	4.537058	15.50604	***0.002321***
3L-2L	26.44400	1	26.44400	27.15590	11	2.468719	10.71163	***0.007427***
1R-2R	19.24973	1	19.24973	40.87370	11	3.715791	5.18052	***0.043837***
3R-2R	41.71031	1	41.71031	27.91597	11	2.537815	16.43552	***0.001902***

ANALYSIS OF STIMULATED UPTAKE IN VENTRAL STRIATUM OF 7 WEEK OLD AND 16 WEEK OLD UNTREATED RATS

SPREADSHEET

	AGE GROUP	1L	2L	3L	1R	2R	3R	1L-2L	3L-2L	1R-2R	3R-2R
Z1 Nacc	3	7.63	3.04	6.85	6.41	2.39	7.08	4.59	3.81	4.02	4.69
Z2 Nacc	3	6.96	6.05	9.61	8.35	4.85	7.9	0.91	3.56	3.5	3.05
Z3 Nacc	3	6.79	3.62	5.57	6.97	3.67	7.09	3.17	1.95	3.3	3.42
Z4 Nacc	3	9.97	4.64	8.71	10.86	4.1	8.92	5.33	4.07	6.76	4.82
Z5 Nacc	3	10.24	6.3	6.1	10.03	4.93	10.82	3.94	-0.2	5.1	5.89
Z6 Nacc	3	6.97	3.71	5.81	8.63	7.37	4.93	3.26	2.1	1.26	-2.44
RAT 1	2	10.16	5.34	12.44	12.71	6.72	10.57	4.82	7.1	5.99	3.85
RAT 2	2	6.29	3.95	5.46	7.19	3.49	5.74	2.34	1.51	3.7	2.25
RAT 3	2	13.04	3.25	9.4	12.84	3.94	8.26	9.79	6.15	8.9	4.32
RAT 4	2	9.45	4.6	11.41	8.73	6.72	9.84	4.85	6.81	2.01	3.12
RAT 5	2	17.19	4.75	17.66	6.85	3.32	13.64	12.44	12.91	3.53	10.32
RAT 6	2	15.69	5.93	11.51	8.83	5.2	12.86	9.76	5.58	3.63	7.66
RAT 7	2	17.79	3.55	11.04	17.41	4.21	11.32	4.21	11.32	13.2	7.11

BREAKDOWN STATISTICS

AGE GROUP	1L Means	1L N	1L Std.Dev.	1L Std.Err.
2	12.80143	7	4.342697	1.641385
3	8.09333	6	1.586804	0.647810
All Grps	10.62846	13	4.055424	1.124772

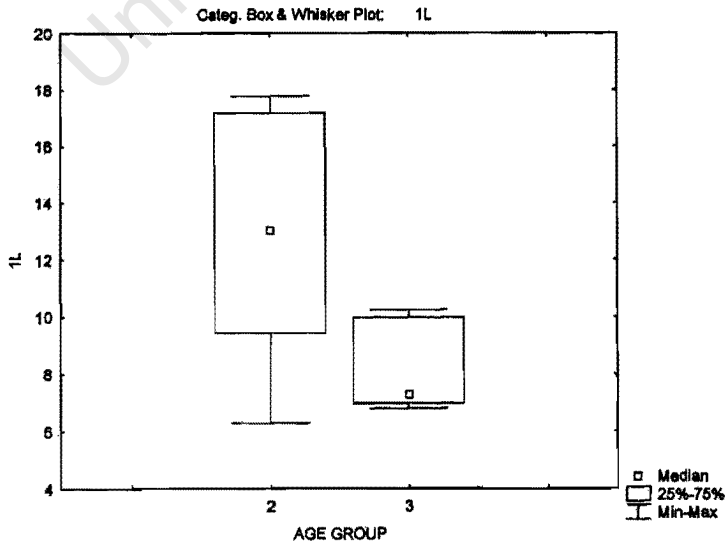

AGE GROUP	2L Means	2L N	2L Std.Dev.	2L Std.Err.
2	4.481429	7	0.965064	0.364760
3	4.560000	6	1.354297	0.552889
All Grps	4.517692	13	1.109753	0.307790

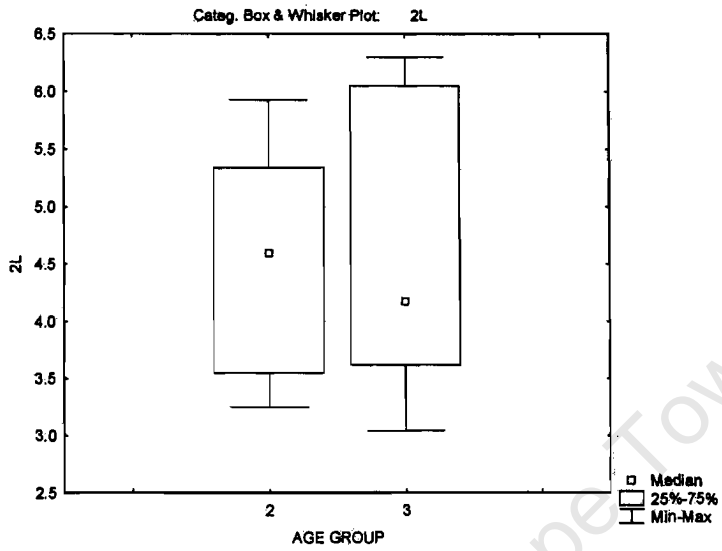

AGE GROUP	3L Means	3L N	3L Std.Dev.	3L Std.Err.
2	11.27429	7	3.641977	1.376538
3	7.10833	6	1.670885	0.682136
All Grps	9.35154	13	3.530979	0.979317

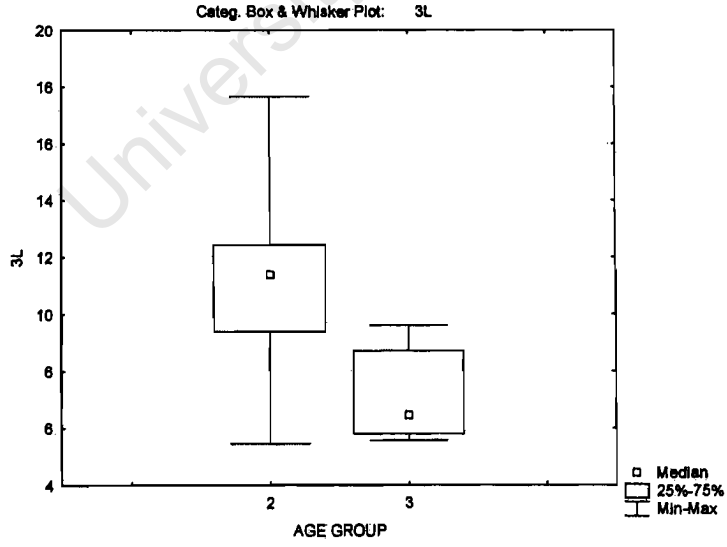

AGE GROUP	1R Means	1R N	1R Std.Dev.	1R Std.Err.
2	10.65143	7	3.832921	1.448708
3	8.54167	6	1.711636	0.698772
All Grps	9.67769	13	3.124855	0.866679

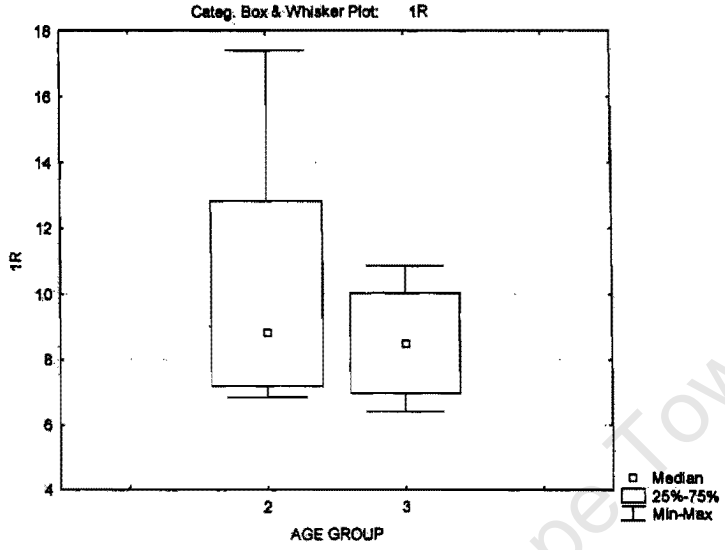

AGE GROUP	2R Means	2R N	2R Std.Dev.	2R Std.Err.
2	4.800000	7	1.444934	0.546134
3	4.551667	6	1.663086	0.678952
All Grps	4.685385	13	1.487602	0.412587

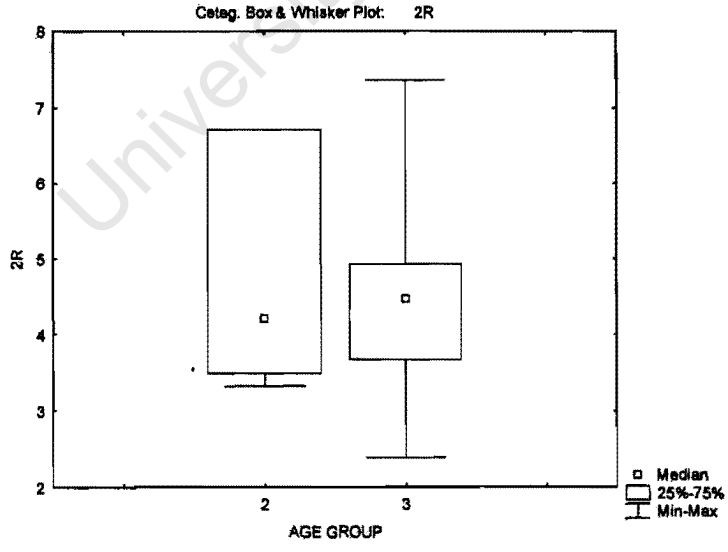

AGE GROUP	3R Means	3R N	3R Std.Dev.	3R Std.Err.
2	10.31857	7	2.707609	1.023380
3	7.79000	6	1.982100	0.809189
All Grps	9.15154	13	2.650267	0.735052

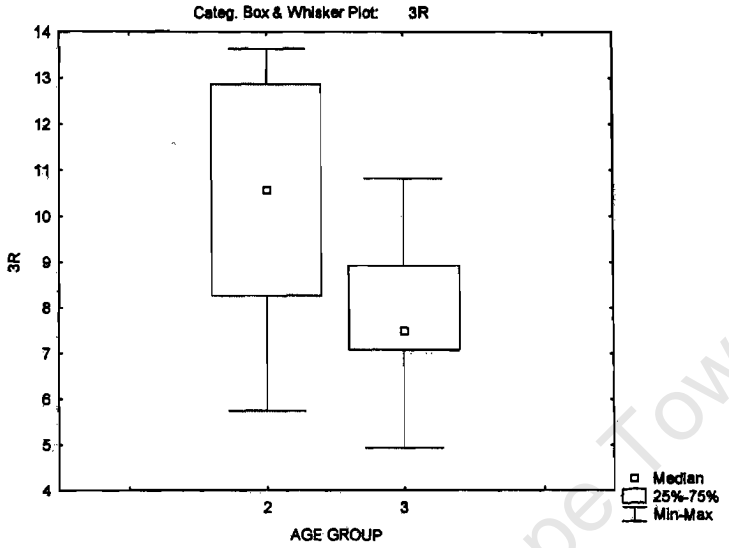

AGE GROUP	1L-2L Means	1L-2L N	1L-2L Std.Dev.	1L-2L Std.Err.
2	6.887143	7	3.736771	1.412367
3	3.533333	6	1.523058	0.621786
All Grps	5.339231	13	3.313094	0.918887

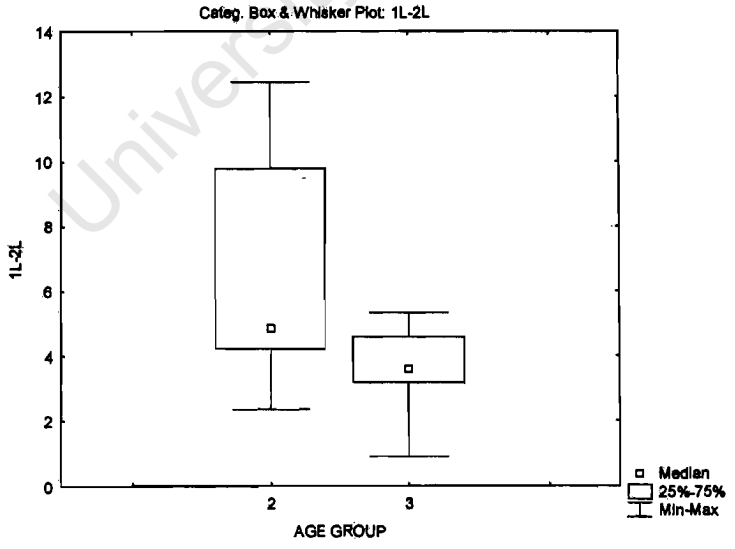

AGE GROUP	3L-2L Means	3L-2L N	3L-2L Std.Dev.	3L-2L Std.Err.
2	7.340000	7	3.779471	1.428506
3	2.548333	6	1.615121	0.659370
All Grps	5.128462	13	3.796140	1.052860

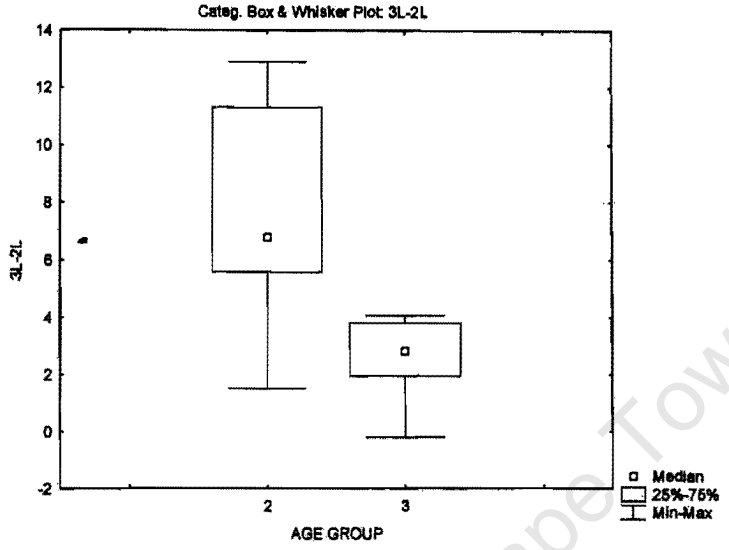

AGE GROUP	1R-2R Means	1R-2R N	1R-2R Std.Dev.	1R-2R Std.Err.
2	5.851429	7	3.937501	1.488235
3	3.990000	6	1.847972	0.754431
All Grps	4.992308	13	3.179267	0.881770

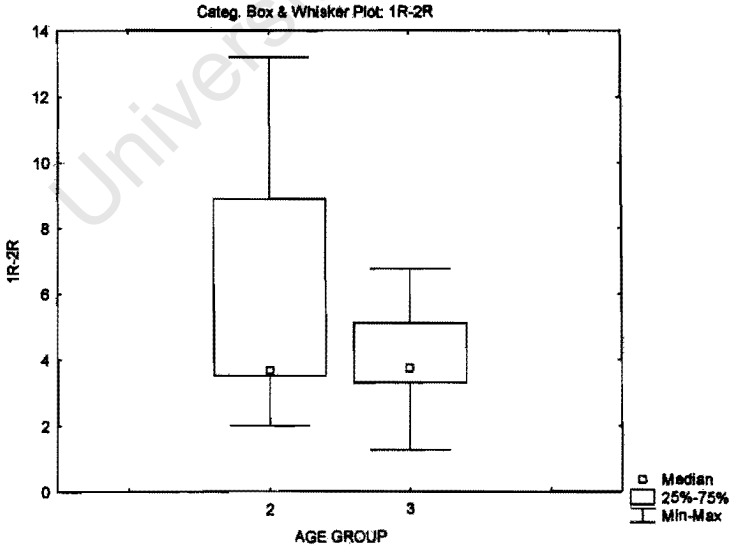

AGE GROUP	3R-2R Means	3R-2R N	3R-2R Std.Dev.	3R-2R Std.Err.
2	5.518571	7	2.910598	1.100103
3	3.238333	6	2.964870	1.210403
All Grps	4.466154	13	3.049318	0.845729

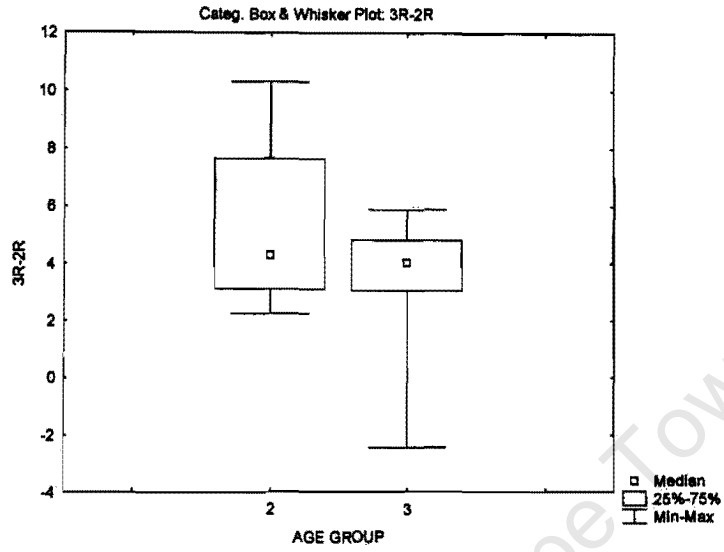

ANALYSIS OF VARIANCE

	SS Effect	df Effect	MS Effect	SS Error	df Error	MS Error	F	p
1L	71.61375	1	71.61375	125.7438	11	11.43126	6.264731	***0.029352***
2L	0.01995	1	0.01995	14.7587	11	1.34170	0.014866	0.905158
3L	56.07051	1	56.07051	93.5433	11	8.50393	6.593481	***0.026154***
1R	14.38046	1	14.38046	102.7962	11	9.34511	1.538823	0.240600
2R	0.19924	1	0.19924	26.3563	11	2.39603	0.083154	0.778429
3R	20.65648	1	20.65648	63.6305	11	5.78459	3.570951	0.085426
1L-2L	36.33982	1	36.33982	95.3793	11	8.67084	4.191036	0.065290
3L-2L	74.17869	1	74.17869	98.7495	11	8.97723	8.262985	***0.015118***
1R-2R	11.19435	1	11.19435	110.0985	11	10.00895	1.118433	0.312928
3R-2R	16.79834	1	16.79834	94.7818	11	8.61652	1.949549	0.190173

ANNEX B

NUMBER OF ROTATIONS CONDUCTED BY SHAM LESIONED AND 6-OHDA LESIONED RATS

	LESION GROUP	QUARTER ROTATIONS	COMPLETE ROTATIONS
K1	1	1419	355
K2	1	1950	488
K3	1	1341	335
K4	1	453	113
K5	1	760	190
M1	1	1104	276
M2	1	595	149
M3	1	-402	-101
M4	1	208	52
M5	1	1700	425
M6	1	707	176
O1	1	705	176
O2	1	1977	494
O4	1	-197	-49
O5	1	1022	256
O7	1	648	162
O10	1	1872	468
K6	2	16	4
K7	2	0	0
K8	2	45	11
M8	2	-220	-55
M9	2	-303	-75
M10	2	26	6.5
M11	2	-278	-69
M12	2	-22	-6
O11	2	-91	-23
O12	2	127	32
O13	2	-134	-34
O14	2	-157	-39
O15	2	-12	-3
O16	2	-80	-20

Breakdown statistics showing mean number of rotations ± sem conducted by 6-OHDA lesioned (group 1) and sham lesioned rats (group 2).

LESION GROUP	QUARTER Means	QUARTER N	QUARTER Std.Dev.	QUARTER Std.Err.	COMPLETE ROTATIONS Means	COMPLETE ROTATIONS N	COMPLETE ROTATIONS Std.Dev.	COMPLETE ROTATIONS Std.Err.
1	933.0588	17	714.9154	173.3925	233.2353	17	178.8129	43.36851
2	-77.3571	14	127.3140	34.0261	-19.3214	14	31.6699	8.46415
All Grps	476.7419	31	735.4492	132.0906	119.1774	31	183.8774	33.02536

TREATMENT GROUP STATISTICS REPORT

COMPARISON OF STIMULATED $^{45}Ca^{2+}$ IN SHAM LESIONED RATS
DORSAL STRIATUM

SPREADSHEET

	LESION GROUP	1L	2L	3L	1R	2R	3R	1L-2L	3L-2L	1R-2R	3R-2R
K6	2	15.49	8.91	13.79	14.75	9.85	15.84	6.58	4.88	4.9	5.99
K7	2	9.96	8.19	10.41	9.11	5.25	13.9	1.77	2.22	3.86	8.65
K8	2	12.15	9.16	12.37	12.28	6.57	12.14	2.99	3.21	5.71	5.57
M9	2	10.92	6.55	11.7	7.12	6.82	8.47	4.37	5.15	0.3	1.65
M11	2	6.15	5.01	8.96	7.89	4.39	10.34	1.14	3.95	3.5	5.95
O11	2	11.01	6.18	8.24	9.41	6.32	9.61	4.83	2.06	3.09	3.29
O13	2	9.71	3.78	6.65	5.2	3.79	7.42	5.93	2.87	1.41	3.63
O14	2	8.16	5.33	9.5	7.63	3.89	7.87	2.83	4.17	3.74	3.98
O15	2	7.38	5.96	5.57	11	6.09	5.19	1.42	-0.39	4.91	-0.9

DESCRIPTIVE STATISTICS

	Valid N	Mean	Minimum	Maximum	Std.Dev.	Standard Error
1L	9	10.10333	6.150000	15.49000	2.776941	0.925647
2L	9	6.56333	3.780000	9.16000	1.840095	0.613365
3L	9	9.68778	5.570000	13.79000	2.679514	0.893171
1R	9	9.37667	5.200000	14.75000	2.911348	0.970449
2R	9	5.88556	3.790000	9.85000	1.880931	0.626977
3R	9	10.08667	5.190000	15.84000	3.368338	1.122779
1L-2L	9	3.54000	1.140000	6.58000	1.984332	0.661444
3L-2L	9	3.12444	-0.390000	5.15000	1.707850	0.569283
1R-2R	9	3.49111	0.300000	5.71000	1.724634	0.574878
3R-2R	9	4.20111	-0.900000	8.65000	2.776236	0.925412

STUDENT T-TEST

	Mean	Std.Dv.	N	Diff.	Std.Dv. Diff.	t	df	p
1L	10.10333	2.776941						
2L	6.56333	1.840095	9	3.540000	1.984332	5.351926	8	*0.000684*
3L	9.68778	2.679514						
2L	6.56333	1.840095	9	3.124444	1.707850	5.488381	8	*0.000582*

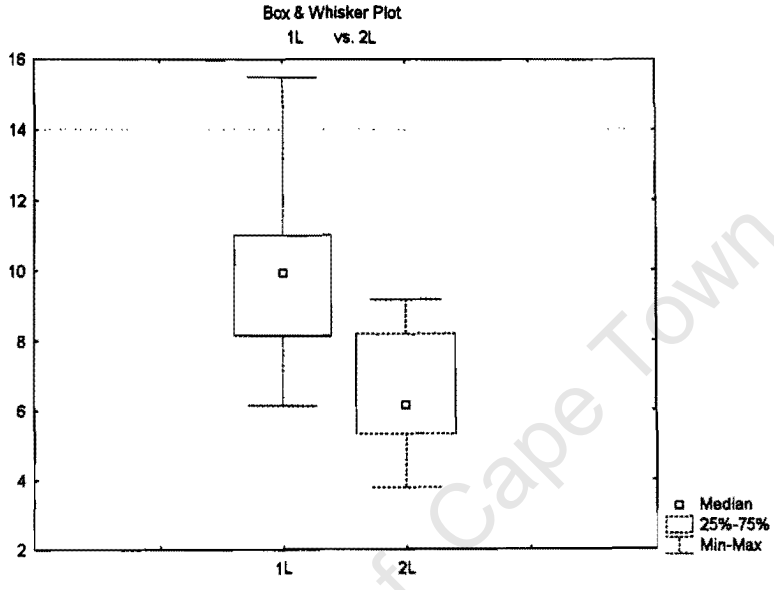

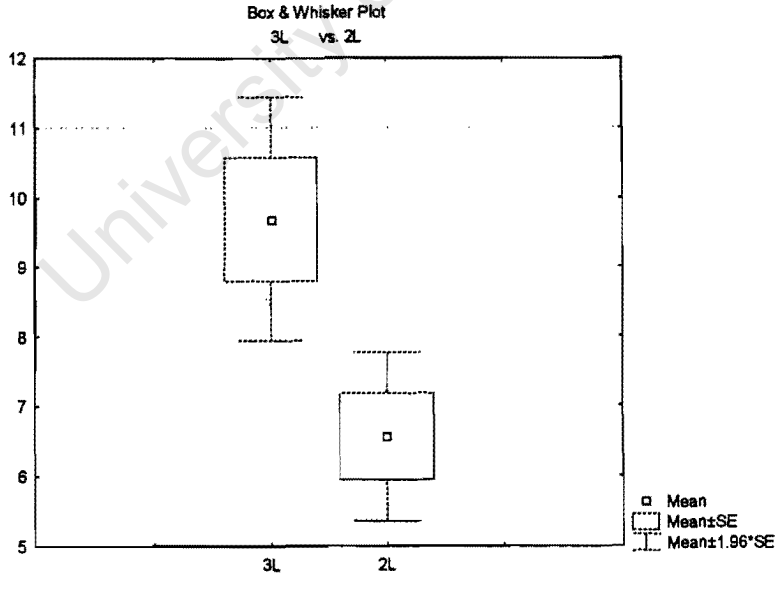

	Mean	Std.Dv.	N	Diff.	Std.Dv. Diff.	t	df	p
1R	9.37667	2.911348						
2R	5.88556	1.880931	9	3.491111	1.724634	6.072787	8	*0.000298*
3R	10.08667	3.368338						
2R	5.88556	1.880931	9	4.201111	2.776236	4.539720	8	*0.001900*

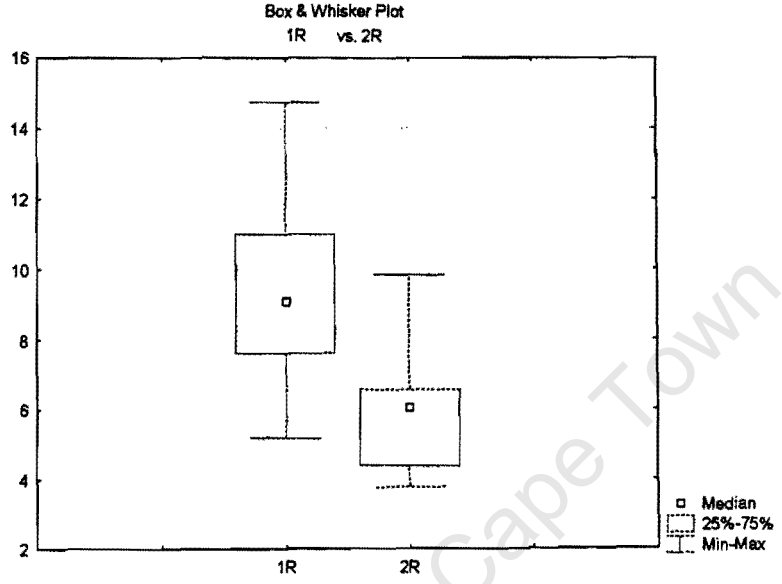

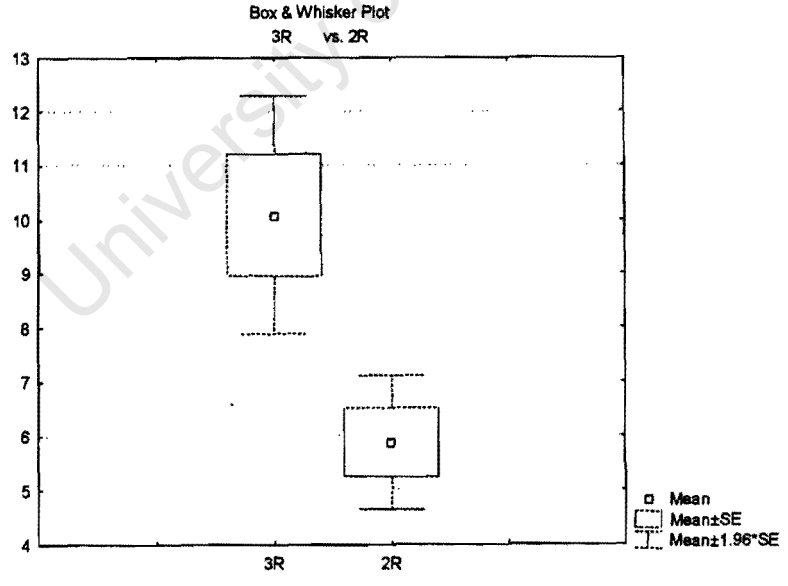

	Mean	Std.Dv.	N	Diff.	Std.Dv. Diff.	t	df	p
1L-2L	3.540000	1.984332						
3L-2L	3.124444	1.707850	9	0.415556	2.006222	0.621400	8	0.551628

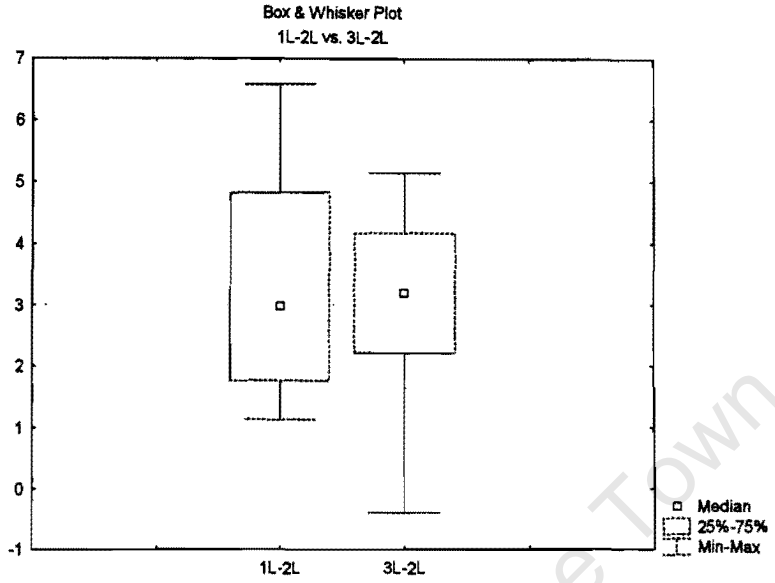

	Mean	Std.Dv.	N	Diff.	Std.Dv. Diff.	t	df	p
1R-2R	3.491111	1.724634						
3R-2R	4.201111	2.776236	9	-0.710000	2.877108	-0.740327	8	0.480263

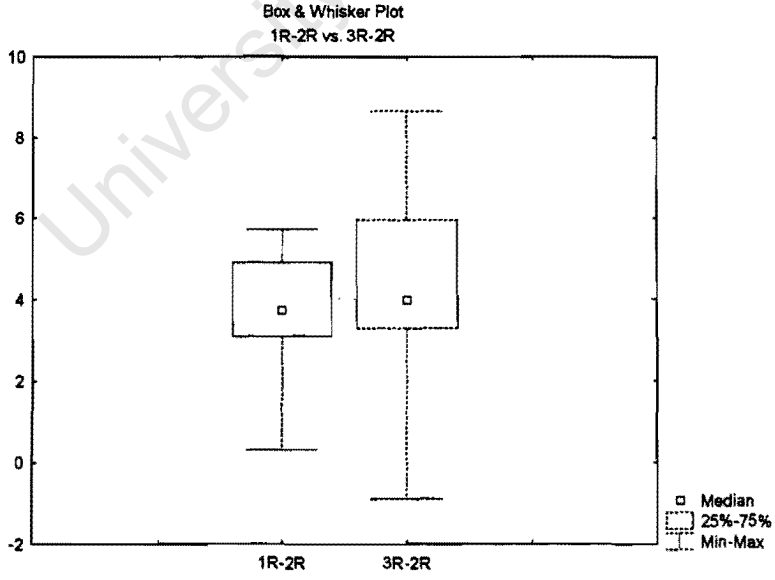

	Mean	Std.Dv.	N	Diff.	Std.Dv. Diff.	t	df	p
1L-2L	3.540000	1.984332						
1R-2R	3.491111	1.724634	9	0.048889	3.024237	0.048497	8	0.962509

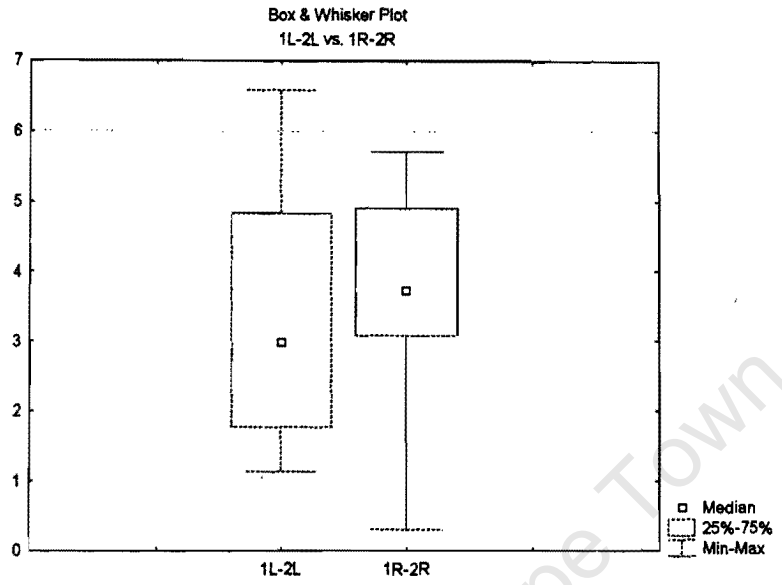

	Mean	Std.Dv.	N	Diff.	Std.Dv. Diff.	t	df	p
3L-2L	3.124444	1.707850						
3R-2R	4.201111	2.776236	9	-1.07667	2.654016	-1.21702	8	0.258276

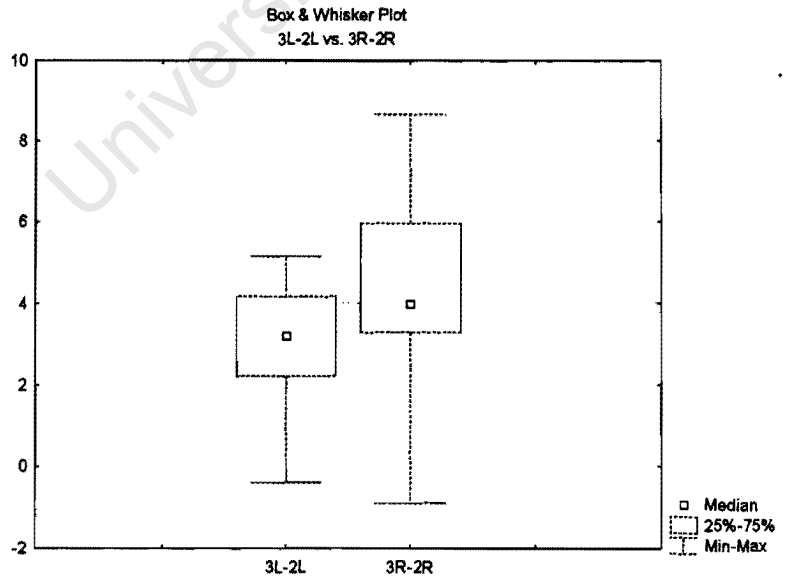

VENTRAL SHAM LESIONED GROUP REPORT (WITHIN GROUP ANALYSIS)

SPREADSHEET

	LESION GROUP	1L	2L	3L	1R	2R	3R
M10	2	5.07	1.87	5.03	3.75	1.97	4.34
O11	2	11.53	4	7.51	12.97	4.47	9.99
O13	2	6.59	1.88	5.19	4.86	1.54	6.88
O14	2	9.1	4.66	7.95	10.15	3.32	8.8
O15	2	8.8	4.03	13.23	8	5.14	10.53
	LESION GROUP	1L-2L	3L-2L	1R-2R	3R-2R		
M10	2	3.2	3.16	1.78	2.37		
O11	2	7.53	3.51	8.5	5.52		
O13	2	4.71	3.31	3.32	5.34		
O14	2	4.44	3.29	6.83	5.48		
O15	2	4.77	9.2	2.86	5.39		

DESCRIPTIVE STATISTICS

	Valid N	Mean	Minimum	Maximum	Std.Dev.	Standard Error
LESION GROUP	5	2.000000	2.000000	2.00000	0.000000	0.000000
1L	5	8.218000	5.070000	11.53000	2.482251	1.110096
2L	5	3.288000	1.870000	4.66000	1.316537	0.588773
3L	5	7.782000	5.030000	13.23000	3.319446	1.484501
1R	5	7.946000	3.750000	12.97000	3.782556	1.691610
2R	5	3.288000	1.540000	5.14000	1.550861	0.693566
3R	5	8.108000	4.340000	10.53000	2.529460	1.131209
1L-2L	5	4.930000	3.200000	7.53000	1.586427	0.709472
3L-2L	5	4.494000	3.160000	9.20000	2.633710	1.177831
1R-2R	5	4.658000	1.780000	8.50000	2.862887	1.280322
3R-2R	5	4.820000	2.370000	5.52000	1.371441	0.613327

STUDENT T-TESTS

	Mean	Std.Dv.	N	Diff.	Std.Dv. Diff.	t	df	p
1L	8.218000	2.482251						
1R	7.946000	3.782556	5	0.272000	1.430164	0.425273	4	0.692519
	Mean	**Std.Dv.**	**N**	**Diff.**	**Std.Dv. Diff.**	**t**	**df**	**p**
2L	3.288000	1.316537						
2R	3.288000	1.550861	5	0.000000	0.918450	0.000000	4	1.000000
	Mean	**Std.Dv.**	**N**	**Diff.**	**Std.Dv. Diff.**	**t**	**df**	**p**
3L	7.782000	3.319446						
3R	8.108000	2.529460	5	-0.326000	2.059352	-0.353975	4	0.741229

	Mean	Std.Dv.	N	Diff.	Std.Dv. Diff.	t	df	p
1L	8.218000	2.482251						
2L	3.288000	1.316537	5	4.930000	1.586427	6.948833	4	***0.002253***

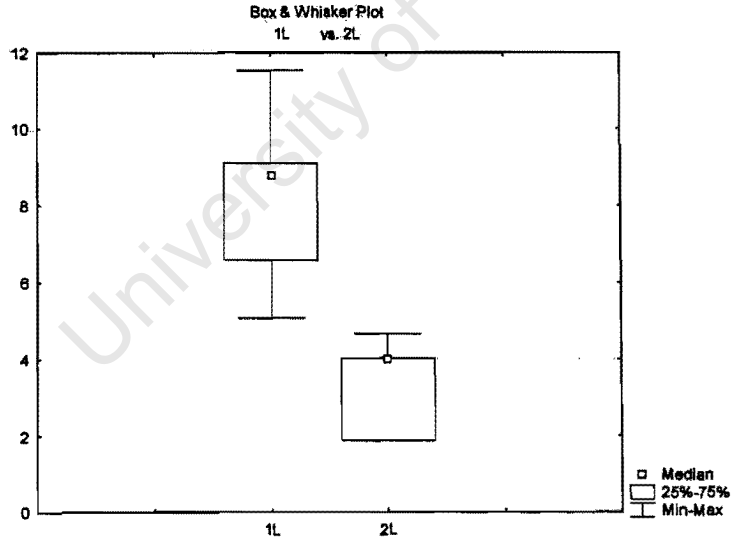

	Mean	Std.Dv.	N	Diff.	Std.Dv. Diff.	t	df	p
3L	7.782000	3.319446						
2L	3.288000	1.316537	5	4.494000	2.633710	3.815488	4	***0.018851***

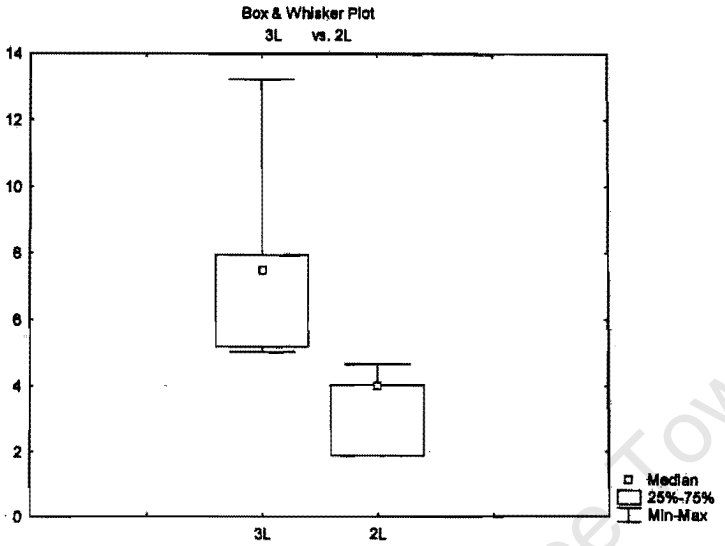

	Mean	Std.Dv.	N	Diff.	Std.Dv. Diff.	t	df	p
1R	7.946000	3.782556						
2R	3.288000	1.550861	5	4.658000	2.862887	3.638148	4	***0.022001***

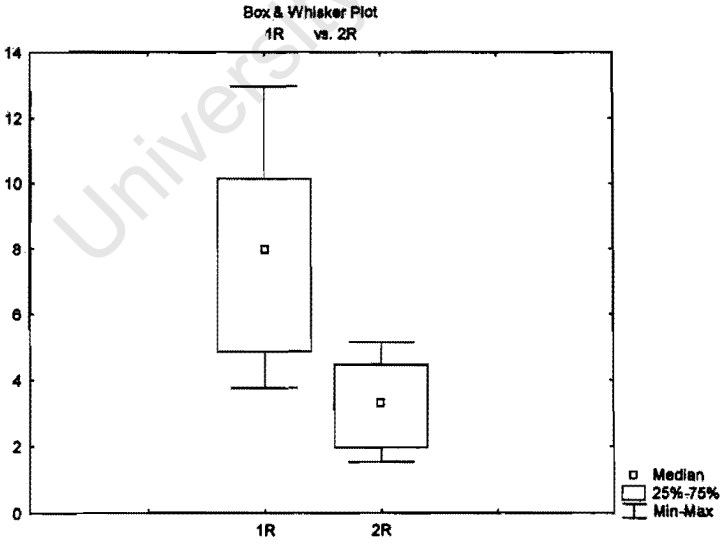

	Mean	Std.Dv.	N	Diff.	Std.Dv. Diff.	t	df	p
3R	8.108000	2.529460						
2R	3.288000	1.550861	5	4.820000	1.371441	7.858777	4	0.001417

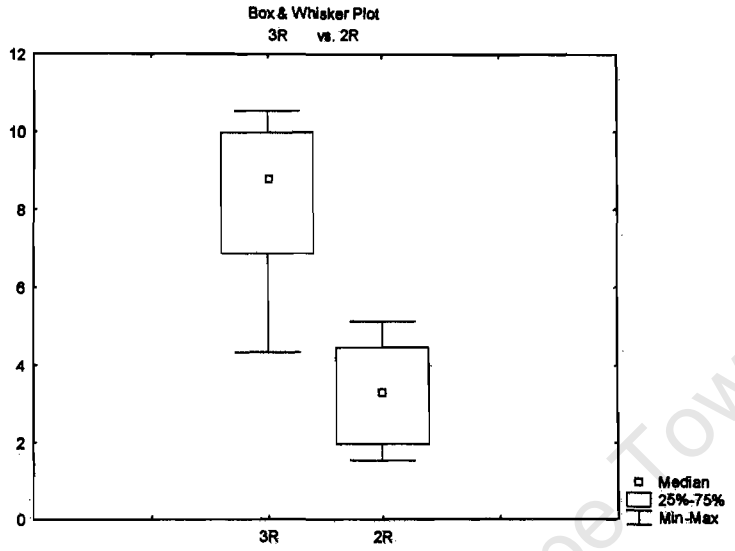

	Mean	Std.Dv.	N	Diff.	Std.Dv. Diff.	t	df	p
1L-2L	4.930000	1.586427						
3L-2L	4.494000	2.633710	5	0.436000	3.087026	0.315814	4	0.767936

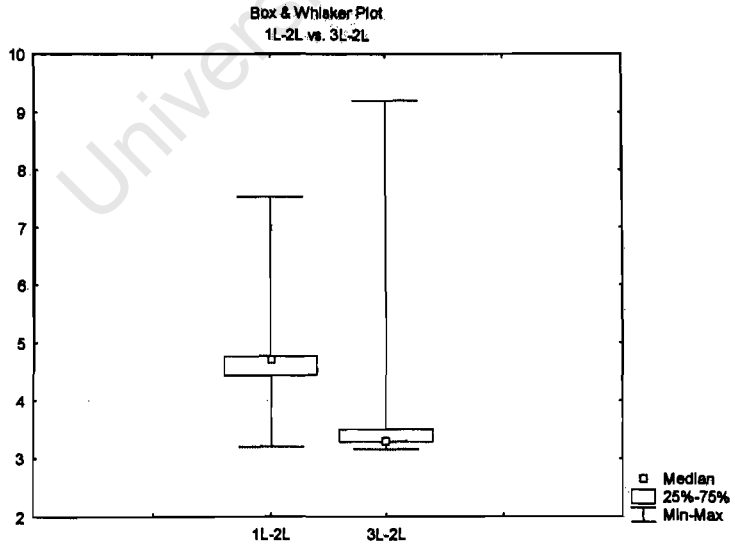

	Mean	Std.Dv.	N	Diff.	Std.Dv. Diff.	t	df	p
1R-2R	4.658000	2.862887						
3R-2R	4.820000	1.371441	5	-0.162000	2.313065	-0.156607	4	0.883141

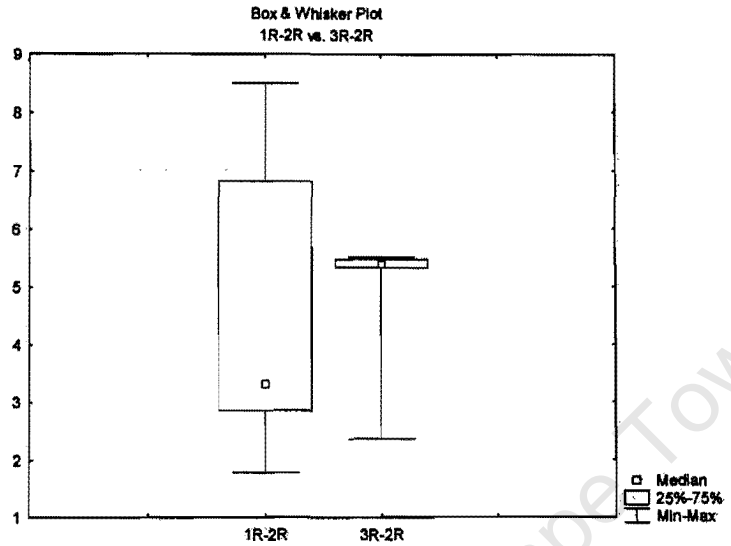

	Mean	Std.Dv.	N	Diff.	Std.Dv. Diff.	t	df	p
1L-2L	4.930000	1.586427						
1R-2R	4.658000	2.862887	5	0.272000	1.862772	0.326508	4	0.760410

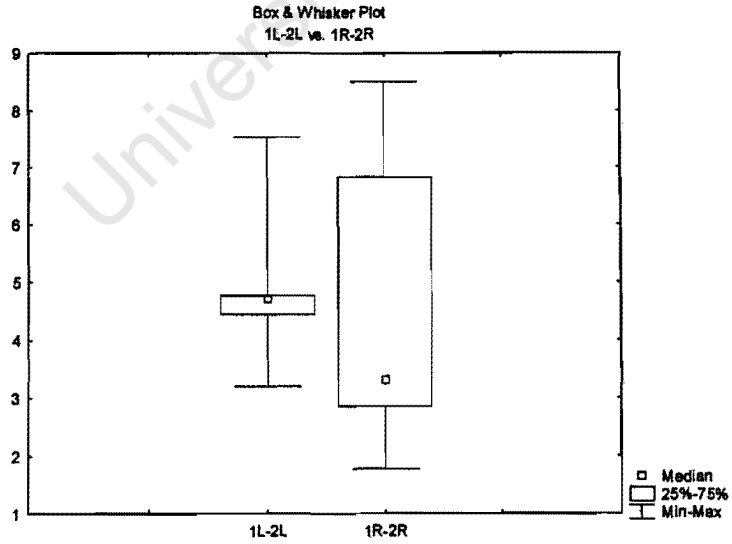

	Mean	Std.Dv.	N	Diff.	Std.Dv. Diff.	t	df	p
3L-2L	4.494000	2.633710						
3R-2R	4.820000	1.371441	5	-0.326000	2.625163	-0.277681	4	0.795018

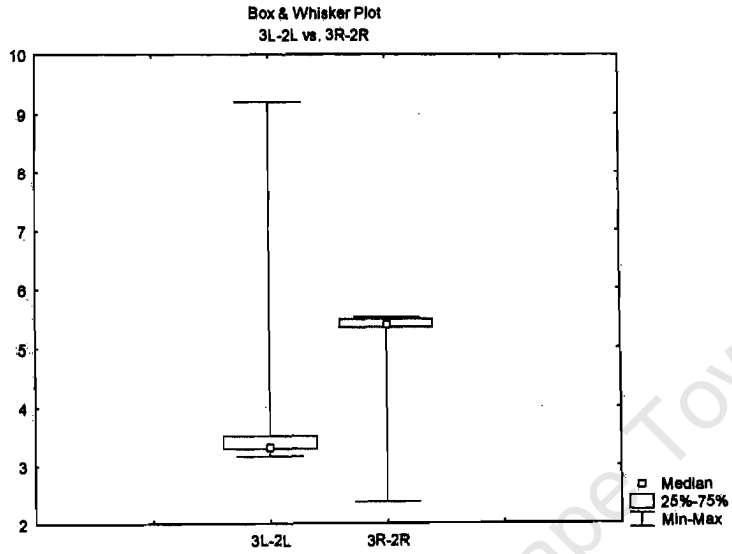

TREATMENT GROUP STATISTICS REPORT

COMPARISON OF STIMULATED $^{45}Ca^{2+}$ IN 6-OHDA LESIONED RATS
DORSAL STRIATUM

SPREADSHEET

	LESION GROUP	1L	2L	3L	1R	2R	3R	1L-2L	3L-2L	1R-2R	3R-2R
K2	1	11.17	6.48	12.87	11.6	7.01	11.86	4.69	6.39	4.59	4.85
K3	1	12.96	9.36	16.1	11.89	7.24	17.16	3.6	6.74	4.65	9.92
K4	1	11.91	4.91	6.86	11.99	3.59	11.16	7	1.95	8.4	7.57
K5	1	8.5	5.27	5.86	10.2	6.48	6.36	3.23	0.59	3.72	-0.12
M1	1	8.18	2.47	9.74	6.38	2.8	5.96	5.71	7.27	3.58	3.16
M5	1	7.58	2.52	7.33	5.73	3.06	6.22	5.06	4.81	2.67	3.16
O1	1	6.56	3.59	8.58	9.99	4.65	10.95	2.97	4.99	5.34	6.3
O5	1	5.43	5.89	10.98	5.06	6.88	10.19	-0.46	5.09	-1.82	3.31
O7	1	8.26	4.24	6.84	8.15	4.14	7.22	4.02	2.6	4.01	3.08
O10	1	6.85	4.42	9.8	7.86	3.99	7.86	2.43	5.38	3.87	3.87

DESCRIPTIVE STATISTICS

	Valid N	Mean	Minimum	Maximum	Std.Dev.	Standard Error
1L	10	8.740000	5.43000	12.96000	2.471841	0.781665
2L	10	4.915000	2.47000	9.36000	2.039996	0.645103
3L	10	9.496000	5.86000	16.10000	3.164119	1.000582
1R	10	8.885000	5.06000	11.99000	2.612854	0.826257
2R	10	4.984000	2.80000	7.24000	1.740174	0.550291
3R	10	9.494000	5.96000	17.16000	3.505815	1.108636
1L-2L	10	3.825000	-0.46000	7.00000	2.038198	0.644535
3L-2L	10	4.581000	0.59000	7.27000	2.187243	0.691667
1R-2R	10	3.901000	-1.82000	8.40000	2.532923	0.800981
3R-2R	10	4.510000	-0.12000	9.92000	2.807288	0.887742

STUDENT T-TESTS

	Mean	Std.Dv.	N	Diff.	Std.Dv. Diff.	t	df	p
1L	8.740000	2.471841						
2L	4.915000	2.039996	10	3.825000	2.038198	5.934514	9	***0.000219***
3L	9.496000	3.164119						
2L	4.915000	2.039996	10	4.581000	2.187243	6.623129	9	***0.000097***

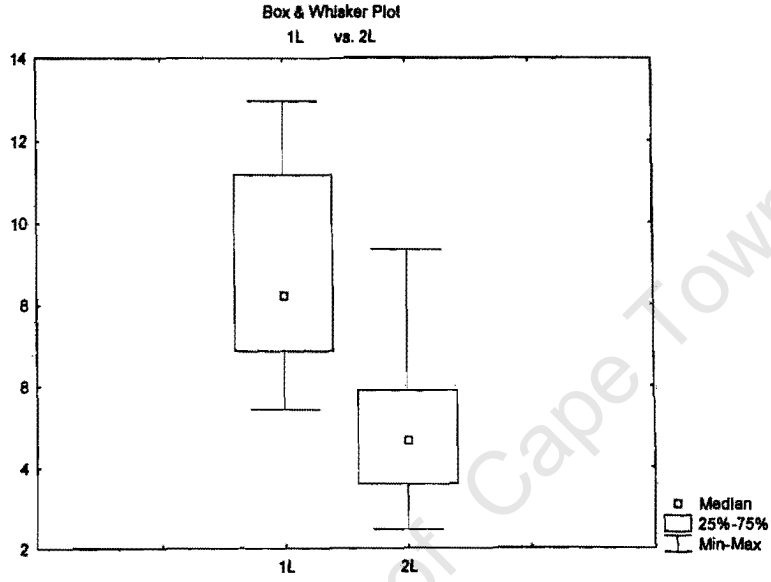

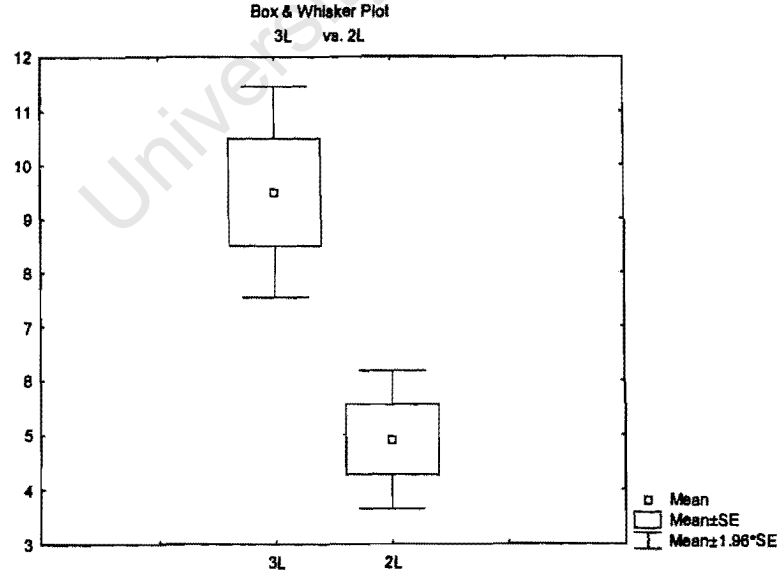

	Mean	Std.Dv.	N	Diff.	Std.Dv. Diff.	t	df	p
1R	8.885000	2.612854						
2R	4.984000	1.740174	10	3.901000	2.532923	4.870280	9	0.000883
3R	9.494000	3.505815						
2R	4.984000	1.740174	10	4.510000	2.807288	5.080302	9	0.000663

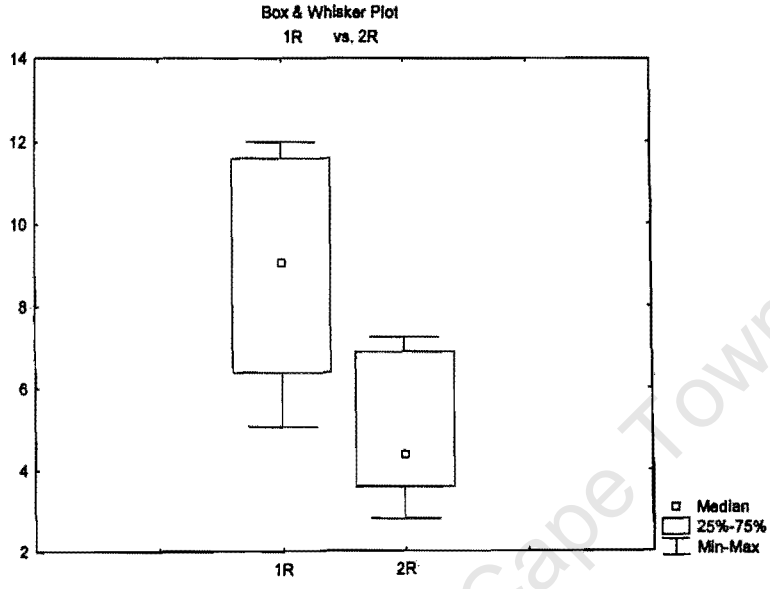

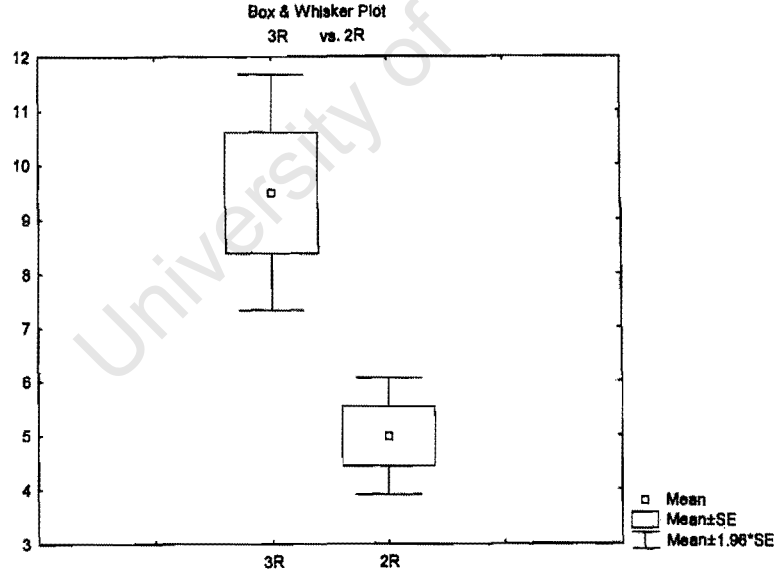

	Mean	Std.Dv.	N	Diff.	Std.Dv. Diff.	t	df	p
1L-2L	3.825000	2.038198						
3L-2L	4.581000	2.187243	10	-0.756000	3.119905	-0.766268	9	0.463140

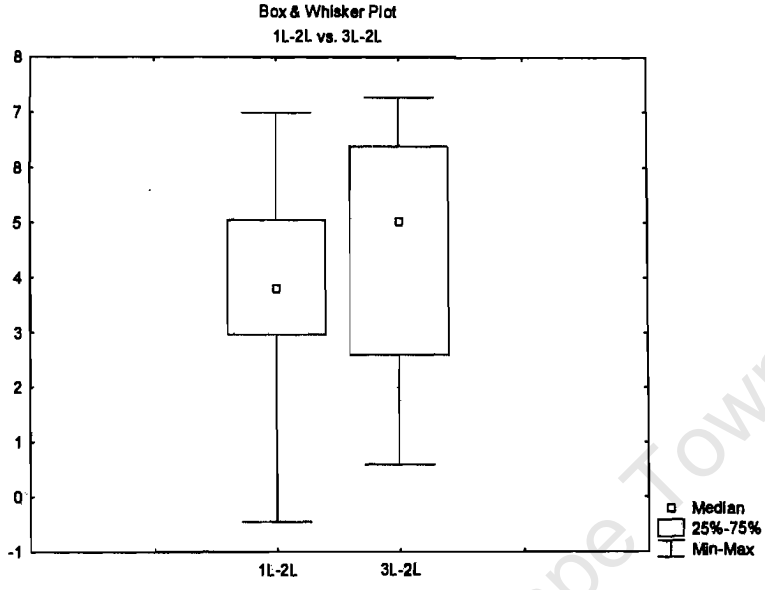

	Mean	Std.Dv.	N	Diff.	Std.Dv. Diff.	t	df	p
1R-2R	3.901000	2.532923						
3R-2R	4.510000	2.807288	10	-0.609000	2.750477	-0.700179	9	0.501512

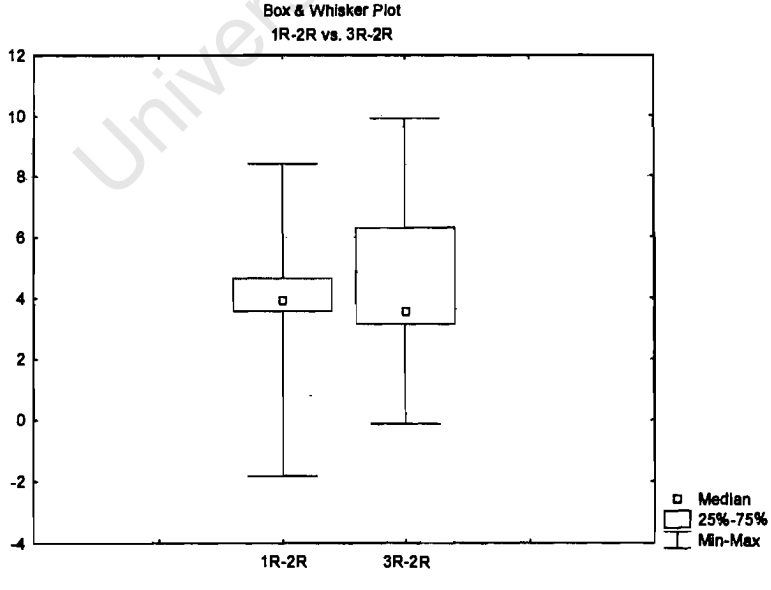

	Mean	Std.Dv.	N	Diff.	Std.Dv. Diff.	t	df	p
1L-2L	3.825000	2.038198						
1R-2R	3.901000	2.532923	10	-0.076000	1.600140	-0.150195	9	0.883923

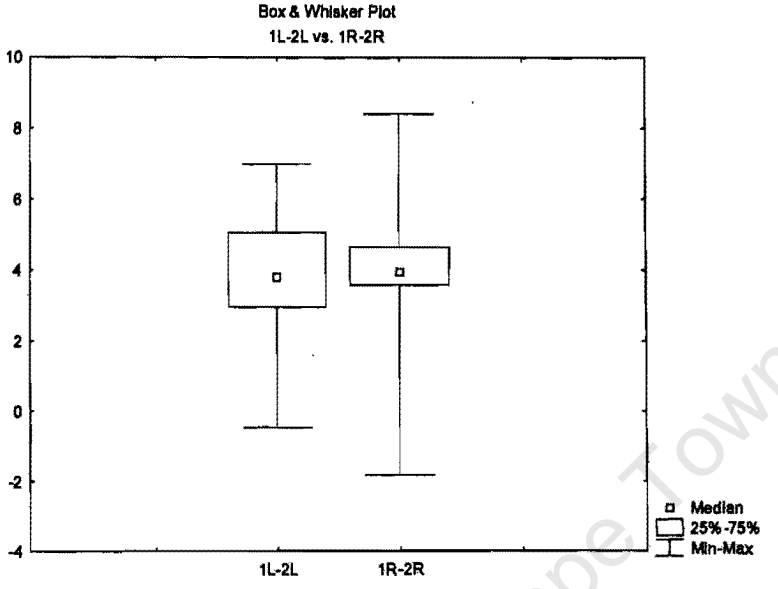

	Mean	Std.Dv.	N	Diff.	Std.Dv. Diff.	t	df	p
3L-2L	4.581000	2.187243						
3R-2R	4.510000	2.807288	10	0.071000	2.819214	0.079640	9	0.938266

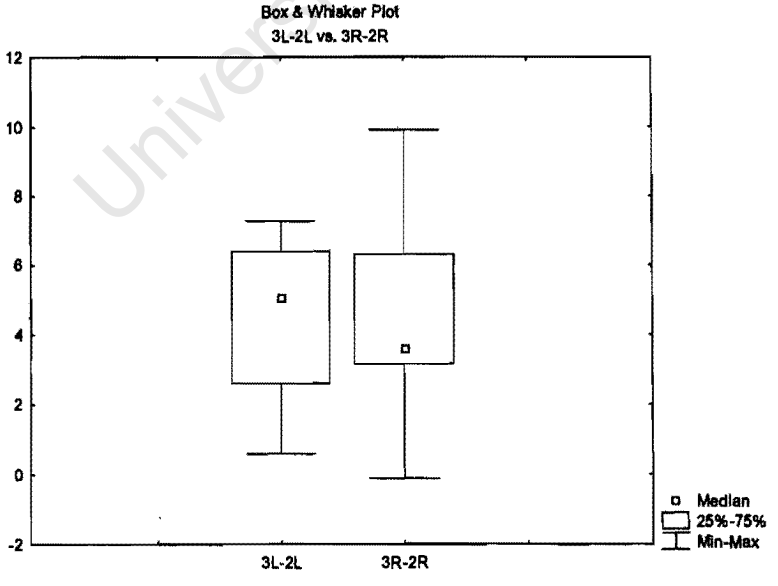

VENTRAL 6-OHDA LESIONED GROUP REPORT (WITHIN GROUP ANALYSIS)

SPREADSHEET

	LESION GROUP	1L	2L	3L	1R	2R	3R
M1	1	9.14	4.31	8.32	12.76	3.13	9.74
O1	1	11.28	4.95	11.48	12.23	4.6	13.4
O5	1	10.41	4.35	11.22	11.37	5.65	11.26
O10	1	7.91	4.34	8.49	7.5	3.08	5.55
	LESION GROUP	1L-2L	3L-2L	1R-2R	3R-2R		
M1	1	4.83	4.01	9.63	6.61		
O1	1	6.33	6.53	7.63	8.8		
O5	1	6.06	6.87	5.72	5.61		
O10	1	3.57	4.15	4.42	2.47		

DESCRIPTIVE ANALYSIS

Descriptive Statistics (Sheet1 in Imported from C:\Documents and Settings\Thabelo\My Documents\Neurosci\FINAL THESIS WRITE UP\RESULTS\SPREADSHEETS\TREATMENT GROUP\NACC 6OHDA ONLY JUNE.xls)

	Valid N	Mean	Minimum	Maximum	Std.Dev.	Standard Error
1L	4	9.68500	7.910000	11.28000	1.473918	0.736959
2L	4	4.48750	4.310000	4.95000	0.308801	0.154401
3L	4	9.87750	8.320000	11.48000	1.705020	0.852510
1R	4	10.96500	7.500000	12.76000	2.379951	1.189975
2R	4	4.11500	3.080000	5.65000	1.242699	0.621349
3R	4	9.98750	5.550000	13.40000	3.317483	1.658741
1L-2L	4	5.19750	3.570000	6.33000	1.266264	0.633132
3L-2L	4	5.39000	4.010000	6.87000	1.520088	0.760044
1R-2R	4	6.85000	4.420000	9.63000	2.274394	1.137197
3R-2R	4	5.87250	2.470000	8.80000	2.630594	1.315297

STUDENT T-TESTS

T-test for Dependent Samples (Sheet1 in Imported from C:\Documents and Settings\Thabelo\My Documents\Neurosci\FINAL THESIS WRITE UP\RESULTS\SPREADSHEETS\TREATMENT GROUP\NACC 6OHDA ONLY JUNE.xls) Marked differences are significant at p < .05000

	Mean	Std.Dv.	N	Diff.	Std.Dv. Diff.	t	df	p
1L	9.68500	1.473918						
1R	10.96500	2.379951	4	-1.28000	1.687503	-1.51703	3	0.226535
	Mean	**Std.Dv.**	**N**	**Diff.**	**Std.Dv. Diff.**	**t**	**df**	**p**
2L	4.487500	0.308801						
2R	4.115000	1.242699	4	0.372500	1.188483	0.626850	3	0.575218
	Mean	**Std.Dv.**	**N**	**Diff.**	**Std.Dv. Diff.**	**t**	**df**	**p**
3L	9.877500	1.705020						
3R	9.987500	3.317483	4	-0.110000	2.183239	-0.100768	3	0.926092

	Mean	Std.Dv.	N	Diff.	Std.Dv. Diff.	t	df	p
1L	9.685000	1.473918						
2L	4.487500	0.308801	4	5.197500	1.266264	8.209187	3	***0.003783***

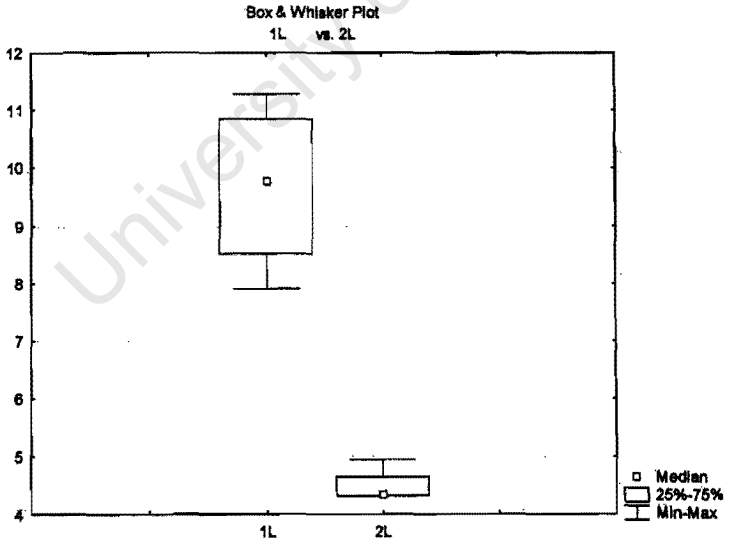

	Mean	Std.Dv.	N	Diff.	Std.Dv. Diff.	t	df	p
3L	9.877500	1.705020						
2L	4.487500	0.308801	4	5.390000	1.520088	7.091696	3	***0.005767***

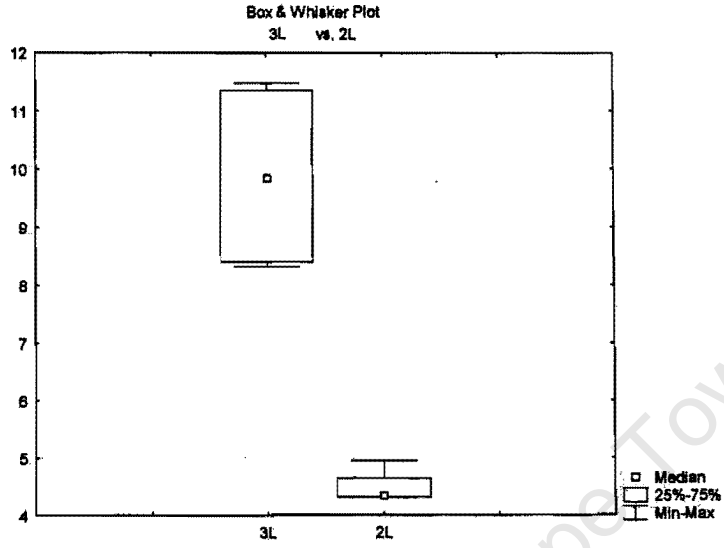

	Mean	Std.Dv.	N	Diff.	Std.Dv. Diff.	t	df	p
1R	10.96500	2.379951						
2R	4.11500	1.242699	4	6.850000	2.274394	6.023583	3	***0.009171***

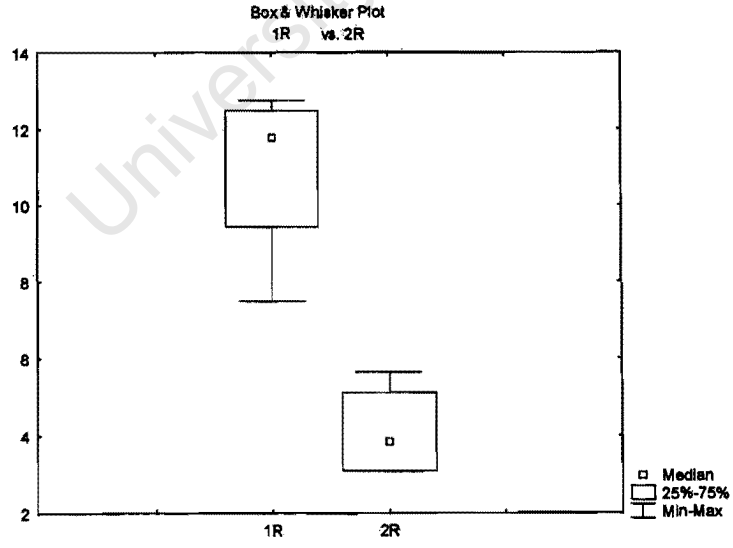

	Mean	Std.Dv.	N	Diff.	Std.Dv. Diff.	t	df	p
3R	9.987500	3.317483						
2R	4.115000	1.242699	4	5.872500	2.630594	4.464771	3	***0.020928***

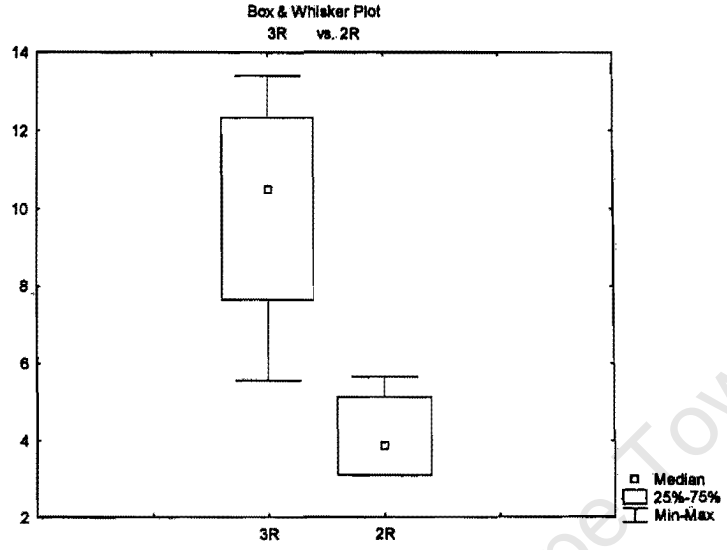

	Mean	Std.Dv.	N	Diff.	Std.Dv. Diff.	t	df	p
1L-2L	5.197500	1.266264						
3L-2L	5.390000	1.520088	4	-0.192500	0.720341	-0.534469	3	0.630090

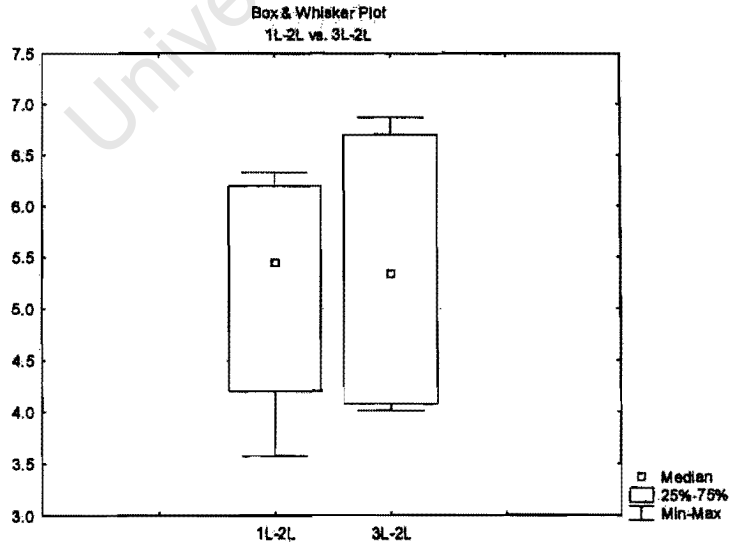

	Mean	Std.Dv.	N	Diff.	Std.Dv. Diff.	t	df	p
1R-2R	6.850000	2.274394						
3R-2R	5.872500	2.630594	4	0.977500	1.869213	1.045895	3	0.372457

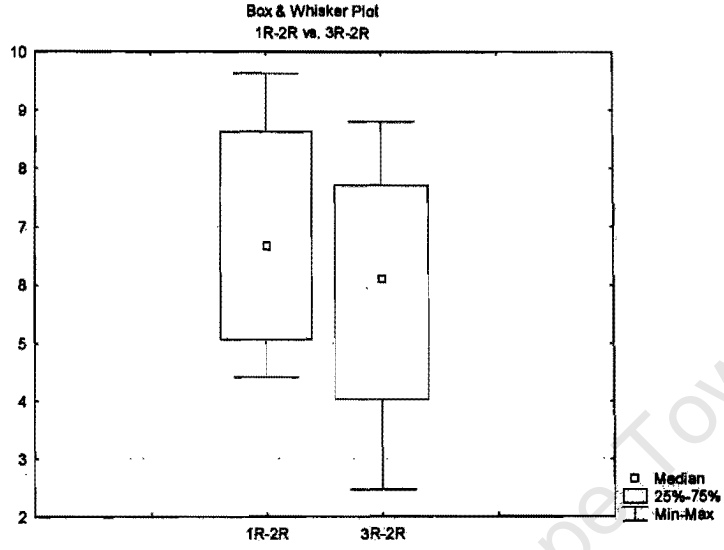

	Mean	Std.Dv.	N	Diff.	Std.Dv. Diff.	t	df	p
1L-2L	5.197500	1.266264						
1R-2R	6.850000	2.274394	4	-1.65250	2.209455	-1.49584	3	0.231584

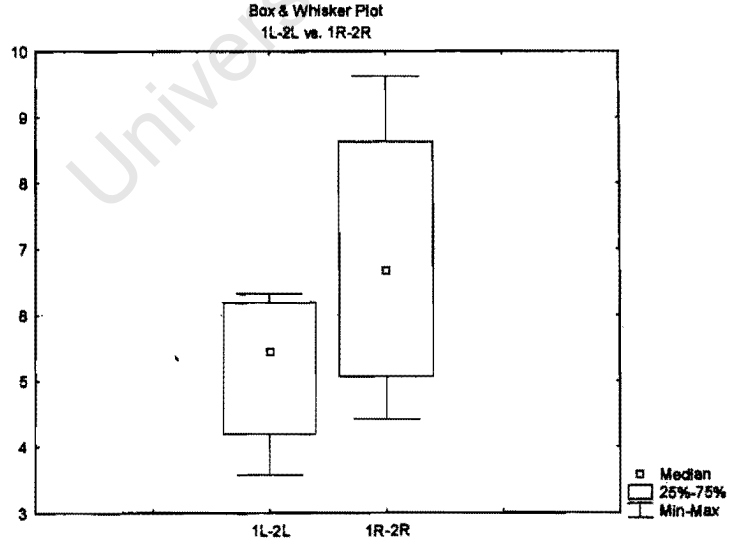

	Mean	Std.Dv.	N	Diff.	Std.Dv. Diff.	t	df	p
3L-2L	5.390000	1.520088						
3R-2R	5.872500	2.630594	4	-0.482500	2.265074	-0.426035	3	0.698801

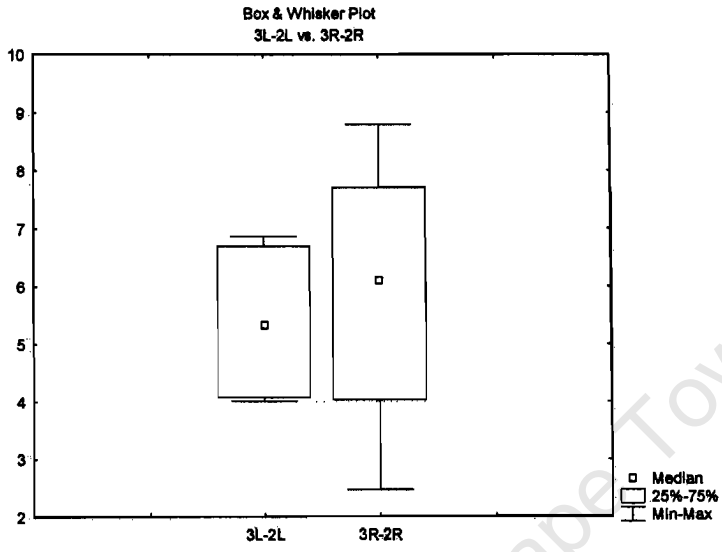

TREATMENT GROUP STATISTICS REPORT

COMPARISON OF STIMULATED $^{45}Ca^{2+}$ IN 6-OHDA LESIONED RATS vs SHAM LESIONED RATS

DORSAL STRIATUM

SPREADSHEET

	LESION GROUP	1L	2L	3L	1R	2R	3R	1L-2L	3L-2L	1R-2R	3R-2R
K2	1	11.17	6.48	12.87	11.6	7.01	11.86	4.69	6.39	4.59	4.85
K3	1	12.96	9.36	16.1	11.89	7.24	17.16	3.6	6.74	4.65	9.92
K4	1	11.91	4.91	6.86	11.99	3.59	11.16	7	1.95	8.4	7.57
K5	1	8.5	5.27	5.86	10.2	6.48	6.36	3.23	0.59	3.72	-0.12
M1	1	8.18	2.47	9.74	6.38	2.8	5.96	5.71	7.27	3.58	3.16
M5	1	7.58	2.52	7.33	5.73	3.06	6.22	5.06	4.81	2.67	3.16
O1	1	6.56	3.59	8.58	9.99	4.65	10.95	2.97	4.99	5.34	6.3
O5	1	5.43	5.89	10.98	5.06	6.88	10.19	-0.46	5.09	-1.82	3.31
O7	1	8.26	4.24	6.84	8.15	4.14	7.22	4.02	2.6	4.01	3.08
O10	1	6.85	4.42	9.8	7.86	3.99	7.86	2.43	5.38	3.87	3.87
K6	2	15.49	8.91	13.79	14.75	9.85	15.84	6.58	4.88	4.9	5.99
K7	2	9.96	8.19	10.41	9.11	5.25	13.9	1.77	2.22	3.86	8.65
K8	2	12.15	9.16	12.37	12.28	6.57	12.14	2.99	3.21	5.71	5.57
M9	2	10.92	6.55	11.7	7.12	6.82	8.47	4.37	5.15	0.3	1.65
M11	2	6.15	5.01	8.96	7.89	4.39	10.34	1.14	3.95	3.5	5.95
O11	2	11.01	6.18	8.24	9.41	6.32	9.61	4.83	2.06	3.09	3.29
O13	2	9.71	3.78	6.65	5.2	3.79	7.42	5.93	2.87	1.41	3.63
O14	2	8.16	5.33	9.5	7.63	3.89	7.87	2.83	4.17	3.74	3.98
O15	2	7.38	5.96	5.57	11	6.09	5.19	1.42	-0.39	4.91	-0.9

BREAKDOWN STATISTICS

LESION GROUP	1L Means	1L N	1L Std.Dev.	1L Std.Err.
1	8.74000	10	2.471841	0.781665
2	10.10333	9	2.776941	0.925647
All Grps	9.38579	19	2.640344	0.605736

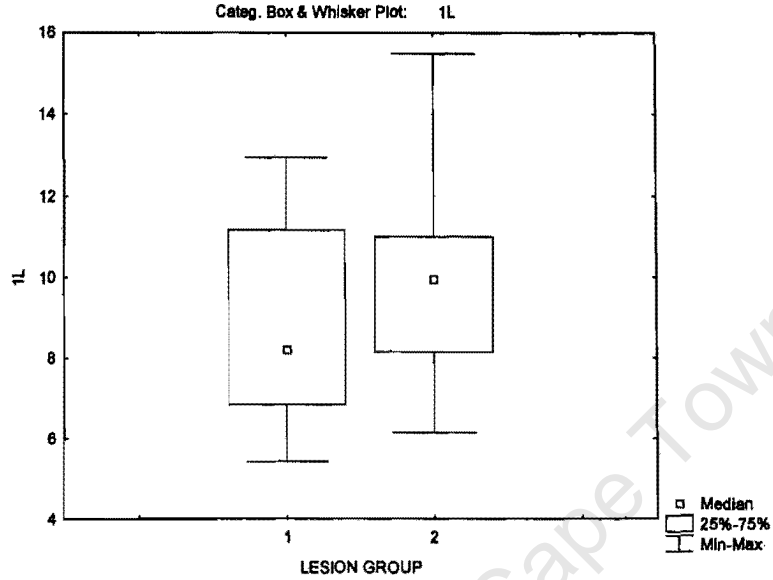

LESION GROUP	2L Means	2L N	2L Std.Dev.	2L Std.Err.
1	4.915000	10	2.039996	0.645103
2	6.563333	9	1.840095	0.613365
All Grps	5.695789	19	2.073803	0.475763

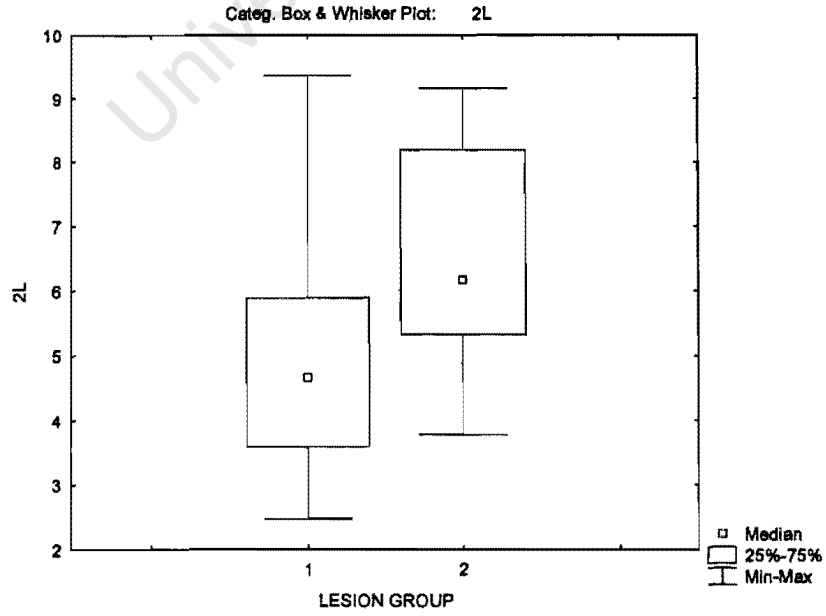

LESION GROUP	3L Means	3L N	3L Std.Dev.	3L Std.Err.
1	9.496000	10	3.164119	1.000582
2	9.687778	9	2.679514	0.893171
All Grps	9.586842	19	2.864703	0.657208

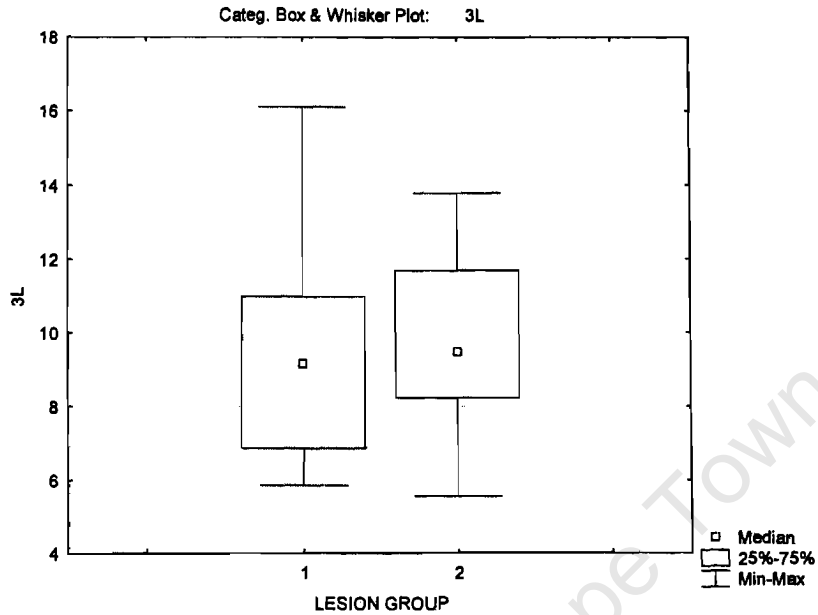

LESION GROUP	1R Means	1R N	1R Std.Dev.	1R Std.Err.
1	8.885000	10	2.612854	0.826257
2	9.376667	9	2.911348	0.970449
All Grps	9.117895	19	2.691506	0.617474

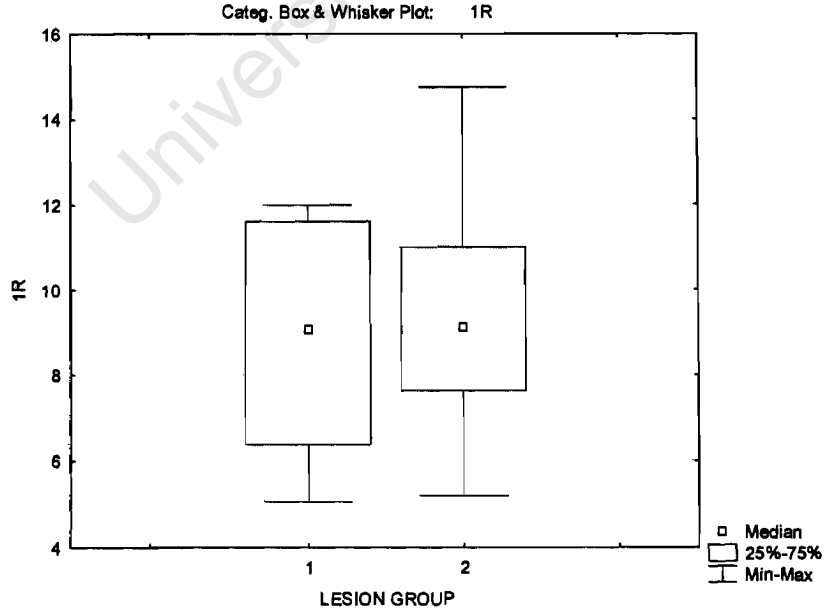

LESION GROUP	2R Means	2R N	2R Std.Dev.	2R Std.Err.
1	4.984000	10	1.740174	0.550291
2	5.885556	9	1.880931	0.626977
All Grps	5.411053	19	1.816700	0.416780

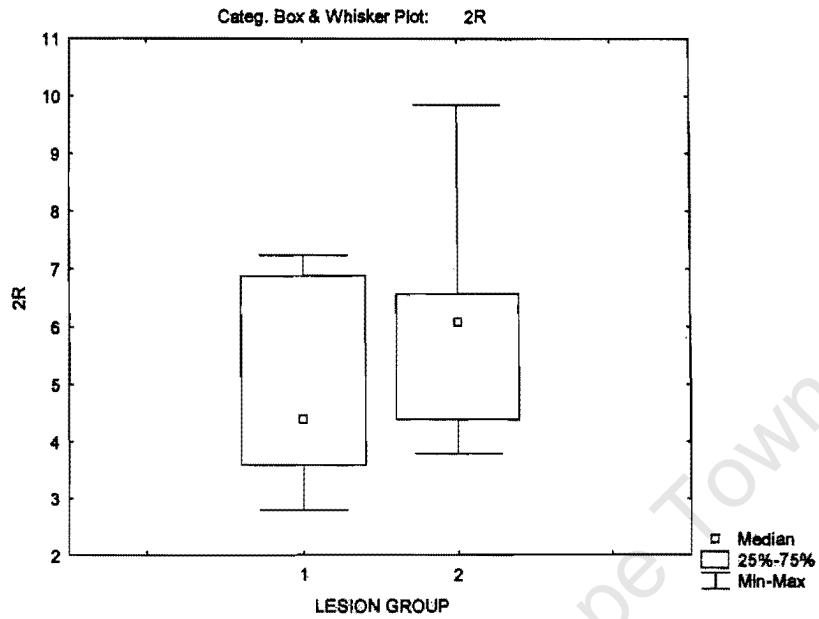

LESION GROUP	3R Means	3R N	3R Std.Dev.	3R Std.Err.
1	9.49400	10	3.505815	1.108636
2	10.08667	9	3.368338	1.122779
All Grps	9.77474	19	3.358621	0.770521

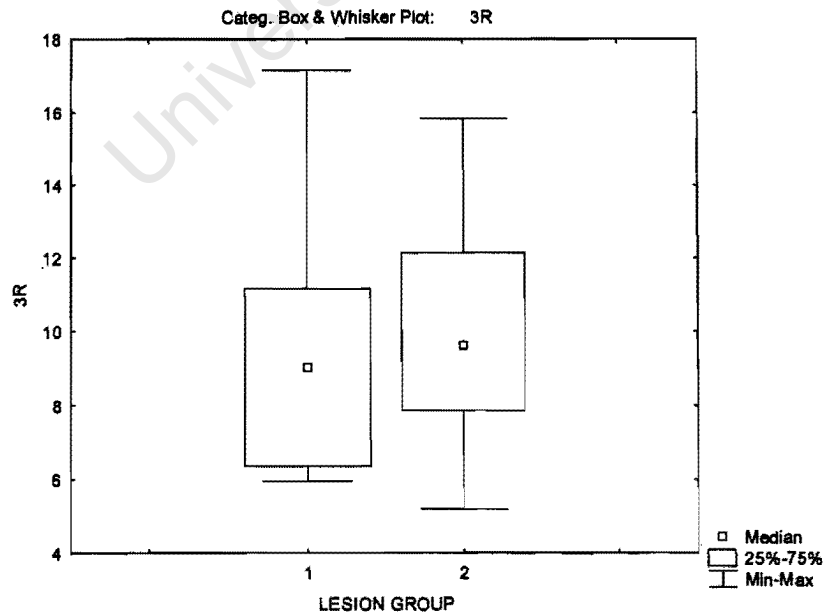

LESION GROUP	1L-2L Means	1L-2L N	1L-2L Std.Dev.	1L-2L Std.Err.
1	3.825000	10	2.038198	0.644535
2	3.540000	9	1.984332	0.661444
All Grps	3.690000	19	1.961768	0.450060

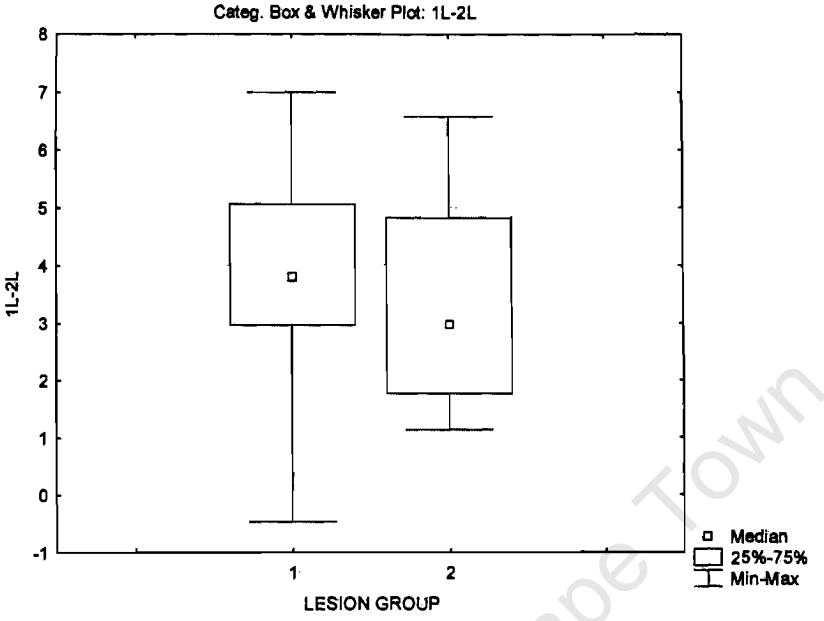

LESION GROUP	3L-2L Means	3L-2L N	3L-2L Std.Dev.	3L-2L Std.Err.
1	4.581000	10	2.187243	0.691667
2	3.124444	9	1.707850	0.569283
All Grps	3.891053	19	2.060741	0.472766

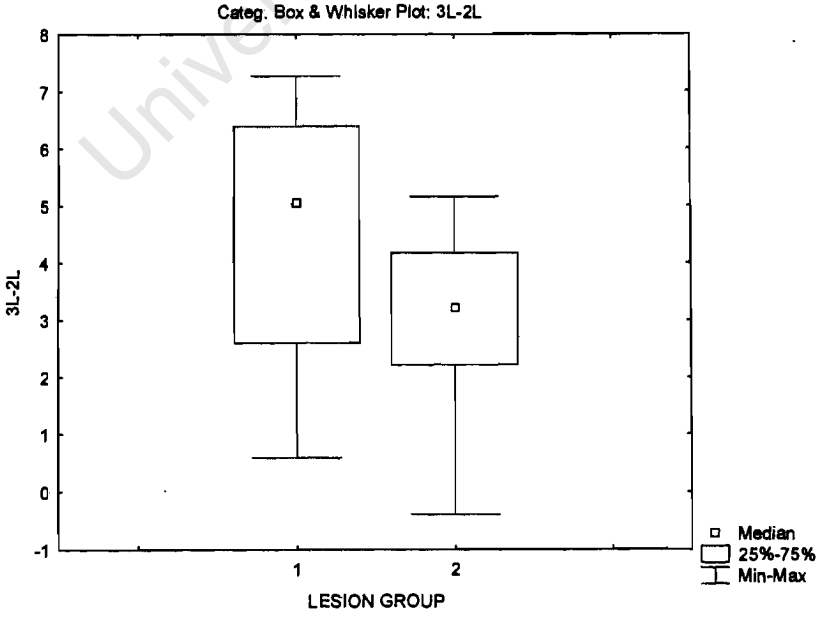

LESION GROUP	1R-2R Means	1R-2R N	1R-2R Std.Dev.	1R-2R Std.Err.
1	3.901000	10	2.532923	0.800981
2	3.491111	9	1.724634	0.574878
All Grps	3.706842	19	2.138691	0.490649

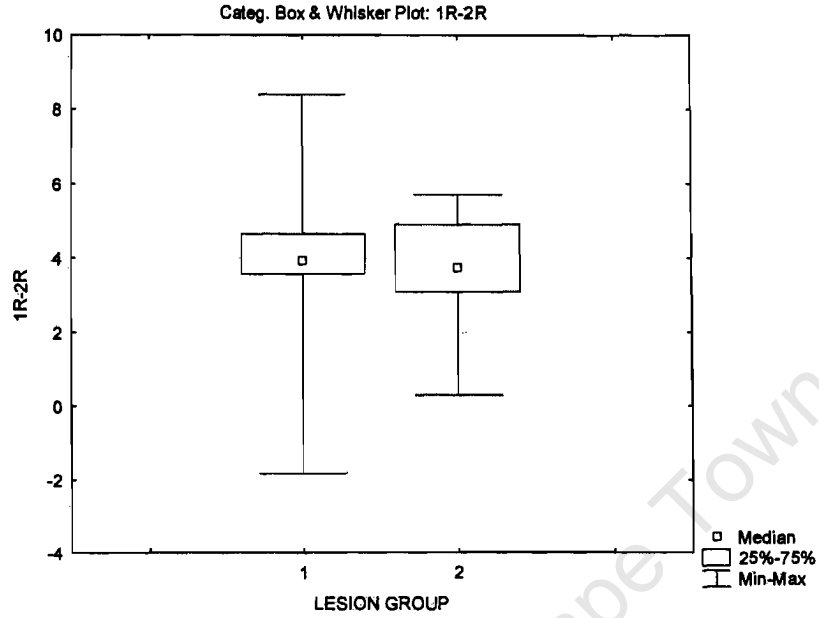

LESION GROUP	3R-2R Means	3R-2R N	3R-2R Std.Dev.	3R-2R Std.Err.
1	4.510000	10	2.807288	0.887742
2	4.201111	9	2.776236	0.925412
All Grps	4.363684	19	2.718656	0.623702

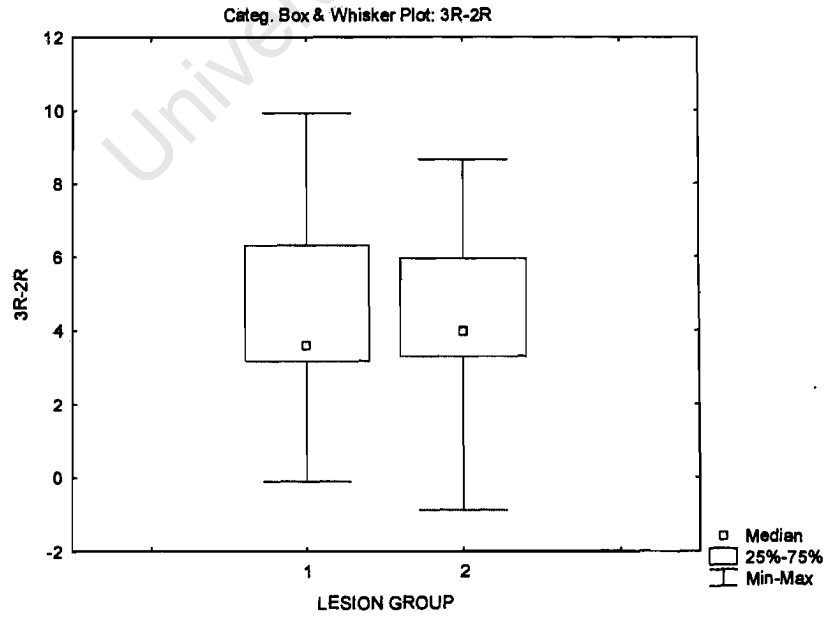

ANALYSIS OF VARIANCE

	SS Effect	df Effect	MS Effect	SS Error	df Error	MS Error	F	p
1L	8.80426	1	8.80426	116.6812	17	6.86360	1.282747	0.273111
2L	12.87001	1	12.87001	64.5419	17	3.79658	3.389897	0.083117
3L	0.17421	1	0.17421	147.5432	17	8.67901	0.020073	0.888998
1R	1.14507	1	1.14507	129.2507	17	7.60298	0.150608	0.702772
2R	3.85012	1	3.85012	55.5571	17	3.26806	1.178104	0.292895
3R	1.66383	1	1.66383	201.3822	17	11.84601	0.140455	0.712463
1L-2L	0.38475	1	0.38475	68.8889	17	4.05229	0.094946	0.761724
3L-2L	10.04947	1	10.04947	66.3903	17	3.90531	2.573281	0.127098
1R-2R	0.79583	1	0.79583	81.5362	17	4.79625	0.165928	0.688840
3R-2R	0.45195	1	0.45195	132.5877	17	7.79928	0.057948	0.812648

ANALYSIS OF UPTAKE IN VENTRAL STRIATUM OF TREATMENT GROUP

SPREADSHEET

	LESION GROUP	1L	2L	3L	1R	2R	3R	1L-2L	3L-2L	1R-2R	3R-2R
M1	1	9.14	4.31	8.32	12.76	3.13	9.74	4.83	4.01	9.63	6.61
O1	1	11.28	4.95	11.48	12.23	4.6	13.4	6.33	6.53	7.63	8.8
O5	1	10.41	4.35	11.22	11.37	5.65	11.26	6.06	6.87	5.72	5.61
O10	1	7.91	4.34	8.49	7.5	3.08	5.55	3.57	4.15	4.42	2.47
M10	2	5.07	1.87	5.03	3.75	1.97	4.34	3.2	3.16	1.78	2.37
O11	2	11.53	4	7.51	12.97	4.47	9.99	7.53	3.51	8.5	5.52
O13	2	6.59	1.88	5.19	4.86	1.54	6.88	4.71	3.31	3.32	5.34
O14	2	9.1	4.66	7.95	10.15	3.32	8.8	4.44	3.29	6.83	5.48
O15	2	8.8	4.03	13.23	8	5.14	10.53	4.77	9.2	2.86	5.39

BREAKDOWN STATISTICS

LESION GROUP	1L Means	1L N	1L Std.Dev.	1L Std.Err.
1	9.685000	4	1.473918	0.736959
2	8.218000	5	2.482251	1.110096
All Grps	8.870000	9	2.119729	0.706576

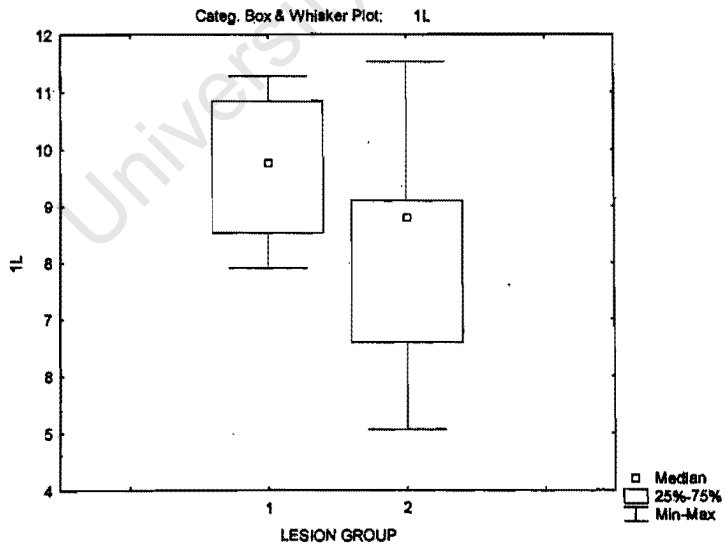

LESION GROUP	2L Means	2L N	2L Std.Dev.	2L Std.Err.
1	4.487500	4	0.308801	0.154401
2	3.288000	5	1.316537	0.588773
All Grps	3.821111	9	1.141079	0.380360

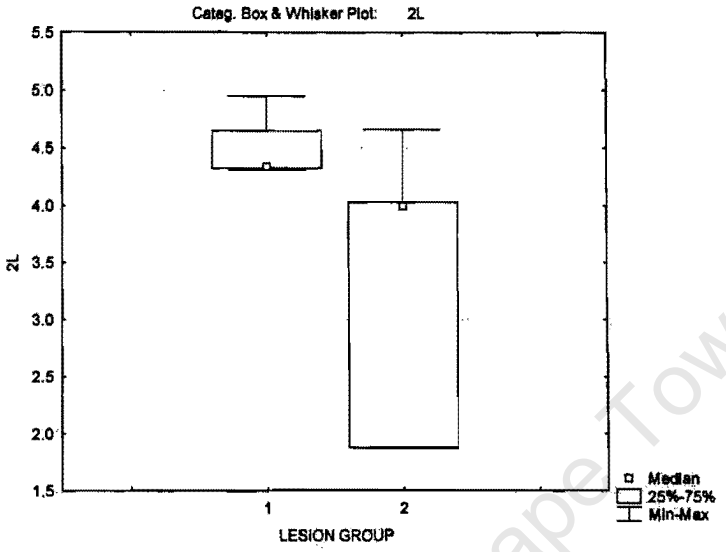

LESION GROUP	3L Means	3L N	3L Std.Dev.	3L Std.Err.
1	9.877500	4	1.705020	0.852510
2	7.782000	5	3.319446	1.484501
All Grps	8.713333	9	2.796297	0.932099

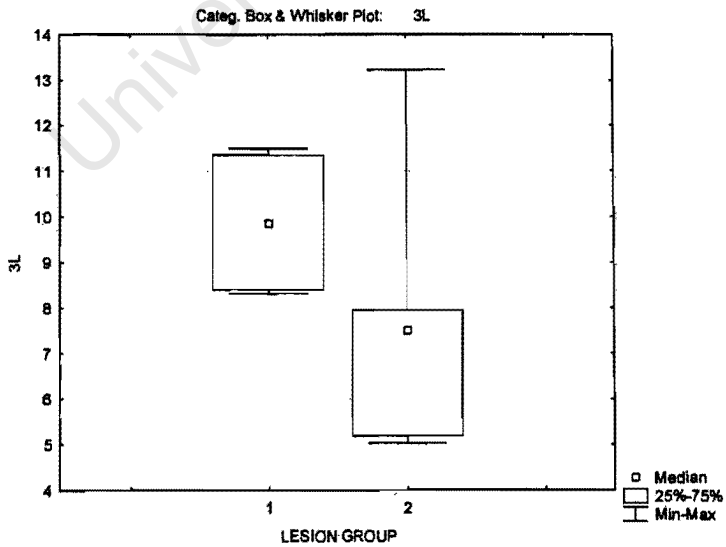

LESION GROUP	1R Means	1R N	1R Std.Dev.	1R Std.Err.
1	10.96500	4	2.379951	1.189975
2	7.94600	5	3.782556	1.691610
All Grps	9.28778	9	3.436524	1.145508

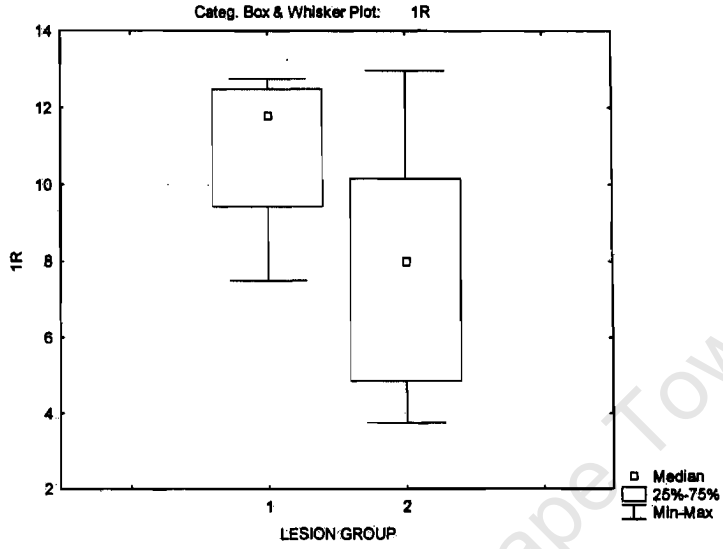

LESION GROUP	2R Means	2R N	2R Std.Dev.	2R Std.Err.
1	4.115000	4	1.242699	0.621349
2	3.288000	5	1.550861	0.693566
All Grps	3.655556	9	1.404164	0.468055

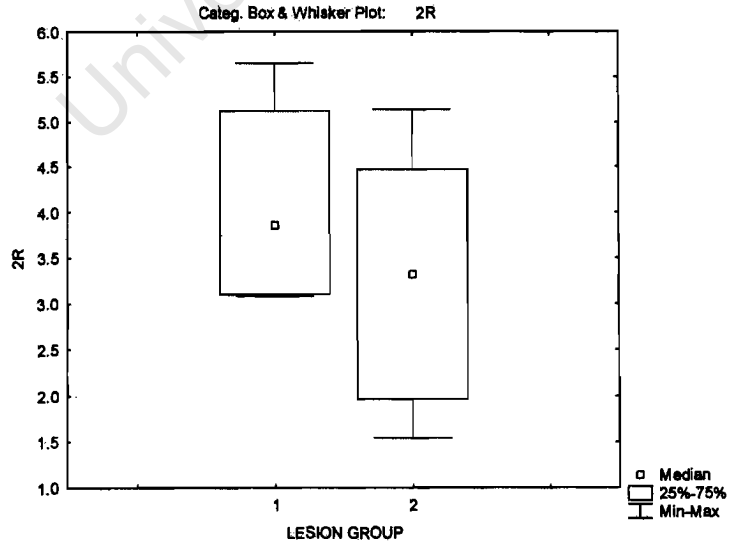

LESION GROUP	3R Means	3R N	3R Std.Dev.	3R Std.Err.
1	9.987500	4	3.317483	1.658741
2	8.108000	5	2.529460	1.131209
All Grps	8.943333	9	2.882269	0.960756

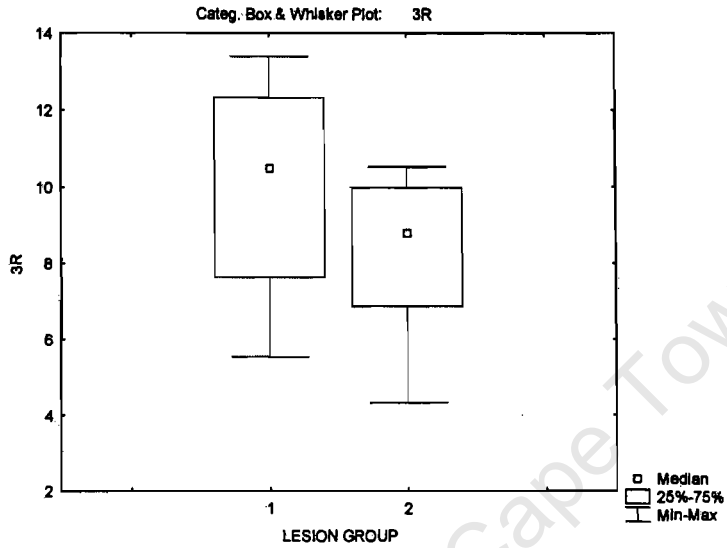

LESION GROUP	1L-2L Means	1L-2L N	1L-2L Std.Dev.	1L-2L Std.Err.
1	5.197500	4	1.266264	0.633132
2	4.930000	5	1.586427	0.709472
All Grps	5.048889	9	1.370962	0.456987

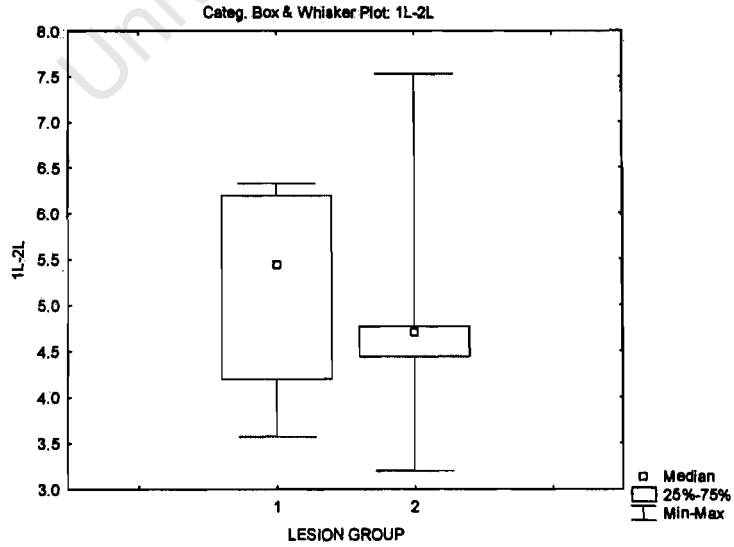

LESION GROUP	3L-2L Means	3L-2L N	3L-2L Std.Dev.	3L-2L Std.Err.
1	5.390000	4	1.520088	0.760044
2	4.494000	5	2.633710	1.177831
All Grps	4.892222	9	2.134882	0.711627

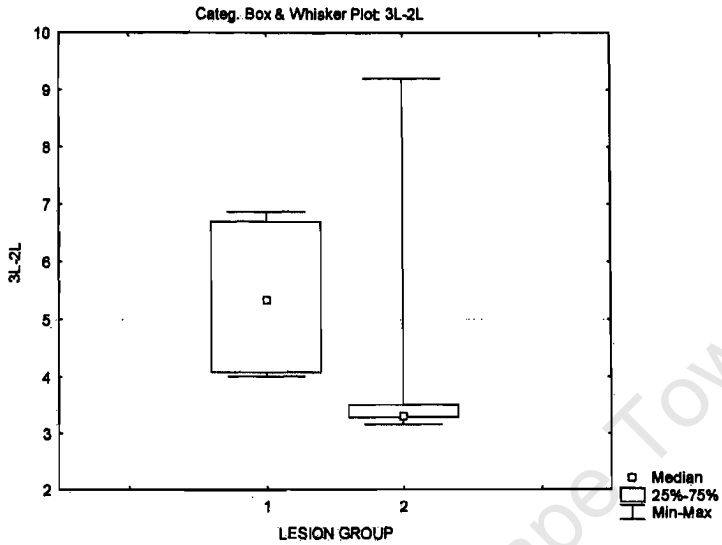

LESION GROUP	1R-2R Means	1R-2R N	1R-2R Std.Dev.	1R-2R Std.Err.
1	6.850000	4	2.274394	1.137197
2	4.658000	5	2.862887	1.280322
All Grps	5.632222	9	2.715248	0.905083

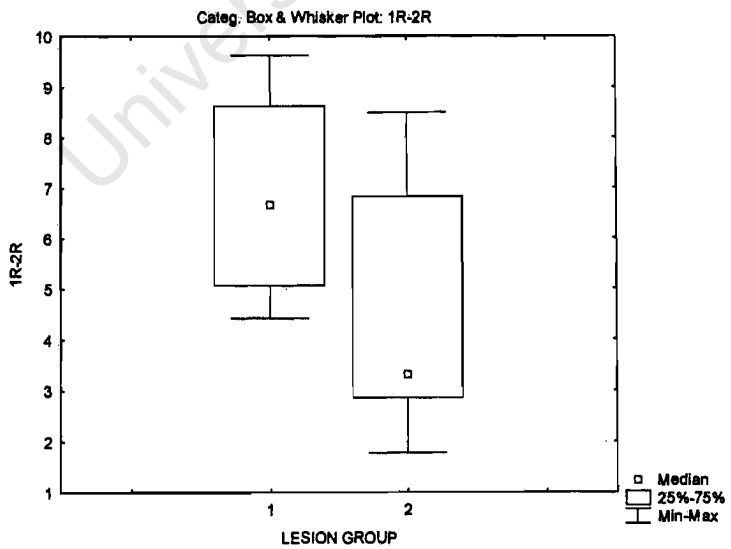

LESION GROUP	3R-2R Means	3R-2R N	3R-2R Std.Dev.	3R-2R Std.Err.
1	5.872500	4	2.630594	1.315297
2	4.820000	5	1.371441	0.613327
All Grps	5.287778	9	1.960394	0.653465

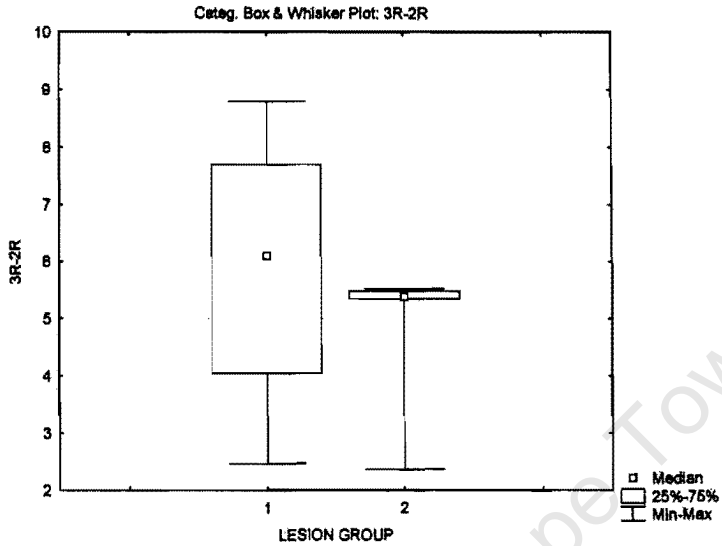

ANALYSIS OF VARIANCE

	SS Effect	df Effect	MS Effect	SS Error	df Error	MS Error	F	p
1L	4.78242	1	4.78242	31.16358	7	4.45194	1.074233	0.334463
2L	3.19733	1	3.19733	7.21916	7	1.03131	3.100271	0.121667
3L	9.75804	1	9.75804	52.79616	7	7.54231	1.293774	0.292785
1R	20.25414	1	20.25414	74.22342	7	10.60335	1.910165	0.209437
2R	1.51984	1	1.51984	14.25358	7	2.03623	0.746402	0.416237
3R	7.85005	1	7.85005	58.60976	7	8.37282	0.937563	0.365162
1L-2L	0.15901	1	0.15901	14.87728	7	2.12533	0.074819	0.792341
3L-2L	1.78404	1	1.78404	34.67772	7	4.95396	0.360123	0.567349
1R-2R	10.67748	1	10.67748	48.30308	7	6.90044	1.547362	0.253563
3R-2R	2.46168	1	2.46168	28.28348	7	4.04050	0.609252	0.460645

DORSO-VENTRAL UPTAKE ANALYSIS

ANALYSIS OF 1ST DORSAL SECTION vs 3RD VENTRAL SECTION.

The first dorsal striatum slice (1L-2L and 1R-2R) which was sectioned was the same slice from which the 3rd ventral striatum (3L-2LV and 3R-2RV) were dissected.

6-OHDA LESIONED RATS
SPREADSHEET

	NUCLEI GROUP	1L-2L	1L-2LV	3L-2L	3L-2LV	1R-2R	1R-2RV	3R-2R	3R-2RV
M1	1	5.71	4.83	7.27	4.01	3.58	9.63	3.16	6.61
O1	1	2.97	6.33	4.99	6.53	5.34	7.63	6.3	8.8
O5	1	-0.46	6.06	5.09	6.87	-1.82	5.72	3.31	5.61
O10	1	2.43	3.57	5.38	4.15	3.87	4.42	3.87	2.47

	Mean	Std.Dv.	N	Diff.	Std.Dv. Diff.	t	df	p
1L-2L	2.662500	2.528891						
3L-2LV	5.390000	1.520088	4	-2.72750	3.763592	-1.44941	3	0.243084

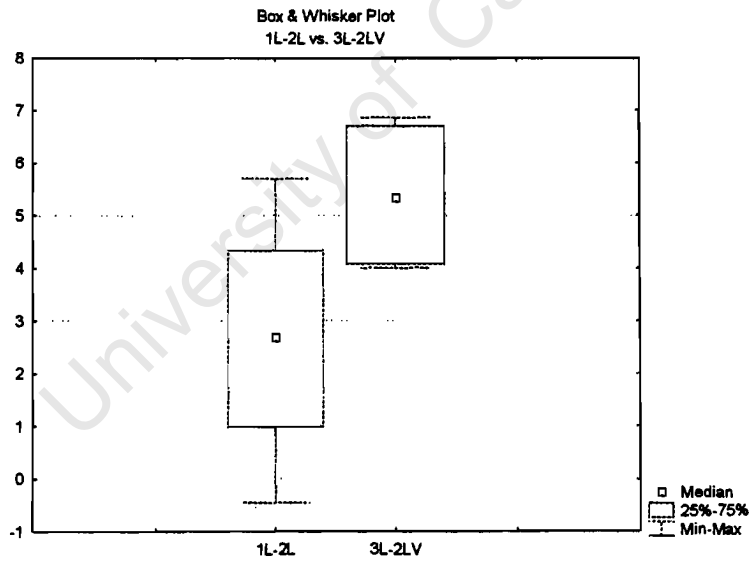

	Mean	Std.Dv.	N	Diff.	Std.Dv. Diff.	t	df	p
1R-2R	2.742500	3.137731						
3R-2RV	5.872500	2.630594	4	-3.13000	3.611546	-1.73333	3	0.181455

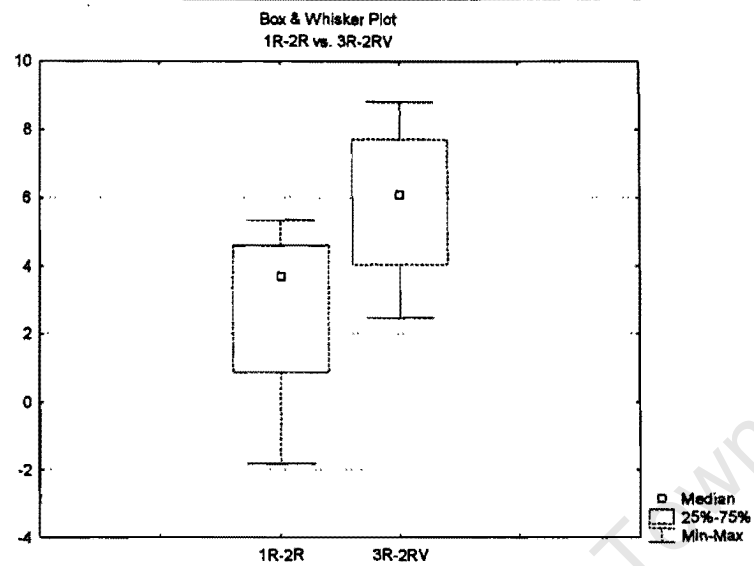

SHAM LESIONED RATS

SPREADSHEET

	NUCLEI GROUP	1L-2L	1L-2LV	3L-2L	3L-2LV	1R-2R	1R-2RV	3R-2R	3R-2RV
M10	1	2.13	3.2	3.08	3.16	1.31	1.78	1.46	2.37
O11	1	4.83	7.53	2.06	3.51	3.09	8.5	3.29	5.52
O13	1	5.93	4.71	2.87	3.31	1.41	3.32	3.63	5.34
O14	1	2.83	4.44	4.17	3.29	3.74	6.83	3.98	5.48
O15	1	1.42	4.77	-0.39	9.2	4.91	2.86	-0.9	5.39

	Mean	Std.Dv.	N	Diff.	Std.Dv. Diff.	t	df	p
1L-2L	3.428000	1.890772						
3L-2LV	4.494000	2.633710	5	-1.06600	4.022621	-0.592561	4	0.585351

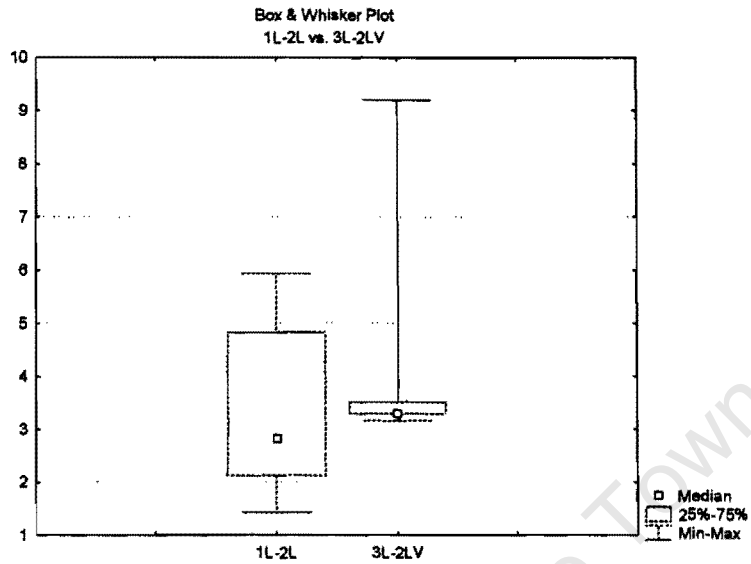

	Mean	Std.Dv.	N	Diff.	Std.Dv. Diff.	t	df	p
1R-2R	2.892000	1.543509						
3R-2RV	4.820000	1.371441	5	-1.92800	1.336552	-3.22557	4	*0.032110*